In Vivo Microdialysis Coupled with Electrophysiology for the Neurochemical Analysis of Epileptic Seizures

by

Eric Wayne Crick
B.S., Western Kentucky University,
Bowling Green, KY, 2002

Submitted to the Department of Chemistry and the Faculty of the
Graduate School of the University of Kansas in partial fulfillment of
the requirements for the degree of Doctor of Philosophy

_____
(Committee Chair)

_____

_____

_____
(Committee Members)

Date defended:_____

The Dissertation Committee for Eric Wayne Crick certifies
that this is the approved version of the following dissertation:

**In Vivo Microdialysis Coupled with Electrophysiology for the
Neurochemical Analysis of Epileptic Seizures**

_____

(Committee Chair)

_____

_____

_____

(Committee Members)

Date approved:_____

Abstract

Eric Wayne Crick, Ph.D.
R.N. Adams Institute for Bioanalytical Chemistry
Department of Chemistry, June 2007
University of Kansas

The focus of this research has been on the development of analytical techniques for the determination of the neurochemistry pertaining to animals that model epilepsy. The utilization of microdialysis sampling coupled with electrophysiological techniques played a vital role in the understanding of these neurochemical changes.

A thorough working knowledge of epilepsy models is essential for the development of new therapies for the neurological disorder. Initial work focused on a well known convulsant, 3-mercaptopropionic acid (3-MPA). An epileptic seizure model employing 3-MPA does not exist. A constant infusion dosing scheme was employed with a steady-state concentration of 3-MPA in the brain. The ability to control the 3-MPA concentration was an excellent independent variable for further experimentation involving the correlation of neurochemical events. A PK-PD study was conducted using simultaneous ECoG recordings.

A major difficulty with microdialysis sampling of neurochemical events is the ability to fully capture the events with sufficient temporal resolution. The sampling frequency is often hindered by the analytical instrumentation commonly available. Liquid chromatography was initially utilized for the neurochemical analysis of 5 minute microdialysis collections. However, it was found that this temporal resolution was not sufficient for obtaining meaningful neurochemical data from the seizure model.

Capillary electrophoresis was also employed, allowing for the neurochemical analysis with 60 second resolution. A biphasic increase in the levels of glutamate and dopamine were observed with the enhanced temporal resolution. Moreover, the levels of glutamate and γ-aminobutyric acid had sustained changes over extended periods of time. It was determined that glutamate receptor desensitization played a crucial role in these findings. The shortcomings of these methods include poor derivatized sample stability and decreased catecholamine sensitivity in a complex analysis of amino acid and biogenic amine neurotransmitters.

To overcome these limitations, additional instrumentation was developed using a dual-parallel electrode detection scheme for capillary electrophoresis. This design provided increased sensitivity by simultaneously operating in the series and parallel-opposed configurations, thereby permitting redox cycling. It also allowed for enhanced selectivity by operating in the parallel-adjacent configuration. This scheme would help to improve the sample stability due to the electroactive nature of the catecholamines.

Acknowledgements

was outstanding, and to Andrew Mayer – your contributions to the CTZ work were invaluable…best of luck with continuing the project.

To my parents, Billy and Leesa, your love and support, from kindergarten through the present, has been endearing. You have always believed in me regardless of where I was in life, and look, I'm almost out of school! To my sister, Rebecca, thank you for putting up with me throughout the years.

Last but not least, I must thank my wife, Leigh. You've lovingly supported everything that I've ever wanted to do. You've quietly put up with my <u>two</u> visits to Europe, not complaining once that you couldn't tag along. I guess I owe you one sometime!

Table of Contents

Chapter 1. Introduction

Chapter 2. Development of a Chemical Seizure Model Using 3-Mercapto-propionic Acid

Chapter 3. Neurochemical Correlation of Glutamate, GABA, and Dopamine to 3-MPA Chemical Seizure Model

Chapter 4. Enhanced Temporal Resolution Neurochemical Analysis Using Capillary Electrophoresis

Chapter 5. Dual-Electrode Detection for Capillary Electrophoresis: Feasibility of a New Dual-Detector Design

Chapter 6. Conclusions and Future Work

List of Tables

List of Figures

Chapter 1.

Introduction

1.1. Epilepsy

Epilepsy is a neurological disorder that affects approximately 1% of the population worldwide [1]. Epilepsy is characterized by recurrent, unprovoked seizures and is defined as two or more unprovoked seizure events [2]. A normal brain is thought to become epileptic due to a fleeting change in behavior as a result of the "disordered, rhythmic firing of populations of central nervous system (CNS) neurons" [3]. Basically, the brain becomes hyperexcitable and inhibition is diminished. This leads to a state of imbalance between the excitatory and inhibitory neurotransmitters in the brain. An estimated 5% of the world's population will have at least one seizure in their lifetime and approximately 20% of that population will end up having recurrent seizures during their lives [4]. McNamara *et al.* estimated that 60% of all epilepsies are partial in nature, or arise from one localized area in the brain. Forty percent of these partial epilepsy cases originate from the limbic system, with limbic epilepsy being the most common form of epilepsy [3]. While 60 - 70% of the world's epileptic population is treated using antiepileptic medication, or antiepileptic drugs (AEDs), approximately one-third of the population is classified as having retractable epilepsy that is not treatable with one or more AEDs in combination [4]. From these

statistics, it is evident that pursuing the area of epilepsy treatments is of utmost importance.

1.2. Treatments for Epilepsy

As mentioned above, the most common treatment for those patients with epilepsy and epileptic seizures is AEDs. While knowledge of epilepsy and related seizures has grown throughout the years, only two-thirds of the epileptic population is efficiently treated for their disorder. This statistic highlights the need for other alternative treatments for epileptic patients. One popular treatment for epilepsy is the ketogenic diet. With the ketogenic diet, mainly prescribed in pediatric epilepsy, the patient is restricted to a diet high in fat, moderate in protein, and low in carbohydrates [5]. This treatment is hypothesized to be effective due to a direct action on the ketone bodies, especially β-aminobutyric acid, an analogue to γ-aminobutyric acid (main inhibitory neurotransmitter). It also causes an increase in the nitric oxide levels in the hippocampus [6]. The ketogenic diet is successful, causing approximately 50 – 90% reduction in seizures in children after a six month time frame [7]. Because the ketogenic diet is less effective in adults, other treatments must be pursued. One of the alternative treatments available is electrical stimulation that causes suppression in seizure activity. Essentially, electrodes are implanted into the brain regions that have been proven to be epileptic. Previously studied brain regions include the cortex, basal ganglia, thalamus, subthalamic nucleus, hippocampus, and vagal nerve [8, 9]. It has

2

been reported that the average reduction in seizure activity is approximately 60 – 90% in experimental studies on animals and humans [8, 10].

With any new treatment or therapy that is developed, the most crucial aspect is to have a critical working knowledge of the underlying neurochemical happenings. These treatments or therapies initially must be modeled with either animals or humans to demonstrate their efficacies; however, there is a lack of available models that describe all of the epilepsies. Therefore, the ability to create viable epileptic seizure models is necessary in order to further the understanding of the chemistries behind them.

1.3. Animal Seizure Models

Animal models of epilepsy and epileptic seizures play a critical role in the understanding treatments that suppress the epileptic activity [11]. These animal models are used to make comparisons to human epilepsy; thus, choosing the appropriate model when studying parameters of epilepsy is of utmost importance. Criteria to consider when choosing an animal model that parallels human epilepsy include clinical symptoms/manifestations, electrophysiological activity, and the therapeutic effect of antiepileptic drugs (AEDs) [12]. The two most common types of animal seizure models are the kindling model (electrical) and the pharmacologically-induced model (chemical) [12].

1.3.1. Electrical Seizure Models

Introduced by Goddard in 1967, the kindling model uses frequencies of electrical stimulation in order to produce epileptic seizures [13]. Typically, bipolar stimulation wires are surgically implanted into animal brains. After the animal has recovered it is given a repeated shock, or stimulation, on a daily interval that results in enhanced electrical excitability of the brain [11]. Kindling has become a rather popular model to induce "spontaneous" epileptic seizures over time [14]. This model then produces information on how the brain learns and memorizes the electrical stimulation, resulting in seizing on its own in the absence of the actual electrical shock. The drawback of this model is that it is very time consuming (days to weeks) and actually produces changes in the neuronal structure and function down to the level of gene expression [15].

1.3.2. Chemical Seizure Models

Chemical means of producing epileptic activity is typically performed by the introduction of chemical convulsants to the animal models. Chemical convulsants can be introduced to the animals systemically or intracerebrally (e.g. kainic acid, picrotoxin, 3-mercaptopropionic acid), or topically (e.g. penicillin) [16, 17]. The chemical seizure models can be broken into two groups based upon the amount of knowledge that is known regarding their mechanisms of action at the neuronal level: 1) those that are used to predict the efficacy of newly developed AEDs, and 2) those

that are used to further enhance the knowledge regarding the generation of seizure activity [18].

The chemical convulsants in the first group have been validated in animal models that have high specificity in the identification of drugs and/or target receptors with clinical efficacy patterns. Examples of these include picrotoxin (selectively blocks $GABA_C$ receptors), pentylenetetrazole (blocks $GABA_A$ receptors), and allylglycine (irreversibly blocks glutamic acid decarboxylase (GAD)). The chemical convulsants listed in the second group use mechanisms not yet completely understood and therefore, could act on one or multiple drug receptors. Refinement of these chemical seizure models could potentially lead to the use of these convulsants in the search for new AEDs. Examples of compounds that belong in the second grouping include penicillin (thought to affect $GABA_B$ receptors), γ-hydroxybutyric acid (thought to inhibit dopamine), and 3-mercaptopropionic acid (thought to act as a competitive inhibitor of GAD) [18].

Animal models of epilepsy are advantageous because they assess seizure causes and consequences. In order to examine changes in the animal after cessation of seizure activity, the survival times of the experiment can be adjusted accordingly and repeated events, such as kindling, can be studied effectively. Limitations of animal models include the difficulty to generalize findings due to differences in animal strains and many of the available models result in status epilepticus (SE), which does not model typical epilepsy [16].

1.4. Electrophysiological Recordings

There are two common ways in which electrophysiological recordings can be made from the brain. Firstly, electroencephalography (EEG) uses disk shaped electrodes placed onto the scalp of the patient. The resulting EEG plot is actually a recording of the voltage differences between two electrodes at two different parts of the brain [11]. EEG voltages result from the summation of all of the synaptic activity occurring around the cortical region under the scalp where the electrodes are located. Secondly, electrophysiological recordings of the brain can be measured by placing electrodes through a hole made in the skull into the cerebral cortex. This type of recording is known as an electrocorticograph, or ECoG. The cortical signals recorded using ECoG are comparable to those collected by EEG. In extreme cases, part of the skull is removed when using ECoG to gain better knowledge of the exact portion of the cortex that is epileptic in order to surgically remove the region [19]. ECoG can also be used after the surgery is complete in order to verify that the epileptic tissue has been removed successfully.

The main advantage of ECoG collections over EEG collections is enhanced spatial resolution. Electrodes placed directly onto the cerebral cortex allow for a more effective measurement of the neuronal activity. In EEG recordings, the skull reduces the electrical signal from the cortex, resulting in lowered output signals and possibly causing critical neuronal events to go unnoticed.

1.5. Microdialysis Sampling

Microdialysis is a sampling technique used to study unbound tissue concentrations of both exogenous and endogenous compounds. This technique has gained exponential attention in the neurosciences during the past three decades, and is the method of choice to study the pharmacokinetics (PK) and the pharmacodynamics (PD) of drug substances in the brain and various other tissues and organs [20].

The dialysis technique was first developed and implemented for the use of sampling in the brain by Bito *et al.* in 1966 [21]. Small dialysis sacs filled with 6% dextran in saline solution were placed into the brains and subcutaneous neck tissues of dogs introducing the idea of a "compartment" enclosed within dialysis membrane which equilibrates to the extracellular surroundings. After 10 weeks of sampling, the dialysis sacs were removed and analyzed for amino acid and electrolyte content. Delgado *et al.* provided a design overhaul in 1972 with the development of the "dialytrode" [22]. The design of the dialytrode included two small stainless steel rods soldered together forming a typical push-pull type cannula with a seven-electrode contact. This dialytrode provided electrical stimulation and recording, as well as chemical injection and collection. In 1974, Understedt *et al.* refined the aforementioned design by implementing thin dialysis tubes, or hollow fibers, into the brain [23]. The purpose of the hollow fibers was to mimic the function of the blood vessels and was only devoid of the blood-brain barrier. [^{3}H]dopamine was perfused through the fibers to establish a true baseline and to observe amphetamine stimulated release of dopamine. Following these initial experiments, the use of microdialysis in

the neurosciences has expanded. Recent neurochemical research using microdialysis has ranged from basic PK-PD correlations for newly developed drugs [24] to studying the effects of traumatic brain injuries [25] and neurological disorders [26].

1.5.1. Theory of Microdialysis Sampling

Microdialysis sampling is based on the principle of dialysis, in which small analytes and water diffuse to and from the tissues or organs of interest through a semi-permeable membrane [27]. An isotonic solution, deficient in the analyte of interest, is perfused through the membrane. This solution, termed the perfusate, is pumped through the microdialysis probe inlet tubing at typical flow rates of 0.5 – 5 µL/min, and is allowed to equilibrate with the fluid located outside the membrane via diffusion across the membrane. The outflow from the microdialysis probe, termed the dialysate, is collected either on-line for real-time analysis or off-line for future analysis [28]. A schematic of a brain microdialysis probe is shown in Figure 1.1. Analytes of interest, located in the surrounding extracellular fluid (ECF), diffuse into the microdialysis probe due to the concentration gradient present [29]. The collected portion represents the free, or unbound, fraction of analytes in the area of interest due to the semi-permeable membrane containing a specific molecular weight cutoff (MWCO) that prohibits large molecules, such as proteins, to pass through the membrane.

1.5.2. Microdialysis Probe Designs

The microdialysis probe design most common in neurochemistry is the concentric cannula, or rigid probe design [30]. The brain is a heterogeneous tissue; thus, high spatial resolution must be considered for the proper probe design. The concentric cannula, as depicted in Figure 1.1, contains an active membrane 0.5 – 4 mm in length and 240 - 350 μm in outer diameter [31]. The probes are placed into supporting guide cannulas which are implanted into discrete brain regions and then anchored and cemented to the skull.

The two other main types of microdialysis probe designs are the flexible cannula probe and the linear probe, as shown in Figures 1.2(A) and 1.2(B). The flexible cannula probe by-passes the rigidity of the concentric design discussed above, and is primarily used for sampling in blood vessels [32]. The linear probe design is primarily used in tissues that are more homogenous in nature, such as the liver, muscle, or heart [20].

Another important consideration of microdialysis probe design is the nature of the semi-permeable membrane. Various options include polyacrylonitrile, polycarbonate, polyethersulfone, and cuprophan [29]. Since analytes have different physical characteristics, chemical interactions of the analyte will vary with each type of membrane. This can greatly affect probe performance and analyte recovery from the sampling site of interest.

Dialysate

Perfusate

ECF

Semipermeable
Membrane

(A)

(B)
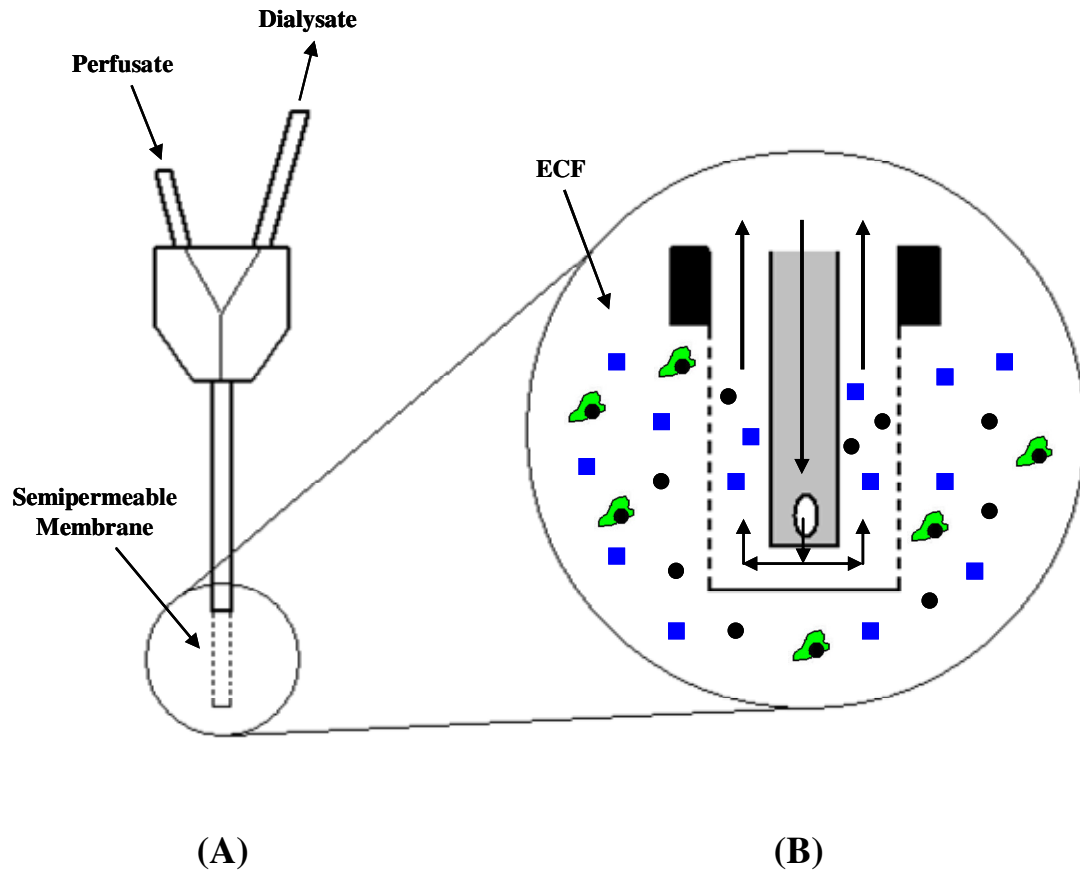
Figure 1.1. Rigid (concentric) cannula microdialysis probe design. (A) Full view of concentric probe. (B) Enlarged view of the semipermeable membrane of probe. The direction of the perfusate flow through the probe is indicated by arrows. Symbols: ■, water; ●, small molecules (will diffuse in/out of the probe); protein-bound small molecules in the ECF (will not diffuse through the membrane).
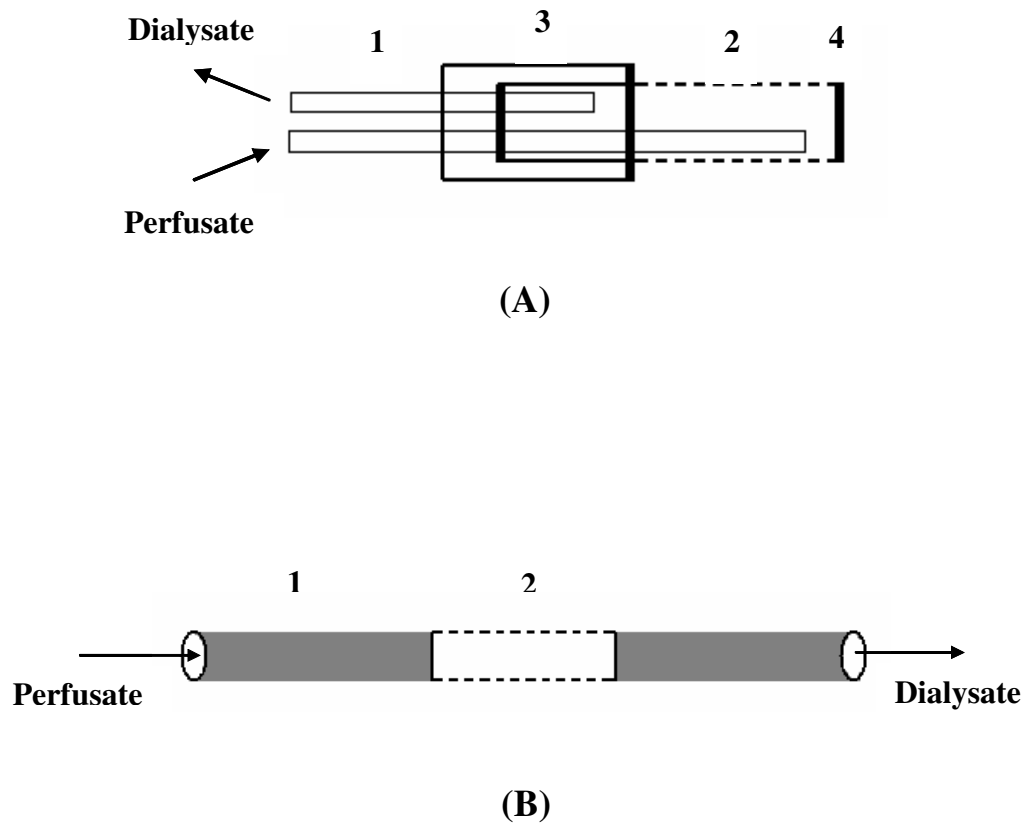
Figure 1.2. Schematic of alternative microdialysis probe designs. (A) Flexible cannula microdialysis probe design. (B) Linear probe design. The direction of the perfusate flow through the probe is indicated by arrows. 1 = polyimide tubing; 2 = semi-permeable membrane; 3 = MRE tubing; 4 = UV glue junction. The process of microdialysis probe fabrication is detailed in Section 2.2.3.1.

1.5.3. Calibration Methods

If using microdialysis as a quantitative sampling technique, the relative recovery of the probe must be known. Due to the constant perfusion of liquid through the probe, a true equilibrium and a 100% relative recovery cannot be established. The relative recovery, shown in Equation 1.1, is the ratio of the dialysate analyte concentration (C_{dial}) and the analyte concentration in the perfusion medium (C_{perf}) [33].

$$\text{Relative Recovery} = (C_{dial}) \,/\, (C_{perf}) \qquad\qquad (1.1)$$

Since the relative recovery never reaches an equilibrated state, the analyte concentration recovered by the microdialysis probe is lower than the analyte concentration in the ECF. There are several factors that affect the performance of the microdialysis probe. These factors include the perfusion rate (controlled by a perfusion pump), the composition of the perfusate, the velocity of the diffusion process (including environmental temperature, MWCO, and semi-permeable membrane area), and the complexity of the sample matrix [29, 34]. A typical calibration method used for an *in vitro* experimental setup includes placing a microdialysis probe into a vial containing a solution mimicking the ECF, also known as artificial cerebral spinal fluid (aCSF), that has a known concentration of the analyte of interest. This solution is maintained at 37 °C and continuously stirred. The probe is then perfused with aCSF that does not contain the analyte. Dialysate samples are

collected, analyzed, and compared with the solution in the vial to determine the relative *in vitro* recovery.

When implanting the microdialysis probe into the brain, the sample matrix changes. There no longer exists a simple, dynamic environment; it has been replaced with a static heterogeneous environment. Therefore, making a comparison between *in vitro* and *in vivo* probe calibration values can be inexact because of these additional factors that may impede the analyte's recovery into the microdialysis probe [35]. These factors include the amount of tissue vascularization, the metabolism rate, and the reuptake of the analyte into cells [27].

In vivo calibration of the microdialysis probe can be accomplished by a few different methods. One established method is no-net-flux. Lonnroth *et al.* first described this method in 1987, and it is considered the one "true" way to perform an *in vivo* microdialysis probe calibration [36]. With the no-net-flux calibration method, the analyte concentration in the sample matrix is first estimated based upon reported literature values. Then concentrations of the analyte, either above or below the estimated concentration, are introduced into the perfusate. If the analyte concentration in the perfusate is greater than that in the brain, the analyte will diffuse through the membrane into the brain. If the analyte concentration in the perfusate is less than that in the brain, the analyte will diffuse into the probe. A plot of the net change in analyte concentration in the dialysate (y-axis) versus the analyte concentration in the perfusate (x-axis) results in a linear relationship, thereby determining the true concentration of the analyte in the brain. When the

concentration in the probe matches the concentration in the brain, no net diffusion occurs. While this method has proven to work very well, it suffers from being very time consuming. Results, similar to those obtained using the no-net-flux method, have been reported by investigators using simpler calibration methods. One simplified method is that of calibration by delivery, or retrodialysis [37]. In this method, once the microdialysis probe has been implanted, a known concentration of the analyte is perfused through the probe. The dialysate is collected, analyzed, and compared to the

$$\text{Relative Delivery} = (C_{perf} - C_{dial}) / (C_{perf}) \qquad (1.2)$$

perfusate. Equation 1.2 represents the comparison of the two substances. This method was compared to no-net-flux method by Song and Lunte, and the calibration value was found to be similar [38]. However, this method does not take into account any changes in analyte recovery of the microdialysis probe throughout the entirety of the experiment. For this quantity to be taken into account, another version of retrodialysis should be considered. In this method, an internal standard is added to the perfusate during the course of the experiment [39]. The diffusion properties of the chosen internal standard should match those of the analyte of interest in order to compare the relative recovery of the internal standard to the relative recovery of the analyte. The advantage of using an internal standard is that probe performance over the course of an experiment does not affect the overall recovery results. The last

method used for *in vivo* calibration is flow rate variation [40]. In this method, the flow rate of the perfusate is varied over the course of the calibration. The concentration of recovered analyte is plotted against the flow rate, and when extrapolated to zero, the analyte concentration can be estimated and the relative recovery of the probe can be measured. The main disadvantage of this method is that the long sampling times required for the low flow rates lead to poor temporal resolution.

1.5.4. Advantages and Limitations

Advantages of microdialysis include the ability to collect multiple samples from the site of action in the animal over long periods of time. Microdialysis samples do not require further sample cleanup as the semi-permeable membrane excludes proteins and other large molecules. Methods such as tissue homogenization, require the sacrifice of multiple animals at different time points in order to complete the study. The homogenates are comprised of both intracellular and extracellular components, proteins, and other large molecules. The total analyte concentration, not the non-protein bound active portion of the analyte, is measured. Another advantage of microdialysis is its ability to exchange fluid with the tissue or organ being sampled. This advantage is particularly important when performing PK studies, given that blood sampling can disturb the distribution and metabolism of drugs, thereby leading to biased results [41]. Microdialysis allows for the collection of a representative sample of all substances in the ECF, providing these substances will

diffuse through the semi-permeable membrane. This characteristic is advantageous compared to fast scan cyclic voltammetry, which only allows for the measurement of electroactive analytes, albeit at much improved temporal resolution. Additionally, fouling of the electrode is an issue [42].

The limitations of microdialysis include the size limitation of the analyte(s) sampled. Microdialysis is a technique primarily for sampling small molecule compounds. Also, the implantation of the microdialysis probes is invasive. This can lead to tissue trauma and gliosis, the formation of a coating of glial cells onto the probe membrane, possibly blocking the membrane function [29]. In the brain, the implantation of the probe impairs important regulatory processes, such as glucose metabolism, blood flow, and neurotransmitter release [43]. Depending upon the parameters to be measured, the time between microdialysis probe implantation and the start of sample collection can be very large since different biological systems need different lengths of time to recover from the probe implantation.

1.5.5. Applications

While this work primarily focuses on microdialysis sampling of the brain, microdialysis can also be used in a variety of organs and tissues. Herrera *et al.* displayed the use of microdialysis for the determination of protein binding [44]. A variety of drugs with known percent binding values to human serum protein ranging from 10% – 98% were studied. Microdialysis was also compared to ultrafiltration, another sampling technique. It was concluded that microdialysis was the preferred

16

technique to monitor protein binding of drugs due to the lesser extent of non-specific adsorption to the membrane and no prior sample cleanup step needed.

For *in vivo* work, microdialysis has been employed to study drug transporters in the central nervous system and also to investigate the BBB permeability of drugs [45, 46]. Microdialysis has recently been shown by Parrot *et al.* to reveal information regarding the neurotransmitter changes in awake epileptic rats [47]. Other sites of interest for microdialysis sampling include the skin to monitor drug penetration [48], the muscle to study the penetration of antimicrobial drugs for surgical procedures [49], and the bone to study the antimicrobial effects of gentamicin in cortical bone as an alternative to bone biopsies [50]. Rooyackers *et al.* demonstrated, by implanting probes into the brain, liver, and intestine simultaneously, that microdialysis sampling is beneficial in measuring human metabolism [51].

Another important use for microdialysis is in PK. For the successful development of new and efficacious drug therapies, a thorough characterization of the drug is necessary to gain a working knowledge of its actions within the body. This characterization includes identifying interactions with specific molecular targets and defining the PK and PD properties [52]. PD classification will be further discussed in Section 2.1.4. PK characterization involves gaining a quantitative understanding of the absorption, distribution, metabolism, and elimination (ADME) of drug entities [53]. PK is classically defined as the study of monitoring the concentration of the drug entity over the time course of the experiment [54].

Microdialysis sampling is a well established technique which can be used for the process of monitoring the PK of different drugs in many different sites in the body [55-58]. The use of microdialysis for PK studies has been reviewed extensively by Davies in 1999 and Elmquist and Sawchuk in 1997 [20, 59]. Among the important discussions of microdialysis is that PK measurements can more accurately determine the ADME parameters, especially metabolism, since the probe can be inserted directly into the tissue or organ or interest and the drug can be delivered directly through the probe. It is advantageous to use microdialysis to monitor a drug's PK in the blood since it doesn't remove any fluid from the animal and alter the total fluid volume [32, 41]. Also, microdialysis samples only contain the collected metabolites, which are devoid of proteins and the enzymes that degrade the metabolites [20]. Microdialysis was found recently by Rambeeck *et al.* to be useful in monitoring the effectiveness of new AED's in patients with intractable epilepsy [60].

Using microdialysis *in vivo* can be quite useful, but the technique is limited to the analytical methodologies available for the analysis of the collected samples. Since perfusion rates are kept relatively low in order to increase the relative recovery as much as possible, the sample size collected is quite small, on the order of 1-5 μL. These small samples, typically analyzed offline, contain a dilute solution of the analytes of interest and these factors present a difficult challenge to the analytical chemist in terms of the simultaneous detection and quantification of the low amounts of analytes recovered [27]. Davies *et al.* reviewed several analytical considerations for the analyses of microdialysis samples [30]. Yang *et al.* [28] and Ruiz-Jiménez *et*

al. [61] demonstrated that the analyses of microdialysis samples can be simplified and analyzed online using liquid chromatography (LC) and capillary electrophoresis (CE), respectively. This technique allows for a significant enhancement in the achievable temporal resolution allowing more information to be derived during the experiment.

1.6. Separations

One of the most important pieces of knowledge at the disposal of the analytical chemist is that of separation science. When a set of biological samples contains numerous analytes, the contents of those samples must be elucidated as efficiently and reproducibly as possible. The ability to perform a separation on a sample is the first step in unlocking the sample information. The second step is accurately determining the analytes within the sample. The marriage of a separation technique to a powerful detection scheme can allow the accurate identification of the contents of the presented sample.

A rugged and robust analytical separation technique is liquid chromatography (LC) [62] (see Section 1.6.1.). LC was developed primarily for the analysis of hydrophobic, non-volatile analytes [63]. The basis of an LC separation is the interaction of the analyte between the mobile phase (liquid) and stationary phase (solid).

Another popular separation technique is capillary electrophoresis (CE) (see Section 1.6.2.). CE, developed for the analysis of charged analytes, is based upon the movement of ions through a capillary by an electric field [63]. Each separation

technique serves individual applications and can be used in combination to provide additional information regarding the problem at hand. CE has the advantage of small sample volumes (0.25 – 1 μL) and high resolution (several million theoretical plates). LC, on the other hand, typically requires larger sample volumes and provides inferior resolution (on the order of 10^5 theoretical plates per column). However, LC is more effective in separating polar compounds. Therefore, in summary, it is important to carefully weigh these considerations in choosing the appropriate separation technique.

1.6.1. Liquid Chromatography

1.6.1.1. Theory

LC is a separation technique that has been used extensively since the 1970's [62]. Figure 1.3 depicts a schematic of a basic LC analytical instrument. The mobile phase reservoirs usually hold 0.5 – 2 liters of solution. The mobile phase should be filtered before use to remove any large particulate matter which could block the remainder of the LC system. A degassing apparatus should also be used in conjunction with the mobile phase reservoir. It is important to remove as much oxygen and other environmental influences as possible as these could cause sample degradation or interferences within the LC system. The pump should handle the pumping of mobile phase at pressures up to 6000 psi. The injector introduces analytes into the system. The analytes are introduced into a flowing stream of mobile phase and carried onto the column. The column, with diameters ranging from 1 – 4.6 mm and lengths ranging from 50 – 250 mm, contains the stationary phase appropriate

for the types of analytes to be separated and will be discussed further in Section 1.6.1.2. The column effluent is passed onto the detector, which monitors the physical and/or chemical properties of the analytes. Different modes of detection are discussed in Section 1.6.1.3. Data are acquired analyzed via a computer attached to receive the detector output. It is common for the entire LC system to be fully automated and operated by the same computer which collects the data [62].

During an isocratic separation, a constant solvent composition is used throughout the elution time of the analytes(s) of interest. A typical instrumental setup for this type of separation is shown in Figure 1.3 [63]. If the analysis time for an isocratic separation is very long or if large amounts of time exist between the early eluting analytes and the late eluting analytes, a second pump can be employed to perform a *gradient* separation [63]. Late eluting peaks in an isocratic separation suffer from the extended interaction with the stationary phase and retention in the column. This results in a very long analysis time and slow experimental throughput. A gradient separation can greatly decrease the analysis time and also help separate a mixture containing a very large number, or different types, of analytes [62].

The analyte retention on the column can be calculated by Equation 1.3:

$$k' = (t_1 - t_0) / (t_0) \qquad (1.3)$$
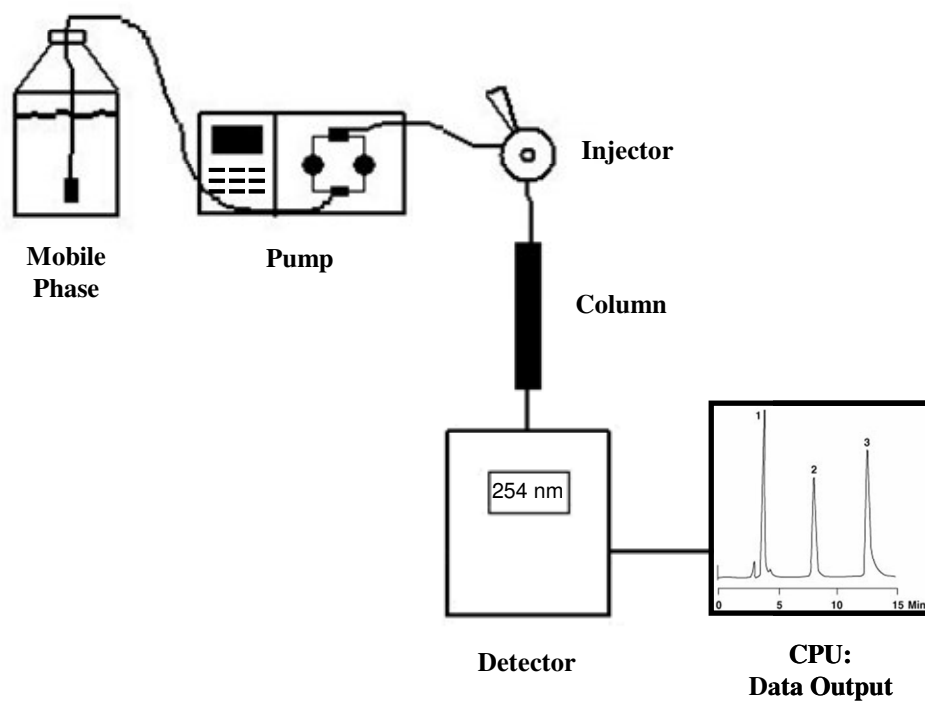
Figure 1.3. Schematic of a typical LC system
used for an isocratic separation.

Mobile
Phase

Pump

Injector

Column

254 nm

Detector

CPU:
Data Output
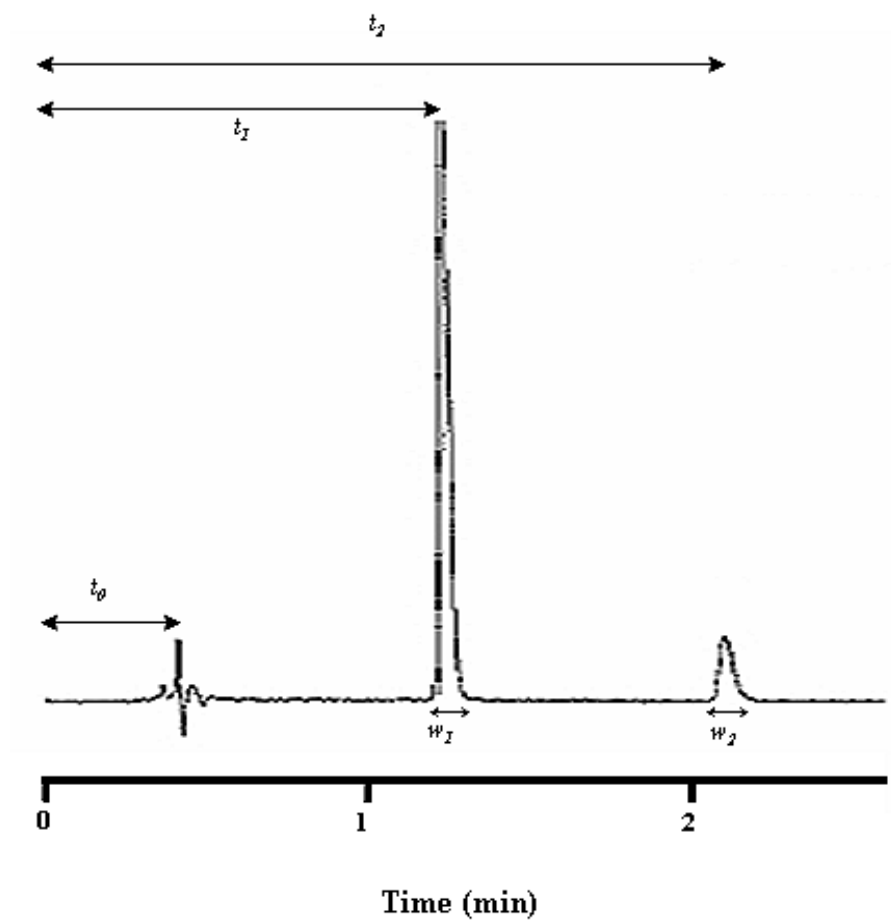
Figure 1.4. A typical LC chromatogram showing the separation of 2 analytes.

where k' represents the capacity factor, t_1 is the elution time for Analyte 1 in the schematic, and t_0 is the elution time for the void, or dead volume. This relationship is shown schematically in Figure 1.4.

The resolution between any two analytes can be calculated as shown in Equation 1.4.

$$R_s = 2(t_2 - t_1) / (w_2 + w_1) \qquad (1.4)$$

R_s is the resolution value, t_2 is the elution time for Analyte 2, t_1 is the elution time for Analyte 1, and w_2 and w_1 are the peak widths at the base for Analytes 2 and 1, respectively.

The ability of the stationary phase to effectively separate two analytes is given by the selectivity (α):

$$\alpha = k'_2 / k'_1 \qquad (1.5)$$

Equation 1.5 shows selectivity to be the ratio of the capacity factor for Analyte 2 (k'_2) to Analyte 1 (k'_1).

The efficiency (N) is a kinetic measurement of how easily an analyte moves through the column and its interaction with the stationary and mobile phases [64].

$$N = 16(t_2 / w)^2 = 5.54(t_2 / w_{0.5})^2 \qquad (1.6)$$

Efficiency is calculated from Equation 1.6 using the elution time for Analyte 2 from Figure 1.4 and either the width at the base of the peak (w) or the peak width at half-height ($w_{0.5}$).

Equation 1.6 can be used also when calculating the height equivalent to a

$$H = L / N \qquad\qquad (1.7)$$

theoretical plate (H).   Equation 1.7 shows that total plate height, H, is calculated by dividing the column length (L) by the efficiency (N). This quantity is related to the van Deemter equation (Equation 1.8), which correlates the individual components of band broadening that make up the total plate height.

$$H = A + B/u + Cu \qquad\qquad (1.8)$$

A represents the analyte dispersion due to multiple flow paths through the stationary phase and mobile phase effects (eddy diffusion), B represents the axial or longitudinal diffusion of the analyte, C represents the dispersion due to the kinetics of the mobile phase within the stationary phase, and u represents the linear flow velocity [64].

Ultra-performance LC (UPLC), which employs particle sizes for the stationary phases that are < 2 μm [65], offers dramatically reduced separation times compared to conventional LC. A separation of eight diuretics using a typical LC setup (2.1 x 100 mm, 5 μm particle size C_{18} column) was achieved with adequate

resolution in just over 10 minutes. When the same separation was performed using UPLC settings (2.1 x 30 mm, 1.7 μm particle size C_{18} column), the result had identical resolution to the previous separation, but was achieved in 1.6 minutes. Similar results for decreases in analysis times and increases in peak efficiencies have been reported for UPLC separations conducted by both Nguyen *et al.* [66] and Olsen *et al.* [67].

1.6.1.2. Modes of Separation

There are two main types of LC separation modes: reversed-phase (RP) and normal-phase (NP). They are each based on the interaction of the analyte with the stationary phase. The choice of which mode to employ should be decided upon by considering the analytes of interest and which stationary phase and mobile phase would be the most efficient for their separation.

RP-LC is the most widely employed mode of separation encompassing approximately 90% of all low molecular weight sample analyses [62, 68]. RP-LC uses a hydrophobic stationary phase and a polar mobile phase, in some cases even 100% aqueous. The dominant molecular interactions in RP-LC are dispersive forces, including hydrophobic and van der Waals interactions [62]. The stationary phases employed in RP-LC are primarily silica based; octyl (C8) and octyldecyl (C18) are the most common ligands [64]. Typical particle sizes that are used in RP-LC packing materials are between 2 – 5 μm. Chemically modified porous silica can be used as well to increase the surface area of the stationary phase thereby retaining analytes for

longer periods of time [62]. For very hydrophobic analytes, an organic modifier may be added to the mobile phase that will lessen the interaction between the analytes and the stationary phase, allowing the analytes to elute faster. For analytes that are small and cationic, the hydrophilicity is such that the analytes may elute with the dead volume and become "lost." A way to increase the retention of these analytes is by adding an ion-pairing agent. The addition of an acid such as 1-octanesulfonic acid (SOS) decreases the charge on the solute, thereby causing the interaction between the analyte and stationary phase to increase, thus retaining the analyte in the column for a longer period of time [69].

NP-LC, in contrast to RP-LC, uses a polar stationary phase and a non-polar solvent as the mobile phase to separate relatively non-polar analytes [62]. The molecular interactions employed in NP-LC are polar forces such as hydrogen bonding. The common stationary phases in NP-LC are typically silica gels or alumina that are modified with dense populations of hydroxyl groups to increase their polarity [62].

1.6.1.3. Detection Strategies

By far, the most common detection strategy for LC is ultraviolet/visible (UV/Vis) absorbance [62]. The UV/Vis detector is used for the detection of analytes containing a chromophore moiety and may be fixed wavelength, variable wavelength, or diode array format. Each type possesses its own advantages in the detection of analytes. The fixed wavelength detector is used primarily as a sensitive detection

scheme with a wide linear range. The variable wavelength and diode array formats can be advantageous when performing method development where the maximum wavelength of absorption of the analyte or metabolite is either not known or is moving based on changing LC conditions [62].

Fluorescence detection is used for analytes containing a fluorophore which absorbs radiation at one wavelength and then emits it a longer wavelength [62]. This detection scheme is highly selective due to the fact that most organic molecules absorb UV/Vis light, but not all will fluoresce. Fluorescence detection is generally more sensitive than UV/Vis absorbance detection, with approximately 3 orders of magnitude more sensitivity [70]. A limitation of this detection strategy is possible fluorescence quenching by the use of improper mobile phase constituents (e.g. highly polar solvents or halide ions) [70].

Electrochemical (EC) detection can be useful for analytes that are ionic or are easily oxidized or reduced [62]. EC detectors are highly sensitive, useful for the trace analysis of biological samples, and typically have nanomolar detection limits [70]. Typical electrode materials range from glassy carbon, carbon paste, gold, gold/mercury amalgams, copper, and platinum [71]. This detection scheme can be quite selective as well due to different electroactive species differing in their optimum oxidation/reduction potentials. A limitation of EC detection is that the electrodes are easily fouled by the contents in the column effluent resulting in decreased performance over time.

Mass spectrometry is a detection strategy of interest, especially in the pharmaceutical industry [62]. This is a highly universal and selective detector for use with LC [64]. Mass spectrometry ultimately allows the analyst to gain important information regarding the molecular weight and structure for individual peaks from the chromatogram. A limitation of mass spectrometry is the high cost of the instrumentation.

1.6.2. Capillary Electrophoresis

1.6.2.1. Theory

CE and the theory behind it was introduced by Jorgenson and Lukacs in 1981 [72]. The researchers used a 75 µm inner diameter (i.d.) x 100 cm capillary to separate amino acids, peptides, and urinary amines at 30 kV. CE is complementary to LC in that the separation is based primarily on size and charge [73]. Advantages of CE over LC are the small volumes needed for both the samples and reagents. This allows the use of alternative chemicals or solvents to help separate the analytes of interest since the cost would be much less [73].

A typical CE setup is shown in Figure 1.5. The high voltage power supply applies voltages ranging from 0 – 30 kV for the separation. The Plexiglas box protects the analyst from harm by enclosing the live voltage. The capillary employed is generally fused silica, with an i.d. of 25 – 100 µm and a length of 20 – 100 cm. The inlet of the capillary is placed in a buffer reservoir located inside the Plexiglas box. The outlet of the capillary is placed into another buffer reservoir that contains an

Capillary

Detector

(Cathode)

30 kV

**High Voltage
Power Supply**

**Plexiglas
Box
(Anode)**

**Buffer
Reservoirs**
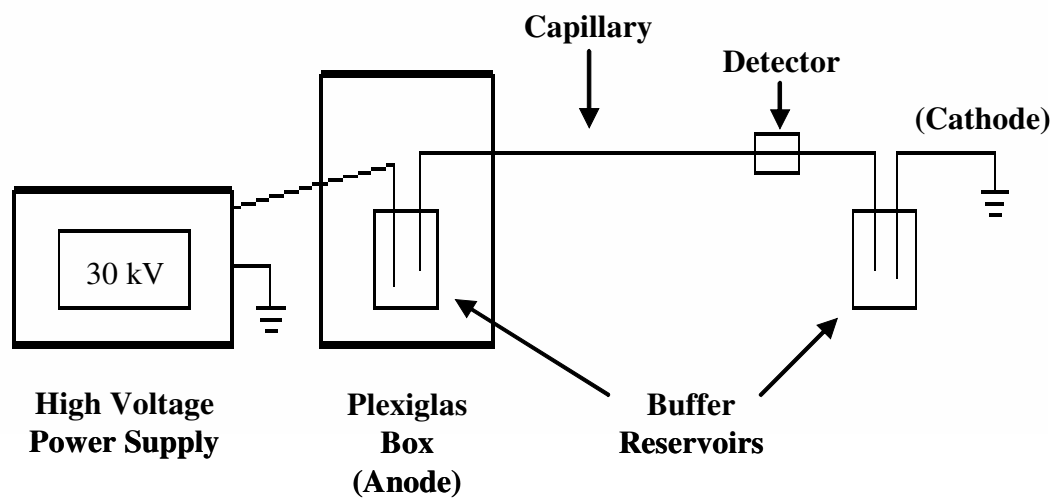
Figure 1.5. Schematic of a typical CE instrument.
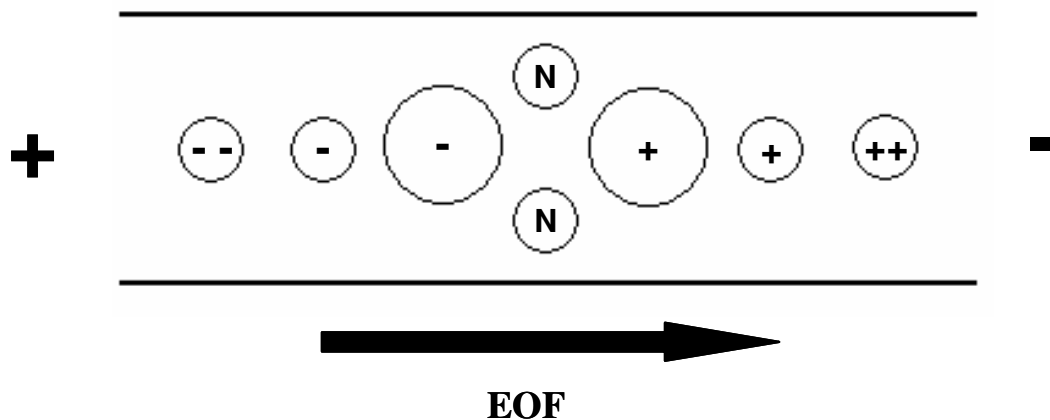
Figure 1.6. Schematic displaying the electrophoretic separation of analytes from the inside of the capillary. The analytes were injected at the anode (+) end of the capillary. The migration order under the conditions shown are as follows: 1st – small, multiply charged cations; 2nd – small, singly charged cations; 3rd – large, singly charged cations; 4th – neutrals; 5th – large, singly charged anions; 6th – small, singly charged anions; 7th – small, doubly charged anions.

electrode to ground the high voltage. Under normal polarity, the inlet of the capillary acts as the anode (+) and the outlet of the capillary acts as the cathode (-). The schematic shown in Figure 1.6 displays the migration order of analytes under normal polarity. The polarity can be reversed in order to change the migration order of the analytes. On-capillary detection can be achieved by removing a small portion of the polyimide coating from the capillary, thereby making a transparent window through which the analyte can be optically detected. A commercial UV detector can be attached to the capillary at this location for analyte detection [73, 74].

As mentioned previously, the separation of analytes in CE is based on the size and charge of the analyte as well as the electric field assisting in the analyte migration. The separation is also based on several forces acting on the analytes. The migration, or electrophoretic mobility, of the analyte is acted upon by two forces, the electrostatic force, F_e (Equation 1.9) and the frictional force, F_f (Equation 1.10) [73, 74].

$$F_e = qE \qquad\qquad (1.9)$$

$$F_f = 6\pi\eta R(\mu_{app}E) \qquad\qquad (1.10)$$

In Equation 1.9, the F_e is the force which pulls an ion toward the electrode of opposing charge and is proportional to the charge on the analyte (q) and the electric field (E). The F_f is the opposing force to the F_e and is proportional to the radius of

the ion (R), the velocity of the ion ($\mu_{app}E$) where μ_{app} is the apparent mobility of the ion, and the viscosity of the run buffer (η). If these two forces are set equal to each

$$\mu_{app} = q / 6\pi\eta R \qquad (1.11)$$

other, as shown, then the electrophoretic mobility of the analyte is a property of both the size and charge [74].

The separation of analytes in CE is also based on the electroosmotic flow (EOF). EOF is a term to describe the bulk flow of solution within the capillary [73]. The inner walls of the fused silica capillary impart a layer of negative charge giving way to SiO⁻ functionalities. These ionized silanol groups attract cations from the buffer and create an electrical double layer appositional to the surface of the fused silica as depicted in Figure 1.7. This electrical double layer is called the Inner Helmholtz layer, or Stern layer. This layer is essentially static and has a thickness of approximately 0.1 nm [74]. A diffuse region formed from hydrated cations in the buffer, termed the Outer Helmholtz layer, is more centrally located in the capillary. When an electric field is applied, this diffuse layer will have "bulk" movement toward the detector. Therefore, the apparent mobility of an analyte is shown in Equation 1.12 and is actually the combination of the electrophoretic

$$\mu_{app} = \mu_{ep} + \mu_{eo} \qquad (1.12)$$
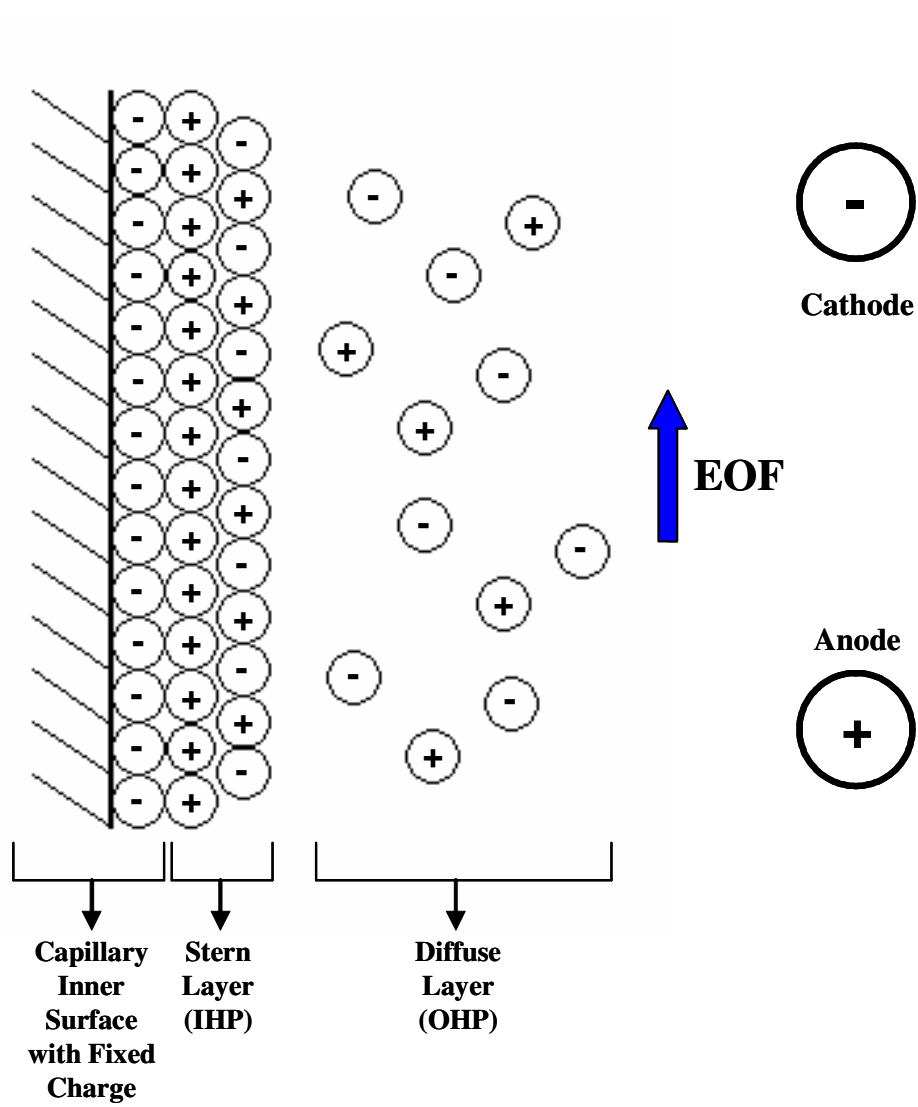
Figure 1.7. Schematic of EOF during normal polarity.

mobility (μ_{ep}) and the electroosmotic mobility (μ_{eo}). The magnitude of the EOF (v_{eo}) is shown in Equation 1.13. It is based on the zeta potential (ζ) of the electrical

$$v_{eo} = \varepsilon \zeta E / \eta \qquad (1.13)$$

double layer, which is determined by the concentration, or ionic strength, of the buffer [74]. It is also proportional to the dielectric constant of the buffer (ε), the electric field (E), and inversely proportional to the viscosity of the buffer (η). The EOF can be changed as a function of pH; hence, the amount of ionization on the fused silica walls change as a function of pH, or with the addition of organic surfactants [73, 75]. When a cationic surfactant, such as tetradecyltrimethylammonium bromide (TTAB), is added to the buffer at a concentration below its critical micelle concentration (CMC), it forms an electrostatic interaction with the silanol groups on the fused silica and reverses the charge inside the capillary as shown in Figure 1.8. The migration order of the analytes change due to the reversal of charge on the capillary wall. The outlet of the capillary now acts as the anode and the inlet the cathode, and the separation potential is reversed.

If the concentration of the surfactant added is above the CMC, micelles are formed. This mode of CE, termed micellar electrokinetic chromatography (MEKC), was first introduced by Terabe *et al.* in 1984 [76]. Micelles are aggregates of surfactant molecules in which the hydrophilic charged "head" portions of the surfactant molecules are pointed outward into solution and the hydrophobic, non-
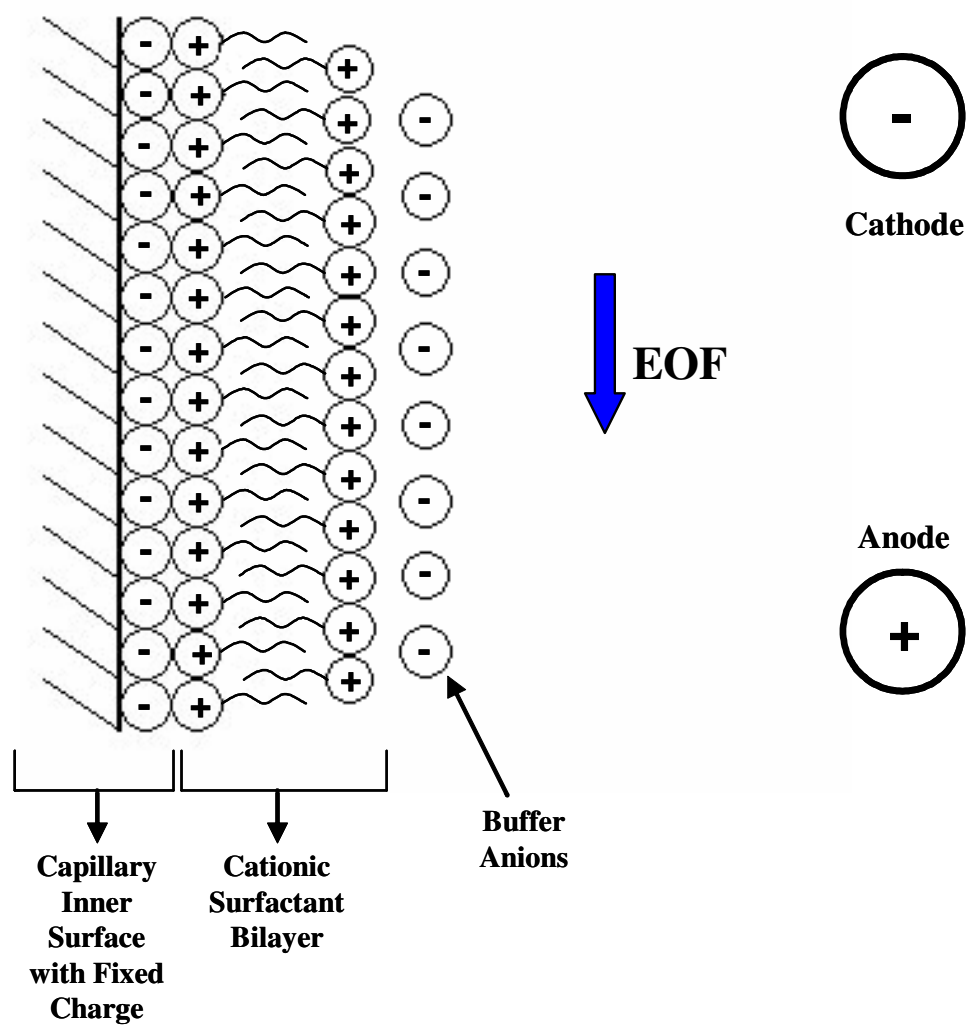
Figure 1.8. Schematic of EOF during reverse polarity.
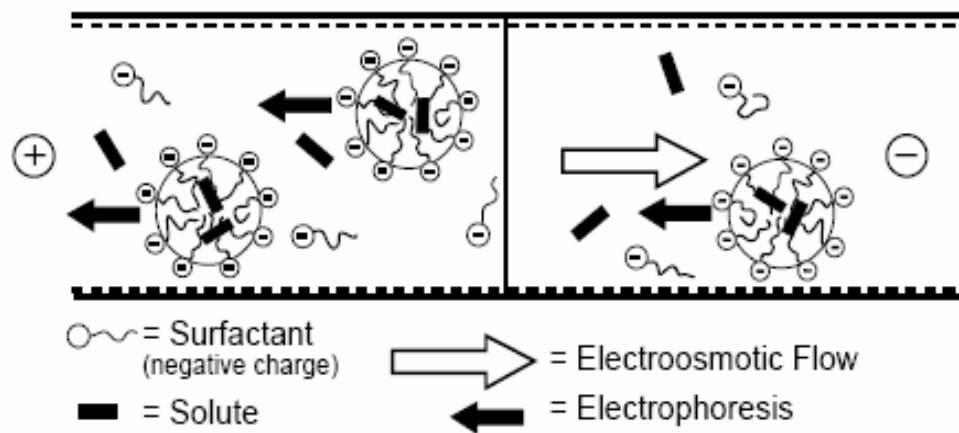
Figure 1.9. Schematic of electrophoresis under MEKC conditions [82].

polar "tail" portions are pointed inward away from the solution (Figure 1.9). MEKC was developed to solve the problem of separating the band of neutral analytes since this band cannot be separated in regular CE mode. By adding the micelles to the run buffer, a pseudostationary phase forms, allowing for the separation of both neutral and ionic analytes [75]. In MEKC, the neutral analytes distribute between the aqueous phase and the micellar phase, mainly based on the hydrophobic nature of the analyte. Even the ionic analytes can possess electrostatic interactions with the charged micellar phase affecting the electrophoretic mobility through the capillary.

The efficiency of the separation in CE is generally much better than LC [73]. Typical efficiency values for LC separations range from 5000 – 10000 plates [63] while multimillion-plate efficiency has been reported using anion stacking in CE [77]. This high level of efficiency arises primarily from the flow profile for the injected sample. In CE, the flow profile is a "plug" as opposed to laminar flow obtained in LC (Figure 1.10). This profile occurs due to the absence of a stationary phase packed within the capillary. If the van Deemter equation (Equation 1.8) is applied for a CE separation, the A and Cu terms are neglible. Equation 1.14 refers to the efficiencies (N) obtainable for a CE separation.

$$N = \mu_{ep} V L_d / 2 D L_t \qquad (1.14)$$

N is proportional to μ_{ep}, the applied voltage (V), and the length to the detector on the capillary (L_d). It is inversely proportional to the total length of the capillary (L_t) and

(A)

Flow

(B)
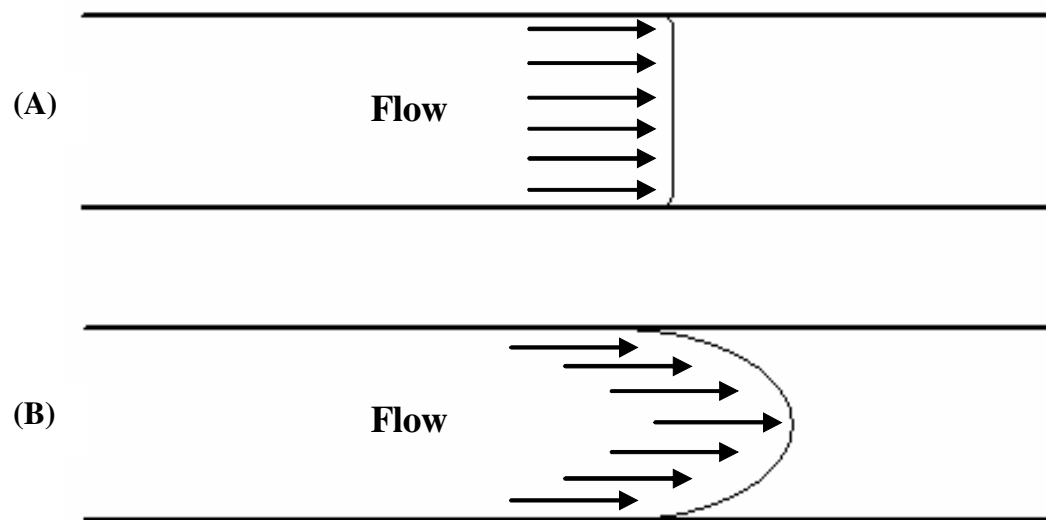
Flow

Figure 1.10. Flow patterns associated with CE and LC. (A) "Plug" flow as obtained in CE separation. (B) Laminar flow as obtained in LC separation.

the diffusion coefficient (D) of the analyte. It would appear from this equation that the efficiency increases just by increasing the separation voltage. However, the effect of Joule heating must be considered [74]. Joule heating occurs as a function of the square of the applied voltage (V) and the conductivity of the buffer (K), and inversely occurs as the square of the length of the capillary (Equation 1.15).

$$\Delta H = KV^2 / L_t^2 \qquad (1.15)$$

Joule heating is greatly reduced by using a capillary of smaller i.d. as this will provide a greater surface-to-volume ratio which allows the dissipation of generated heat.

The conventional CE setup is slowly being replaced by microchip CE. In the microchip CE format, substrates such as glass or fused silica are used which allow for the high voltages to be supplied for the separations [74]. Small channels for the flow of buffer are fabricated into the substrates with widths of 20 – 100 μm and depths of 5 – 20 μm [74]. Various designs are available for fabrication to assure the most efficient separation possible. The main advantage of the microchip format is the reduction in analysis times from minutes to seconds. Sandlin *et al.* recently described the use of a microchip CE device coupled directly to microdialysis for the analysis of glutamate and aspartate from the brain of a rat [78]. The ultimate goals of these microchip CE devices are mass production, relatively cheap cost, and ease of disposability. The present limitation to the use of microchip CE is the expensive cost of the detection schemes.

1.6.2.2. Detection Strategies

The detection schemes used in CE are either on-capillary schemes or off-capillary schemes. The most commonly employed on-capillary approach is UV absorbance detection [64]. Since detection is performed on-capillary, the i.d. of the capillary forms the light path. Beer's law states that the concentration is directly dependent upon the length of the light path [63]. This leads to a signal reduction in CE-UV as compared to LC-UV, which has a longer path length. Different approaches may be taken to enhance the UV detector performance. A "bubble cell" widens the capillary at the window and "z-flow cells" connect the separation capillary to a separate detection capillary. Both approaches increase the sensitivity approximately three and 50 times, respectively; however, resolution is compromised in both approaches [79, 80].

Another type of on-capillary detection for CE is fluorescence or laser-induced fluorescence (LIF) detection. This type of detection scheme offers very high selectivity over UV absorbance detection, as well as up to a 1000-fold decrease in the detection limits [81]. The drawback of LIF detection is that a high number of analytes do not possess native fluorescence. Therefore, a derivatization step is required which can complicate the analysis and cause dilution of the analytes.

Off-capillary approaches are gaining popularity in CE. One of the most popular off-capillary strategies is EC detection. EC detection is inexpensive and sensitive compared to the previously mentioned detection schemes. EC detection is based on the electrochemical oxidation or reduction of the analyte that occurs on the

surface of the electrode; therefore, the limits of detection (LODs) are not compromised as with the on-capillary methods [82]. With CE, the electrode alignment can either be end-capillary or in-capillary. When end-capillary detection is employed, an electrode with a surface area larger than the i.d. of the capillary is aligned with the outlet of the capillary and the migrating analytes are detected electrochemically. With the use of in-capillary detection, a decoupling system must be employed in order to separate the current due to the separation voltage from the current associated with the electrode [73]. Additionally, EC lends itself to miniaturization for use in microchip CE. Xu *et al.* has recently reviewed the use of EC detection for microchip CE systems [83]. This approach offers significant advantages in temporal resolution when coupled to microdialysis sampling for the analysis of neurotransmitters versus conventional CE [78].

1.7. Overview of Research

This dissertation investigates some of the neurochemical mechanisms that underlie a novel chemically-induced seizure model for the study of epilepsy. Microdialysis sampling from the brain of a rat model is coupled with electrophysiological recording and this combination acts as the basis of the developed seizure model. The microdialysis samples are analyzed using the techniques and theory discussed in this chapter.

Chapter two discusses the development of a chemically-induced seizure model using the convulsant, 3-mercaptopropionic acid. Different dosing strategies

were employed to determine the PK of this convulsant and also to investigate maintaining a steady-state of the convulsant within the brain. The PK data obtained from the rat was compared with the electrical activity from the brain, thereby giving PK-PD correlations [84].

Chapter three discusses the neurochemical changes that were observed using the chemical seizure model. The analytes of interest were the amino acid neurotransmitters and the biogenic amine neurotransmitters. These compounds were analyzed using LC coupled with both fluorescence and EC detection schemes.

Chapter four discusses the development of CE methodology in order to increase the temporal resolution of neurotransmitter collection during the chemical seizure model. Increased temporal resolution will help to decipher the results obtained from Chapter 3 when a longer sampling time was employed. In this chapter, CE is coupled to both LIF and UV detection schemes to further enhance the understanding of the results obtained with LC (discussed in Chapter 3).

Chapter five discusses the development of a newly designed dual-electrode detector for CE. The design was implemented in order to gain sensitivity for the analysis of a variety of analytes. An evaluation of this detection scheme is discussed with emphasis on redox cycling.

1.8. References

[1]. Stafstrom, C.E., *Epilepsy: a review of selected clinical syndromes and advances in basic science.* J. Cereb. Blood Flow Metab., **2006**, 26: 983-1004.

[2]. **http://www.who.int/mediacentre/factsheets/fs165/en/** (**Accessed January 2007**).

[3]. McNamara, J.O., Huang, Y.Z., and Leorard, A.S., *Molecular signaling mechanisms underlying epileptogenesis.* Sci. STKE, **2006**, 2006: 1-22.

[4]. Arroyo, S., Brodie, M.J., Avanzini, G., Baumgartner, C., Chiron, C., Dulac, O., French, J.A., and Serratosa, J.M., *Is refractory epilepsy preventable?* Epilepsia, **2002**, 43: 437-444.

[5]. Huffman, J. and Kossoff, E.H., *State of the ketogenic diet(s) in epilepsy.* Curr. Neurol. Neurosci. Rep., **2006**, 6: 332-340.

[6]. Bough, K.J. and Stafstrom, C.E., *The ketogenic diet: scientific principles underlying its use.* Neurol. Dis. Ther., **2004**, 64(Epilepsy): 263-284.

[7]. Kossoff, E.H., McGrogan, J.R., Bluml, R.M., Pillas, D.J., Rubenstein, J.E., and Vining, E.P., *A modified Atkins diet is effective for the treatment of intractable pediatric epilepsy.* Epilepsia, **2006**, 47: 421-424.

[8]. Albensi, B.C., *A comparison of drug treatment versus electrical stimulation for suppressing seizure activity.* Drug News Perspect., **2003**, 16: 347-352.

[9]. Hodaie, M., Wennberg, R.A., Dostrovsky, J.O., and Lozano, A.M., *Chronic anterior thalamus stimulation for intractable epilepsy.* Epilepsia, **2002**, 43: 603-608.

[10]. Osorio, I., Frei, M.G., Sunderam, S., Giftakis, J., Bhavaraju, N.C., Schaffner, S.F., and Wilkinson, S.B., *Automated seizure abatement in humans using electrical stimulation.* Ann. Neurol., **2005**, 57: 258-268.

[11]. Fisher, R.S., *Animal models of the epilepsies.* Brain Res. Rev., **1989**, 14: 245-278.

[12]. Netopilova, M. and Drsata, J., *3-mercaptopropionic acid, a useful tool in experimental epilepsy studies.* Folia Pharm. Univ. Carol., **1995**, 19: 63-78.

[13]. Goddard, G.V., *Development of epileptic seizures through brain stimulation at low intensity.* Nature, **1967**, 214: 1020-1021.

[14]. Morimoto, K., Fahnestock, M., and Racine, R.J., *Kindling and status epilepticus models of epilepsy: rewiring the brain.* Prog. Neurobiol., **2004**, 73: 1-60.

[15]. Mody, I., *The molecular basis of kindling.* Brain Pathol., **1993**, 3: 395-403.

[16]. Cole, A.J., Koh, S., and Zheng, Y., *Are seizures harmful: what can we learn from animal models?* Prog. Brain Res., **2002**, 135: 13-23.

[17]. Netopilova, M., Haugvicova, R., Kubova, H., Drsata, J., and Mares, P., *Influence of convulsants on rat brain activities of alanine aminotransferase and aspartate aminotransferase.* Neurochem. Res., **2001**, 26: 1285-1291.

[18]. De Deyn, P.P., D'Hooge, R., Marescau, B., and Pei, Y.-Q., *Chemical models of epilepsy with some reference to their applicability in the development of anticonvulsants.* Epilepsy Res., **1992**, 12: 87-110.

[19]. Keene, D.L., Whiting, S., and Ventueyra, E.C.G., *Electrocorticography.* Epileptic Disord., **2000**, 2: 57-63.

[20]. Davies, M.I., *A review of microdialysis sampling for pharmacokinetic applications.* Anal. Chim. Acta, **1999**, 379: 227-249.

[21]. Bito, L., Davson, H., Levin, E., Murray, M., and Snider, N., *The concentrations of free amino acids and other electrolytes in cerebraospinal fluid, in vivo dialysate of brain, and blood plasma of the dog.* J. Neurochem., **1966**, 13: 1057-1067.

[22]. Delgado, J.M.R., DeFeudis, F.V., Roth, R.H., Ryugo, D.K., and Mitruka, B.M., *Dialytrode for long term intracerebral perfusion in awake monkeys.* Arch. Int. Pharmacodyn., **1972**, 198: 9-21.

[23]. Ungerstedt, U. and Pycock, C., *Functional correlates of dopamine neurotransmission.* Bull. Schweiz. Akad. Med. Wiss., **1974**, 30: 44-55.

[24]. Hocht, C., Opezzo, J.A.W., Bramuglia, G.F., and Taira, C.A., *Application of microdialysis for pharmacokinetic-pharmacodynamic modelling.* Expert Opin. Drug Discov., **2006**, 1: 289-301.

[25]. Ungerstedt, U. and Rostami, E., *Microdialysis in Neurointensive Care.* Curr. Pharm. Des., **2004**, 10: 2145-2152.

[26]. Kostrzewa, R.M., Nowak, P., Kostrzewa, J.P., Kostrzewa, R.A., and Brus, R., *Peculiarities of L-dopa treatment of Parkinson's disease.* Amino Acids, **2005**, 28: 157-164.

[27]. Chaurasia, C.S., *In vivo microdialysis sampling: theory and applications.* Biomed. Chromatogr., **1999**, 13: 317-332.

[28]. Yang, C.-S., Tsai, P.-J., Chen, W.-Y., Tsai, W.-J., and Kuo, J.-S., *On-line derivatization for continuous and automatic monitoring of brain extracellular glutamate levels in anesthetized rats: a microdialysis study.* J. Chromatogr. B, **1999**, 734: 1-6.

[29]. Plock, N. and Kloft, C., *Microdialysis - theoretical background and recent implementation in applied life-sciences.* Eur. J. Pharm. Sci., **2005**, 25: 1-24.

[30]. Davies, M.I., Cooper, J.D., Desmond, S.S., Lunte, C.E., and Lunte, S.M., *Analytical considerations for microdialysis sampling.* Adv. Drug Deliv. Rev., **2000**, 45: 169-188.

[31]. **http://www.microdialysis.com/, (Accessed February 2007)**.

[32]. Telting-Diaz, M., Scott, D.O., and Lunte, C.E., *Intravenous microdialysis sampling in awake, freely-moving rats.* Anal. Chem., **1992**, 64: 806-810.

[33]. Wages, S.A., Church, W.H., and Justice Jr., J.B., *Sampling considerations for on-line microbore liquid chromatography of brain dialysate.* Anal. Chem., **1986**, 58: 1849-1856.

[34]. Moghaddam, B. and Bunney, B.S., *Ionic composition of microdialysis perfusing solution alters the pharmacological responsiveness and basal outflow of striatal dopamine.* J. Neurochem., **1989**, 53: 652-654.

[35]. Hsiao, J.K., Ball, B.A., Morrison, P.F., Mefford, I.N., and Bungay, P.M., *Effects of different semipermeable membranes on in vitro and in vivo performance of microdialysis probes.* J. Neurochem., **1990**, 54: 1449-1452.

[36]. Lonnroth, P., Jansson, P.-A., and Smith, U., *A microdialysis method allowing characterization of intercellular water space in humans.* Am. J. Physiol., **1987**, 16(Endocrinol. Metab.): E228-E231.

[37]. Stahle, L., Arner, P., and Ungerstedt, U., *Drug distribution studies with microdialysis III: extracellular concentration of caffeine in adipose tissue in man.* Life Sci., **1991**, 49: 1853-1858.

[38]. Song, Y. and Lunte, C.E., *Comparison of calibration by delivery versus no net flux for quantitative in vivo microdialysis sampling.* Anal. Chim. Acta, **1999**, 379: 251-262.

[39]. Larsson, C.I., *The use of an "internal standard" for control of the recovery in microdialysis.* Life Sci., **1991**, 49: PL73-PL78.

[40]. Jacobson, I., Sandberg, M., and Hamberger, A., *Mass transfer in brain dialysis devices - a new method for the estimation of extracellular amino acids concentration.* J. Neurosci. Methods, **1985**, 15: 263-268.

[41]. Hocht, C., Opezzo, J.A.W., and Taira, C.A., *Validation of a new intraarterial microdialysis shunt probe for the estimation of pharmacokinetic parameters.* J. Pharm. Biomed. Anal., **2003**, 31: 1109-1117.

[42]. Lu, Y., Peters, J.L., and Michael, A.C., *Direct comparison of the response of voltammetry and microdialysis to electrically evoked release of striatal dopamine.* J. Neurochem., **1998**, 70: 584-593.

[43]. Robinson, T.E. and Justice Jr., J.B., *Microdialysis in the Neurosciences*, ed. J.P. Huston. **1991**, Amsterdam: Elsevier.

[44]. Herrerra, A.M., Scott, D.O., and Lunte, C.E., *Microdialysis sampling for determination of plasma protein binding of drugs.* Pharm. Res., **1990**, 7: 1077-1081.

[45]. Dash, A.K. and Elmquist, W.F., *Separation methods that are capable of revealing blood-brain barrier permeability.* J. Chromatogr. B, **2003**, 797: 241-254.

[46]. Sawchuk, R.J. and Elmquist, W.F., *Microdialysis in the study of drug transporters in the CNS.* Adv. Drug Deliv. Rev., **2000**, 45: 295-307.

[47]. Parrot, S., Sauvinet, V., Riban, V., Depaulis, A., Renaud, B., and Denoroy, L., *High temporal resolution for in vivo monitoring of neurotransmitters in awake epileptic rats using brain microdialysis and capillary electrophoresis with laser-induced fluorescence detection.* J. Neurosci. Methods, **2004**, 140: 29-38.

[48]. Schnetz, E. and Fartasch, M., *Microdialysis for the evaluation of penetration through the human skin barrier - a promising tool for future research?* Eur. J. Pharm. Sci., **2001**, 12: 165-174.

[49]. Karjagin, J., Pahkla, R., and Starkopf, J., *Perioperative penetration of metronidazole into muscle tissue: a microdialysis study.* Eur. J. Clin. Pharmacol., **2004**, 59: 809-813.

[50]. Stolle, L.B., Arpi, M., Jorgensen, P.H., Riegels-Nielsen, P., and Keller, J., *In situ gentamicin concentrations in the cortical bone.* Acta Orthop. Scand., **2003**, 74: 611-616.

[51]. Rooyackers, O., Thorell, A., Nygren, J., and Ljungqvist, O., *Microdialysis methods for measuring human metabolism.* Curr. Opin. Clin. Nutr. Metab. Care, **2004**, 7: 515-521.

[52]. Takimoto, C.H., *Basic pharmacokinetics and pharmacodynamic principles.* Cancer Treat. Res., **2001**, 106(Cancer Chemoprevention): 85-101.

[53]. Rescigno, A., *Foundations of pharmacokinetics.* Pharmacol. Res., **2000**, 42: 527-538.

[54]. Shargel, L. and Yu, A., *Applied Biopharmaceutics & Pharmacokinetics*. 4th ed, ed. C.L. Mehalik. **1999**, New York: McGraw-Hill.

[55]. Kaddoumi, A., Nakashima, M.N., Maki, T., Matsumura, Y., Nakamura, J., and Nakashima, K., *Liquid chromatography studies on the pharmacokinetics of phentermine and fenfluramine in brain and blood microdialysates after intraperitoneal administration to rats.* J. Chromatogr. B, **2003**, 791: 291-303.

[56]. Scott, D.O. and Lunte, C.E., *In vivo microdialysis sampling in the bile, blood, and liver of rats to study the disposition of phenol.* Pharm. Res., **1993**, 10: 335-342.

[57]. Verbeeck, R.K., *Blood microdialysis in pharmacokinetic and drug metabolism studies.* Adv. Drug Deliv. Rev., **2000**, 45: 217-228.

[58]. Weiss, D.J., Lunte, C.E., and Lunte, S.M., *In vivo microdialysis as a tool for monitoring pharmacokinetics.* Trends Analyt. Chem., **2000**, 19: 606-616.

[59]. Elmquist, W.F. and Sawchuk, R.J., *Application of microdialysis in pharmacokinetic studies.* Pharm. Res., **1997**, 14: 267-288.

[60]. Rambeeck, B., Jurgens, U.H., May, T.W., Pannek, H.W., Behne, F., Ebner, A., Gorji, A., Straub, H., Speckmann, E.-J., Pohlmann-Eden, B., and Loscher, W., *Comparison of brain extracellular fluid, brain tissue, cerebrospinal fluid, and serum concentrations of antiepileptic drugs measured intraoperatively in patients with intractable epilepsy.* Epilepsia, **2006**, 47: 681-694.

[61]. Ruiz-Jimenez, J. and de Castro, M.D.L., *Coupling microdialysis to capillary electrophoresis.* Trends Analyt. Chem., **2006**, 25: 563-571.

[62]. *HPLC for Pharmaceutical Scientists*, ed. Y. Kazakevich and R. Lobrutto. **2007**, Hoboken: John Wiley & Sons, Inc.

[63]. Harris, D.A., *Quantitative Chemical Analysis*. 5th ed. **1999**, New York: W. H. Freeman and Company.

[64]. Cunico, R.L., Gooding, K.M., and Wehr, T., *Basic HPLC and CE of Biomolecules*. **1998**, Richmond: Bay Bioanalytical.

[65]. Swartz, M.E., *UPLC: an introduction and review*. J. Liq. Chromatogr. Relat. Technol., **2005**, 28.

[66]. Nguyen, D.T.-T., Guillarme, D., Rudaz, S., and Veuthey, J.-L., *Fast analysis in liquid chromatography using small particle size and high pressure.* J. Sep. Sci., **2006**, 29: 1836-1848.

[67]. Olsen, B.A., Castle, B.C., and Myers, D.P., *Advances in HPLC technology for the determination of drug impurities.* Trends Analyt. Chem., **2006**, 25: 796-805.

[68]. Dorsey, J.G., Cooper, W.T., Siles, B.A., Foley, J.P., and Barth, H.G., *Liquid chromatography: theory and methodology.* Anal. Chem., **1998**, 70: 591R-644R.

[69]. *High-performance liquid chromatography of peptides and proteins: separation, analysis, and conformation* ed. C.T. Mant and R.S. Hodges. **1991**, Boca Raton: CRC Press, Inc.

[70]. *A Practical Guide to HPLC Detection*, ed. D. Parriott. **1993**, San Diego: Academic Press, Inc.

[71]. Lunte, S.M., Lunte, C.E., and Kissinger, P.T., *Electrochemical detection in liquid chromatography and capillary electrophoresis*, in *Laboratory Techniques in Electroanalytical Chemistry*, P.T. Kissinger and W.R. Heineman, Editors. **1996**, Marcel Dekker, Inc.: New York.

[72]. Jorgenson, J.W. and Lukacs, K.D., *Free-zone electrophoresis in glass capillaries.* Clin. Chem., **1981**, 27: 1551-1553.

[73]. Lunte, S.M. and Radzik, D.M., *Principles of Capillary Electrophoresis*, in *Pharmaceutical and Biomedical Applications of Capillary Electrophoresis*, S.M. Lunte and D.M. Radzik, Editors. **1996**, Elsevier: Oxford.

[74]. *Handbook of Capillary Electrophoresis*. 2nd ed, ed. J.P. Landers. **1997**, Boca Raton: CRC Press, Inc.

[75]. Schiewe, J., *Principles of capillary electrophoresis.* Drugs Pharmaceut. Sci., **2003**, 128: 1-21.

[76]. Terabe, S., Otsuka, K., Ichikawa, K., Tsuchiya, A., and Ando, T., *Electrokinetic separations with micellar solutions and open-tubular capillaries.* Anal. Chem., **1984**, 56: 111-113.

[77]. Arnett, S.D., *Improving Sensitivity for Capillary Electrophoresis for the Analysis of Physiological Samples*. **2005**, University of Kansas: Dissertation.

[78]. Sandlin, Z.D., Shou, M., Shackman, J.G., and Kennedy, R.T., *Microfluidic electrophoresis chip coupled to microdialysis for in vivo monitoring of amino acid neurotransmitters.* Anal. Chem., **2005**, 77: 7702-7708.

[79]. Heiger, D.N., Kaltenbach, P., and Sievert, H.-J.P., *Diode array detectors for capillary electrophoresis.* Electrophoresis, **1994**, 15: 1234-1247.

[80]. Moring, S.E., Pairaud, C., Albin, M., Locke, S., Thibault, P., and Tindall, G.W., *Enhancement of UV detection sensitivity for capillary electrophoresis.* American Lab., **1993**, 25: 32-39.

[81]. Liu, C.-M. and Tzeng, Y.-M., *Applications of capillary electrophoresis in pharmaceutical drug design.* J. Food Drug Anal., **1998**, 6: 391-404.

[82]. O'Shea, T.J., *Electrochemical Detection for Capillary Electrophoresis*, in *Pharmaceutical and Biomedical Applications of Capillary Electrophoresis*, S.M. Lunte and D.M. Radzik, Editors. **1996**, Elsevier: Oxford.

[83]. Xu, X., Li, L., and Weber, S.G., *Electrochemical and optical detectors for capillary and chip separations.* Trends Analyt. Chem., **2007**, 26: 68-79.

[84]. Crick, E.W., Osorio, I., Bhavaraju, N.C., Linz, T.H., and Lunte, C.E., *An investigation into the pharmacokinetics of 3-mercaptopropionic acid and development of a steady-state chemical seizure model using in vivo microdialysis and electrophysiological monitoring.* Epilepsy Res., **2007**, 74: 116-125.

Chapter 2.

Development of a Chemical Seizure Model Using
3-Mercaptopropionic Acid

2.1. Introduction

2.1.1. Background and Significance

The goal of this study was to develop a chemical seizure model using the convulsant, 3-mercaptopropionic acid (3-MPA). A pharmacodynamics (PD) approach was taken, combining *in vivo* microdialysis sampling with electrophysiological methods to simultaneously monitor the real-time 3-MPA concentration in the brain and the corresponding electrocorticographic (ECoG) activity.

3-MPA disrupts the excitatory/inhibitory balance in the brain. However, quantitative data about the changes in the main excitatory neurotransmitter, glutamate (Glu), and the main inhibitory neurotransmitter, γ-aminobutyric acid (GABA), as a function of the concentration of 3-MPA in the brain, are lacking. Knowledge of the concentration of 3-MPA in the brain would serve as an important independent variable when investigating changes in the Glu/GABA ratio. Also, a correlation could be formed between the changes in Glu and GABA and the seizure frequency or rate and intensity.

The ability to monitor the concentration of 3-MPA in real-time using *in vivo* microdialysis would allow for the regulation and achievement of a steady-state concentration of the convulsant. This strategy will enable the investigation of seizure frequency or rate and intensity under conditions that either eliminate, or precisely track fluctuations of the independent variable (convulsant concentration in the brain), thus allowing for more accurate interpretation of the results and a better insight into seizure dynamics.

2.1.2. Current Analytical Uses for 3-Mercaptopropionic Acid

Other than its use as a convulsant, 3-MPA has been used in a wide range of applications. One application for its use is as a natural environmental sequester for transition metals in fresh and salt waters [1]. Another application for the use of 3-MPA is its ability to form a self-assembled monolayer on a gold surface. This arrangement allows for studies of the interactions of gold nanoparticles for the purpose of distance-sensitive labels or proximity probes [2], the detection of target analytes in pharmaceutical drugs using flow injection analysis [3], and the analysis of important metals in humans using a peptide-thiol modified biosensor [4]. Another important use for 3-MPA is its use as a convulsant to study epilepsy. O'Connell *et al.* [5] and Towfighi *et al.* [6] used 3-MPA to induce neuronal lesions which allowed a study of the regional brain damage resulting from status epilepticus. 3-MPA has also been used to study the pharmacokinetics (PK) and effectiveness of different antiepileptic drugs (AEDs) [7, 8].

2.1.3. Mechanism of Action of 3-Mercaptopropionic Acid

The mechanisms of action and the seizures induced by 3-MPA [9-11] have been well characterized [12-14]. Glutamic acid decarboxylase (GAD), the enzyme that converts Glu to GABA, is competitively inhibited by 3-MPA administration to rats, thereby decreasing GABA concentrations in the brain [15-20]. The resulting imbalance between Glu and GABA, the main excitatory and inhibitory neurotransmitters in the brain, respectively, can sequentially lead to two types of generalized seizures: first myoclonic and then tonic-clonic seizures [12, 21].

Myoclonic seizures are brief jerks of the muscles of the face and forelimbs. These types of seizures are usually non-violent and last for 2 - 3 seconds. Because the 3-MPA resides within the animal for longer periods of time, the brief muscle jerks turn into tonic-clonic seizures and the muscles of the face, forelimbs, and upper body act together to form violent "jumping" actions. These seizures usually last for 1- 3 minutes and greatly affect the breathing patterns of the animal.

The affect of 3-MPA on brain electrical activity has been extensively studied [21]. 3-MPA seizures elicit rhythmical spikes in electrical activity which soon changes to sudden, violent outbursts of electrical spikes.

2.1.4. Specific Aims of Research

The main goal for this research was to use 3-MPA as a convulsant for the development of a chemical seizure model. First, the protein binding and PK of 3-MPA were studied. In order to gain quantitative knowledge on the kinetic processes

of 3-MPA after it was dosed, it was necessary to fit the obtained data to a mathematical model to simplify the complex biological system. For the PK modeling, a noncompartmental model, or "model-independent" PK was employed. This model is based upon the mathematical description of the useful PK values from the sampling sites of interest including maximum concentrations (C_{max}), maximum times to plateau at those concentrations (T_{max}), area under the curve (AUC), and the elimination half-life ($t_{1/2}$) [22]. Using a noncompartmental PK analysis eliminates the possibility of choosing the "incorrect" compartmental model, calculating the incorrect PK parameters for further reference, and is automated quite readily on available PK software packages such as WinNonlin (Pharsight Corporation) or SummitPK (Summit Research Services).

Once the PK of 3-MPA, based on bolus dosing, was revealed, a chemical seizure model in which steady-state concentrations of the convulsant were maintained within the brain compartments was developed. The steady-state concentration is important because it serves as an independent variable for future experiments correlating the convulsant concentration in the brain to the changes observed with neurochemical events. The ECoG data were also simultaneously monitored. These results were used to explore the PD of 3-MPA. PD is a measure of the effect of the drug entity (typically at a receptor within the site of action) over the time course of the experiment [23]. The drug interaction with different receptors within the tissue or organ dosed results in a cascade of molecular responses leading to different pharmacological or toxicological actions. PD analyses are equally important as PK

analyses when developing new drug therapies or treatments. PK-PD modeling has grown in popularity in response to the development of new drugs. PK-PD models help to relate the intensity of the pharmacological response to the concentration of the drug in the site of interest over the course of the experiment [23, 24]. All of these data were combined in order to further understand the PK-PD relationship for the developed 3-MPA seizure model.

If successful, this chemical seizure model can help to gain better knowledge of deep brain stimulation treatments. These types of treatments are over 75% successful in slowing / reducing the number of seizures observed in the clinical setting [25, 26]. Electrical stimulation can be implemented during the seizures created by 3-MPA to impede further activity, thereby providing insight into the neurochemistry of epileptic seizures.

2.2. Materials and Methods

2.2.1. Chemicals / Reagents

Monobasic sodium phosphate, dibasic sodium phosphate, sodium chloride, potassium chloride, magnesium chloride, calcium chloride, disodium ethylenediamine tetraacetate (Na_2EDTA), 85% *o*-phosphoric acid, methanol, and 0.3 μm alumina powder were obtained from Fisher Scientific (Pittsburgh, PA). 3-Mercaptopropionic acid and lyophilized human plasma were obtained from Sigma-Aldrich (St. Louis, MO). Triple-distilled mercury was obtained from Bethlehem Apparatus Company (Hellertown, PA). Ketamine HCl was obtained from Fort Dodge Animal Health (Fort

Dodge, IA). Xylazine was obtained from Lloyd Laboratories (Shenandoah, IA). Acepromazine was obtained from Boehringer Ingelheim Vetmedica, Inc. (St. Joesph, MO). All solutions were prepared in 18.2 MΩ distilled, deionized water (Labconco, Kansas City, MO) and filtered through 0.22 μm pore size polyethersulfone (PES) membrane filters prior to use unless otherwise noted.

2.2.2. Instrumentation

A liquid chromatographic system with electrochemical detection was used to analyze the microdialysis samples. In total, 2 μL of each microdialysis sample was directly injected onto a Synergi 4μ Hydro-RP column (150 x 2.0 mm, Phenomenex, Torrance, CA). The liquid chromatographic system consisted of a Shimadzu LC-20AD pump, and a Rheodyne 9725i PEEK sample injector valve connected to a Phenomenex C18 guard column. The mobile phase was adapted from Stenken *et al.* [27] and consisted of a phosphate buffer and methanol (80:20, v:v). The phosphate buffer was made of 25 mM monobasic sodium phosphate and 0.5 mM Na$_2$EDTA with the pH adjusted to 2.5 using 85% *o*-phosphoric acid.

The electrochemical detector consisted of a thin-layer gold mercury (Au/Hg) amalgam electrode. Preparation of the gold electrode was described by Allison and Shoup [28]. In brief, a 3 mm gold electrode embedded in a PEEK block (Bioanalytical Systems, West Lafayette, IN) was polished with 0.3 μm alumina powder then rinsed with 100% methanol followed by copious amounts of water. Triple-distilled mercury was placed onto the surface of the electrode and allowed to

remain for 5 minutes before removal with the edge of a notecard. The amalgamation process occurred overnight and then the electrode was placed into the electrochemical flowcell. 3-MPA was indirectly detected at the electrode via the oxidation of mercury from the electrode surface as the thiol passes over based on Equation 2.1 shown below.

$$2\ RSH\ +\ Hg\ \longrightarrow\ Hg(SR)_2\ +\ 2\ H^+\ +\ 2\ e^- \tag{2.1}$$
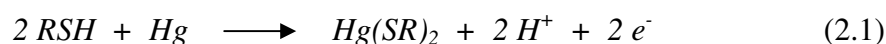
The optimal detection potential was determined from a hydrodyanamic voltammagram (HDV) of 3-MPA (Figure 2.1). This potential was controlled by an LC-4C potentiostat (Bioanalytical Systems, West Lafayette, IN). The data were collected at 10 Hz and processed using a Chrom&Spec Chromatography Data System (Ampersand International, Beachwood, OH). The electrode was set at a potential of +100 mV versus a Ag/AgCl reference electrode. The detection of 3-MPA at the Au/Hg electrode is shown schematically in Figure 2.2. The linear range of this LC-EC method was checked before each experiment and was found to be linear between $1 - 200\ \mu M$. The limit of detection (LOD) of 3-MPA in microdialysis samples was determined to be 500 nM.
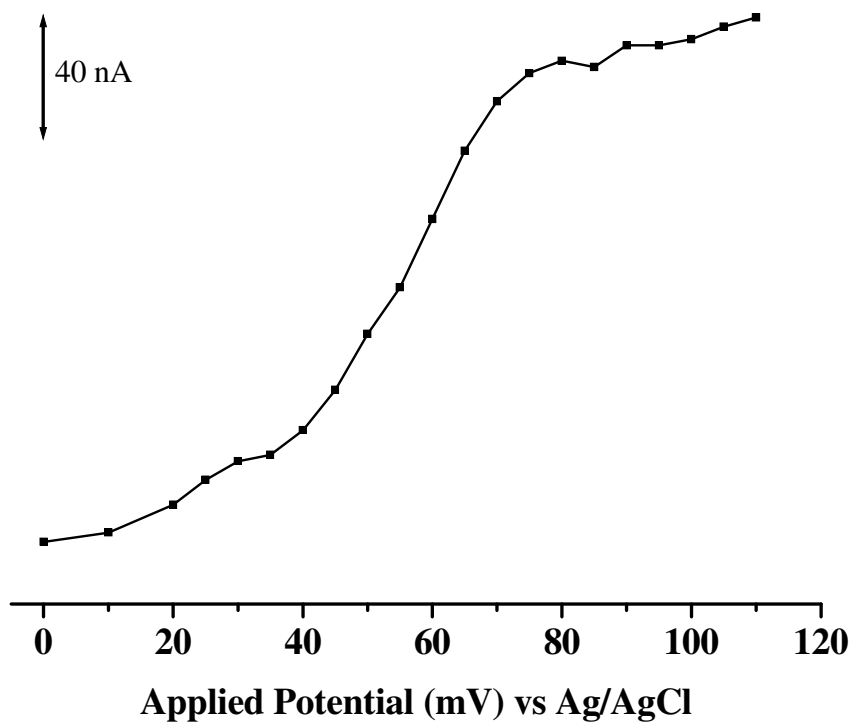
Figure 2.1. Hydrodynamic voltammagram of 100 μM 3-MPA. All conditions as described in Section 2.2.2.

(A)

HS⎯⎯⎯⎯C(=O)⎯OH

(B)
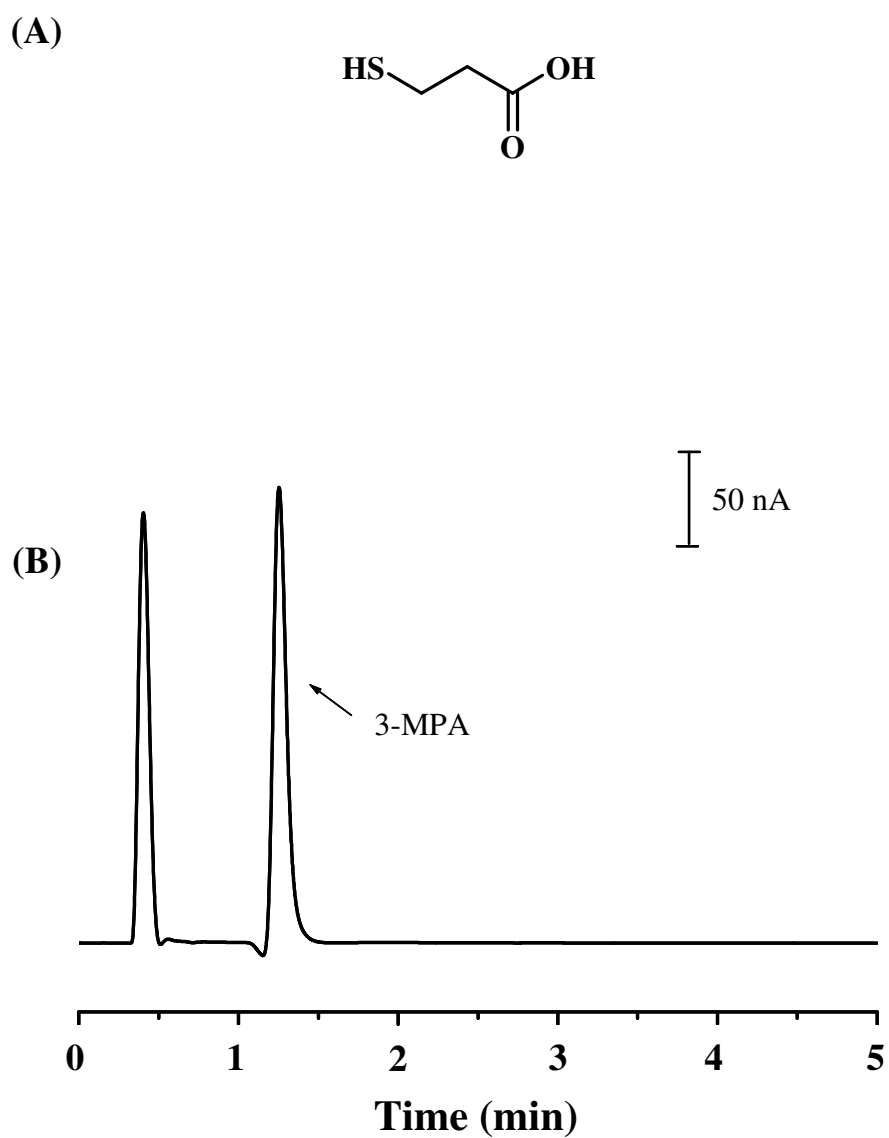
Figure 2.2. Typical chromatogram of 3-MPA. (A) Structure of 3-MPA. (B) LC-EC analysis of 3-MPA from microdialysate. Detection at +100 mV vs Ag/AgCl.

2.2.3. Experimental

2.2.3.1. 3-MPA Protein Binding

To evaluate the extent to which 3-MPA binds to proteins, a method of ultracentrifugation was employed. Ultracentrifugation is an effective method for studying small molecule-protein binding interactions [29, 30]. Lyophilized human plasma was reconstituted in deionized water to a volume of 5 mL. 40 µL of a 1 mM 3-MPA solution was added to 360 µL of the reconstituted human plasma giving a final concentration of 100 µM 3-MPA. This drug-plasma mixture was prepared in Microcon® Ultracel YM-30 ultracentrifugation tubes with a MWCO of 30 kDa. The solution was first vortexed for 1 minute. The ultracentrifuge tubes were then placed into a micro-centrifuge (Model 235C, Fisher Scientific) and centrifuged at a fixed speed of 12,400 rpm for 12 minutes. The filtrates were collected and analyzed using the LC-EC method discussed in Section 2.2.2. Equation 2.2 was used to determine the extent of plasma protein binding for 3-MPA. In Equation 2.2, *T* represents the total concentration of

$$\% \ Binding = (\ [T-F]\ /\ T\ )\ x\ 100\% \tag{2.2}$$

3-MPA added to the plasma and *F* represents the free fraction of 3-MPA which was collected in the filtrate. The experiment was repeated two times, leading to a total of three repetitions for the protein binding measurement.

60

2.2.3.2. *Vascular Probe Fabrication*

Vascular microdialysis probes were manufactured in-house using a modification to a previous probe design [31]. A 12-inch section of polyimide tubing, 170 μm o.d. and 122 μm i.d. (MicroLumen Inc., Tampa, FL), was placed through a 10 mm piece of micro-renathane (MRE-033) tubing, 838 μm OD and 356 μm ID (Braintree Scientific Inc., Braintree, MA) leaving a 10 mm protrusion of the polyimide tubing at the end. A 14 mm section of 40 kDa MWCO polyacrylonitrile (AN69$_{HF}$) hollow fiber microdialysis membrane (Hospal Industries, Lyon, France) was placed over the exposed polyimide tubing and guided into the MRE-033 tubing a distance of 3 mm. UV glue (UVEXS, Sunnyvale, CA) was used to seal the end of the semi-permeable membrane leaving a 1 mm gap between the polyimide tubing and the end of the membrane, as well as the connection with the MRE-033 tubing. The UV glue was activated using a ELC-450 UV light system (Electro-Lite Corporation, Danbury, CT) with conditions of 5.0 W/cm^2 (365 nm) for five seconds. A six inch piece of polyimide tubing was placed 3 mm into the top of the MRE-033 tubing and affixed with UV glue. A 20 mm length of polyethylene tubing (PE-50), 965 μm OD and 580 μm ID (Fisher Scientific, Pittsburgh, PA) was placed over the two pieces of polyimide tubing and secured with UV glue. The final product had a semi-permeable membrane 10 mm in length.

2.2.3.3. Surgical Procedures

Male Wistar rats weighing 300 - 450 grams (Charles River Laboratories, Wilmington, MA) were used. The animals were kept on 12 hour light-dark cycles and allowed free access to food and water prior to the experiment. The research described herein was conducted in compliance with all applicable federal statutes and regulations related to animals and experiments involving animals and adheres to the principles stated in the Guide for the Care and Use of Laboratory Animals, NIH publication 86-23, 1996 edition.

Brain. On the day of the experiment, rats were pre-anesthetized with isoflurane. A subcutaneous injection of 67.5 mg/kg ketamine: 3.4 mg/kg xylazine: 0.67 mg/kg acepromazine was then administered for full anesthesia. Supplemental doses of 100 mg/mL ketamine were given at a rate of 0.2 mL/hr to maintain the same plane of anesthesia. The anesthetized rat was placed on a stereotaxic frame (Harvard Appartus, Holliston, MA) and then connected to a Homeothermic Blanket Control Unit (Harvard Apparatus, Holliston, MA) where the body temperature was maintained at 37.0 ± 0.3 °C. A midline incision was made on the scalp and the skull was exposed. Four electrodes (1 mm o.d. stainless steel screws (Ace Hardware, Lawrence, KS)) were placed over the cortex to record ECoG activity. Two of the four electrodes were placed over the right hemisphere 4.2 mm anterior and 5.8 mm posterior and -1.4 mm lateral with respect to bregma. The third electrode was used as a ground electrode on the right hemisphere 5.8 mm posterior and +1.4 mm lateral with respect to bregma, and the other electrode was used as reference (nasion).

Prior to the implantation, the brain microdialysis probes were placed into a vial containing the perfusion medium, artificial cerebral spinal fluid (aCSF) [145 mM NaCl, 2.7 mM KCl, 1.0 mM $MgCl_2$, 1.2 mM $CaCl_2$, 0.45 mM NaH_2PO_4, and 2.33 mM Na_2HPO_4, pH 7.4], and connected using FEP (fluorinated ethylene propylene; 0.014 in. i.d., 0.033 in. o.d.) tubing to a 1 mL syringe containing aCSF. A CMA/100 microsyringe pump perfused aCSF through the microdialysis probes at a rate of 2 µL/min for approximately one hour as suggested by the manufacturer to remove any trapped air bubbles and to wet the probe prior to implantation.

Microdialysis intracerebral guide cannulas (CMA Microdialysis Inc., North Chelmsford, MA) were implanted into the brain with the following coordinates: posterior 0.2 mm, lateral +3.2 mm, ventral 3.5 mm (striatum) and anterior 5.6 mm, lateral +4.8 mm, ventral 5.0 mm (hippocampus) both with respect to the bregma [32]. The guide cannulas were fixed to the skull surface with Duralay dental cement (Worth, IL). A CMA/12 microdialysis probe with a 4 mm membrane (CMA Microdialysis Inc., North Chemlsford, MA) was then placed through the guide cannula into the striatum and a CMA/12 microdialysis probe with a 2 mm membrane was placed into the hippocampus.

Jugular Vein. A small incision was made in the neck, and the right jugular vein was dissected and ligated. An incision was made in the vein distal to the ligature, and the vascular microdialysis probe was inserted toward the heart and affixed in place with suturing. Tissue staples were used to close the neck incision.

Femoral Vein Cannulation. A small incision was made over the left groin, and the femoral vein was dissected and ligated. An incision was made in the vein distal to the ligature, and a 25 mm length of MRE-033 tubing was inserted into the femoral vein a distance of 5 cm and then affixed properly by suturing. The skin incision was closed with tissue staples.

2.2.4. Brain and Vascular Probe Calibration

The *in vitro* vascular microdialysis probe calibration was determined prior to the experiment. The semi-permeable membrane of the probe was placed into a bath of aCSF that was stirred and heated to 37 °C. A solution of 25 µM 3-MPA prepared in aCSF was delivered through the probe at a flow rate of 1 µL/min and the dialysate was collected and analyzed.

Following the implantation of the electrodes and the brain and vascular microdialysis probes, the rat was connected to a CMA/100 microsyringe pump (CMA Microdialysis Inc., North Chelmsford, MA). Both microdialysis probes were perfused with a solution of 25 µM 3-MPA at a rate of 1 µL/min for three hours to allow for *in vivo* microdialysis probe calibration. Then both probes were flushed with aCSF at a rate of 1 µL/min for three hours to allow for cleansing and stabilization of the probe environment.

Equation 1.2, listed in Section 1.5.3., was used to determine the relative delivery for each probe. The concentration of 3-MPA in the dialysate was obtained using this probe correction factor.

2.2.5. ECoG Collection

ECoG recordings were obtained beginning 30 minutes prior to dosing with 3-MPA to measure the baseline. The signals were acquired through a Biomedical amplifier (SA Instruments, San Diego, CA) using a 0.1 Hz high pass filter, a 6000 Hz low pass filter, a sampling rate of 15 kHz and a NIDAQ PCI 6731 data acquisition card (National Instruments, Austin, TX). The data were stored in the computer hard drive and analyzed, using custom built software [33, 34]. The total number of seizures, their duration, and intensity were determined using an algorithm developed by Osorio *et al*. [34, 35]. Seizures were detected by filtering the ictal component from the raw ECoG using a wavelet spectral filter that enhances frequencies between 8-42 Hz, and computing, in real-time, the ratio of the median power of the filtered foreground (2 seconds) to the median power of the filtered background (30 minutes). The resulting ratio is an estimate of the instantaneous seizure content of the ECoG. For this study, seizures were defined as any automated detection with a maximal ratio that reached or exceeded a threshold of 22.

2.2.6. Noncompartimental Pharmacokinetics Analysis

Noncompartmental PK analysis was performed on the data using WinNonlin (Pharsight Corporation, Mountain View, CA). The parameters of interest obtained from the blood and brain microdialysates were the elimination constant (K_e), time to achieve maximum concentration (T_{max}), maximum concentration (C_{max}), the area

under the curve (AUC_{inf}), and the area under the curve per dose administered (AUC_{inf}/Dose). The paired t-test was used to study statistical significance of the data.

2.3. Results and Discussion

2.3.1. 3-MPA Protein Binding

A concentration of 100 µM 3-MPA was used to evaluate the extent of protein binding within human plasma. The value obtained for the protein binding of 3-MPA to human plasma was $53.1 \pm 2.6\%$ (n = 3). Therefore, the remaining 46.9% of the dosed 3-MPA is available for use as an effective pharmacological convulsive agent.

2.3.2. In Vitro *Microdialysis Probe Performance*

The *in vitro* calibration of the vascular and brain microdialysis probes measured a value of $77.2 \pm 5.8\%$ (n = 8) and $50.1 \pm 3.3\%$ (n = 4) delivery of 3-MPA, respectively, at a flow rate of 1 µL/min. The high delivery values obtained for 3-MPA display no problems such as difficulty diffusing through or adsorbing to the semi-permeable membrane. Therefore, microdialysis was a viable sampling technique for 3-MPA collection from the rats.

2.3.3. In Vivo *Microdialysis Probe Performance*

The *in vivo* calibration of the vascular and brain microdialysis probes measured a value of $63.0 \pm 11.2\%$ (n = 28) and $38.1 \pm 10.5\%$ (n =31) delivery of 3-MPA, respectively, at a flow rate of 1 µL/min. There is no significant difference

between the *in vitro* and *in vivo* results obtained for the vascular microdialysis probes. The lower average value for the *in vivo* results could be a consequence of the vascular probe placement into the jugular vein. If any part of the semi-permeable membrane of the probe was resting against a wall of the jugular vein, then there was not a completely dynamic environment surrounding the probe as in an *in vitro* study. The decreased value of the brain probe performance is expected due to the static environment within the brain tissue.

2.3.4. Bolus Dosing with ECoG Analysis

Control experiments were conducted by injecting a bolus dose of 0.9% saline to the rat while recording the ECoG response. These experiments were performed to ensure that no part of the experiment outside of 3-MPA administration induced convulsive activity. No changes were observed from basal ECoG activity during these "sham" injections (Figure 2.3).

The convulsant was administered as an (intraperitoneal) i.p. bolus dose at two different concentrations, 50 mg/kg (n = 5) and 100 mg/kg (n = 5) to compare effects at two different concentrations. The resulting PK curves are shown in Figure 2.4. Semi-logarithmic concentration versus time plots are shown for 3-MPA in the blood and in the brain. The slopes of the concentration-time curves appear parallel for the blood and brain in the 50 mg/kg 3-MPA dose. However, this is not the case for the 100 mg/kg 3-MPA dose. The slopes of the blood and brain concentration-time curves for the higher dose appear to converge onto each other, and if extrapolated, may cross paths. One major observation of these experiments was that the rats dosed with the
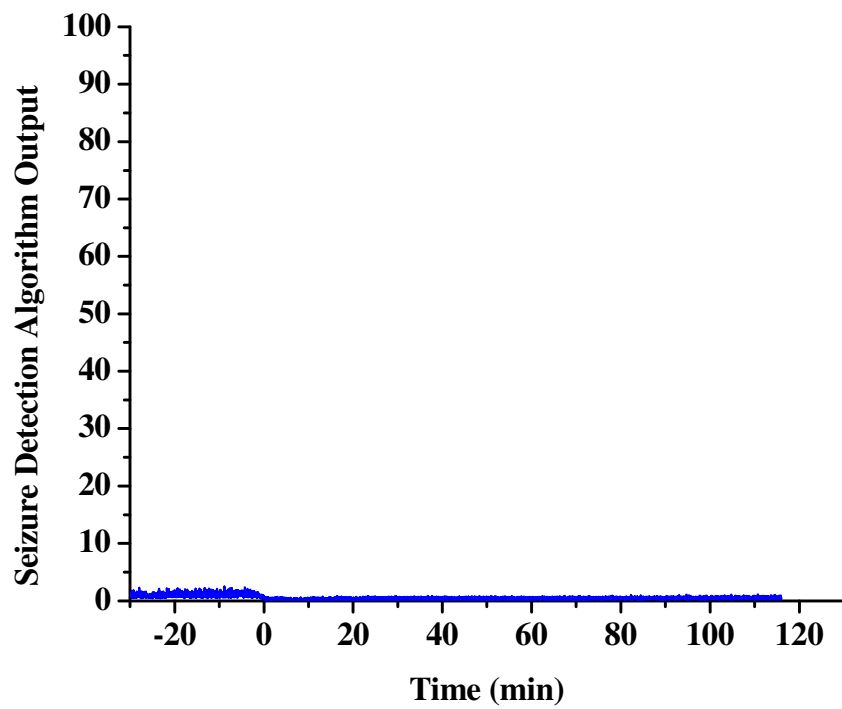
Figure 2.3. ECoG plot of saline injection. Cortical brain activity following a "sham" dose of saline administered at t = 0 minutes.
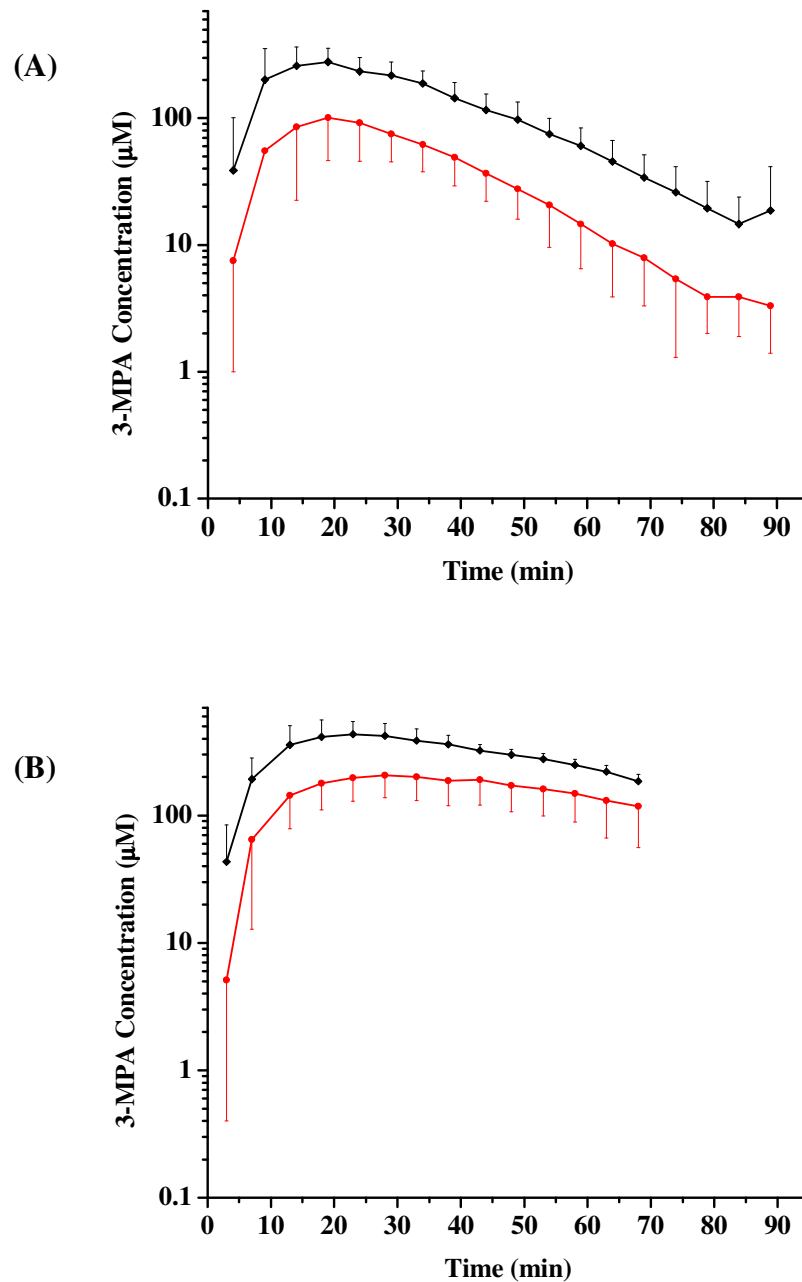
Figure 2.4. Semilog pharmacokinetics curves from blood and brain microdialysates for 3-MPA bolus dosing (n = 5). A, 50 mg/kg IP bolus dose; B, 100 mg/kg IP bolus dose. [Blood microdialysate (♦), brain microdialysate (●)]. 3-MPA was administered at t = 0 minutes on the x-axis.

higher concentration of 3-MPA did not survive as long as those dosed with the lower concentration. At the conclusion of the 50 mg/kg bolus dosing experiments, the average concentration of 3-MPA remaining in the brain was approximately 5 μM, whereas for the rats dosed with 100 mg/kg, the final brain concentration measured was approximately 120 μM. This shows that saturation was occurring in the brain with the higher dose of 3-MPA.

The tabulated PK parameters (Table 2.1) showed this effect also. There are significant differences in the pharmacokinetics data between the 50 mg/kg and 100 mg/kg doses. The maximum concentration (C_{max}) for the brain was significantly different ($p < 0.05$) between the two doses. This was a much smaller difference than that observed for the blood C_{max} values. The K_e values are very similar in the blood and the brain for the 50 mg/kg dose as was depicted on the semi-log concentration-time curves (Figure 2.3(A)). At the 100 mg/kg dose, where the slopes appear to converge upon one another, the K_e values for the blood and brain differed ($p < 0.05$). The time to reach maximum concentration (T_{max}) differs significantly ($p < 0.10$) between the blood and brain for the 100 mg/kg dose. The area under the curve normalized to the administered dose (AUC_{inf}/Dose) ($p < 0.01$) values differed significantly between the blood and the brain for both doses administered.

Comparing the blood and brain PK across doses had significant differences as well. The K_e values for the blood and brain both differed ($p < 0.01$) beween the 50 mg/kg and the 100 mg/kg doses. There was also a difference ($p < 0.05$) for the T_{max}

Table 2.1. Pharmacokineics parameters for 50 mg/kg and 100 mg/kg bolus dosing.

	50 mg/kg Bolus Dose[a]		100 mg/kg Bolus Dose[a]	
	Blood	**Brain**	**Blood**	**Brain**
K_e (min^{-1})	0.052 ± 0.012	0.060 ± 0.016	0.026 ± 0.014[b]	0.018 ± 0.014[b]
T_{max} (min)	15.0 ± 4.5	18.0 ± 2.2	21.0 ± 2.7[b]	31.0 ± 8.4[b]
C_{max} (μM)	308.7 ± 114.0[d]	101.6 ± 55.2[d]	448.9 ± 122.1[c]	211.0 ± 69.6[c]
AUC_{inf} (mg min μL^{-1})	1125 ± 387	353 ± 178	3171 ± 641	2168 ± 973
AUC_{inf}/Dose (min μL^{-1})	23 ± 8[d]	7 ± 4[d]	32 ± 6	22 ± 10

a: n = 5 rats
b: $p < 0.10$
c: $p < 0.05$
d: $p < 0.01$

for both the blood and the brain across doses. The C_{max} for the brain differed significantly ($p < 0.05$) between the two doses, whereas the blood C_{max} values did not. The AUC_{inf}/Dose differed ($p < 0.05$) for both the brain and the blood PK.

The blood/brain data are shown in Table 2.2. For the 50 mg/kg dose, the K_e is around 1. There was a noticeable difference ($p < 0.05$) in the K_e blood/brain values between the two doses, however. The other significant difference was with the AUC_{inf} blood/brain values for each dose ($p < 0.05$). The AUC_{inf} in the brain at 50 mg/kg 3-MPA was 31% of the AUC_{inf} in the blood while at 100 mg/kg, it was 68%. The average maximum concentration of 3-MPA in the brain is 33% of the C_{max} in the blood for the 50 mg/kg dose, whereas for the 100 mg/kg dose, it is 47%. These values do not differ significantly.

These data again point to a saturation effect occurring in the brain upon administration of higher doses of 3-MPA. The AUC_{inf}/Dose blood/brain data differs between doses ($p < 0.05$). At the 50 mg/kg dose, the AUC_{inf} of 3-MPA in the brain is on average 3.5 times less than the 3-MPA in the blood. However, at the 100 mg/kg dose, the brain 3-MPA is only 1.5 times less than that in the blood. This again shows the saturation effect that is dose dependent in the rat.

A typical raw ECoG displaying 3-MPA seizure activity using single channel continuous recording is shown in Figure 2.5. These raw data are filtered through a seizure detection algorithm [34, 35] to provide pertinent information regarding the dosing scheme applied. A typical ECoG recording after manipulation via the seizure detection algorithm is shown in Figures 2.6(A) and 2.6(B) for the administration of a

Table 2.2. Pharmacokineics parameters for blood/brain ratio for 50 mg/kg and 100 mg/kg bolus dosing.

	50 mg/kg Bolus Dose[a]	100 mg/kg Bolus Dose[a]
K_e (min^{-1})	0.89 ± 0.14^b	1.52 ± 0.47^b
T_{max} (min)	0.82 ± 0.18	0.72 ± 0.22
C_{max} (μM)	3.36 ± 1.06	2.64 ± 1.97
AUCinf (mg min μL^{-1}) AUCinf/Dose (min μL^{-1})	3.54 ± 1.27^c	1.59 ± 0.40^c

a: n = 5 rats
b: p < 0.10
c: p < 0.05

Figure 2.5. Raw electrocortigram showing a typical 3-MPA seizure. Seizure onset was at approximately 2765 seconds and termination was at 2808 seconds and "interictal" epileptiform discharges, recorded from 2 subdural electrodes placed symmetrically on each side of bregma.
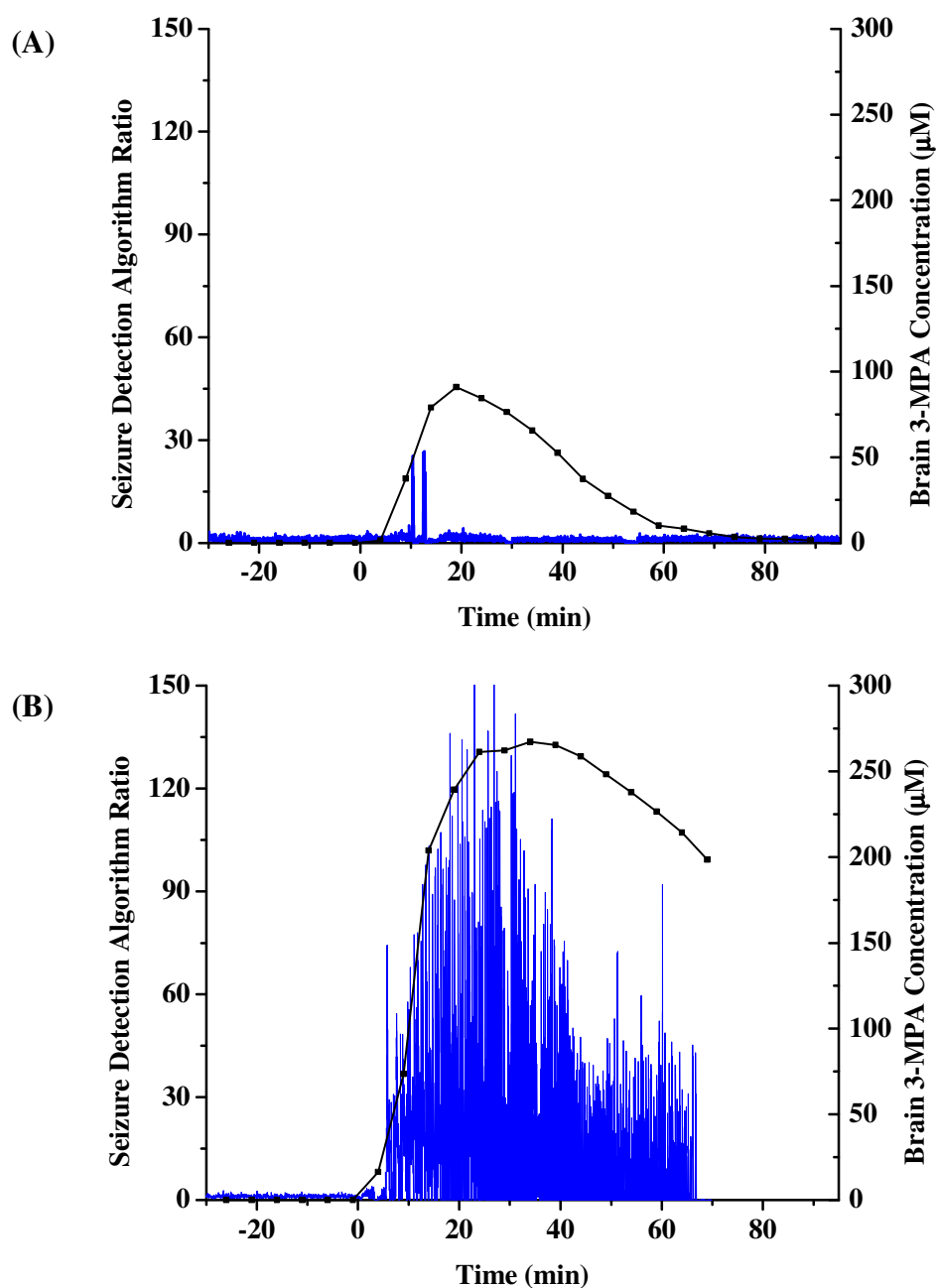
Figure 2.6. Example seizure detection algorithm ratio plots. A, representative data for brain 3-MPA concentration superimposed onto the ECoG recording for a 50 mg/kg bolus dose; B, representative data for brain 3-MPA concentration superimposed onto the ECoG recording for a 100 mg/kg bolus dose. The x-axis denotes the time (t = 0 corresponds to the 3-MPA (■) administration), and the y-axis denotes an estimate of the seizure content (intensity) of the raw ECoG signal. Increases in the algorithm ratio to 22 or above correspond to seizures.

50 mg/kg bolus dose and a 100 mg/kg bolus dose, respectively. Seizure detections are denoted by increases in the algorithm ratio at or above 22. After administration of the 50 mg/kg dose (Figure 2.6(A)) short-lived seizure activity occurred on average within 11.3 minutes. For the 100 mg/kg dose (Figure 2.6(B)), seizure activity occurred on average within 8.5 minutes and was much longer lived. The ECoG data from the bolus dosing is displayed in Table 2.3. The latency period for the onset of seizures after administration of the bolus doses corresponded to a slightly higher average concentration in the brain at onset (92 µM versus 58 µM, respectively). This represents a statistically significant difference in the concentrations at seizure onset ($p < 0.05$). There is a 67-fold increase in the average number of seizures detected for the 100 mg/kg dose compared to the 50 mg/kg dose ($p < 0.01$). The corresponding seizure duration times show that the average seizure lasts longer for the 50 mg/kg dose (1.72 s) than for the 100 mg/kg dose (1.03 s). This is directly related to the total number of seizures observed for each experiment. For the 100 mg/kg dose, there are more total seizures observed per experiment and their average duration is shorter than the lower dose administered. The range for the seizure durations for the 100 mg/kg dose is also less variable than the 50 mg/kg dose as shown by the average standard deviation. The maximum seizure intensity (R_{max}) is higher for the corresponding higher bolus dose, but not statistically different from that of the lower dose.

It is inferred from the PK curves and the ECoG data that, in the brain, the minimum effective concentration (MEC) of 3-MPA needed to induce seizure activity is 50 µM and the minimum toxic concentration (MTC) for the convulsant is 200 µM.

Table 2.3. ECoG data for 50 mg/kg and 100 mg/kg bolus dosing.

	50 mg/kg Bolus Dose[a]	100 mg/kg Bolus Dose[a]
Latency to Seizure Onset (s)	680.7 ± 123.5	510.2 ± 305.2
Brain [3-MPA] at Seizure Onset (μM)	57.6 ± 37.2	91.9 ± 28.3
Number of Seizures Detected	9 ± 2^{b}	603 ± 85^{b}
Average of the Average Seizure Duration (s)	1.72 ± 4.00	1.03 ± 2.11
R_{max}	61.7 ± 38.1	123.8 ± 69.5

a: n = 4 rats
b: $p < 0.01$

These values arise from combining the results shown in Figures 2.6(A) and (B) and the ECoG data from Table 2.3. After the administration of the 3-MPA dose in Figure 2.6(A), the true seizure activity is observed after the concentration of convulsant in the brain has reached a value of 50 μM, therefore, this is the value for the MEC. As for the MTC, from Figure 2.6(B), after a concentration of 200 μM is reached, the convulsant saturated the brain tissue and eliminated at a much slower rate than the lower dose (discussed above). From visual observations of the respiration of the animals, this saturation in the convulsant concentration correlated very closely to the time in which the animals went into a state of respiratory distress. Therefore, the MTC was determined as 200 μM.

2.3.5. Steady-State Dosing Schemes

2.3.5.1. Multiple Dosing Regimens with ECoG Analysis

In the next portion of the study, two multiple dosing regimens were employed in an attempt to obtain a steady concentration of 3-MPA in the brain. Based on the single dose PK, the first dosing regimen consisted of administering an i.p. loading dose of 50 mg/kg followed by two i.p. maintenance doses of 46.7 mg/kg at 30 minute intervals. These values were derived by using the maintenance dosing equation (Equation 2.3) shown below [36].

$$Maintenance\ Dose = Loading\ Dose * (1 - e^{-Ke*\tau}) \qquad (2.3)$$

A τ of 30 minutes represented approximately one elimination half-life for the 50 mg/kg dose. The second dosing regimen consisted of administering an i.p. loading dose of 50 mg/kg followed by two i.p. maintenance doses of 42.3 mg/kg at 45 minute intervals. The τ of 45 minutes represented approximately two elimination half-lives for the loading dose.

Figures 2.7 and 2.8 depict the concentration-time curves for the two models. For the first model, τ = 30 minutes, the maximum concentration in the brain of 310 µM occurred approximately 30 minutes before the rat died. When a maintenance dose was administered every 30 minutes (Figure 2.7), an accumulation of 3-MPA was observed in the brain which led to a toxic effect with a maximum concentration in the brain of 310 µM. This is well above the noted MTC of 200 µM. When maintenance dosing was extended to every 45 minutes, the maximum concentration in the brain was 175 µM. The timing of the maintenance dose was extended to 45 minutes (Figure 2.8) allowing more of the 3-MPA to eliminate from the brain before additional dosing. In this case, the rat's seizure activity ceased before each successive dose. Only one experiment of each dosing regimen was carried out due to the lethal effect of the first dosing regimen. These results are consistent with the bolus dosing experiments in which the hypothesized MTC in the brain is 200 µM. Neither dosing regimen achieved a steady 3-MPA concentration in the brain.
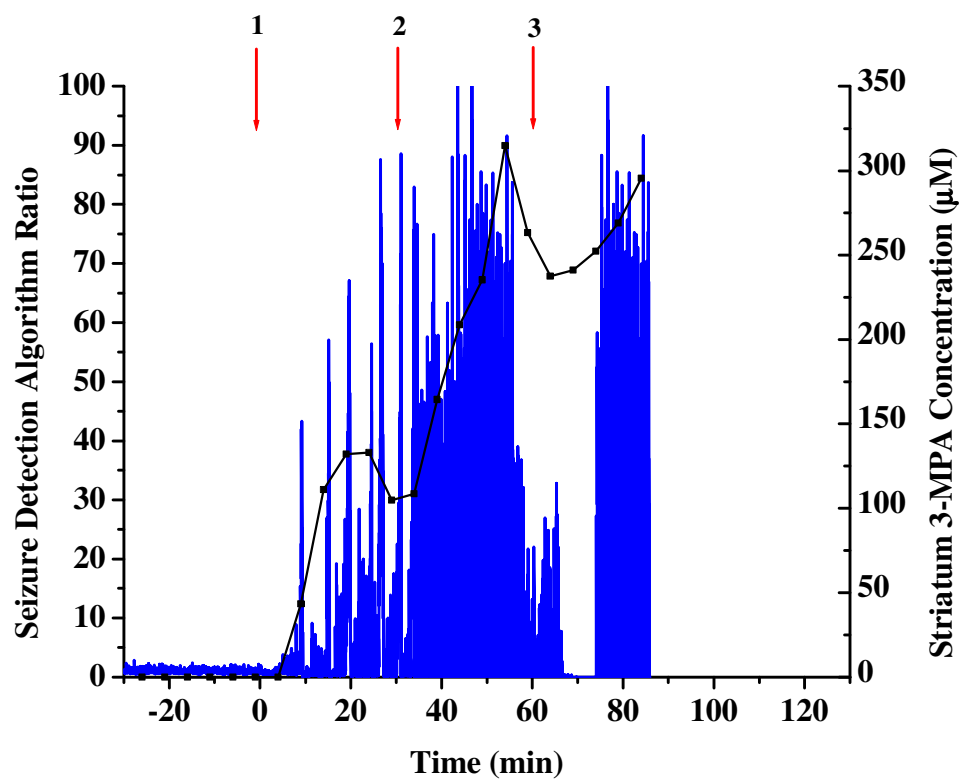
Figure 2.7. Concentration-time curves for multiple dosing scheme of 3-MPA (τ = 30 minutes). 50 mg/kg IP bolus dose administered at t = 0 minutes on the x-axis with booster doses of 46.7 mg/kg (n = 1 rat); [1 = administration of loading dose; 2,3 = administration of booster doses]
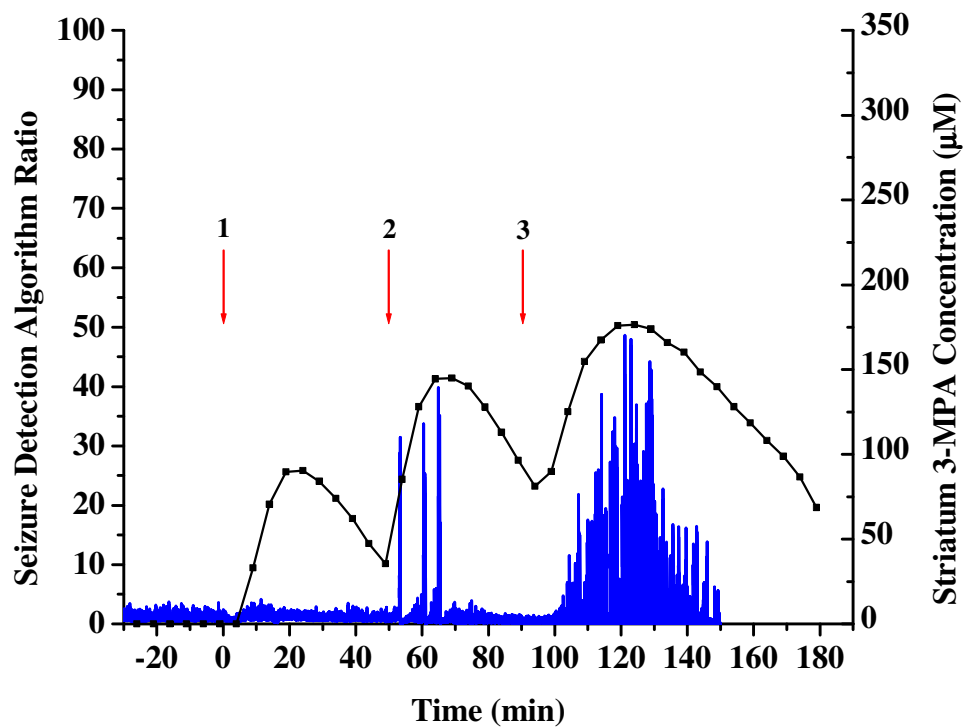
Figure 2.8. Concentration-time curves for multiple dosing scheme of 3-MPA (τ = 45 minutes). 50 mg/kg IP bolus dose administered at t = 0 minutes on the x-axis with booster doses of 42.3 mg/kg (n = 1 rat). [1 = administration of loading dose; 2,3 = administration of booster doses]

2.3.5.2. Constant Infusion Dosing with ECoG Analysis

Due to not being able to achieve a steady-state 3-MPA concentration in the brain using a multiple bolus dosing regimen, the next set of experiments used a loading dose followed by a constant infusion in an attempt to attain and maintain a steady-state concentration of 3-MPA in the brain. Based upon the initial PK studies, a bolus dose of 50 mg/kg was enough to achieve a short-lived seizure state in the rat. These data correlate well with those reported by Mares *et al.* [12] in which the median convulsant dose (CD_{50}) of 3-MPA in an adult rat was noted as 50 mg/kg. Therefore, a 60 mg/kg loading dose of 3-MPA was chosen, which was higher than the reported CD_{50} in order to assure seizure activity would occur before the infusion took effect. The i.v. bolus dose was immediately followed by a constant femoral infusion of 3-MPA at 50 mg/kg/min which was stopped 50 minutes after the initial administration. Figures 2.9(A) and 2.9(B) show the concentration-time curves using this constant infusion regimen for the blood and the brain. Figure 2.9(B) shows success 20 minutes after the loading dose / start of infusion with a steady 3-MPA concentration in the brain. Figure 2.10 displays a typical experimental data set with the 3-MPA concentration-time plot superimposed onto the corresponding EcoG recording. The time interval between 20 – 50 minutes, denoted in a box on each plot, was the time during which a steady brain concentration of 3-MPA was achieved. This time frame is a parameter that could be shortened or broken into segments to study differences in seizure activities due to 3-MPA. It was found that 30 minutes of steady-state convulsant in the brain was the longest time acceptable for inducing
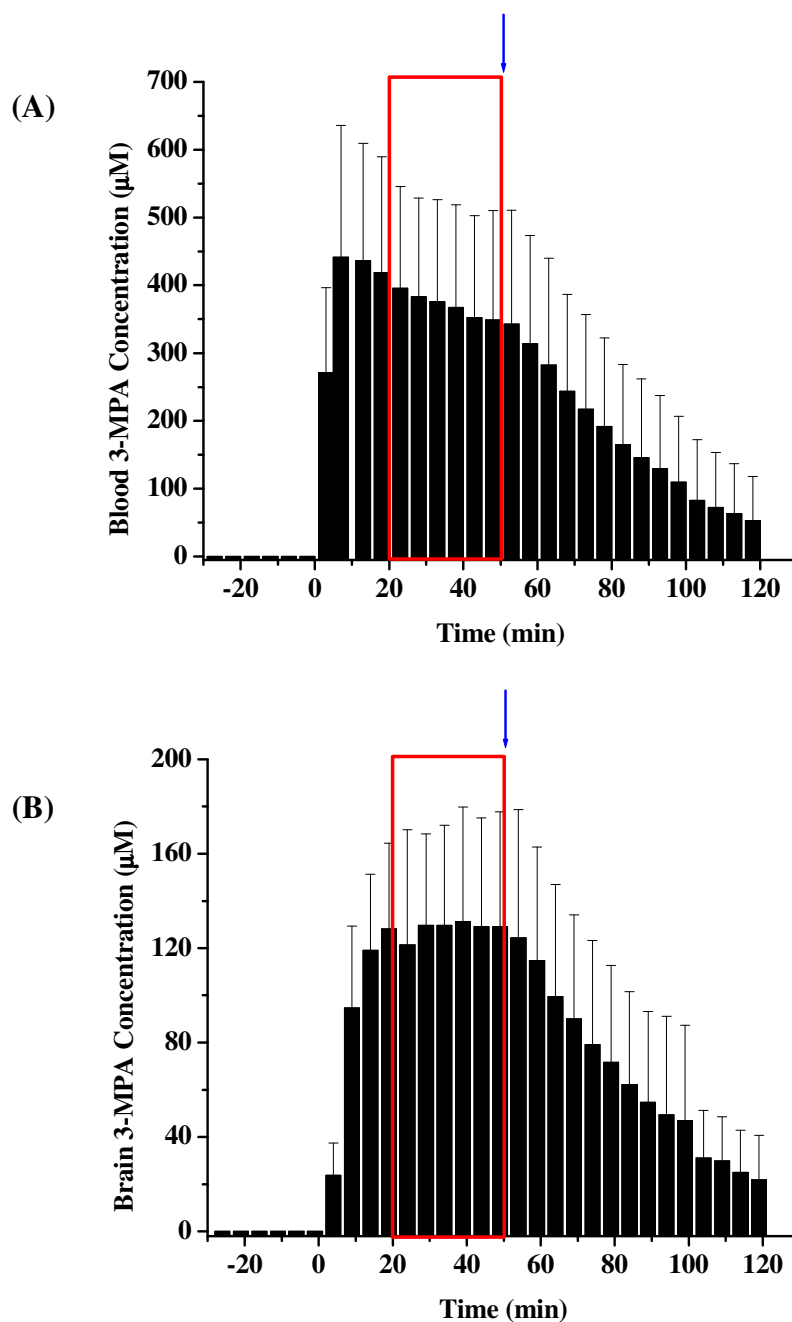
Figure 2.9. Blood and brain concentration profiles for constant infusion dosing of 3-MPA. A, average blood 3-MPA concentration (n = 9 rats); B, average brain 3-MPA concentration in striatum (n = 16 rats); 3-MPA was administered at t = 0 minutes. The boxes in each plot (t = 20-50 minutes) represent the time when a steady-state concentration of 3-MPA was achieved in the brain. The arrow represents the time in which the infusion was stopped.
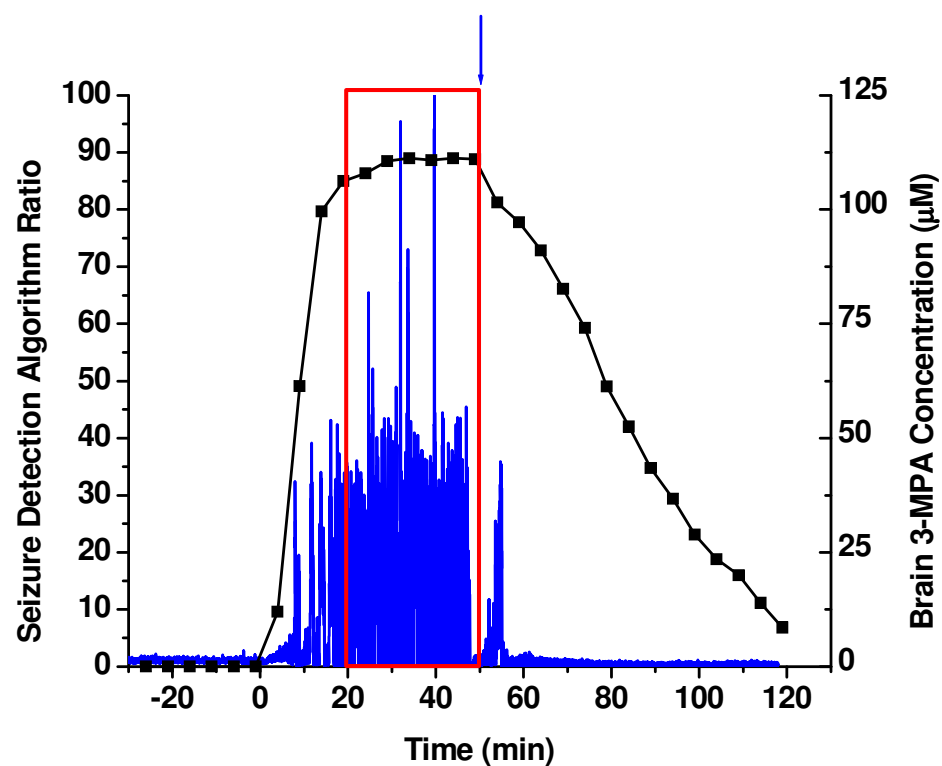
Figure 2.10: A representative plot displaying ECoG activity superimposed onto the corresponding brain [3-MPA] during constant infusion dosing. 3-MPA was administered at t = 0 minutes. All other conditions same as Figure 2.9.

Table 2.4. ECoG data for constant infusion dosing.

	60 mg/kg Bolus + 50 mg/kg/min Infusion[a]
Latency to Seizure Onset (s)	363.2 ± 148.8
Brain [3-MPA] at Seizure Onset (μM)	45.2 ± 19.1
Number of Seizures Detected	592 ± 187
Average of the Average Seizure Duration (s)	0.87 ± 1.78
R_{max}	71.8 ± 22.2

a: n = 6 rats

seizure activity and still obtaining meaningful data after cessation of the 3-MPA infusion.

Table 2.4 displays the ECoG data for the constant infusion dosing scheme. Seizure activity using the constant infusion dosing was obtained on average within 6.1 minutes, and the seizures were long-lived resembling those of the 100 mg/kg bolus dose. The average number of seizures obtained with the constant infusion dosing (592) differed significantly ($p < 0.05$) with the average number of seizures obtained with the 50 mg/kg bolus dose (9), but not with the 100 mg/kg dose (603). The average seizure intensity for this scheme, while more similar in value to the 50 mg/kg bolus dose, was not significantly different from either of the intensities arising from the administered bolus doses. Interestingly, the difference in latency to first seizure is not explained by the 3-MPA concentration, since the infusion model's did not differ statistically from that of the 50 mg/kg dose, but it did differ from the 100 mg/kg dose ($p < 0.05$). This could be explained by the dosing routes. The bolus dosing was administered i.p., while the loading dose for the infusion model was administered i.v. The 3-MPA concentration at the time of seizure onset could be closer to the 50 mg/kg dose due to the smaller amount of the convulsant introduced during the loading dose followed by the infusion with a small steady amount of convulsant.

The elimination PK for the infusion model (Table 2.5(A)) for the blood and brain are significantly different ($p < 0.01$) compared to that of the bolus dose of 50 mg/kg 3-MPA (data from Table 2.2). However, the infusion model elimination PK

86

are more similar to the 100 mg/kg bolus dose of 3-MPA. As with the 100 mg/kg

bolus dose, saturation within the brain was again observed with the constant infusion

model. This accumulative effect within the brain during the infusion model can be

discussed comparatively to that of the 100 mg/kg bolus dose. The infusion model

elimination kinetics (Table 2.5) showed that these data did not differ significantly

when compared against the 100 mg/kg dose. These data pointed to more 3-MPA

residing within the brain when the infusion occurs. This may explain why all of the

3-MPA is not eliminated before the experiment is finished. The rats only survived

approximately 70 minutes after the removal of the infusion of 3-MPA and the average

concentration in the brain upon death was 10 μM. The slow elimination kinetics are

believed to play a role in this effect.

Table 2.5. Elimination pharmacokinetics for constant infusion model. (A), average data from the blood (n = 9 rats) and brain (n = 16 rats); (B), Blood/Brain ratios for elimination parameters.

	Dosing Scheme	Sample	K_e (min^{-1})
(A)	**Constant Infusion**	**Blood**	0.034 ± 0.019
		Brain	0.030 ± 0.011
(B)	**Constant Infusion**	**Blood/Brain**	1.34 ± 0.48

The blood/brain K_e data for the infusion model (Table 2.5(B)) are significantly different from the 50 mg/kg bolus dose ($p < 0.01$), whereas there was no difference between this value and the 100 mg/kg bolus dose. This was to be expected noting the differences observed in the individual K_e data.

Using the constant infusion dosing regimen for 3-MPA produced the desired steady-state convulsant concentration within the brain. The parameters of administered concentration and length of infusion can be controlled with this steady-state dosing model in order to keep the animal between the MEC and MTC.

2.3.5.2.1. Comparison of Striatum versus Hippocampus Dosing

The final set of experiments compared two different brain regions, the striatum and the hippocampus, and used the constant infusion dosing scheme. The hippocampus was selected due to its closeness in resemblance to human limbic and temporal lobe epilepsy, which comprises 40% of all human epilepsies [37]. Again, an i.v. loading dose of 60 mg/kg 3-MPA was administered immediately followed by an i.v. infusion of 50 mg/kg/min. The infusion was ceased at 50 minutes post-introduction. Microdialysis samples were collected every 5 minutes from the striatum and hippocampus. Histology to verify the proper location of the microdialysis probes within the striatum and hippocampus was performed at Lawrence Memorial Hospital - Pathology Department using haematoxylin and eosin (H&E) staining. Example slices from both the striatum and hippocampus are shown in Figures 2.11 and 2.12, respectively.

(A)

(B)

4 mm
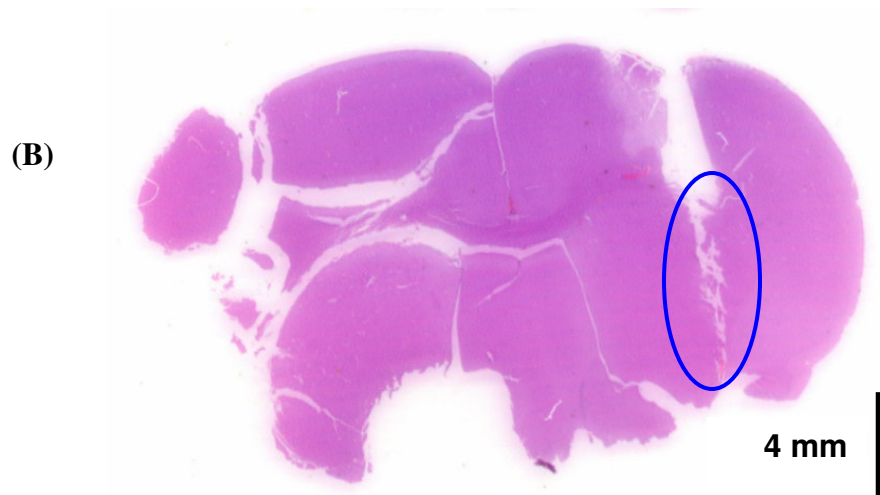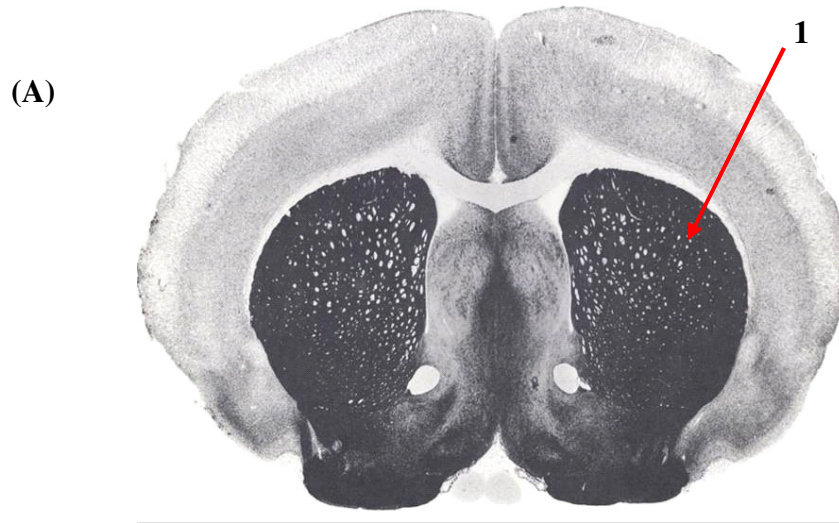
Figure 2.11. Histology of the striatum. (A) Photograph of brain slice displaying the striatal region (1) taken from Paxinos and Watson [29]. (B) Actual histological slide noting the microdialysis probe placement within the striatum. The area circled in blue represents the probe membrane. [A/P: +0.2mm; M/L: +3.2mm; D/V: -3.5mm]
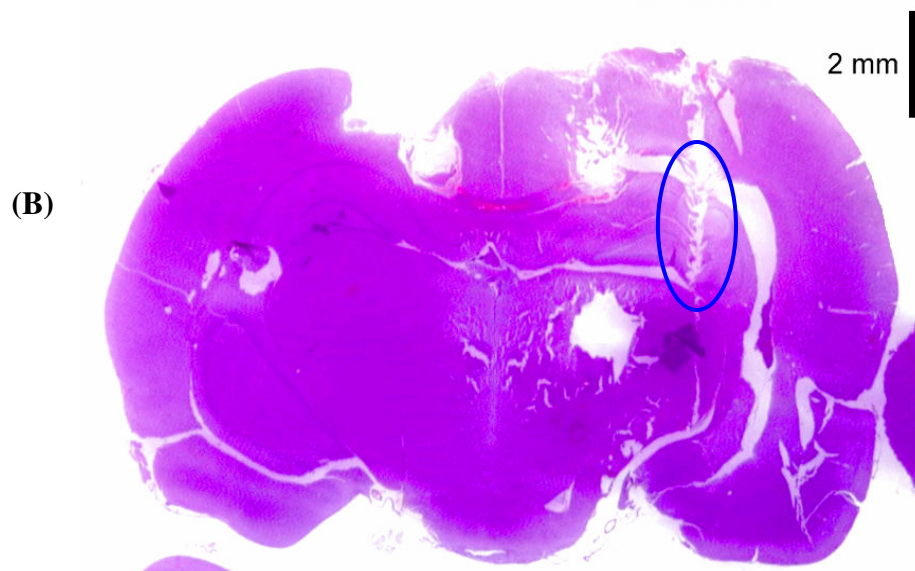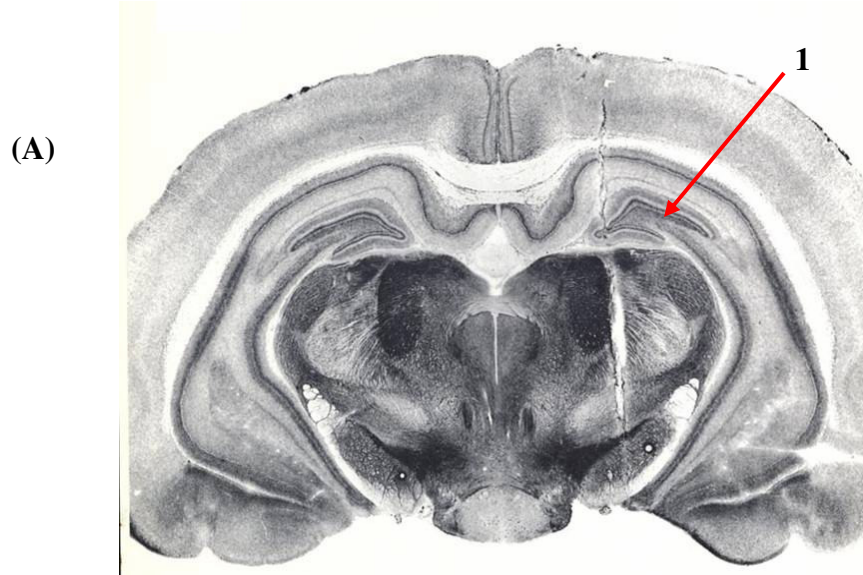
Figure 2.12. Histology of the hippocampus. (A) Photograph of brain slice displaying the hippocampal region (1) taken from Paxinos and Watson [29]. (B) Actual histological slide noting the microdialysis probe placement within the hippocampus. The area circled in blue represents the probe membrane. [A/P: -5.6mm; M/L: +4.8mm; D/V: -5.0mm]

Figures 2.13(A) and 2.13(B) detail brain concentration-time plots for the constant infusion dosing regimen. A steady-state concentration of 3-MPA was observed in both the hippocampus and the striatum approximately 20 minutes following the administration of the convulsant. However, the average C_{max} of 3-MPA achieved within the hippocampus was approximately 31% higher than that obtained in the striatum (193 μM vs 140 μM). Table 2.6 details these observations. The C_{max} differed significantly ($p < 0.05$) between the striatum and hippocampus during the steady-state phase of the infusion model. While still below the previously noted MTC of 200 μM for the striatum, the concentration in the hippocampus was slowly approaching this value. This would then further the finding that 30 minutes of steady-state convulsant in the brain was an acceptable time frame to induce seizures without the possibility of crossing the MTC threshold.

Table 2.6. Comparison of constant infusion dosing model in striatum and hippocampus (n = 3 rats).

	C_{max} (μM)[a]	K_e (min^{-1})
Striatum	139.9 ± 15.6	0.020 ± 0.007
Hippocampus	192.5 ± 5.3	0.023 ± 0.003

a: $p < 0.05$
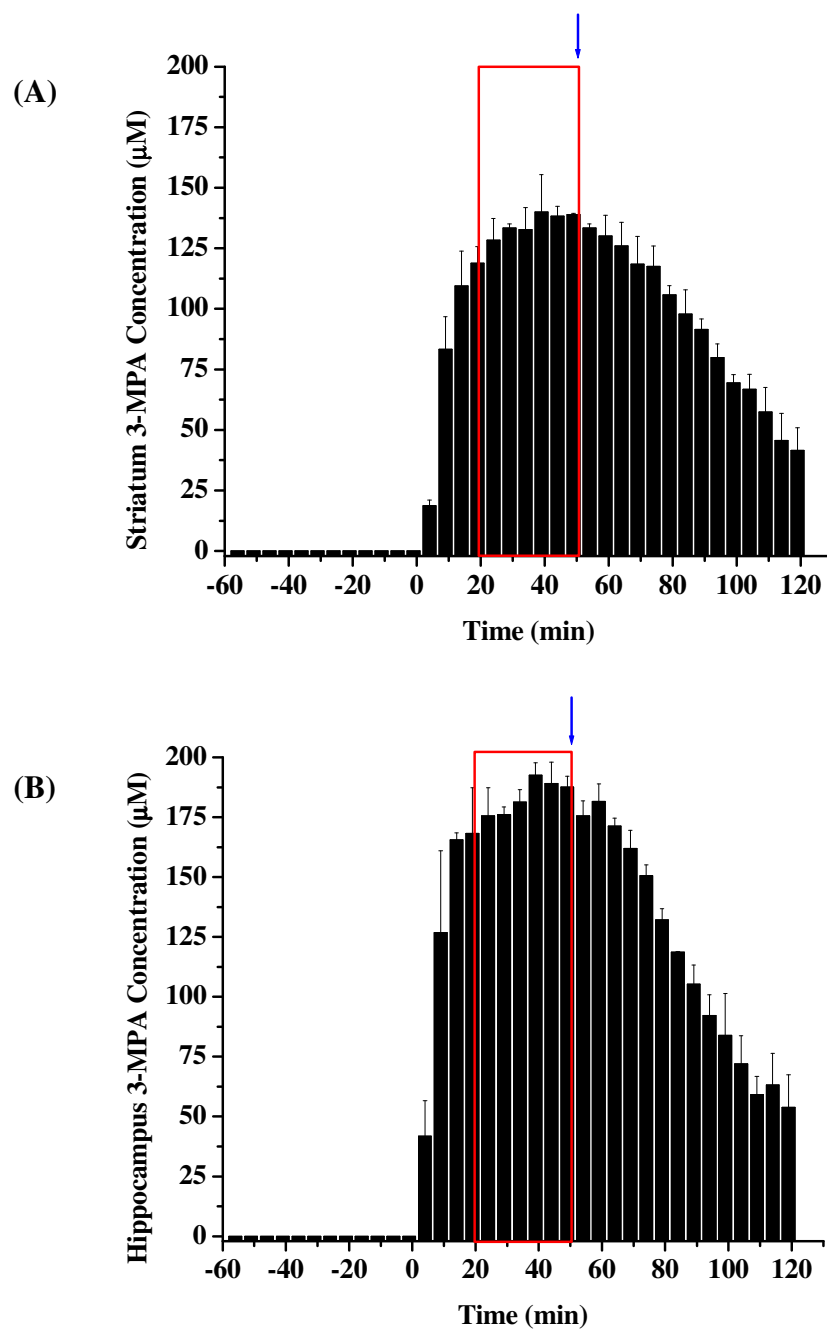
Figure 2.13. Brain concentration-time profiles for constant infusion dosing of 3-MPA. [3-MPA] measured from the (A) striatum and (B) hippocampus simultaneously (n = 3 rats). 3-MPA was administered at t = 0 minutes All other conditions same as Figure 2.9.

The K_e did not differ significantly between the striatum and hippocampus (Table 2.6); the 3-MPA eliminated from the hippocampus at a comparable rate to that of the striatum. While it appeared from Figure 2.13(B) that the 3-MPA eliminates more rapidly from the hippocampus than the striatum, there was no statistical difference between the two brain regions.

2.3.5.3. Anticonvulsant Dosing

In order to verify that the 3-MPA seizure model developed in this study was inducing hyperexcitable cortical brain tissue, a well known anticonvulsant, diazepam, was administered to block the seizure activity. Diazepam, a benzodiazepine having a central nervous system depressant effect, is an antiepileptic drug which is administered routinely for epileptic fits [37]. Theoretically, a dose of diazepam, which is also a GABA agonist, increases the seizure threshold by increasing inhibition in the brain. This would cause the seizures elicited by 3-MPA to become non-existent due to the reversal of the action of the convulsant.

Thirty minutes after beginning the constant infusion dosing experiment (10 minutes into the steady-state 3-MPA concentration), a 20 mg/kg i.v. bolus dose of diazepam was administered. Figure 2.14(A) and 2.14(B) display the typical results from this experiment. In Figure 2.14(A), a dose of diazepam alone did not to affect baseline brain activity. In Figure 2.14(B), approximately three minutes following the administration of 20 mg/kg diazepam, the seizure activity ceased. This plot was overlayed with the concentration of 3-MPA in the brain during the experiment and
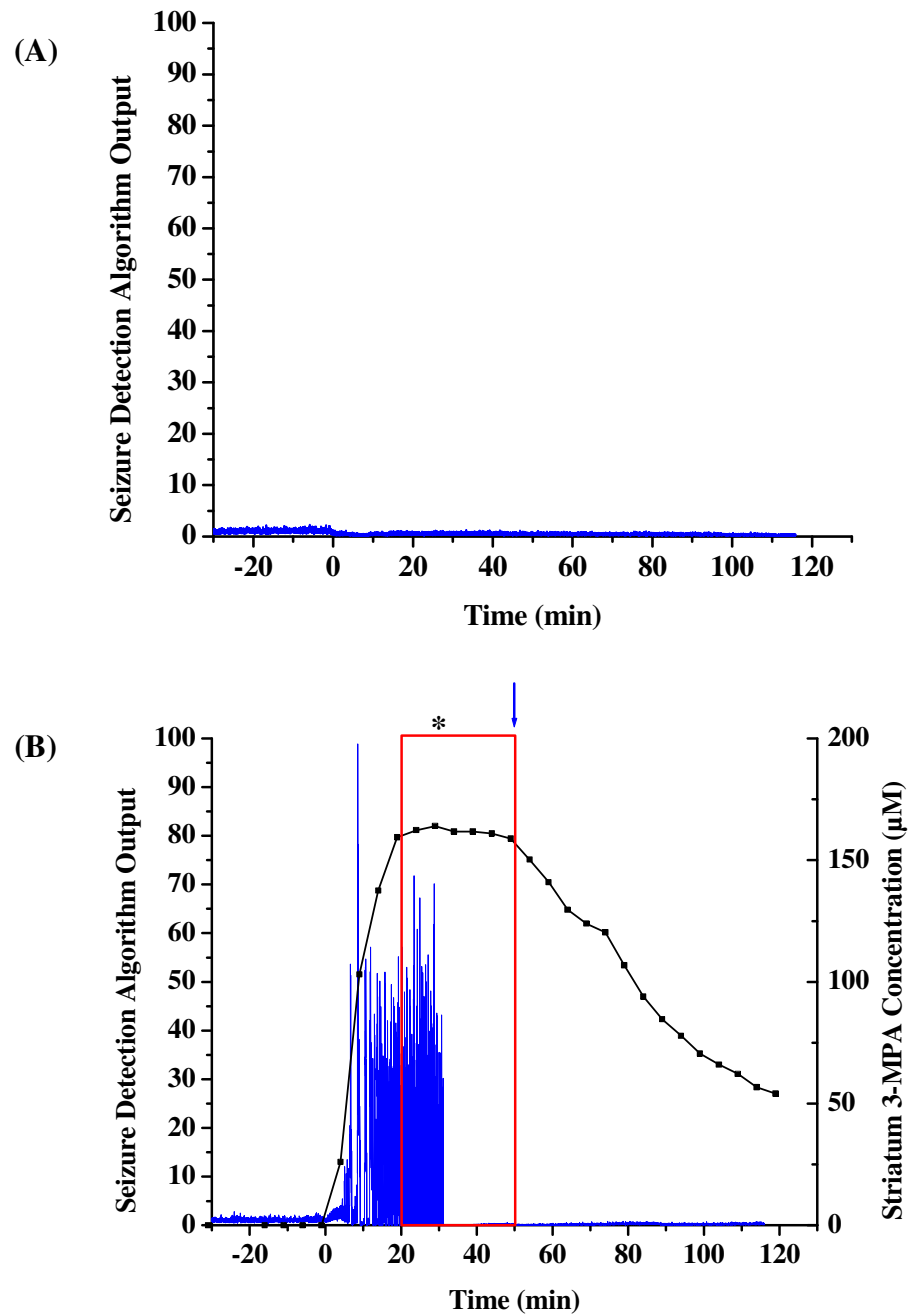
Figure 2.14. ECoG activity following diazepam administration. (A) Example ECoG plot displaying background cortical brain activity following a "sham" dose of 20 mg/kg diazepam administered at t = 0 minutes. (B) A representative plot displaying ECoG recording with the corresponding brain 3-MPA concentration superimposed. 3-MPA was administered at t = 0 minutes. 20 mg/kg diazepam administered at t = 30 minutes (*). All other conditions same as Figure 2.9.

shows that while the steady-state of 3-MPA remained in the brain until the infusion was removed, the seizure activity stopped. Therefore, the developed seizure model was effective for the study of epileptic activity and also the manipulation of the seizure activity without affecting the dosing scheme.

2.4. Conclusions

This is the first known study that reports on the PK of the known convulsant, 3-MPA. The concentration of 3-MPA in the brain (both striatum and hippocampus) was successfully monitored *in vivo* and in real-time. The model was also able to maintain a steady concentration within the brain for a given time period which lead to a PK-PD correlation for this model. This chemical seizure model allows for the future analysis of neurochemical events as they are related to the convulsant concentration in the brain. Having this independent variable accessible for future experiments allows for a better correlation of the neurochemical changes that occur due to the administration of 3-MPA and thus with epileptic seizures.

2.5. References

1.   Hu, H., Mylon, S.E., and Benoit, G., *Distribution of the thiols glutathione and 3-mercaptopropionic acid in Connecticut lakes.* Limnol. Oceanogr., **2006**, 51: 2763-2774.

2.   Sendroiu, I.E., Mertens, S.F.L., and Schiffrin, D.J., *Plasmon interactions between gold nanoparticles in aqueous solution with controlled spatial separation.* Phys. Chem. Chem. Phys., **2006**, 8: 1430-1436.

3.   Pedrosa, V.A., Lowinsohn, D., and Bertotti, M., *FIA determination of paracetamol in pharmaceutical drugs by using gold electrodes modified with a 3-mercaptopropionic acid monolayer.* Electroanalysis, **2006**, 18: 931-934.

4.   Chow, E., Wong, E.L.S., Bocking, T., Nguyen, Q.T., Hibbert, D.B., and Gooding, J.J., *Analytical performance and characterization of MPA-Gly-Gly-His modified sensors.* Sens. Actuators B Chem., **2005**, 111-112: 540-548.

5.   O'Connell, B.K., Towfighi, J., Kofke, W.A., and Hawkins, R.A., *Neuronal lesions in mercaptopropionic acid-induced status epilepticus.* Acta Neuropathol., **1988**, 77: 47-54.

6.   Towfighi, J., Kofke, W.A., O'Connell, B.K., Housman, C., and Graybeal, J.M., *Substantial nigra lesions in mercaptopropionic acid induced status epilepticus: A light and electron microscopic study.* Acta Neuropathol., **1989**, 77: 612-620.

7.   de Sarro, G., Ferreri, G., Gareri, P., Russo, E., de Sarro, A., Gitto, R., and Chimirri, A., *Comparative anticonvulsant activity of some 2,3-benzodiazepine derivatives in rodents.* Pharmacol. Biochem. Behav., **2003**, 74: 595-602.

8.   Hocht, C., Lazarowski, A., Gonzalez, N.N., Auzmendi, J., Opezzo, J.A.W., Bramuglia, G.F., Taira, C.A., and Giradi, E., *Nimodipine restores the altered hippocampal phenytoin pharmacokinetics in a refractory epileptic model.* Neurosci. Lett., **2007**, 413: 168-172.

9.   Loscher, W., *3-mercaptopropionic acid: Convulsant properties, effects on enzymes of the gamma-aminobutyric acid system in mouse brain and antagonism by certain anticonvulsant drugs, aminooxyacetic acid and gabaculine.* Biochem. Pharmacol., **1979**, 28: 1397-1407.

10. Sprince, H., Parker, C.M., Josephs, J.A., and Magazino, J., *Convulsant activity of homocysteine and other short-chain mercaptoacids: Protection therefrom.* Annals NY Acad. Sci., **1969**, 166: 323-325.

11. Sprince, H., Parker, C.M., and Smith, G.G., *3-mercaptopropionic acid: Convulsant and lethal properties compared with other sulfur-convulsants; protection therefrom.* Agents Actions, **1970**, 1: 231-233.

12. Mares, P., Kubova, H., Zouhar, A., Folbergrova, J., Koryntova, H., and Stankova, L., *Motor and electrocorticographic epileptic activity induced by 3-mercaptopropionic acid in immature rats.* Epilepsy Res., **1993**, 16: 11-18.

13. Netopilova, M., Drsata, J., Haugvicova, R., Kubova, H., and Mares, P., *Inhibition of glutamate decarboxylase activity by 3-mercaptopropionic acid has different time course in the immature and adult rat brains.* Neurosci. Lett., **1997**, 226: 68-70.

14. Skerritt, J.H. and Johnston, G.A.R., *Enhancement of excitant amino acid release from rat brain slices by the convulsant 3-mercaptopropionic acid.* Brain Res., **1983**, 258: 165-169.

15. Arnaiz, G.R.d.L., Canal, M.A.d., and Roberts, E.D., *Alteration of GABA system and purkinje cells in rat cerebellum by the convulsant 3-mercaptopropionic acid.* J. Neurochem., **1972**, 19: 1379-1385.

16. Arnaiz, G.R.d.L., Canal, M.A.d., Robiolo, B., and Pacheco, M.M.d., *The effect of the convulsant 3-mercaptopropionic acid on enzymes of the gamma-aminobutyric acid system in the rat cerebral cortex.* J. Neurochem., **1973**, 21: 615-623.

17. Fan, S.G., Wusteman, M., and Iversen, L.L., *3-mercaptopropionic acid inhibits GABA release from rat brain slices in vitro.* Brain Res., **1981**, 229: 379-387.

18. Timmerman, W., Zwaveling, J., and Westerink, B.H.C., *Characterization of extracellular GABA in the substantia nigra reticulata by means of brain microdialysis.* Naunyn-Schmiedeberg's Arch. Pharmacol., **1992**, 345: 661-665.

19. Lamar, C., *Mercaptopropionic acid: A convulsant that inhibits glutamate decarboxylase.* J. Neurochem., **1970**, 17: 165-170.

20. Tunnicliff, G., *Action of inhibitors on brain glutamate decarboxylase.* Int. J. Biochem., **1990**, 22: 1235-1241.

21. Netopilova, M. and Drsata, J., *3-mercaptopropionic acid, a useful tool in experimental epilepsy studies.* Folia Pharm. Univ. Carol., **1995**, 19: 63-78.

22. Welling, P.G., *Pharmacokinetics: Processes, Mathematics, and Applications.* 2nd ed. **1997**, Washington, DC: American Chemical Society.

23. Shargel, L. and Yu, A., *Applied Biopharmaceutics & Pharmacokinetics.* 4th ed, ed. C.L. Mehalik. **1999**, New York: McGraw-Hill.

24. Li, Y., Peris, J., Zhong, L., and Derendorf, H., *Microdialysis as a tool in local pharmacodynamics.* AAPS J., **2006**, 8: E222-E235.

25. Hamani, C., Hodaie, M., and Lozano, A.M., *Present and future of deep brain stimulation for refractory epilepsy.* Acta Neurochir. (Wein), **2005**, 147: 227-229.

26. Osorio, I., Frei, M.G., Sunderam, S., Giftakis, J., Bhavaraju, N.C., Schaffner, S.F., and Wilkinson, S.B., *Automated seizure abatement in humans using electrical stimulation.* Ann. Neurol., **2005**, 57: 258-268.

27. Stenken, J.A., Puckett, D.L., Lunte, S.M., and Lunte, C.E., *Detection of N-acetylcysteine, cysteine and their disulfides in urine by liquid chromatography with a dual-electrode amperometric detector.* J. Pharm. Biomed. Anal., **1990**, 8: 85-89.

28. Allison, L.A. and Shoup, R.E., *Dual electrode liquid chromatography detector for thiols and disulfides.* Anal. Chem., **1983**, 55: 8-12.

29. Laue, T., *Analytical ultracentrifugation: a powerful 'new' technology in drug discovery.* Drug Discov. Today, **2004**, 1: 309-315.

30. Lebowitz, J., Lewis, M.S., and Schuck, P., *Modern analytical ultracentrifugation in protein science: A tutorial review.* Protein Sci., **2002**, 11: 2067-2079.

31. Telting-Diaz, M., Scott, D.O., and Lunte, C.E., *Intravenous microdialysis sampling in awake, freely-moving rats.* Anal. Chem., **1992**, 64: 806-810.

32. Watson, C. and Paxinos, G., *The Rat Brain: In Stereotax Coordinates.* 2nd ed. **1986**, San Diego: Academic Press.

33. Osorio, I., Frei, M.G., Manly, B.F.J., Sunderam, S., Bhavaraju, N.C., and Wilkinson, S.B., *An introduction to contingent (closed-loop) brain electrical*

stimulation for seizure blockage, to ultra-short-term clinical trials, and to multidimensional statistical analysis of therapeutic efficacy. J. Clin. Neurophysiol., **2001**, 18: 533-544.

34.   Osorio, I., Frei, M.G., and Wilkinson, S.B., *Real-time automated detection and quantitative analysis of seizures and short-term prediction of clinical onset.* Epilepsia, **1998**, 39: 615-627.

35.   Osorio, I., Frei, M.G., Giftakis, J., Peters, T., Ingram, J., Turnbull, M., Herzog, M., Rise, M.T., Schaffner, S., Wennberg, R.A., Walczak, T.S., Risinger, M.W., and Ajmone-Marsan, C., *Performance reassessment of a real-time seizure-detection algorithm on long ECoG series.* Epilepsia, **2002**, 43: 1522-1535.

36.   Schoenwald, R.D., *Pharmacokinetic principles of dosing adjustments understanding the basics* **2001**, Pennsylvania: Technomic. 258.

37.   Siegel, G.J., Agranoff, B.W., Albers, R.W., Fisher, S.K., and Uhler, M.D., eds. *Basic Neurochemistry: Molecular, Cellular, and Medical Aspects*. 6th ed. **1999**, Lippincott Williams & Wilkins: Philadelphia.

Chapter 3.

Neurochemical Correlation of Glutamate, GABA, and Dopamine to 3-MPA Chemical Seizure Model

3.1. Introduction

3.1.1. Background and Significance

Epileptic seizures are known to result from imbalances within the neurotransmitter systems in the brain. Historically, epileptic seizures have been viewed as hyperexcitable events [1, 3, 4]. This collection of research all point to the excitatory and inhibitory amino acid neurotransmitters, specifically glutamate (Glu) and γ-aminobutyric acid (GABA), and the biogenic amine neurotransmitters, in particular dopamine (DA), as the main components of interest in gaining a more thorough neurochemical understanding of epilepsy. The inner workings of how Glu, GABA, DA, and all other important transmitters can be described as complex at best. Much work has been accomplished in order to understand the relationships between the amino acid and biogenic amine neurotransmitters in many different areas of the brain, including the striatum [2, 5-9], hippocampus [10], nucleus accumbens [11], and ventral tegmental area [12, 13], but many of the findings are still unexplained.

A comprehensive understanding of how neurotransmitter systems are interconnected to various epileptic seizure models is invaluable to the advancement of treatments for epilepsy and the development of new antiepileptic drugs (AEDs). The

ability to better understand the neurophysiology of epilepsy and epileptic seizures would allow for better animal seizure models to be developed which mimic more closely human epilepsy. As introduced in Chapter 2, a good working knowledge of the neurotransmitter systems in relation to 3-MPA is non-existent. The ability to obtain data, regarding the changes in neurotransmission in different brain regions during the 3-MPA chemical seizure model, is critical in strengthening the developed model for its further use in the understanding of generalized seizures in the laboratory and clinical settings.

3.1.2. Amino Acid Neurotransmitters

The structures of the amino acid neurotransmitters of interest are shown in Figure 3.1. The main amino acids of interest are Glu, the major excitatory neurotransmitter, and GABA, the major inhibitory neurotransmitter. Other amino acids such as glycine (Gly), aspartate (Asp), and arginine (Arg) can be monitored but are not of critical importance to this research as the mechanism of action of 3-MPA directly affects the Glu/GABA system (as discussed in Section 2.1.3.). Figure 3.2 displays the biochemical synthesis of Glu and GABA.

In the brain, across all regions, a certain Glu/GABA ratio exists [1]. This balance in excitation/inhibition is what prevents the brain from being epileptic. Disruptions to this fine balance within the brain, such as the administration of 3-MPA, will cause the inhibitory threshold to lower, resulting in epileptic seizures. An
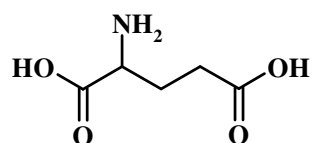
Glutamate (Glu)

pKa ~ 2.17(most basic)
pKa ~ 9.76 (most acidic)
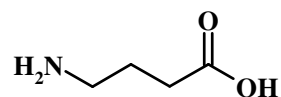
γ-Hydroxybutyric Acid (GABA)

pKa ~ 4.44(most basic)
pKa ~ 11.24 (most acidic)

Figure 3.1. Amino acid neurotransmitters of interest. The pKa values were obtained using SciFinder® Scholar 2006.
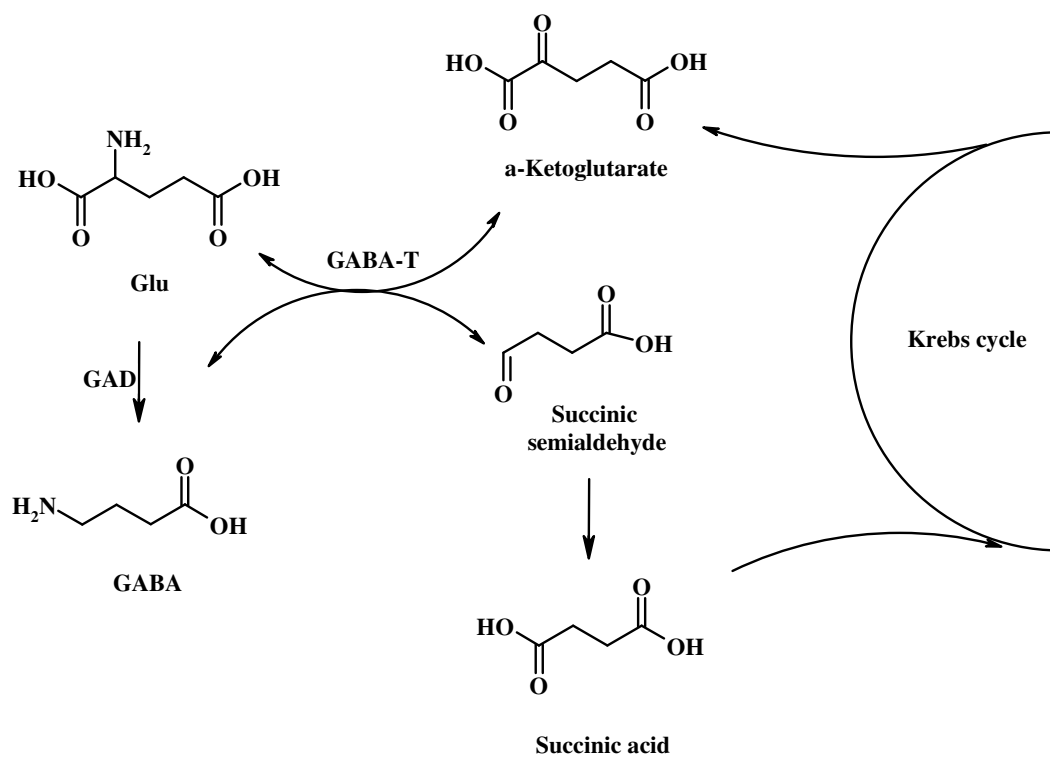
Figure 3.2. Glu and GABA biosynthesis. Adapted from Siegel *et al.* [1].

accurate interpretation of the deviations within the Glu/GABA ratio will help to further understand the mechanism of 3-MPA induced seizures.

3.1.3. Biogenic Amine Neurotransmitters

The biogenic amine neurotransmitters of interest are shown in Figure 3.3. These are DA, norepinephrine (NE), serotonin (5-HT), and any of their metabolites that can be monitored, including 3,4-dihydroxyphenylacetic acid (DOPAC) and homovanillic acid (HVA). Figures 3.4 and 3.5 show the biosynthetic pathways for the biogenic amines.

It is believed that the biogenic amine neurotransmitters, along with the amino acid neurotransmitters, play an extensive role in regulating the initiation and spread of seizure activity [4]. Evidence for the correlation of glutamateric and dopaminergic neurotransmission has been reported extensively in the literature [14-16]. It is believed that glutamate and N-methyl-D-aspartate (NMDA) act together to facilitate increases in DA release in the striatum [17]. Knowledge of DA neurotransmission as well as other biogenic amines and its correlation with the amino acid neurotransmitters would greatly enhance the effective understanding of the developed 3-MPA seizure model.

3.1.4. Current Analytical Methodologies Used for the Determination of Neurotransmitters in Biological Samples

The majority of literature available suggests the use of (liquid chromatography) LC and capillary electrophoresis (CE) instrumentation for the
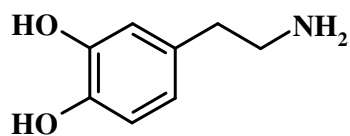
Dopamine (DA)

pKa ~ 9.39 (most acidic)
pKa ~ 10.11 (most basic)
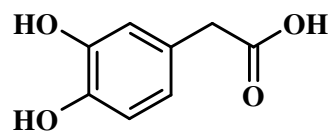
**3,4-Dihydroxyphenylacetic acid
(DOPAC)**

pKa ~ 4.42 (most acidic)
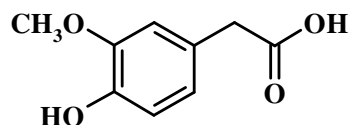
Homovanillic acid (HVA)

pKa ~ 4.39 (most acidic)
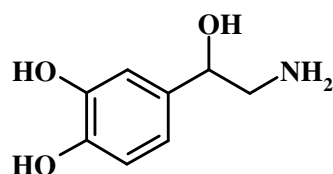
Norepinephrine (NE)

pKa ~ 9.57 (most acidic)
pKa ~ 8.36 (most basic)
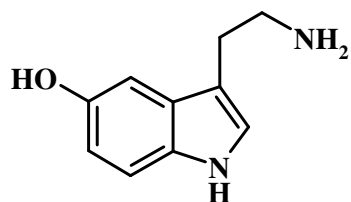
**5-Hydroxytryptamine
(5-HT)**

pKa ~ 9.61 (most acidic)
pKa ~ 10.31 (most basic)
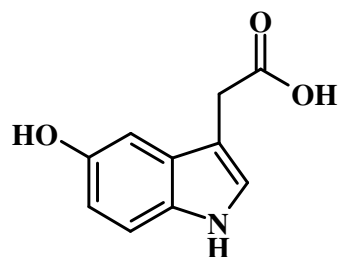
**5-Hydroxyindole-3-acetic acid
(5-HIAA)**

pKa ~ 4.54 (most acidic)

Figure 3.3. Biogenic amine neurotransmitters of interest. The pKa values were obtained using SciFinder® Scholar 2006.
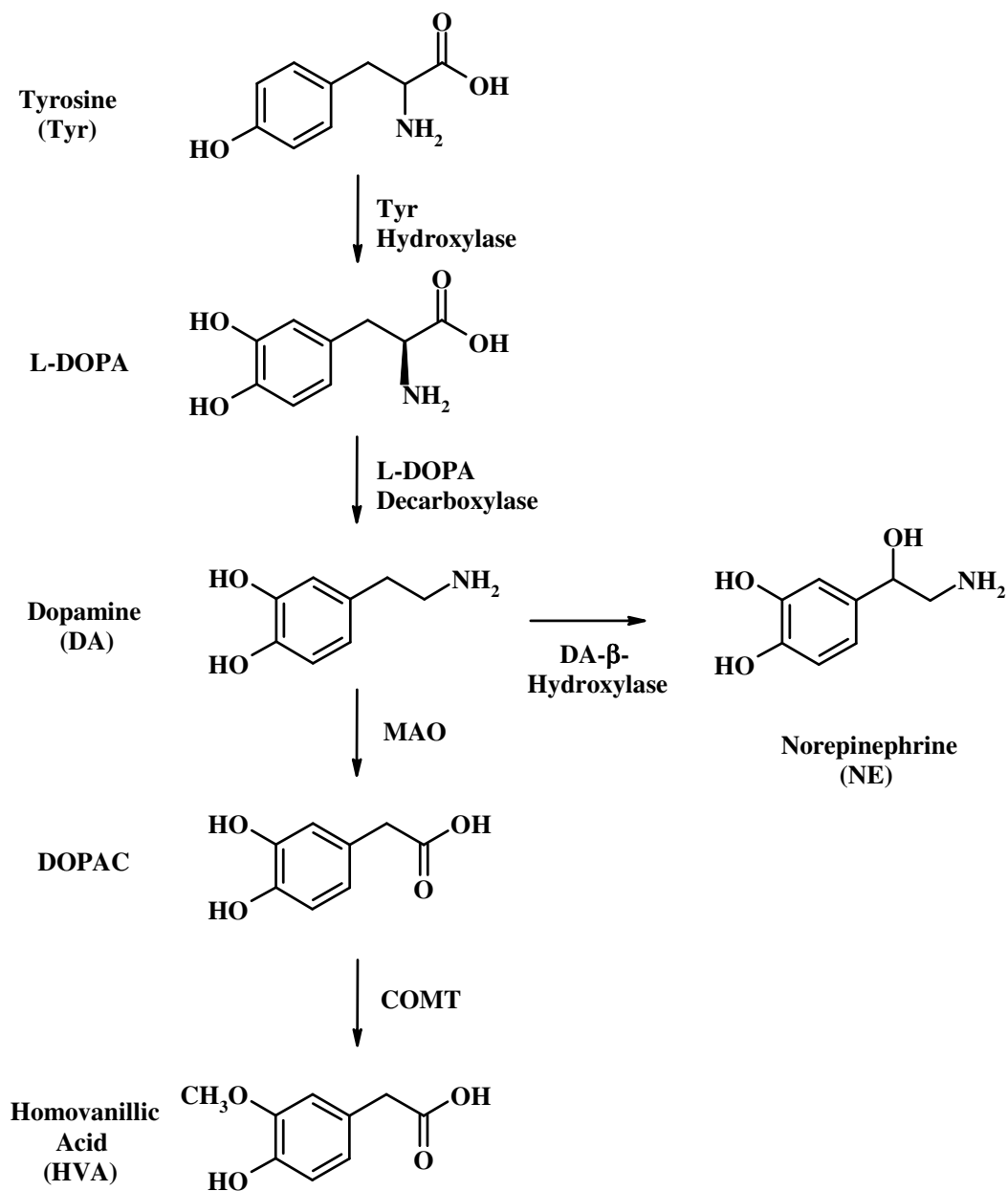
Figure 3.4. Biosynthesis of catecholamines. Adapted from
Seigel *et al*. [1].
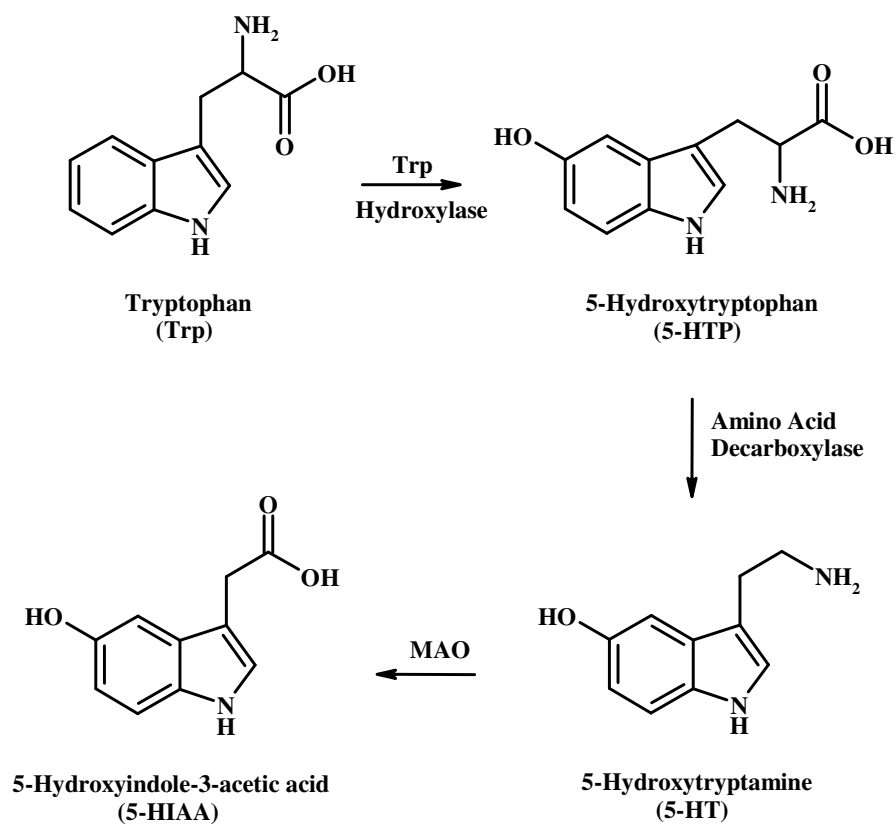
Figure 3.5. Major metabolites of tryptophan.

purpose of separating and detecting amino acid and biogenic amine neurotransmitters from biological samples. LC coupled with both electrochemical (EC) and fluorescence detection has been used extensively for these determinations. The biogenic amine neurotransmitters have been analyzed from a wide array of matrices including brain microdialysates [18], brain homogenates [19], and urine [20] using LC-EC. LC-Fluorescence has been used for the detection of amino acid neurotransmitters in brain microdialysate samples in regard to PK-PD relationships and brain injury [21-23].

CE coupled with laser-induced fluorescence (LIF) is predominately used for the detection of amino acid neurotransmitters in biological matrices. Several authors have used this technique to detect these neurotransmitters in epileptic rat brains [24], pharamacologically-manipulated rat brain microdialysates [25], and urine / blood samples [26]. Other common modes of detection of these neurotransmitters include the use of analyte specific sensors, such as for Glu [27] and voltammetry for analytes such as DA [28].

3.1.5. Sample Derivatization Schemes

As discussed in Section 3.1.4., the analysis of amino acid neurotransmitters in microdialysis samples is commonly accomplished using LC and CE separation methods with various detection schemes. However, the native amino acids in the microdialysates do not contain fluorescent or electroactive moieties. Therefore, the

microdialysis samples must first be derivatized in order to become fluorescent or electroactive.

The two most common derivatization schemes employed for the analysis of the amino acid neurotransmitters via LC are *o*-phthalaldehyde (OPA) and naphthalene-2,3-dicarboxyaldehyde (NDA). OPA derivatization was first introduced by Simons and Johnson in 1976 [29]. OPA is an effective reagent for the purpose of selectively derivatizing primary amines in the presence of an alkyl thiol (e.g. β-mercaptoethanol (βME)), as the reducing agent in the formation 1-alkylthio-2-alkylisoindoles which are both fluorescent and electroactive [29]. The OPA/βME method was employed by Lindroth and Mopper the same year for the separation and analysis of amino acids and ammonia in seawater [30]. While OPA is an attractive derivatizing reagent due to its lack of fluorescence or electroactive moieties, the main drawback in using OPA/βME as a derivatization scheme for primary amines is the instability of the products formed. Jacobs *et al*. studied the OPA/βME more closely and found that while the derivatized products are formed within one minute, the fluorescent isoindoles quickly degrade to form non-fluorescent by-products [31]. This discovery severely limited the possibility of OPA/βME being used as an effective pre-column labeling technique, especially for coupling with automated LC analysis. In 1987, Jacobs offered a new reducing agent for use with OPA which helped form more stable derivatives [32]. It was shown that the substitution of sulfite for βME created N-alkyl-1-isoindole sulfonates which were stable for upwards of 5 hours [32, 33].

An alternative derivatization agent, NDA, was first introduced in 1986 by Carlson *et al*. [34]. NDA is selective in the labeling of primary amines. When NDA is coupled with the cyanide ion (CN^-) as a nucleophile, N-substituted-1-cyanobenz[f]isoindole adducts are formed (Figure 3.6). de Montigny *et al*. used the NDA/CN^- reaction to assay the amino acids following an enzymatic hydrolysis of glucogon [35]. The authors showed that the N-substituted-1-cyanobenz[*f*]isoindole adducts are stable for over 11 hours, which is the main advantage of the NDA/CN^- derivatization scheme over OPA/βME derivatization. The NDA/CN^- derivatization scheme has since been used extensively for the LC and CE analysis of amino acid neurotransmitters as elevated levels of these play a large role in disorders such as depression [21], sleep states [36], and epilepsy [24].

3.1.6. Specific Aims of Research

The goal of this research was to apply LC methods in order to determine the changes, or lack thereof, in the amino acid and biogenic amine neurotransmitters from the striatum and hippocampus as related to the 3-MPA chemical seizure model discussed in Chapter 2. Existing LC methods were modified to include the analysis of both the concentration of the convulsant in the brain and the biogenic amines using dual-electrode electrochemical detection (LC-EC), as well as derivatized microdialysis samples to detect the amino acid neurotransmitters using fluorescence detection (LC-Fluorescence). As two analytical instruments were required for the sample analyses, the temporal resolution of the experiments discussed herein was 5
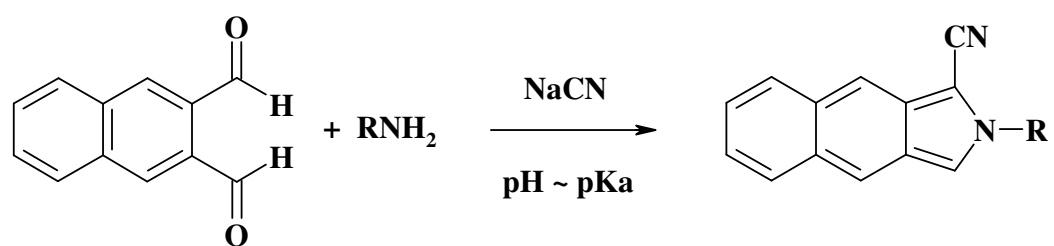
Figure 3.6. NDA/CN- reaction scheme with primary amines.

minutes. This was the minimum volume which could be collected and subsequently split for analysis on both LC instruments.

The neurotransmitter data were used to correlate with simultaneously obtained ECoG data (discussed in Chapter 2). Further PK-PD relationships were established between the concentration of the convulsant in the brain and any deviations in the neurotransmitter systems. Also, the biogenic amine and amino acid neurotransmitters were studied for possible correlations or modulatory actions.

3.2. Materials and Methods

3.2.1. Chemicals / Reagents

Monobasic sodium phosphate, disodium ethylenediamine tetraacetate (Na$_2$EDTA), 85% o-phosphoric acid, acetonitrile, methanol, and 0.3 µm alumina powder were obtained from Fisher Scientific (Pittsburgh, PA). Ammonium acetate, 1-octanesulfonic acid [sodium salt] (SOS), sodium tetraborate decahydrate, boric acid, L-glutamic acid (Glu), L-aspartic acid (Asp), L-arginine (Arg), γ-amino-n-butyric acid (GABA), DL-2-aminoadipic acid (AAP), sodium cyanide, 3,4-dihydroxybenzylamine (DHBA), 3,4-dihydroxyphenethylamine hydrochloride (DA), L-arterenol (NE), homovanillic acid (HVA), 3,4-dihydroxyphenylacetic acid (DOPAC), 5-hydroxytryptamine (5-HT), 5-hydroxyindoleacetic acid (5-HIAA), cyclothiazide, and (-)-2-amino-6-mercaptopurine riboside were obtained from Sigma-Aldrich (St. Louis, MO). Naphthalene-2,3-dicarboxaldehyde (NDA) was obtained from Invitrogen (Carlsbad, CA). All solutions were prepared in 18.2 MΩ distilled,

deionized water (Labconco, Kansas City, MO) and filtered through 0.22 μm pore size membrane filters prior to use unless otherwise noted.

3.2.2. Microdialysis Sample Considerations

Following brain surgery, the animals were allowed to recover (under anesthesia at a rate of 0.2 mL of 100 mg/mL ketamine administered intramuscular (i.m.) every 1.5 hours) for a period of 6 hours. During this time, the environment surrounding the microdialysis probe is allowed to "recover" from the trauma suffered during the microdialysis probe implantation. It is well noted that during the time period following the implantation of a brain microdialysis probe that gliosis occurs [37, 38]. Also during this time period, the brain tissue function becomes disturbed due to the excess neurochemical release of numerous cellular storage compartments as well as increased glucose metabolism and decreased blood flow [38]. The time lapse between the implantation of the brain probe and the commencement of the experiment can last from 30 minutes to 24 hours or longer depending upon the analyte(s) of interest for the study. However, it is necessary that the appropriate length of time has passed in order to be able to monitor a steady basal level of the analyte(s).

Upon collection of the microdialysis sample, care must be taken in regards to the sample storage if the sample cannot be analyzed immediately. For the experiments discussed in this Chapter, two different LC instruments were employed to accomplish all of the required analyses (LC-EC and LC-Fluorescence). The first

step after sample collection was to split the sample into 2.5 µL aliquots into two separate vials. Then a volume of an analytical internal standard (IS) was added to each vial. This IS was prepared in 0.1 M perchloric acid. The purpose of the perchloric acid was to severely slow the rate of autooxidation of the analytes present in the sample matrix, aCSF. It has been shown that the addition of perchloric acid to an aCSF matrix containing neurotransmitters, especially the catecholamines, which are very low in concentration, will help to assist in the stability of the sample [39-41]. If the microdialysis samples cannot be analyzed immediately, they should be placed into a -20 °C laboratory freezer which also helps to control the sample degradation.

3.2.3. Instrumentation

3.2.3.1. Amino Acid Neurotransmitters

2.5 µL of the microdialysis sample was taken and derivatized using an adapted NDA/CN$^-$ scheme from Robert *et al*. [42]. Briefly, to a 2.5 µL dialysate sample, 1.5 µL of the internal standard (α-aminoadipic acid prepared in aCSF), 1 µL of 500 mM borate : 87 mM CN$^-$ (100 : 20 v:v), and 0.5 µL of 3 mM NDA was added. The sample was then mixed by vortex and allowed to react at room temperature for one minute prior to the injection of 5 µL of sample.

The derivatized microdialysis sample was directly injected onto a Synergi 4µ Hydro-RP column (150 x 2.0 mm, Phenomenex, Torrance, CA). A binary LC-Fluorescence was used to analyze the samples. The liquid chromatographic system consisted of two Shimadzu LC-10ADvp pumps, a Shimadzu 20 µL SUS micro-mixer,

114

and a Rheodyne 9725i PEEK sample injector valve connected to a Phenomenex C18 guard column. The binary gradient system was controlled by a Shimadzu SCL-10A$_{VP}$ system controller. Mobile phase A consisted of 50 mM ammonium acetate and 0.5 mM Na$_2$EDTA with the pH adjusted to 6.8 using concentrated glacial acetic acid. Tetrahydrofuran (THF) was added making the final composition 95% acetate buffer : 5% methanol (v:v). Mobile phase B was 100% methanol. This method was adapted from Shah *et al*. [43].

The Shimadzu RF-10A$_{XL}$ fluorescence detector was operated at an excitation wavelength of 442 nm and an emission wavelength of 490 nm [42, 44]. The data were collected at 2.5 Hz and processed using version 7.3 EZStart Chromatography Software (Shimadzu Scientific Instruments, Columbia, MD). A typical chromatogram displaying microdialysate is shown in Figure 3.7.

3.2.3.2. Biogenic Amine Neurotransmitters

To the remaining 2.5 µL of microdialysis sample, 0.3 µL of internal standard (DHBA prepared in 0.1 M perchloric acid) was added. The sample was then mixed by vortex and 2.5 µL was injected immediately.

The microdialysis sample was injected onto a Zorbax C18 Eclipse-XDB (3.5 µm) column (75 x 2.1 mm, Agilent, Palo Alto, CA). An LC-EC system was used to analyze the samples. The LC system consisted of a Shimadzu LC-20AD pump, and a Rheodyne 9725i PEEK sample injector valve connected to a Phenomenex C18 guard column. The mobile phase was adapted from Agilent, Inc. [45] and consisted of 140
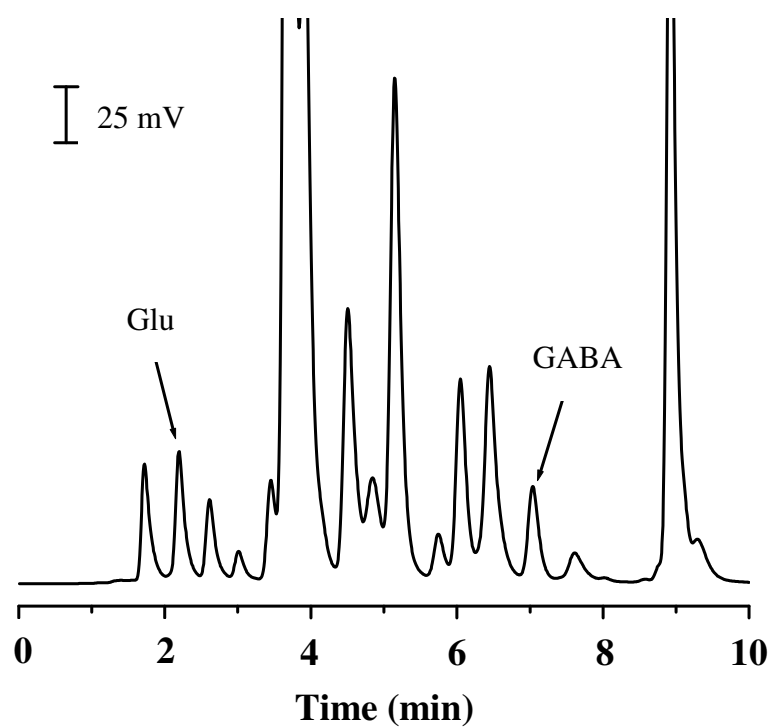
Figure 3.7. Typical LC-Fluorescence chromatogram from brain dialysate. Glu and GABA are clearly baseline resolved.

mM monobasic sodium phosphate, 0.75 mM SOS, and 20 mM Na$_2$EDTA with the pH adjusted to 3.5 using 85% *o*-phosphoric acid. Methanol was then added making the final composition 91% phosphate buffer : 9% methanol (v:v).

The dual-electrode electrochemical detector consisted of one gold-mercury (Au/Hg) amalgam electrode and one glassy carbon (GC) electrode. Preparation of the Au/Hg was as described in Section 2.2.2. The GC electrode was polished during the 0.3 μm alumina powder step. The schematic of this dual electrode is shown in Figure 3.8. The potentials were controlled by two LC-4C potentiostats (Bioanalytical Systems, West Lafayette, IN) with W1 operating the Au/Hg electrode and W2 operating the GC electrode. The data were collected at 10 Hz and processed using a Chrom&Spec Chromatography Data System (Ampersand International, Beachwood, OH). A hydrodynamic voltammagram (HDV) was taken at the GC electrode for all of the biogenic amine neurotransmitters and their metabolites of interest (Figure 3.9). A typical two channel chromatogram displaying the dual detection of 3-MPA and the biogenic amines is shown in Figure 3.10 holding W1 at +100 mV versus Ag/AgCl (as determined in Chapter 2) and W2 at +750 mV versus Ag/AgCl.

3.2.3.3. Cyclothiazide

In order to quantify the cyclothiazide (CTZ) in the brain, CE-UV was performed using a P/ACE MDQ (Beckman Coulter, Palo Alto, CA) and a modified method from Thomas *et al*. [46]. Fused silica separation capillaries with an i.d. of 50 μm and o.d. of 360 μm (Polymicro Technologies, Phoenix, AZ) and a length of 61.5
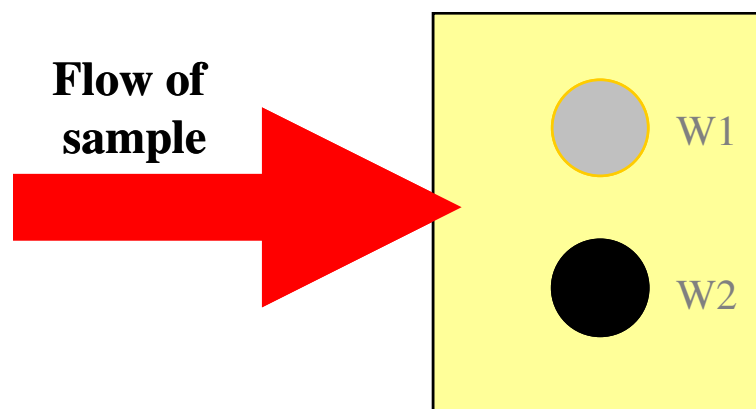
Figure 3.8. Dual Au/Hg and GC working electrode for LC-EC. The configuration of these electrodes is in parallel-adjacent mode and the flow of sample passes over both electrodes simultaneously. LC-EC operating conditions match those described in Section 3.2.3.2.
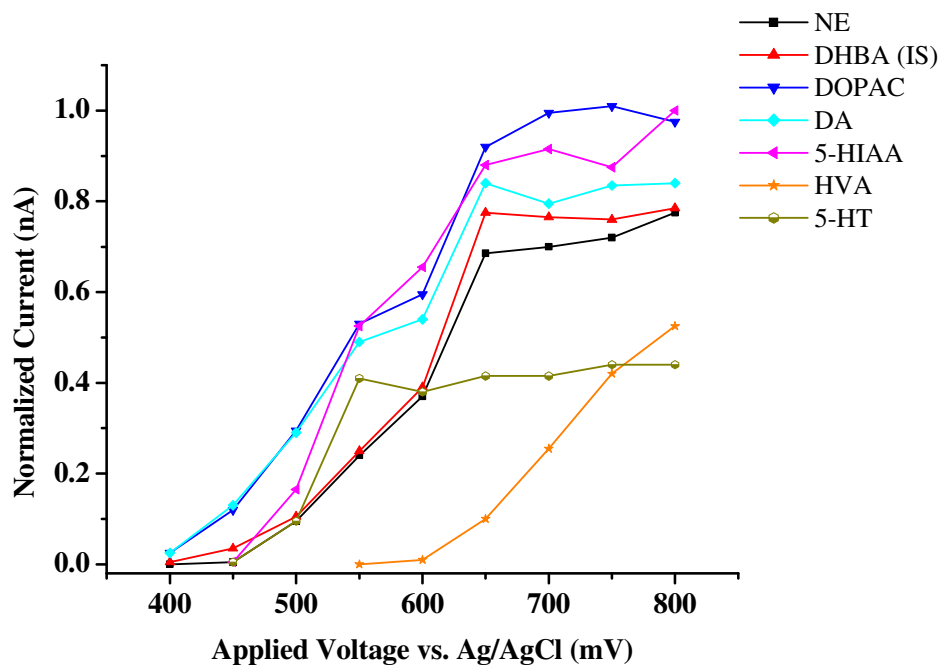
Figure 3.9. HDVs for representative biogenic amine neurotransmitters. All LC-EC conditions match those discussed in Section 3.2.3.1.
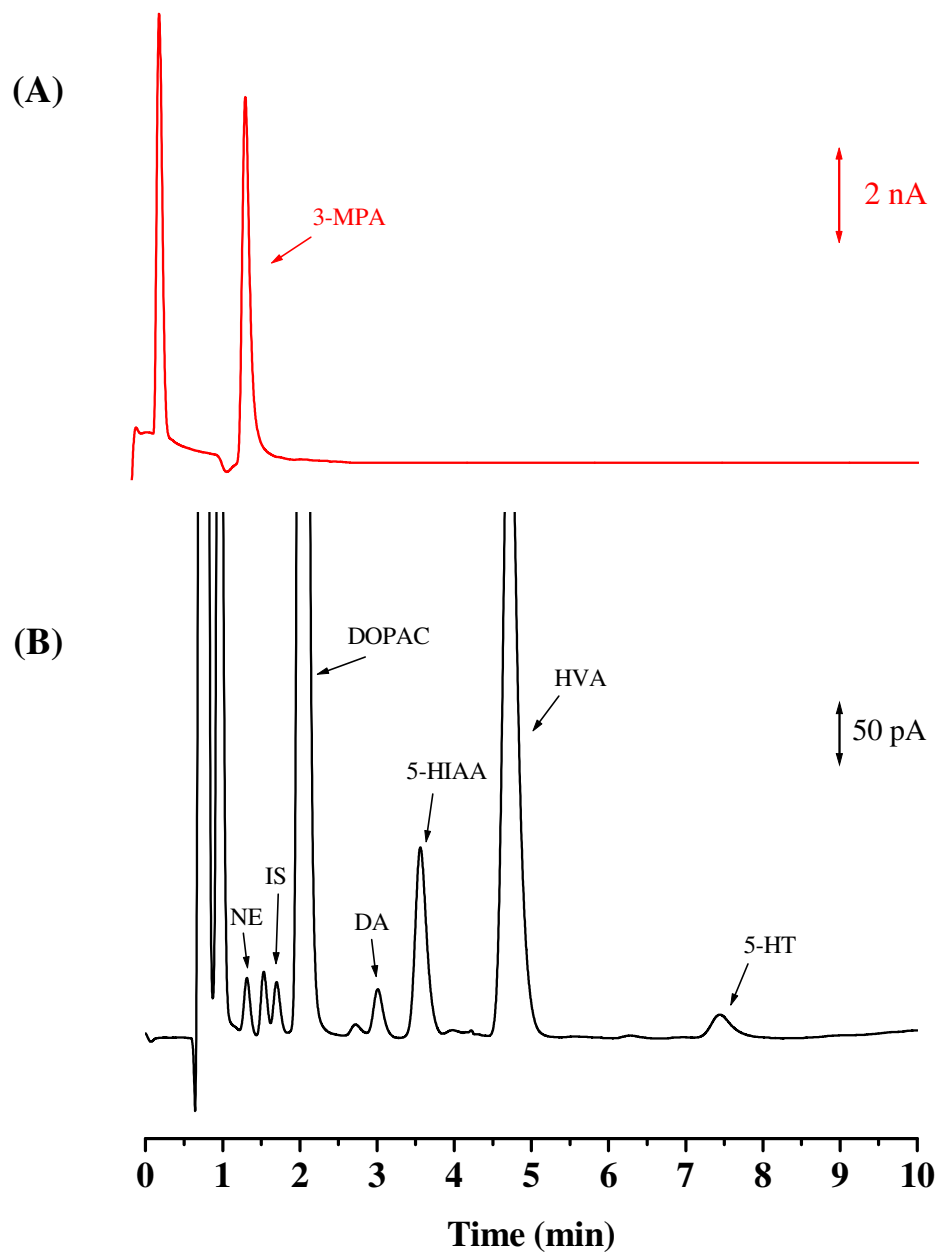
Figure 3.10. Representative 2 channel LC-EC chromatogram. (A) 3-MPA detected at Au/Hg electrode at +100 mV versus Ag/AgCl; (B) Biogenic amines detected at GC electrode at +750 mV versus Ag/AgCl.

cm were used. An active window was created by burning off a 3 mm length of the polyimide coating from the fused silica capillary 10 cm from the outlet, and then cleaning the outside of the capillary with copious amounts of methanol. The data were acquired using a 32 Karat Gold software package (Beckman Coulter, Palo Alto, CA) at 4 Hz.

The background electrolyte (BGE) for the CE-UV analyses was 50 mM boric acid at pH 9.6. The pH was adjusted using 0.1 M NaOH. Prior to use, the BGE was filtered through a 0.22 μm syringe membrane filter (Millipore, Bedford, MA). UV absorbance detection was performed at 230 nm.

Daily, before use, the separation capillary was "activated" by conditioning with 100% methanol (10 min), water (2 min), 0.1 M HCl (5 min), water (2 min), 0.1 M NaOH (10 min), water (2 min), and BGE (10 min) sequentially at a pressure of 20 psi. Prior to the first use of the BGE, an Ohm's Plot was conducted in order to determine the linear range where Joule heating was effectively dissipated. The separation voltage for these experiments was 25 kV. Between injections, the capillary was flushed with 0.1 M NaOH (1.5 min), water (0.5 min), and BGE (2 min) sequentially at 20 psi to rinse the capillary of any remaining analytes and to maintain a uniform charge density on the silanol groups of the capillary.

An electropherogram showing CTZ collected from the microdialysis probe is shown in Figure 3.11. This separation scheme afforded the ability to see both the (R-) and (S-) enantiomers of CTZ in one analysis. This was advantageous as it allowed each enantiomer to be monitored for its modulatory effect within the striatum.
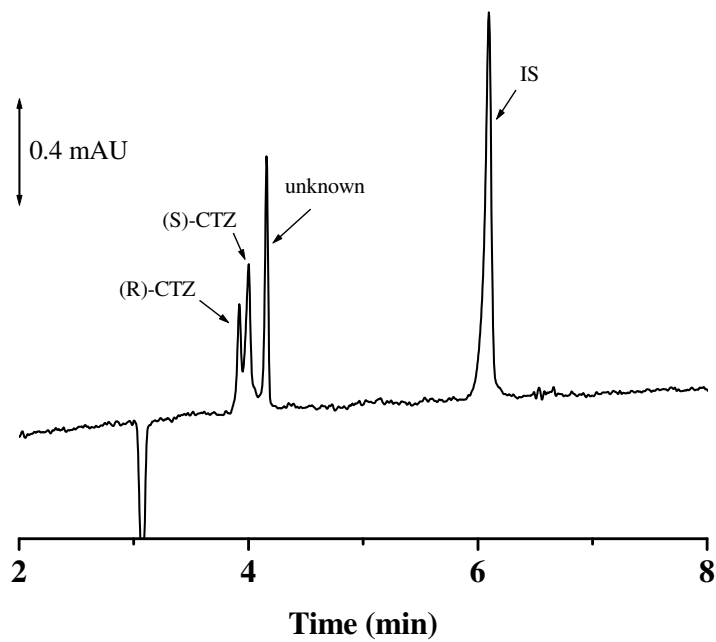
Figure 3.11. Electropherogram displaying CTZ in brain dialysate. The (R)- and (S)- enantiomers as well as the IS are clearly resolved. CE-UV conditions match those described in Section 3.2.3.3.

3.3. Results and Discussion

3.3.1. Striatal Neurotransmission

The amino acid and biogenic amine neurotransmitters were monitored within the striatum using implanted brain microdialysis probes. The constant infusion dosing method discussed in Chapter 2 was employed for this research. The striatum is the site for very large stores of Glu and GABA and would be an opportune location to study the 3-MPA chemical seizure model [1].

Excitatory amino acids, especially Glu, are released into the striatum from the afferent neuronal pathways coming from brain regions such as sensorimotor, cortex, and thalamus. High concentrations of GABA exist in the striatum and the efferent neurons project to brain regions such as the pallidum and the substantia nigra. Biogenic amines, such as DA, also project into the striatum from the substantia nigra. A detailed discussion follows below regarding the interactions which occur among all of these transmitter systems. This information will enable an investigation into any changes that occur in neurotransmission and relate these changes to the 3-MPA chemical seizure model.

Due to the trauma caused during the microdialysis probe implantation and the gliosis processes which follow, the first experimental parameter which had to be determined was the length of time required for the environment surrounding the probe to form a new steady basal level. For Glu, GABA, and the monoamines, a control experiment was conducted in which microdialysis samples were collected directly after probe implantation at a flow rate of 1 μL/min. The results from this experiment

are shown in Figures 3.12(A) and (B). It was determined that the probe must be implanted and continuously perfused with aCSF for a minimum of four hours before background (basal) sample collection could begin. Also before the neurotransmitter analysis could be performed for the 3-MPA seizure model, "sham" injections of saline had to be administered to the animal to ensure that the dosing procedure was not eliciting large effects on the amino acid neurotransmitters. Figure 3.13 displays the results from the striatum after the administration of an intravenous (i.v.) bolus dose and infusion of saline. No significant changes from basal values were detected due to this dosing procedure.

Data were collected and analyzed on 5 minute sampling intervals for the determination of Glu and GABA using the 3-MPA seizure model. Figure 3.14(A) shows a representative plot of the percent change from basal for both Glu and GABA over the time course of one experiment. The average Glu and GABA deviations against the basal levels after the administration of 3-MPA are shown in Figure 3.14(B). Significant differences compared to the basal levels exist for both Glu and GABA. Glu increased an average of 100% above basal values, and GABA decreased an average of 50% of basal values. Glu was significantly ($p < 0.05$) different compared to basal values when the 3-MPA was held at a steady-state concentration. After the cessation of the 3-MPA infusion, Glu remained increased ($p < 0.10$) from the basal values. GABA decreased significantly ($p < 0.01$) throughout a large portion of the experiment.
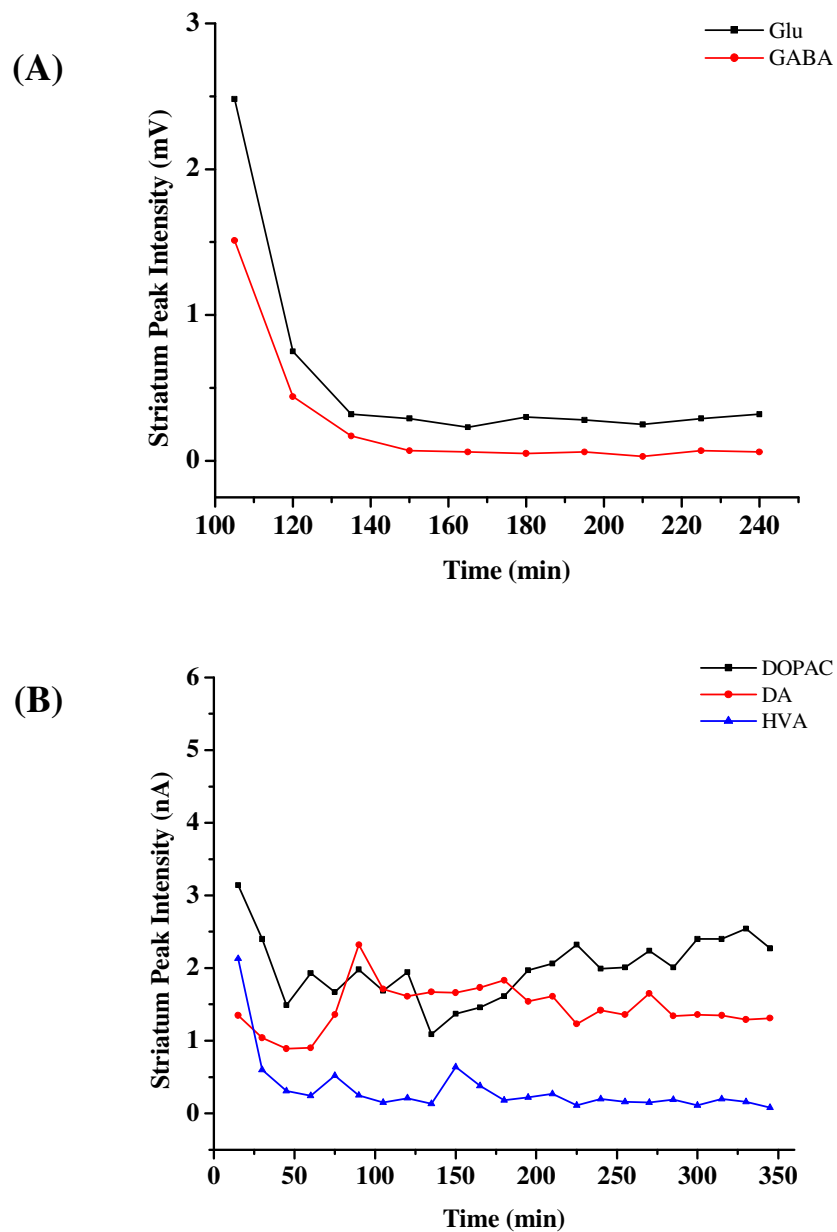
Figure 3.12. Time profiles for neurotransmitters after microdialysis probe implantation into striatum. (A) Changes in representative amino acid (n = 1 rat) and (B) biogenic amine neurotransmitters (n = 1 rat) versus time profiles.
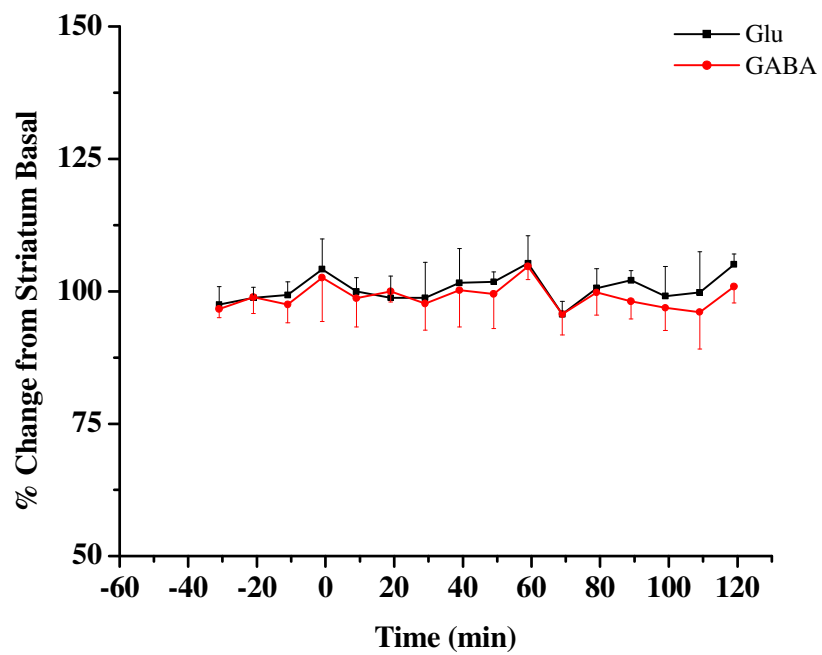
Figure 3.13. Glu and GABA time profiles from the striatum after saline dosing (n = 2 rats). Saline was administered at t = 0 minutes.

Figure 3.14. Percent deviation for amino acid transmitters versus time profiles for constant infusion dosing of 3-MPA measured from the striatum (n = 3 rats). 3-MPA was administered at t = 0 minutes. Boxes represent the time in which a steady-state concentration of 3-MPA was achieved in each region. The arrow represents the time in which the infusion was stopped. (A) Glu and GABA deviations versus time in one example experiment; (B) Glu and GABA deviations versus time (n = 12 rats). [* = p < 0.10; ** = p < 0.05; *** = p < 0.01]

These results were not expected. It was thought that in Glu and GABA would return to basal levels soon after the cessation of the 3-MPA i.v. infusion. The results from one example experiment as well as the overall average from 12 experiments show that this is not the case. Actually, Glu and GABA remained in a "seizure state" for quite a period of time following the removal of the 3-MPA i.v. infusion. GABA began to return to basal levels near the end of the experiment, but Glu continuously increased.

One possible explanation for this sustained increase in Glu over the entirety of the experiment lies with the Glu receptors themselves. Glu transmission in the striatum has been debated heavily in the literature over the past two decades. The content of Glu in the extracellular space is very complex. Several authors have noted that the source of extracellular Glu is multifaceted, coming from possible sources such as synaptic release and release from astrocytes and glial cells [10, 47]. A very high density of Glu transporters are located on the astrocytes which surround the synapse [48]. The Glu transporters on the astrocytes, along with ones on the glial cells, are responsible for the reuptake of Glu from the extracellular space [1]. Regardless of the cause of excess Glu release / spillover into the synaptic cleft, it is believed that upon excess excitation, Glu is not being properly taken back into the cells by the reuptake receptors or transporters [1, 10]. A possible reason for this is Glu receptor desensitization.

It is known that Glu activates two main types of receptors upon its release: α-amino-3-hydroxy-5-methylisoxazole-4-propionic acid (AMPA) and N-methyl-D-

aspartate (NMDA) type receptors [1, 49, 50]. Both AMPA and NMDA receptors are categorized as ionotropic, or ligand-gated, Glu receptors [1]. These ligand-gated ion channels operate by transforming chemical signals into electrical impulses. When a chemical neurotransmitter binds to a post-synaptic receptor, the channel opens allowing the passage of ions, specifically potassium (K^+) and sodium (Na^+), into the cell. Other ions, such as calcium (Ca^{2+}) are kept from entering the cell due to the GluR2 subunit on the AMPA receptor [1]. If Ca^{2+} were to enter the cell, the cell could potentially die due to excitotoxicity. During epileptiform activity, the AMPA receptor is known to become activated due to excess excitatory activity [1]. AMPA receptors by design coordinate "fast" synaptic transmission. If the time in which Glu resides in the synaptic cleft is greater than the time in which the AMPA receptor is open, the receptor may become desensitized [50]. The molecular basis of the Glu receptor desensitization was recently deciphered by Sun *et al.* and dealt with conformational changes due to the rearrangement of the dimer interface created upon the binding of the neurotransmitter to the receptor [51]. Essentially, when the Glu receptor becomes desensitized, it will enter a permanently "closed" state, thereby not allowing the reuptake of Glu into the cell. Many authors have observed Glu receptor desensitization occur when an excess of excitatory neurotransmission has occurred [50, 52, 53]. It was discovered in the early 1990's that AMPA receptor desensitization could be selectively blocked with CTZ [50, 53]. An *in vitro* study using brain slices showed that AMPA post-synaptic currents (PSCs) were depressed upon the addition of Glu. The pre-treatment of these brain slices with 60 μM CTZ

caused the kinetics of the closing of the AMPA receptor, not the NMDA receptor, to be considerably increased from approximately 0.1 ms initially to approximately 1 ms with the addition of CTZ while in the presence of Glu [50, 53]. Other authors have since shown the same millisecond timescales on *in vivo* and cell culture models using patch clamp techniques [52, 54, 55]. With the previous working knowledge of the selective effect upon AMPA receptors, the use of CTZ to possibly "resensitize" the AMPA receptors was explored while using the 3-MPA seizure model in order to try and explain the sustained release of Glu throughout the experiments. Results from these studies are discussed in Section 3.3.1.1.

The biogenic amines were also analyzed using a 5 minute sampling interval. Figure 3.15 shows an example of the experimental results which match the striatal experimental results shown in Figure 3.14(A) for changes in the levels of biogenic amines after the administration of the 3-MPA seizure model. The first interesting piece of information extracted from this plot was the biphasic change associated with DA. This was somewhat unexpected as other authors have reported primarily monophasic changes with DA in regards to epileptic seizures [6]. A collection of six experiments from the striatum are shown in Figure 3.16(A). Upon closer inspection of the basal monoamine levels, it was observed that the only other neurotransmitters with significant changes from the basal levels were the metabolites of DA as shown in Figure 3.16(B). Both DOPAC and HVA decreased a maximum of approximately 40% from basal levels. This decrease in the metabolites of DA was very similar to a report presented by Segovia and Mora in which NMDA was used to excite Glu and
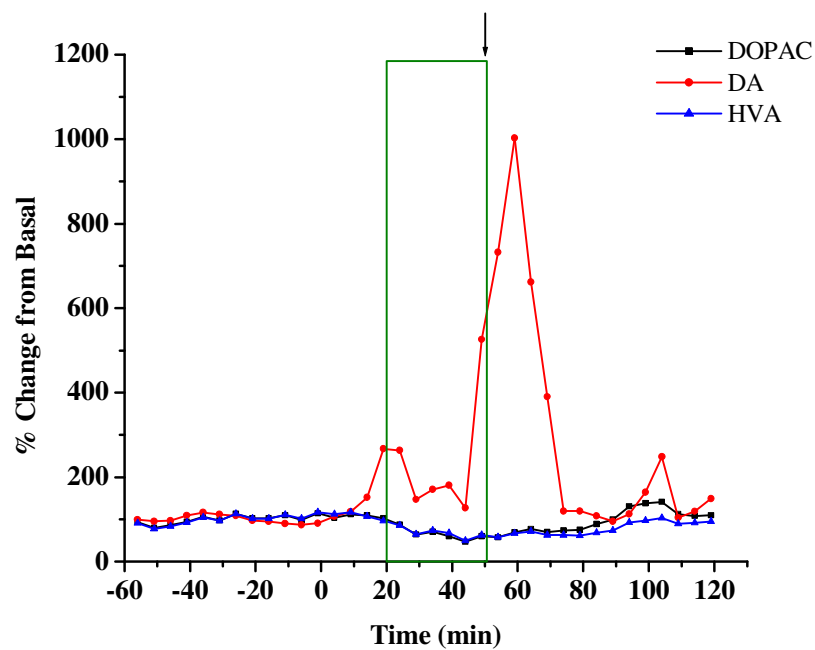
Figure 3.15. Example experiment displaying striatal changes in representative biogenic amines. Percent change versus time profile for constant infusion dosing of 3-MPA measured from the striatum (n = 1 rat). 3-MPA was administered at t = 0 minutes. All other details as stated in Figure 3.14.
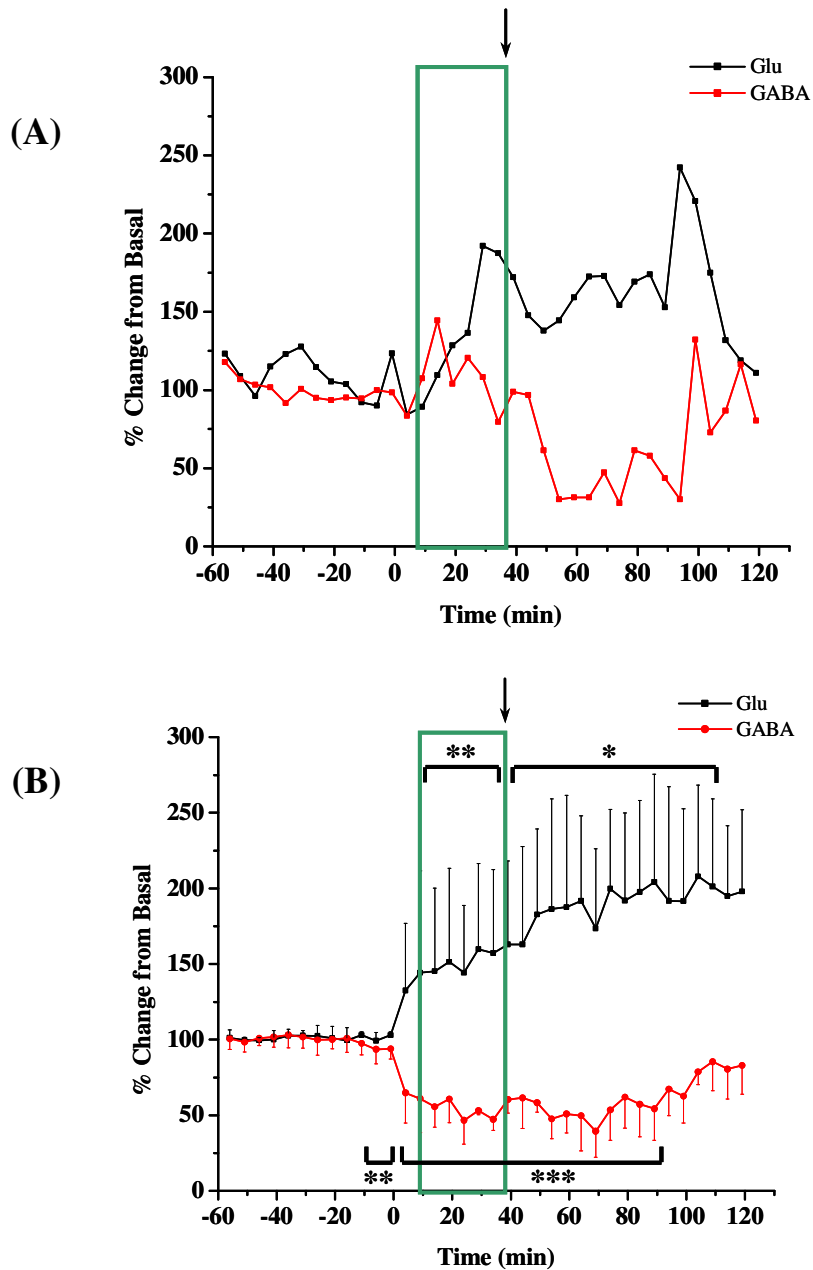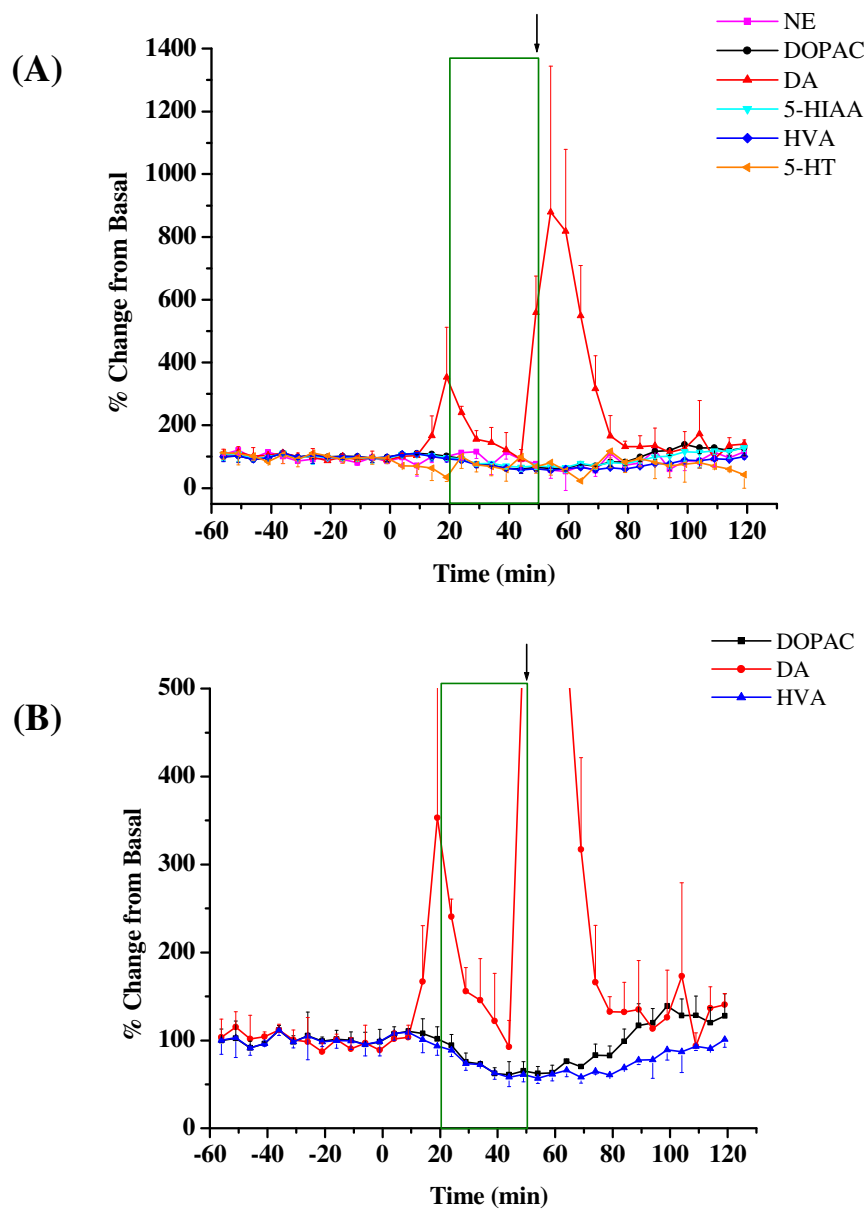
Figure 3.16. Percent deviation for biogenic amine transmmitters versus time profiles for constant infusion dosing of 3-MPA measured from striatum. (A) Compiled data from striatal experiments (n = 6 rats); (B) Closer look at the changes in DA, DOPAC, and HVA. 3-MPA was administered at t = 0 minutes. All other details as stated in Figure 3.14.

132

DA [56]. Other biogenic amines, including NE, 5-HT and 5-HIAA were not significantly different from the recorded basal values. These data could result from 1) the very small quantity of 5-HT projections into the striatum and 2) the 5 minute temporal resolution of the microdialysis technique.

Due to the pronounced and reproducible biphasic increase in DA activity observed within the striatum, further analysis of the data was performed in order to look at this phenomenon more closely and attempt to decipher a cause for its occurrence. Table 3.1 illustrates the median time for each of the phasic spikes in DA activity. The Δt values which represent the spacing between the biphasic spiking within the striatum was also very reproducible. These data could be explained by looking into a mechanism which correlates the DA activity with the aforementioned Glu activity. As discussed in Section 3.1.1., there has been much debate over the relationship between Glu and DA. It is well known that the striatum is a key component of the motor system. The striatum is comprised of glutamatergic afferent neurons which descend from the cortex via the corticostriatal pathway and dopaminergic afferent neurons that project from the substantia nigra pars compacta via the nigro-striatal pathway [57]. Figure 3.17 portrays an adaptation of the circuitry within the basal ganglia [2]. Bouyer *et al*. in 1984 discovered that the descending glutamatergic and dopaminergic projections form appositional contacts thereby suggesting the possibility of cross-communication between these terminals [14]. Many authors believe that glutamatergic neuronal activity works to modulate the dopaminergic neuronal activity [8, 9, 11, 58-62] while others believe the opposite

Table 3.1: Time trends within biphasic spiking of dopamine activity.

	Median Time (t) for 1st DA Spike (min)	Median Time (t) for 2nd DA Spike (min)	Δt (min)
Rat 1	19	59	40
Rat 2	19	59	40
Rat 3	19	54	35
Rat 4	24	54	30
Rat 5	39	89	50
Rat 6	14	54	40
Avg ± SD	22 ± 9	62 ± 14	39 ± 7
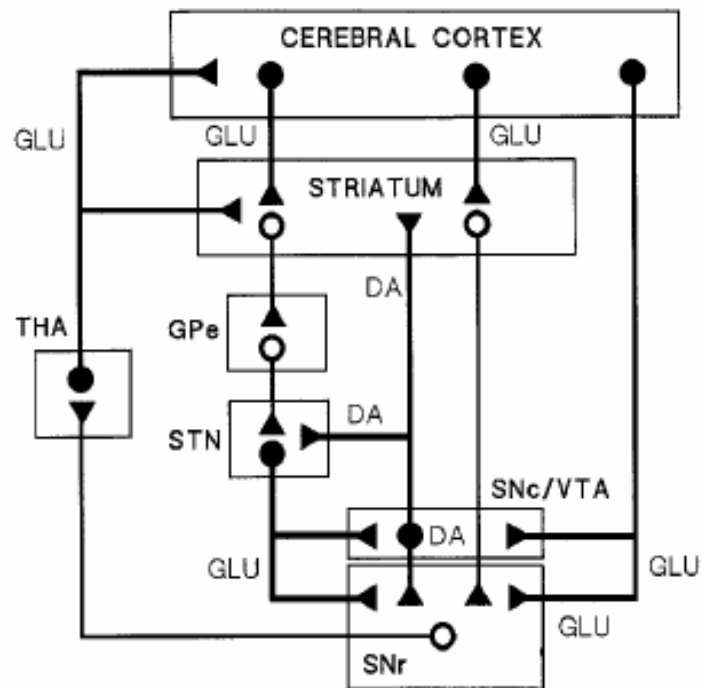
Figure 3.17. Diagram showing the glutamatergic and dopaminergic neuronal circuitry within the basal ganglia. Adapted from Morari *et al*. [2]. GPe (pars externa of globus pallidus); PPN (peduncolopontine nucleus); SNc (pars compacta of substantia nigra); SNr (pars reticula of substantia nigra); STN (subthalamic nucleus); THA (thalamus); VTA (ventral tegmental area).

is true [7, 63]. This modulatory relationship has been strengthened with the discovery that DA synapses contain DA receptors as well as both AMPA and NMDA receptors. The opposite also holds true, Glu synapses contain AMPA, NMDA and DA receptors [12].

With the data obtained in this set of experiments, it was difficult to make a correlation between the Glu and DA activity within the striatum. The main problem lies in the temporal resolution (5 minutes) of the analysis. For example, a biphasic increase in DA transmission was observed with each phasic release lasting, on average, 20 minutes and 37 minutes, respectively. The observed increase in Glu and decrease in GABA were "sustained" releases over time. Glu was observed twice to have a distinguishable biphasic response (see Figure 3.14(A)); however, it was difficult to begin to make correlations between the two neuronal systems. "Fast" neurochemical events have been electrically monitored to transpire on the timescale of 0.5 – 5 milliseconds [1, 53]. In order to monitor neurochemical events on this timescale, the implementation of microelectrodes (e.g. carbon fiber electrodes to monitor DA) should be considered. The temporal resolution of these microelectrodes can be as small as 100 milliseconds [64-66]. Since the changes in the neurotransmitter levels that are observed within this research are prolonged over the span of approximately 20 minutes or more (in the case of DA) or sustained over the course of the experiment (in the case of Glu and GABA), it was decided the first route for improving the experimental conditions in order to illustrate possible

correlation between Glu and DA was to improve the temporal resolution of the brain microdialysis sampling. This issue will be further discussed in more detail Chapter 4.

3.3.1.1. Glutamate Receptor Desensitization

The initial hypothesis of these experiments was that CTZ would "resensitize" the Glu receptors, thereby leading to more Glu reuptake into the cells and less Glu in the extracellular space as monitored by microdialysis. To test this hypothesis, the experimental protocol described in Chapter 2 for the steady-state 3-MPA dosing model was modified to include the perfusion of CTZ through the brain microdialysis probe. Briefly, the addition of 100 µM CTZ was added to the perfusion medium which was altered to include 1% ethanol in the aCSF for CTZ solubility purposes.

Initial control experiments were conducted using only 100 mM CTZ prepared in the new perfusion medium, 1% ethanol in aCSF. Figures 3.18(A) and (B) show there to be slight decreases in the levels of the Glu and GABA and an increase in DA that is not significantly different from basal values.

It was also important to know the concentration of CTZ which was being delivering through the brain microdialysis probe into the striatum. This was determined using the protocol described in Section 2.2.4. The average amount of CTZ delivered into the striatum was $82.6 \pm 4.6\%$ for the (R-) enantiomer (n = 3) and $89.8 \pm 4.9\%$ for the (S-) enantiomer (n = 3). The (S-) enantiomer passes through the microdialysis probe membrane more easily than the (R-) enantiomer. Figure 3.19 displays a plot revealing the average concentration versus time obtained within the
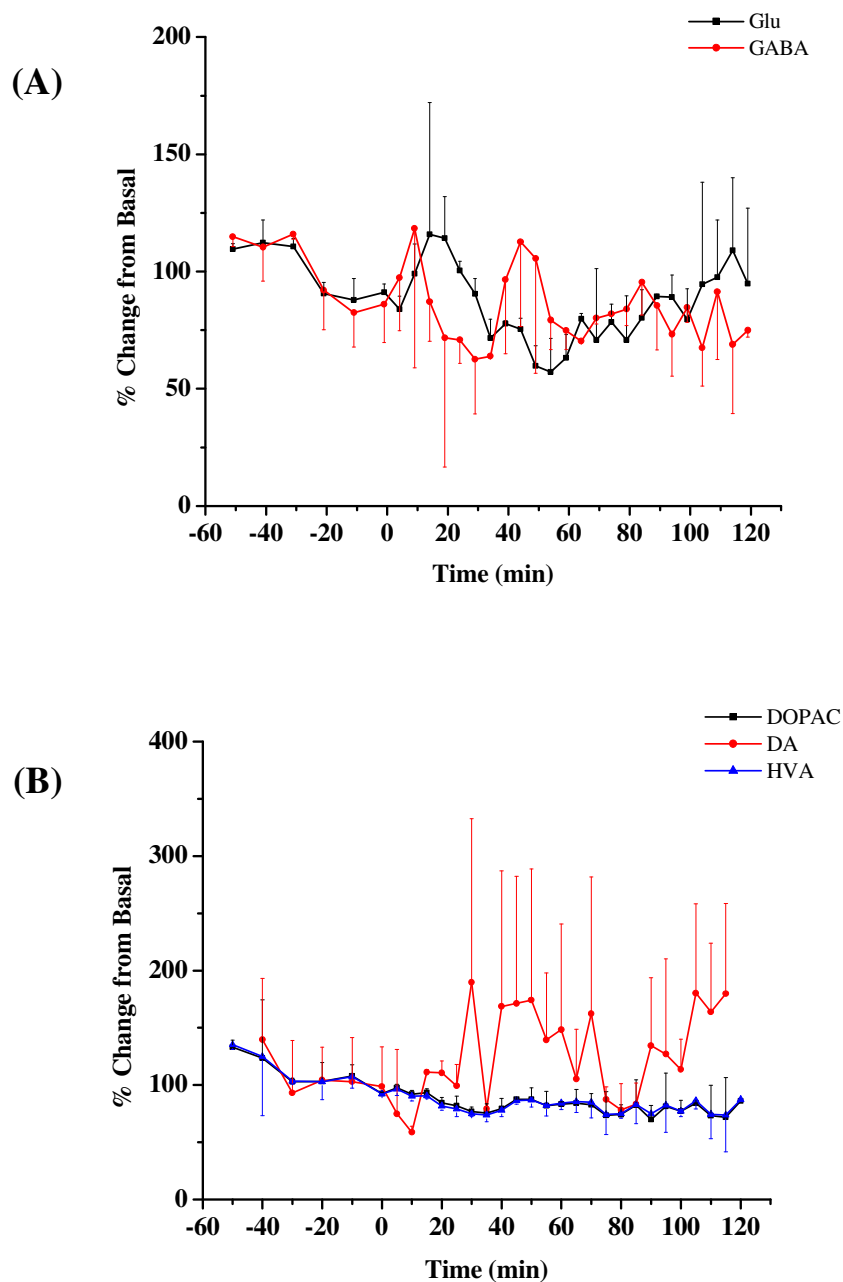
Figure 3.18. Percent changes versus time profiles for amino acid and biogenic amine neurotransmitters with perfusion of 100 µM CTZ control experiments (n = 2). CTZ was administered at t = 0 minutes. (A) Glu and GABA data from the striatum; (B) Representative biogenic amine data from the striatum.
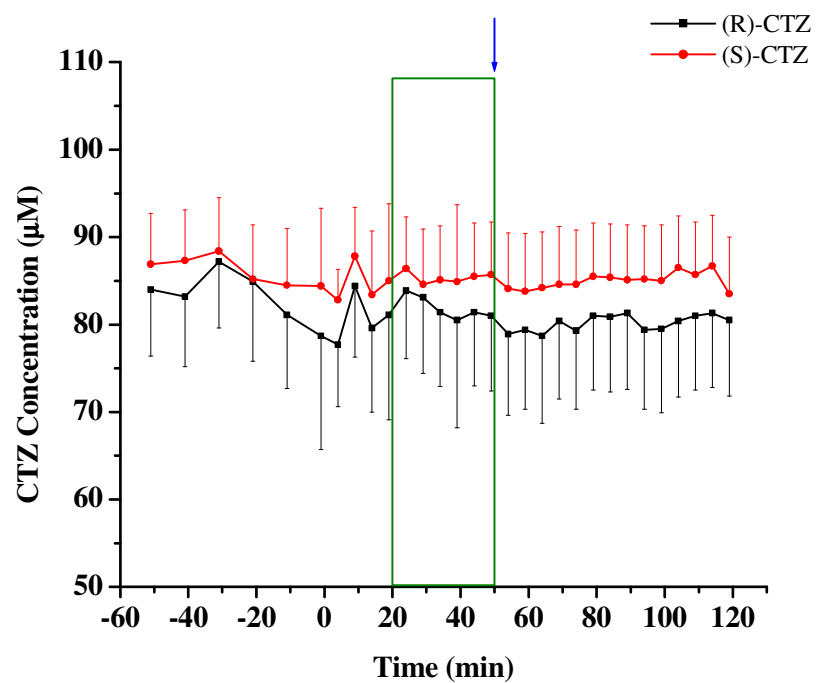
Figure 3.19. Striatal concentration versus time profiles for (R)- and (S)-CTZ (n = 3 rats). CTZ was perfused through the brain microdialysis probe beginning immediately following the probe implantation. 3-MPA was administered at t = 0 minutes. All other details as stated in Figure 3.14.

striatum for each enantiomer. From this plot, it appears that both enantiomers are delivered very efficiently into the striatum, and that the (S-) enantiomer resides within the striatum at a higher concentration (though not significantly) than the (R)-enantiomer. This was consistent with the microdialysis probe calibration results showing that neither enantiomer of CTZ plays a large role on the observed effects.

The effect of CTZ upon the amino acid and biogenic amine neurotransmitters was quite remarkable. Figure 3.20(A) reveals the average Glu and GABA data collected from three experiments. The Glu showed no significant changes for the duration of the experiment when compared to the basal levels. This was greatly different from the Glu results mentioned in Section 3.3.1 where CTZ was not used. The GABA data also proved to be quite interesting when compared with the previous GABA data without the perfusion of CTZ. Without the use of CTZ, the GABA levels after the administration of 3-MPA decreased approximately 50% for a sustained period of time. In this CTZ study, GABA fell only briefly to approximately 80% of the basal level. This was an unexpected change, but upon further review of the literature, CTZ is also known to potentially inhibit the $GABA_A$ receptor, which are contained at a high density within the striatum [54, 55]. This inhibition was believed to be caused by Ca^{2+} mobilization within the glutamatergic NMDA receptor. This receptor blockade would lead to reduced transmission of GABA and subsequently cause GABA levels in the extracellular space to increase.

The effect of CTZ on the biogenic amines was also unexpected. Figure 3.20(B) displays the biogenic amine neurotransmitter data from the collection of three

(A)

(B)
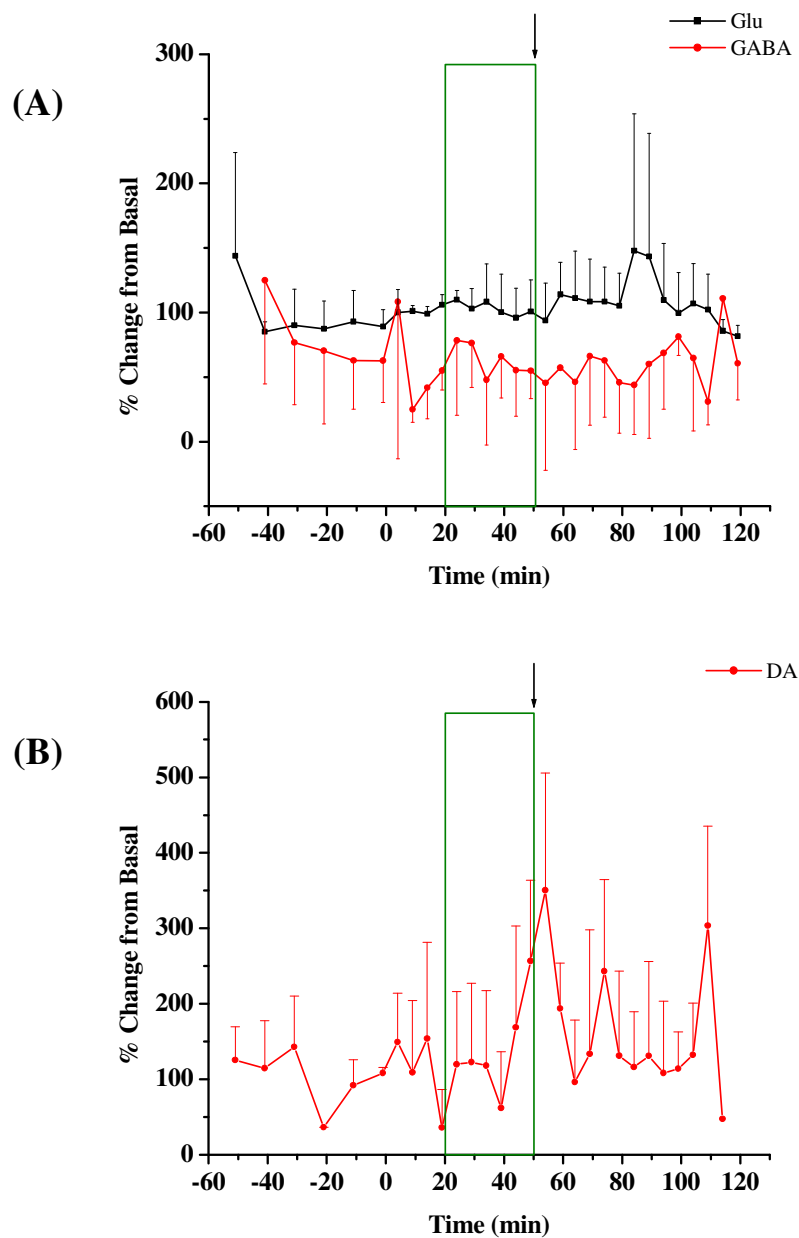
Figure 3.20. Percent change versus time profiles for amino acid and biogenic amine neurotransmitters using 100 mM CTZ perfusion (n = 3 rats). 3-MPA was administered at t = 0 minutes. All other details as stated in Figure 3.13.

experiments. Only the DA data are shown for clarity, as all remaining biogenic amines did not significantly change versus the basal values. DA showed, at best, monophasic activity in the region of 40 – 65 minutes. The data collected within this time frame were significantly ($p < 0.10$) different when compared to the basal values.

It appears for the level of amino acid neurotransmission, CTZ affected both the Glu and GABA receptors inducing a shift in the excitation/inhibition balance which is classically thought to occur within the brain. Taking into account the biogenic amines, DA was the neurotransmitter which showed deviations from basal with any significance. The loss of the first phasic spike in DA activity, associated with striatal DA release without using CTZ, is very interesting as it strengthens the possible observation of an interaction between Glu and DA within the striatum. This idea will again be revisited in Chapter 4.

The ECoG data from the CTZ experiments are shown in Table 3.2. While there was a significant decrease in the activity Glu and GABA when perfusing CTZ through the striatum, there are no significant changes in the ECoG activity. The latency to seizure onset was extended when CTZ was used by approximately 400 seconds, but it was not significantly different from experiments in which CTZ was not present. This could introduce the idea that 3-MPA is acting by another mechanism to induce the seizure activity rather than rather than the classically viewed Glu/GABA imbalance. However, this would have to be further investigated using local electrical recording within the striatum, not from the cortex.

Table 3.2: ECoG data for CTZ experiments.

	60 mg/kg bolus + 50 mg/kg/min infusion[a]	60 mg/kg bolus + 50 mg/kg/min infusion: Perfusion of CTZ[b]
Latency to Seizure Onset (s)	363.2 ± 148.8	770.7 ± 299.6
Number of Seizures Detected	592 ± 187	531 ± 193
Average of the Average Seizure Duration (s)	0.87 ± 1.78	1.6 ± 0.5
R_{max}	71.8 ± 22.2	33.5 ± 5.9

a: n = 12 rats
b: n = 3 rats

3.3.2. Hippocampal Neurotransmission

The amino acid and biogenic amine neurotransmitters were also monitored within the hippocampus using implanted brain microdialysis probes. The constant infusion dosing method described in Chapter 2 was again employed for the experiments discussed within this section. These experiments were conducted as dual probe experiments (n = 3) with the aforementioned experiments within the striatum. The hippocampus was chosen for its closeness in resemblance to human limbic and temporal lobe epilepsy, which comprises 40% of all human epilepsies [1, 67].

The hippocampus is a very popular location to study synaptic activity due to the unidirectional flow of neuronal activity originating and ending in the entorhinal cortex forming a closed loop flow of information [67]. Very high quantities of inhibitory neurons as well as excitatory neurons lie all along the closed loop pathway allowing the conductance of neurotransmission.

Again, the length time needed to reach a new "stable" baseline of neurotransmitter activity was monitored. These results are shown in Figures 3.21(A) and (B). From this, it was clear that waiting a minimum of 4 hours before the collection of basal microdialysis samples was again appropriate for sampling within the hippocampus at a flow rate of 1 µL/min. Control experiments were also conducted to determine any changes in the hippocampal neurotransmitters due to the experimental protocol. These results are illustrated in Figure 3.22. No significant deviations occurred due to dosing saline. Figures 3.23(A) and (B) display the average results from the experiments conducted within the hippocampus for the amino acid
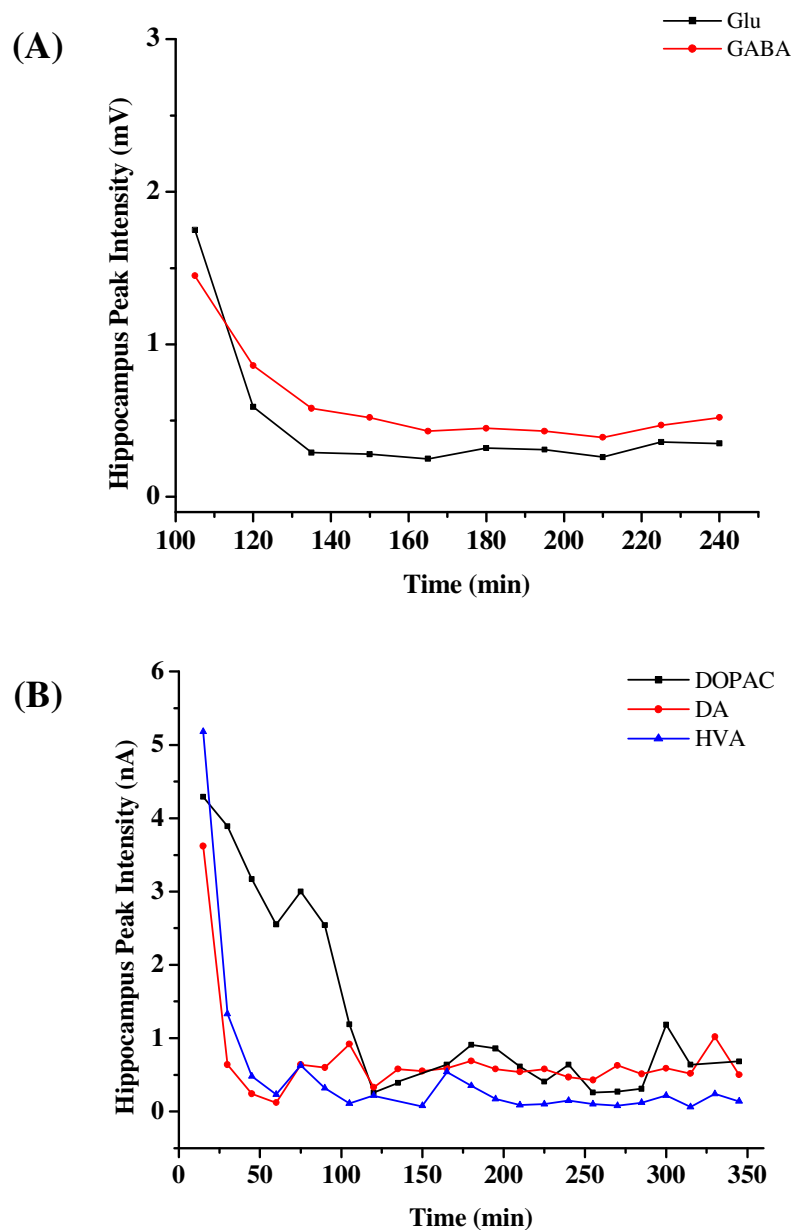
Figure 3.21. Time profiles for neurotransmitters after microdialysis probe implantation into hippocampus. (A) Changes in representative amino acid (n = 1 rat) and (B) biogenic amine neurotransmitters (n = 1 rat) versus time profiles.
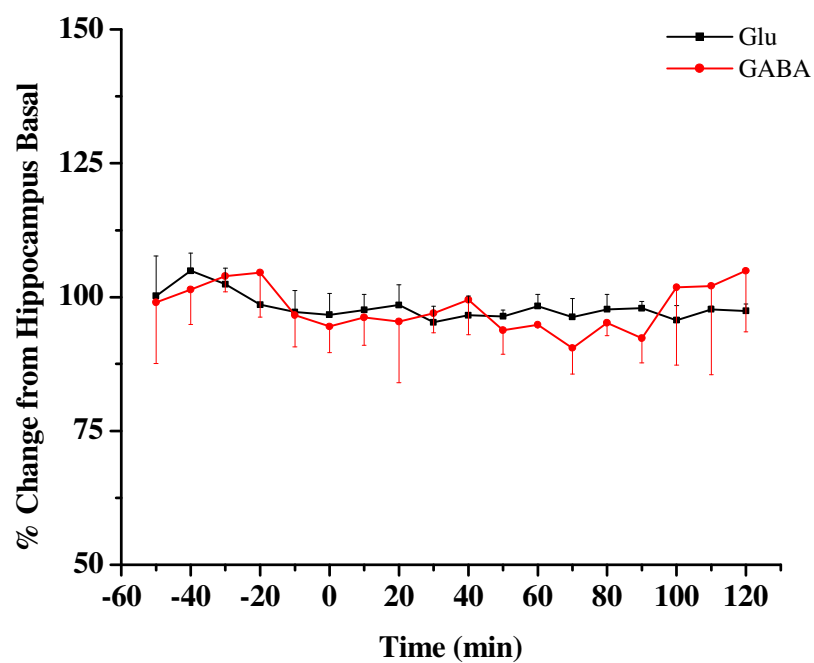
Figure 3.22. Glu and GABA time profiles from the hippocampus for saline dosing (n = 2 rats). Saline was administered at t = 0 minutes.
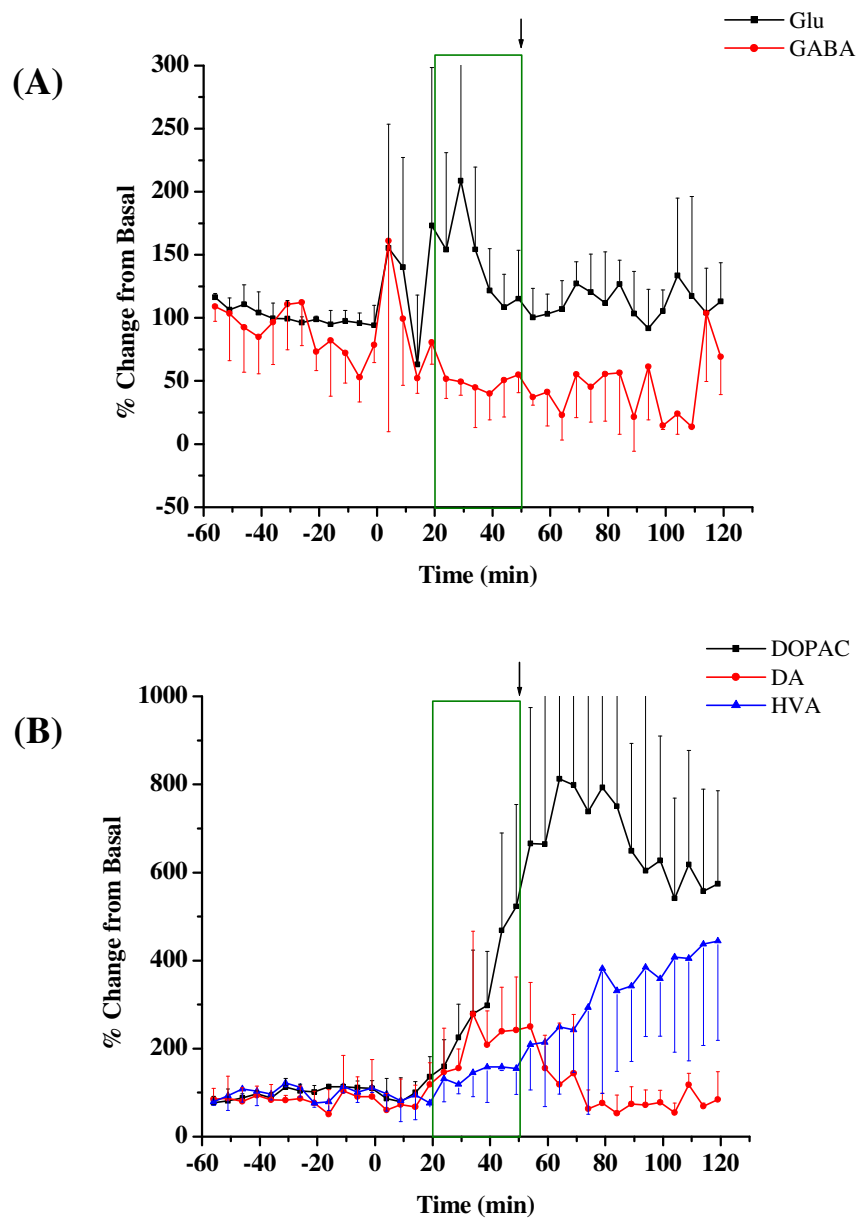
Figure 3.23. Changes in hippocampal neurotransmission. (A) amino acid and (B) biogenic amine neurotransmitters versus time profiles for constant infusion dosing of 3-MPA measured from the hippocampus (n = 3 rats). 3-MPA was administered at t = 0 minutes. All other details as stated in Figure 3.12.

and the biogenic amine neurotransmitters, respectively. Neither Glu nor GABA were observed to change significantly from basal values. The major observed change within the biogenic amines was with the metabolites of DA. DA itself did not significantly change when compared to the basal levels; DOPAC and HVA also did not significantly change (paired t-test). However, there was an increase noted in DOPAC which peaked approximately 60 minutes after 3-MPA administration (10 minutes after the removal of the 3-MPA i.v. infusion). Also, a sustained release of HVA over time (beginning approximately at the time of the removal of the 3-MPA i.v. infusion) was observed. These results contradict corresponding hippocampal literature in which convulsant dosing occurred. Pena and Tapia used 4-aminopyridine to induce seizure activity and obtained large increases in Glu activity [68]. Girardi *et al*. used 3-MPA to induce seizure activity, but at a much higher dose of 145 mg/kg i.p. in order to induce changes in neurotransmission within hippocampus [69]. This movement of Glu was most predominant with the astrocytes, as increased amounts of 3-MPA modified the astrocyte functionality.

More in depth work will need to be completed within the hippocampus to fully gain an understanding of the observed results. Although the concentration of 3-MPA is higher in the hippocampus than the striatum using the developed chemical seizure model, the concentration may not be enough to correspond to changes in the levels of neurotransmitters. Also, the analytical methodologies may not be providing sufficient temporal resolution in order to monitor the changes in all neurotransmission effectively.

3.4. Conclusions

The 3-MPA chemical seizure model which was described in Chapter 2 was applied to obtain a more detailed analysis of amino acid and biogenic amine neurotransmission as they were associated with the seizures elicited by 3-MPA. Within the striatum, large and significant changes were observed for both Glu and GABA which were sustained over a period of time. The reason behind this sustained release was determined to be Glu receptor desensitization. Upon the intracranial administration of CTZ, the Glu levels significantly decreased compared to the previous experiments. An increase in the level of GABA was also observed, displaying a hypothesized increase in the inhibition of the $GABA_A$ receptor. A large and reproducible biphasic increase in DA release was observed within the striatum with a resulting decrease in DOPAC and HVA, both metabolites of DA.

Within the hippocampus, no significant changes were determined for amino acid or biogenic amine neurotransmission; however, further experimentation is required in order to assess these findings. Initial improvements which could be made include improving the temporal resolution of the microdialysis sampling method. The present 5 minute microdialysis sampling times could possibly result in missing important neurochemical events. This idea will be discussed in Chapter 4.

3.5. References

[1]. Siegel, G.J., Agranoff, B.W., Albers, R.W., Fisher, S.K., and Uhler, M.D., eds. *Basic Neurochemistry: Molecular, Cellular, and Medical Aspects*. 6th ed. **1999**, Lippincott Williams & Wilkins: Philadelphia.

[2]. Morari, M., Marti, M., Sbrenna, S., Fuxe, K., Bianchi, C., and Beani, L., *Reciprocal dopamine-glutamate modulation of release in the basal ganglia.* Neurochem. Int., **1998**, 33: 383-397.

[3]. Nyitrai, G., Kekesi, K.A., and Juhasz, G., *Extracellular level of GABA and Glu: in vivo microdialysis-HPLC measurements.* Curr. Top. Med. Chem., **2006**, 6: 935-940.

[4]. Starr, M.S., *The role of dopamine in epilepsy.* Synapse, **1996**, 22: 159-194.

[5]. Adams, B.A., Bradberry, C.W., and Moghaddam, B., *NMDA antagonist effects on striatal dopamine release: Microdialysis studies in awake monkeys.* Synapse, **2002**, 43: 12-18.

[6]. Bert, L., Parrot, S., Robert, F., Desvignes, C., Denoroy, L., Suaud-Chagny, M.-F., and Renaud, B., *In vivo temporal sequence of rat striatal glutamate, aspartate and dopamine efflux during apomorphine, nomifensine, NMDA and PDC in situ administration.* Neuropharmacology, **2002**, 43: 825-835.

[7]. Konradi, C., ed. *Dopamine modulation of responses mediated by excitatory amino acids in the neostriatum.* Catecholamines: Bridging Basic Science with Clinical Medicine, ed. D.S. Goldstein, G. Eisenhofer, and R. McCarty. **1998**, Academic Press: San Diego. 724-729.

[8]. Shimizu, N., Duan, S., Hori, T., and Oomura, Y., *Glutamate modulates dopamine release in the striatum as measured by brain microdialysis.* Brain Res. Bull., **1990**, 25: 99-102.

[9]. Takahata, R. and Moghaddam, B., *Target-specific glutamatergic regulation of dopamine neurons in the ventral tegmental area.* J. Neurochem., **2000**, 75: 1775-1778.

[10]. Clinckers, R., Gheuens, S., Smolders, I., Meurs, A., Ebinger, G., and Michotte, Y., *In vivo modulatory action of extracellular glutamate on the anticonvulsant effects of hippocampal dopamine and serotonin.* Epilepsia, **2005**, 46: 828-836.

[11]. Youngren, K.D., Daly, D.A., and Moghaddam, B., *Distinct actions of endogenous excitatory amino acids on the outflow of dopamine in the nucleus accumbens.* J. Pharmacol. Exp. Ther., **1993**, 264: 289-293.

[12]. Chen, B.T. and Rice, M.E., *Synaptic regulation of somatodendritic dopamine release by glutamate and GABA differs between substantia nigra and ventral tegmental area.* J. Neurochem., **2002**, 81: 158-169.

[13]. Karreman, M., Westerink, B.H.C., and Moghaddam, B., *Excitatory amino acid receptors in the ventral tegmental area regulate dopamine release in the ventral striatum.* J. Neurochem., **1996**, 67: 601-607.

[14]. Bouyer, J.J., Park, D.H., Joh, T.H., and Pickel, V.M., *Chemical and structural analysis of the relation between cortical inputs and tyrosine hydroxylase-containing terminals in rat neostriatum.* Brain Res., **1984**, 302: 267-275.

[15]. Moghaddam, B. and Bolinao, M.L., *Glutamatergic antagonists attenuate ability of dopamine uptake blockers to increase extracellular levels of dopamine: implications for tonic influence of glutamate on dopamine release.* Synapse, **1994**, 18: 337-342.

[16]. Moghaddam, B. and Gruen, R.J., *Do endogenous excitatory amino acids influence striatal dopamine release?* Brain Res., **1991**, 544: 329-330.

[17]. Morari, M., O'Connor, W.T., Ungerstedt, U., and Fuxe, K., *N-methyl-D-aspartic acid differentially regulates extracellular dopamine, GABA, and glutamate levels in the dorsolateral neostriatum of the halothane-anesthetized rat: an in vivo microdialysis study.* J. Neurochem., **1993**, 60: 1884-1893.

[18]. Kehr, J., Hu, X.-J., Yoshitake, T., and Scheller, D., *Determination of the dopamine agonist rotigotine in microdialysates from the rat brain by microbore column liquid chromatography with electrochemical detection.* J. Chromatogr. B, **2007**, 845: 109-113.

[19]. Patel, B.A., Arundell, M., Parker, K.H., Yeoman, M.S., and O'Hare, D., *Simple and rapid determination of serotonin and catecholamines in biological tissue using high-performance liquid chromatography with electrochemical detection.* J. Chromatogr. B, **2005**, 818: 269-276.

[20]. Zydron, M., Baranowski, J., Bialkowski, J., and Baranowska, I., *HPLC-FL/ED in the analysis of biogenic amines and their metabolites in urine.* Sep. Sci. Tech., **2005**, 40: 3137-3148.

[21]. Clarke, G., O'Mahony, S., Malone, G., and Dinan, T.G., *An isocratic high performance liquid chromatography method for the determination of GABA and glutamate in discrete regions of the rodent brain.* J. Neurosci. Methods, **2007**, 160: 223-230.

[22]. Qureshi, A.I., Ali, Z., Suri, M.F.K., Shuaib, A., Baker, G., Todd, K., Guterman, L.R., and Hopkins, L.N., *Extracellular glutamate and other amino acids in experimental intracerebral hemorrhage: An in vivo microdialysis study.* Crit. Care Med., **2003**, 31: 1482-1489.

[23]. Zuo, G.C., Yang, J.Y., Hao, Y., Dong, Y.X., and Wu, C.F., *Ethanol and acetaldehyde induce similar changes in extracellular levels of glutamate, taurine and GABA in rat anterior cingulate cortex.* Toxicol. Lett., **2007**, 169: 253-258.

[24]. Parrot, S., Sauvinet, V., Riban, V., Depaulis, A., Renaud, B., and Denoroy, L., *High temporal resolution for in vivo monitoring of neurotransmitters in awake epileptic rats using brain microdialysis and capillary electrophoresis with laser-induced fluorescence detection.* J. Neurosci. Methods, **2004**, 140: 29-38.

[25]. Parrot, S., Bert, L., Mouly-Badina, L., Sauvinet, V., Colussi-Mas, J., Lambas-Senas, L., Robert, F., Bouilloux, J.-P., Suaud-Chagny, M.-F., Denoroy, L., and Renaud, B., *Microdialysis monitoring of catecholamines and excitatory amino acids in the rat and mouse brain: recent developments based on capillary electrophoresis with laser-induced fluorescence detection - a mini-review.* Cell. Mol. Neurobiol., **2003**, 23: 793-804.

[26]. Hsieh, M.-H. and Chang, H.-T., *Discontinuous electrolyte systems for improved detection of biologically active amines and acids by capillary electrophoresis with laser-induced native fluorescence detection.* Electrophoresis, **2005**, 26: 187-195.

[27]. Oldenziel, W.H., Dijkstra, G., Cremers, T.I.F.H., and Westerink, B.H.C., *Evaluation of hydrogel-coated glutamate microsensors.* Anal. Chem., **2006**, 78: 3366-3378.

[28]. Greco, P.G., Meisel, R.L., Heidenreich, B.A., and Garris, P.A., *Voltammetric measurement of electrically evoked dopamine levels in the striatum of the anesthetized Syrian hamster.* J. Neurosci. Methods, **2006**, 152: 55-64.

[29]. Simons, S.S. and Johnson, D.F., *The structure of the fluorescent adduct formed in the reaction of o-phthalaldehyde and thiols with amines.* J. Am. Chem. Soc., **1976**, 98: 7098-7099.

[30]. Lindroth, P. and Mopper, K., *High performance liquid chromatographic determination of subpicomole amounts of amino acids by precolumn fluorescence derivatization with o-phthaldialdehyde.* Anal. Chem., **1979**, 51: 1667-1674.

[31]. Jacobs, W.A., Leburg, M.W., and Madaj, E.J., *Stability of o-phthalaldehyde-derived isoindoles.* Anal. Biochem., **1986**, 156: 334-340.

[32]. Jacobs, W.A., *o-Phthalaldehyde-sulfite derivatization of primary amines for liquid chromatography-electrochemistry.* J. Chromatogr., **1987**, 392: 435-441.

[33]. Rowley, H.L., Martin, K.F., and Marsden, C.A., *Determination of in vivo amino acid neurotransmitters by high-performance liquid chromatography with o-phthalaldehyde-sulphite dervatization.* J. Neurosci. Methods, **1995**, 57: 93-99.

[34]. Carlson, R.G., Srinivasachar, K., Givens, R.S., and Matuszewski, B.K., *New derivatizing agents for amino acids and peptides. 1. Facile synthesis of N-substituted-1-cyanobenz[f]isoindoles and their spectroscopic properties.* J. Org. Chem., **1986**, 51: 3978-3983.

[35]. de Montigny, P., Stobaugh, J.F., Givens, R.S., Carlson, R.G., Srinivasachar, K., Sternson, L.A., and Higuchi, T., *Naphthalene-2,3-dicarboxaldehyde/cyanide ion: A rationally designed fluorogenic reagent for primary amines.* Anal. Chem., **1987**, 59: 1096-1101.

[36]. Lena, I., Parrot, S., Deschaux, O., Muffat-Joly, S., Sauvinet, V., Renaud, B., Suaud-Chagny, M.-F., and Gottesmann, C., *Variations in extracellular levels of dopamine, noradrenaline, glutamate, and aspartate across the sleep-wake cycle in the medial prefrontal cortex and nucleus accumbens of freely moving rats.* J. Neurosci. Res., **2005**, 81: 891-899.

[37]. Plock, N. and Kloft, C., *Microdialysis - theoretical background and recent implementation in applied life-sciences.* Eur. J. Pharm. Sci., **2005**, 25: 1-24.

[38]. Robinson, T.E. and Justice Jr., J.B., *Microdialysis in the Neurosciences*, ed. J.P. Huston. **1991**, Amsterdam: Elsevier.

[39]. Kankaanpaa, A., Meririnne, E., Ariniemi, K., and Seppala, T., *Oxalic acid stabilizes dopamine, serotonin, and their metabolites in automated liquid chromatography with electrochemical detection.* J. Chromatogr. B, **2001**, 753: 413-419.

[40]. Thorre, K., Pravda, M., Sarre, S., Ebinger, G., and Michotte, Y., *New antioxidant mixture for long term stability of serotonin, dopamine, and their metabolites in automated microbore liquid chromatography with dual electrochemical detection.* J. Chromatogr. B, **1997**, 694: 297-303.

[41]. Zhang, X., Fuller, R.R., Dahlgren, R.L., Potgieter, K., Gillette, R., and Sweedler, J.V., *Neurotransmitter sampling and storage for capillary electrophoresis analysis.* Fresenius J. Anal. Chem., **2001**, 369: 206-211.

[42]. Robert, F., Bert, L., Parrot, S., Denoroy, L., Stoppini, L., and Renaud, B., *Coupling on-line brain microdialysis, precolumn derivatization and capillary electrophoresis for routine minute sampling of o-phosphoethanolamine and excitatory amino acids.* J. Chromatogr. A, **1998**, 817: 195-203.

[43]. Shah, A.J., Crespi, F., and Heidbreder, C., *Amino acid neurotransmitters: separation approaches and diagnostic value.* J. Chromatogr. B, **2002**, 781: 151-163.

[44]. Brajter-Toth, A. and Chambers, J.Q., eds. *Electroanalytical Methods for Biological Materials.* **2002**, Marcel Dekker, Inc.: New York.

[45]. Agilent Technologies, I., *Analysis of Catecholamines.* Product Catalog, **2003-2004**.

[46]. Thomas, B.R., Fang, X.G., Chen, X., Tyrrell, R.J., and Ghodbane, S., *Validated micellar electrokinetic capillary chromatography method for quality control of the drug substances hydrochlorothiazide and chlorothiazide.* J. Chromatogr. B, **1994**, 657: 383-394.

[47]. Timmerman, W. and Westerink, B.H.C., *Brain microdialysis of GABA and glutamate: what does it signify?* Synapse, **1997**, 27: 242-261.

[48]. Pfrieger, F.W. and Barres, B.A., *New views on synapse-glia interactions.* Curr. Opin. Neurobiol., **1996**, 6: 615-621.

[49]. David, H.N., Ansseau, M., and Abraini, J.H., *Dopamine-glutamate reciprocal modulation of release and motor responses in the rat caudate-putamen and nucleus accumbens of "intact" animals.* Brain Res. Rev., **2005**, 50: 336-360.

[50]. Trussell, L.O., Zhang, S., and Raman, I.M., *Desensitization of AMPA receptors upon multiquantal neurotransmitter release.* Neuron, **1993**, 10: 1185-1196.

[51]. Sun, Y., Olson, R., Horning, M., Armstrong, N., Mayer, M., and Gouaux, E., *Mechanism of glutamate receptor desensitization.* Nature, **2002**, 417: 245-253.

[52]. Tran, M.N., Higgs, M.H., and Lukasiewicz, P.D., *AMPA receptor kinetics limit retinal amacrine cell excitatory synaptic responses.* Vis. Neurosci., **1999**, 16: 835-842.

[53]. Vyklicky, L., Patneau, D.K., and Mayer, M., *Modulation of excitatory synaptic transmission by drugs that reduce desensitization at AMPA/Kainate receptors.* Neuron, **1991**, 7: 971-984.

[54]. Deng, L. and Chen, G., *Cyclothiazide potentially inhibits gamma-aminobutyric acid type A receptors in addition to enhancing glutamate responses.* Proc. Natl. Acad. Sci. U.S.A., **2003**, 100: 13025-13029.

[55]. Jaffe, E.H. and L., F., *Glutamate receptor desensitization block potentiates the stimulated GABA release through external Ca^{2+}-independent mechanisms from Granule cells of olfactory bulb.* Neurochem. Res., **2001**, 26: 1177-1185.

[56]. Segova, G. and Mora, F., *Role of nitic oxide in modulating the release of dopamine, glutamate, and GABA in striatum of the freely moving rat.* Brain Res. Bull., **1998**, 45: 275-279.

[57]. Castaneda, T.R., de Prado, B.M., Prieto, D., and Mora, F., *Circadian rhythms of dopamine, glutamate and GABA in the striatum and nucleus accumbens of the awake rat: modulation by light.* J. Pineal Res., **2004**, 36: 177-185.

[58]. Aultman, J.M. and Moghaddam, B., *Distinct contributions of glutamate and dopamine receptors to temporal aspects of rodents working memory using a clinically relevant task.* Psychopharmacology, **2001**, 153: 353-364.

[59]. Jedema, H.P. and Moghaddam, B., *Glutamatergic control of dopamine release during stress in the rat prefrontal cortex.* J. Neurochem., **1994**, 63: 785-788.

[60]. Kretschmer, B.D., *Modulation of the mesolimbic dopamine system by glutamate: Role of NMDA receptors.* J. Neurochem., **1999**, 73: 839-848.

[61]. Nieoullon, A., Kerkerian, L., and Dusticier, N., *Presynaptic controls in the neostriatum: Reciprocal interactions between the nigro-striatal dopaminergic neurons and the cortico-striatal glutamatergic pathway.* Exp. Brain Res., **1983**, Supp. 7: 54-65.

[62]. Pistis, M., Ferraro, L., Pira, L., Flore, G., Tanganelli, S., Gessa, G.L., and Devoto, P., *Δ^9-Tetradydrocannabinol decreases extracellular GABA and increases extracellular glutamate and dopamine levels in the rat prefrontal cortex: an in vivo microdialysis study.* Brain Res., **2002**, 948: 155-158.

[63]. Bamford, N.S., Zhang, H., Schmitz, Y., Wu, N.-P., Cepeda, C., Levine, M.S., Schmauss, C., Zakharenko, S.S., Zablow, L., and Sulzer, D., *Heterosynaptic dopamine neurotransmission selects sets of corticostriatal terminals.* Neuron, **2004**, 42: 653-663.

[64]. Budygin, E.A., Kilpatrick, M.R., Gainetdinov, R.R., and Wightman, R.M., *Correlation between behavior and extracellular dopamine levels in rat striatum: comparison of microdialysis and fast-scan cyclic voltammetry.* Neurosci. Lett., **2000**, 281: 9-12.

[65]. Budygin, E.A., Phillips, P.E.M., Robinson, D.L., Kennedy, A.P., Gainetdinov, R.R., and Wightman, R.M., *Effect of acute ethanol on striatal dopamine neurotransmission in ambulatory rats.* J. Pharmacol. Exp. Ther., **2001**, 297: 27-34.

[66]. Robinson, D.L., Venton, J.L., Heien, M.L.A., and Wightman, R.M., *Detecting subsecond dopamine release with fast-scan cyclic voltammetry.* Clin. Chem., **2003**, 49: 1763-1773.

[67]. Bradford, H.F., *Glutamate, GABA and Epilepsy.* Prog. Neurobiol., **1995**, 47: 477-511.

[68]. Pena, F. and Tapia, R., *Relationships among seizures, extracellular amino acid changes, and neurodegeneration induced by 4-aminopyridine in rat hippocampus: A microdialysis and electroencephalographic study.* J. Neurochem., **1999**, 72: 2006-2014.

[69]. Girardi, E., Ramos, A.J., Vanore, G., and Brusco, A., *Astrocytic response in hippocampus and cerebral cortex in an experimental epilepsy model.* Neurochem. Res., **2004**, 29: 371-377.

Chapter 4.

Enhanced Temporal Resolution Neurochemical Analysis
Using Capillary Electrophoresis

4.1. Introduction

4.1.1. Background and Significance

As stated in Chapter 3, "fast" neurochemical events have been electrically monitored to transpire on the timescale of 0.5 – 5 milliseconds [1, 2]. Many authors, beginning in the late 1970's with R. N. Adams [3, 4], have attempted to track these changes, primarily focusing on dopamine (DA), by electrochemical means [5-8]. Other authors have also attempted to understand the role of certain ions, such as potassium and chloride, within neurological disorders [9, 10]. While these typical carbon fiber (CF) electrodes perform very accurately at monitoring neurochemical changes, they are limited in functionality due to their inability to monitor multiple analytes simultaneously. This continues to be one area where microdialysis prevails. However, microdialysis has traditionally suffered from inadequate temporal resolution. This can prove problematic when neurochemical events are to be monitored. The insufficiencies in temporal resolution can primarily be attributed to the limited concentration detection limits of the analytical methods.

Microdialysis has more recently been reported for monitoring neurochemical events at temporal resolutions ranging from 6 - 30 seconds [11-15]. The ability to collect sub-minute samples using microdialysis is dependent upon different

parameters including the outer diameter of the probe, the thickness of the semi-permeable membrane, the internal volume of the probe, the perfusion rate, and the diffusion coefficient of the analyte of interest. For example, DA has a diffusion coefficient of 6.9×10^{-6} cm^2/s measured in water [16]. In the research from Chapter 3, the brain microdialysis probe used in the rat striatum had an outer diameter of 400 μm and a semi-permeable membrane length of 4 mm and thickness of 50 μm. When the microdialysis probe is perfused at a flow rate of 1 μL/min, the dead volume of the probe is approximately 0.5 μL, hence a delay time of 30 seconds. Considering the time for DA to diffuse across the probe membrane (~500 milliseconds), the fastest temporal resolution that this experiment could achieve is approximately 31 seconds. This sampling frequency could be significantly enhanced with the use of smaller diameter microdialysis probes and thinner semi-permeable membranes.

Due to the limited sample volumes obtained with higher temporal resolution microdialysis sampling, liquid chromatography (LC) methods are no longer applicable for the analysis of these samples [17]. Typical volumes required for injection onto an LC system range from > 2 μL [18]. Capillary electrophoresis (CE) is a separation technique that provides the ability to inject pL – nL sample volumes, therefore, the analysis of typical microdialysate collections of 0.5 – 1 μL are not problematic [17].

High temporal resolution sampling requires that highly sensitive methods be utilized for the analysis. Although CE is appropriate for the analysis of microdialysis samples, the use of a sensitive detection scheme is crucial. A typical detection

scheme used for CE is UV-Vis absorbance (UV). Unfortunately, CE-UV suffers from lowered concentration detection limits because of the small volume of the sample as well as the small detector pathlength (typically 25 – 75 μm). Common limits of detection (LODs) for CE-UV analyses are approximately 1 μM [19]. Owing to the fact that biologically relevant concentrations of several amino acids and most biogenic amines are in the picomolar (pM) – nanomolar (nM) range, CE-UV is not a viable option [19]. A very common, although expensive, route for the detection of amino acids and biogenic amines using CE instrumentation is laser-induced fluorescence (LIF) detection. CE-LIF allows enable low concentration detection limits to be obtained, approaching subnanomolar concentrations for amino acids and biogenic amines [20]. Taking advantage of the primary amine functionality on the amino acid and biogenic amine neurotransmitters, which are easily converted to a fluorescent product using NDA/CN⁻ (refer to Section 3.1.5.), LIF can be employed for the analysis of the minute volumes in the microdialysis samples.

4.1.2. Specific Aims of Research

The goal of this research was to use CE methods in order to improve the temporal resolution achieved with the LC methods discussed in Chapters 2 and 3. The temporal resolution for this research was improved to 60 seconds using CE, as opposed to the 5 minute sample collections discussed in Chapter 3 for the study of amino acid and biogenic amine neurotransmission. As higher temporal resolution produces smaller sample volumes, it also produces a large number of samples. CE-

LIF using an autosampler was employed for the analysis of NDA/CN$^-$ derivatized amino acid and biogenic amine neurotransmitters of interest - glutamate (Glu), γ-aminobutyric acid (GABA), and DA, as discussed in Chapter 3. The metabolites of DA, 3,4-dihydroxyphenylacetic acid (DOPAC) and homovanillic acid (HVA), were analyzed by CE-UV.

The 60 second microdialysis sample collections were analyzed and compared to data obtained from 5 minute microdialysis samples to identify whether more information could be extracted upon a higher sampling frequency. Again, a comparison was made between the Glu-DA correlation for the 60 second samples as well as between the 60 second and 5 minute sample collections (Chapter 3).

4.2. Materials and Methods

4.2.1. Chemicals / Reagents

Methanol, hydrochloric acid, and sodium hydroxide were obtained from Fisher Scientific (Pittsburgh, PA). Sodium tetraborate decahydrate, lithium tetraborate, lithium dodecyl sulfate (LDS), tetradecyltrimethylammonium bromide (TTAB), L-glutamic acid (Glu), L-aspartic acid (Asp), L-arginine (Arg), γ-amino-n-butyric acid (GABA), β-alanine (β-Ala), sodium cyanide, 3,4-dihydroxyphenethylamine hydrochloride (DA), L-arterenol (NE), homovanillic acid (HVA), 3,4-dihydroxyphenylacetic acid (DOPAC), and 4-hydroxybenzoic acid (4-HBA) were obtained from Sigma-Aldrich (St. Louis, MO). Naphthalene-2,3-dicarboxaldehyde (NDA) was obtained from Invitrogen (Carlsbad, CA). All

solutions were prepared in 18.2 MΩ distilled, deionized water (Labconco, Kansas City, MO) and filtered through 0.22 μm pore size membrane filters prior to use unless otherwise noted.

4.2.2. Instrumentation

4.2.2.1. CE with UV-Vis Absorbance Detection (CE-UV)

Separations were performed on a Beckman P/ACE MDQ (Beckman Coulter, Palo Alto, CA) with UV absorbance detection at 214 nm. Fused silica separation capillaries with an i.d. of 50 μm and o.d. of 360 μm (Polymicro Technologies, Phoenix, AZ) and a length of 61.5 cm were used. An active window was created by burning off a 3 mm length of the polyimide coating from the fused silica capillary 10 cm from the outlet, and then cleaning the outside of the capillary with copious amounts of methanol. The data were acquired using a 32 Karat Gold software package (Beckman Coulter, Palo Alto, CA) at 4 Hz.

The background electrolyte (BGE) for the CE-UV analyses was 75 mM sodium tetraborate, 0.5 mM TTAB, pH 8.4. The pH was adjusted using 0.1 M HCl. Prior to use, the BGE was filtered through a 0.22 μm syringe membrane filter (Millipore, Bedford, MA).

Daily, before use, the separation capillary was "activated" by conditioning with 100% methanol (10 min), water (2 min), 0.1 M HCl (5 min), water (2 min), 0.1 M NaOH (10 min), water (2 min), and BGE (10 min) sequentially at a pressure of 20 psi. Prior to the first use of the BGE, an Ohm's Plot was conducted in order to

determine the linear range where Joule heating was effectively dissipated. The separation voltage for these experiments was -20 kV. Between injections, the capillary was flushed with 0.1 M NaOH (1.5 min), water (0.5 min), and BGE (2 min) sequentially at 20 psi to rinse the capillary of any remaining analytes and to maintain a uniform charge density on the silanol groups of the capillary.

4.2.2.2. CE with Laser-Induced Fluorescence Detection (CE-LIF)

Separations were performed on a Beckman P/ACE MDQ (Beckman Coulter, Palo Alto, CA) with and external ZETALIF LIF detector (Picometrics, France). The LIF detector was comprised of an OmniChrome He/Cd laser (Melles Griot, Carlsbad, CA) with an excitation wavelength of 442 nm and an emission filter at 490 nm. Fused silica separation capillaries with an i.d. of 50 μm and o.d. of 360 μm (Polymicro Technologies, Phoenix, AZ) and a length of 75 cm were used. An active window was created by burning off a 3 mm length of the polyimide coating from the fused silica capillary 15 cm from the outlet, and then cleaning the outside of the capillary with copious amounts of methanol. The data were acquired using a 32 Karat Gold software package (Beckman Coulter, Palo Alto, CA) at 4 Hz.

The background electrolyte (BGE) for the CE-LIF analyses was adapted from Siri *et al*. [21] and was comprised of 22.5 mM lithium tetraborate, 20 mM LDS, pH 9.2 (unadjusted). Prior to use, the BGE was filtered through a 0.22 μm syringe membrane filter (Millipore, Bedford, MA).

162

Daily, before use, the separation capillary was "activated" by conditioning with 100% methanol (10 min), water (3 min), 0.1 M HCl (10 min), water (3 min), 0.1 M NaOH (15 min), water (3 min), and BGE (10 min) sequentially at a pressure of 20 psi. Prior to the first use of the BGE, an Ohm's Plot was conducted in order to determine the linear range where Joule heating was effectively dissipated. The separation voltage for these experiments was 21 kV. Between injections, the capillary was flushed with 100% methanol (2 min), 0.1 M NaOH (3 min), water (1 min), and BGE (3 min) sequentially at 20 psi to rinse the capillary of any remaining analytes and to minimize the adsorption of the LDS to the wall of the capillary.

4.2.3. Experimental

The experimental protocol for this research is as described in Section 2.3.5.2. This research was limited to only the striatum because this region is of great interest based on the research discussed in Chapter 3. The main difference with this research was that a higher temporal resolution was employed and microdialysis samples were collected every 2.5 minutes initially, and then further improved to 60 second collections at a perfusion rate of 1 μL/min.

To each sample, an appropriate volume of internal standard (IS) (discussed in more detail below) which was contained in 0.1 M $HClO_4$ was added. The samples were then placed into the freezer at -20 °C until analysis.

4.3. Results and Discussion

4.3.1. CE-UV Method Development

In order to efficiently separate the metabolites of DA, the pKa values of both DOPAC and HVA must be taken into consideration. These are acids with pKa values of 4.42 and 4.39, respectively. If a BGE is used which is greater than pH 6, both of these compounds will be anionic. Since these are the only two analytes which were monitored with CE-UV, a method utilizing the anionic nature of the compounds was developed.

It is very common in CE to separate analytes with acid moieties, such as phenolic acids, with a sodium tetraborate BGE [22, 23]. Due to the similarities in the analytes of interest with phenolic acids, the first BGE studied was that of sodium tetraborate. A CE method originally used by Qian *et al*. was modified for the separation of these anionic metabolites of DA via the addition of TTAB in order to reverse the electroosmotic flow (EOF) [24]. A concentration of 75 mM sodium tetraborate was used with the addition of 0.5 mM TTAB. The pH was adjusted to 8.4 with 0.1 M HCl. Figure 4.1(A) displays an example electropherogram with standards of DOPAC and HVA. The IS employed for this analysis was 4-HBA. The separation conditions used clearly resolved DOPAC and HVA from the other peaks present within the dialysate.

With this method, DOPAC and HVA were linear in the range of 5 - 50 μM. Detection limits, calculated with S/N = 3, were 2 μM for DOPAC and 3 μM for
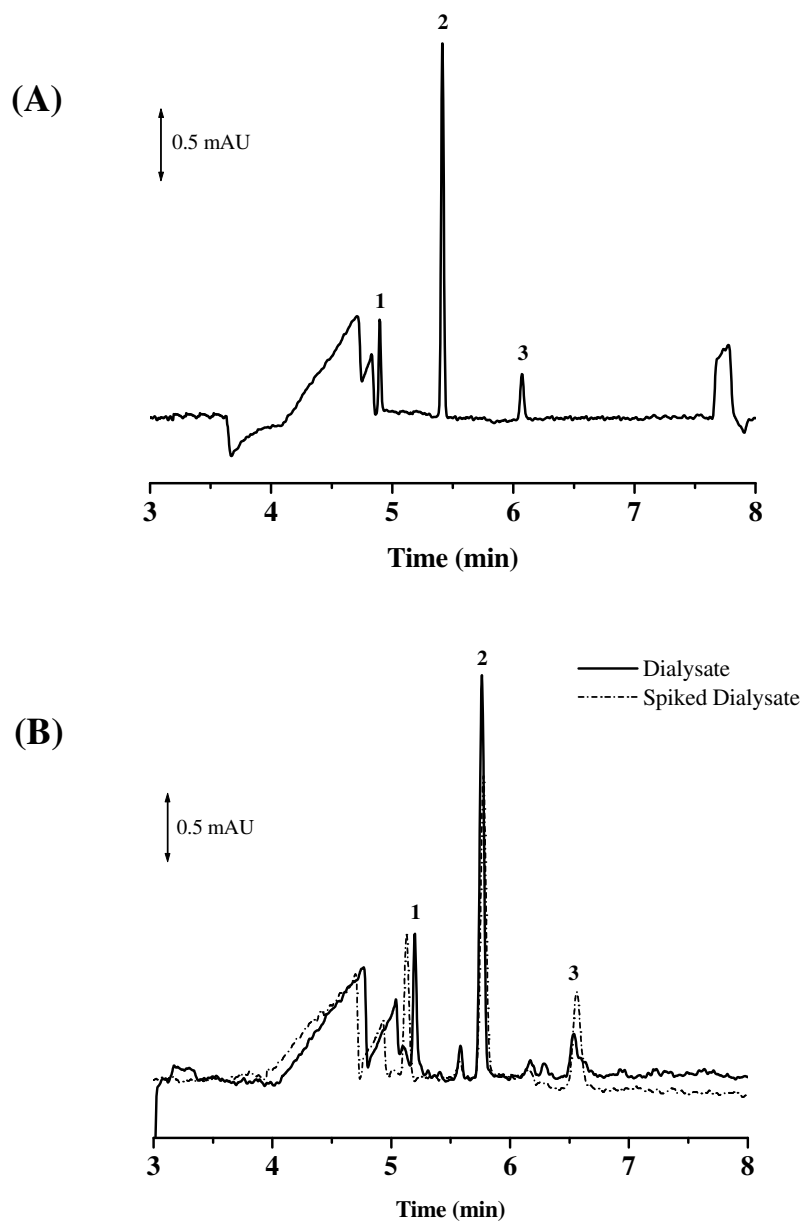
Figure 4.1. CE-UV electropherograms displaying DOPAC and HVA. (A) 10 mM DOPAC and HVA standard injection; (B) Microdialysate injection with DOPAC and HVA mixture spiked in for peak identification. All CE-UV conditions are as described in Section 4.2.2.1. [1 = DOPAC; 2 = 4-HBA (IS); 3 = HVA].

HVA. Figure 4.1(B) shows a representative microdialysate sample after spiking with a DOPAC and HVA standard for peak identification.

4.3.2. CE-LIF Method Development

A 2.5 μL volume of standard or microdialysate sample was used and the NDA/CN⁻ derivatization was carried out by adding 0.3 μL of an IS, 0.5 μL of 500 mM borate : 87 mM sodium cyanide (100:20 v:v), and 0.3 μL of 3 mM NDA. A representative standard electropherogram is displayed in Figure 4.2. The IS for this analysis was β-Ala. The LODs for the neurotransmitters of interest using the 2.5 μL sample size are listed in Table 4.1.

Table 4.1. CE-LIF LODs for amino acid and biogenic amine neurotransmitters of interest. Values are using a S/N = 3.

	LOD for using 2.5 minute microdialysis sample (nM)	LOD for using 60 second microdialysis sample (nM)
Glu	0.7	1.0
GABA	0.5	0.8
DA	1.0	1.5
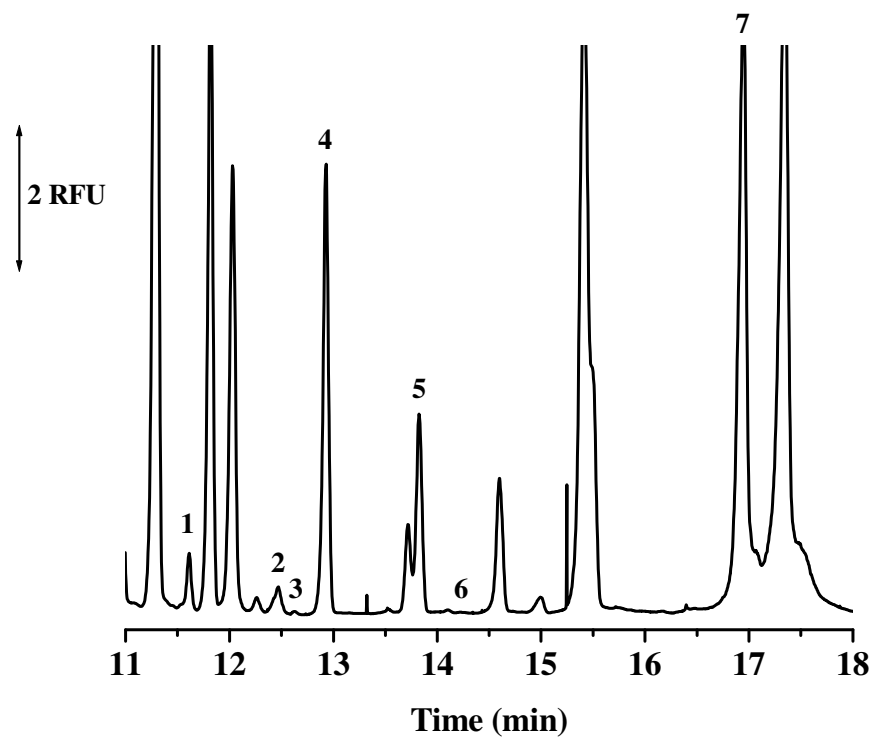
Figure 4.2. CE-LIF electropherograms displaying amino acid and biogenic amine neurotransmitters from striatal microdialysate. All CE-LIF conditions are as described in Section 4.2.2.2. [1 = β-Ala (IS); 2 = GABA; 3 = NE; 4 = Glu; 5 = Asp; 6 = DA; 7 = Arg]

For the analysis of the 60 second microdialysis samples, the method was re-evaluated due to a larger dilution of the sample. When 2.5 µL volume of microdialysis sample was derivatized, the sample was diluted by 30.5%. If a 60 second microdialysis sample was diluted up to 2.5 µL and then derivatized, the dilution factor would grow to 73.2% and the detection of the nanomolar biogenic amines would be greatly affected. Therefore, the samples were used as collected, and only 1 µL of microdialysate was derivatized using the previously described protocol. This resulted in a dilution factor of 52.4%. The method was linear over a tested concentration range of 0.5 – 2 µM for Glu, Asp and Arg, and 5 – 1000 nM for NE, DA and GABA. The LODs using a derivatized 60 second microdialysis sample for the main neurotransmitters of interest are also listed in Table 4.1.

The limitation of using this protocol, as stated earlier, was that the dilution of the sample did not allow for low concentrations of DA to be analyzed. Therefore, the sample had to be analyzed twice - once using a smaller dynamic range setting to encompass the DA, NE, and GABA, and subsequently using a larger dynamic range setting to encompass the Asp, Arg, and Glu. In Figure 4.2, a larger dynamic range setting was employed in order to detect Glu. Figure 4.3(A) illustrates an electropherogram using a smaller dynamic range setting which enabled the analysis of DA and GABA. Figure 4.3(B) shows the same microdialysis sample spiked with a DA and GABA standard for peak identification.
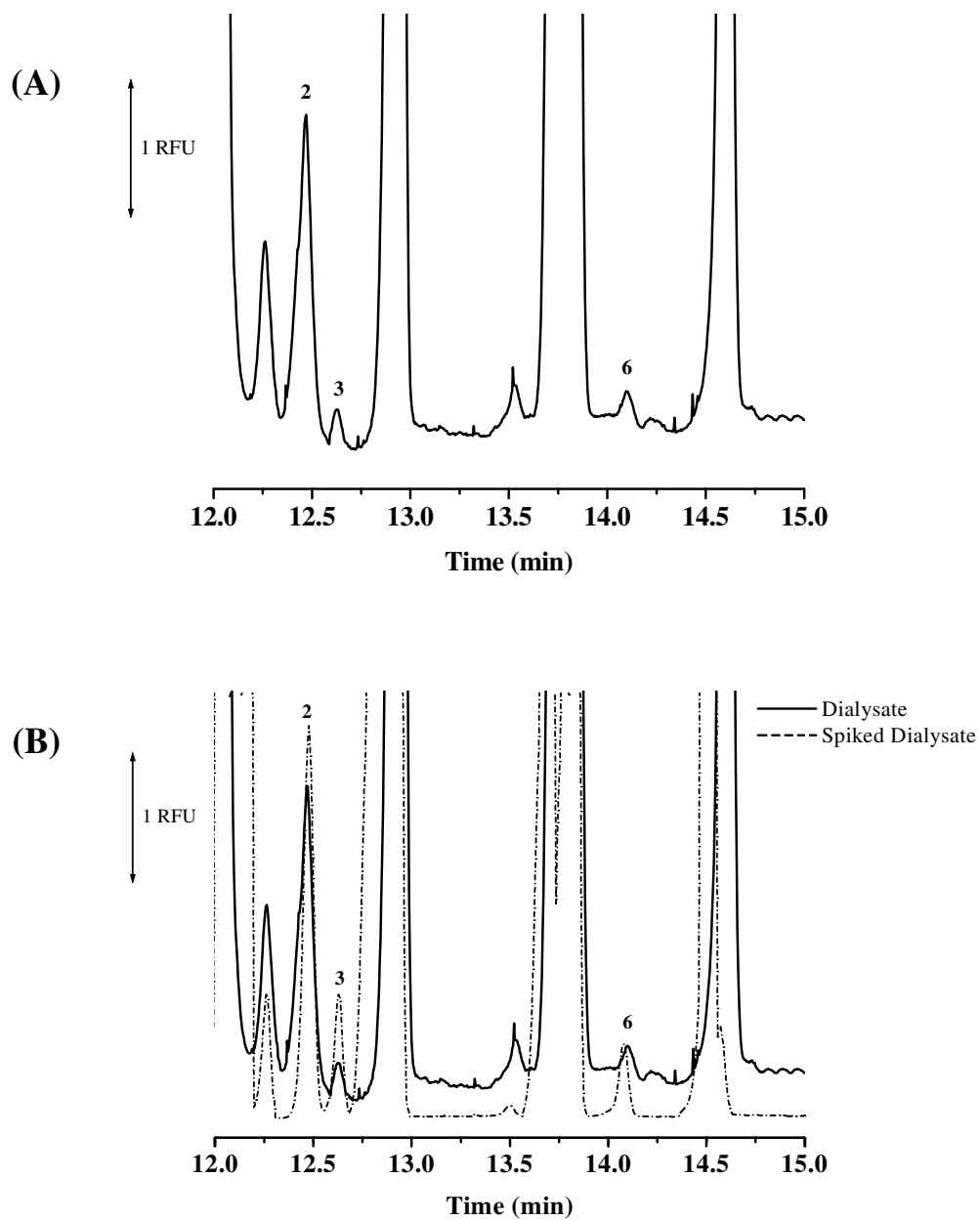
Figure 4.3. CE-LIF electropherograms displaying GABA and DA. (A) Microdialysate injection identifying GABA and DA; (B) Microdialysate injection with GABA and DA mixture spiked for peak identification. All CE-LIF conditions are as described in Section 4.2.2.2. [2 = GABA; 3 = NE; 6 = DA].

4.3.3. Derivatized Microdialysis Sample Stability

Since a commercially available CE-LIF with an autosampler was being employed for the separation and detection of the amino acid and biogenic amine neurotransmitters, the stability of the derivatized microdialysis samples needed to be determined. Figure 4.4 displays a plot of the amino acid neurotransmitters (Glu and GABA) and biogenic amine neurotransmitter (DA) of interest. The plot shows that derivatized Glu and GABA are stable for well over 11 hours as has been reported in literature [25, 26]. However, DA rapidly degrades, losing approximately 20% of its derivatized product within the first 4 hours. The striatal dopamine concentration has been reported ranging between 10 - 18 nM [27, 28]. Since the derivatized DA samples degrade at this rate, the LODs (Table 4.1) will quickly be approached. Therefore, to assure that the smallest derivatized DA sample loss would occur, the autosampler portion of the CE-LIF was not used.

4.3.4. 2.5 Minute Temporal Resolution

For this set of experiments, the sampling frequency was enhanced to 2.5 minutes in order to raise the level of understanding of the associated neurochemical changes. Figure 4.5(A) depicts the amino acid neurotransmitter data using a 2.5 minutes sampling frequency. For Glu, a couple of small areas of spiking can be observed between 15 - 20 mintues and between 40 - 45 mintues. However, these areas are not very definitive in true deviations from the basal values. There was again a sustained increase in Glu near the end of the experiment. For GABA, there was
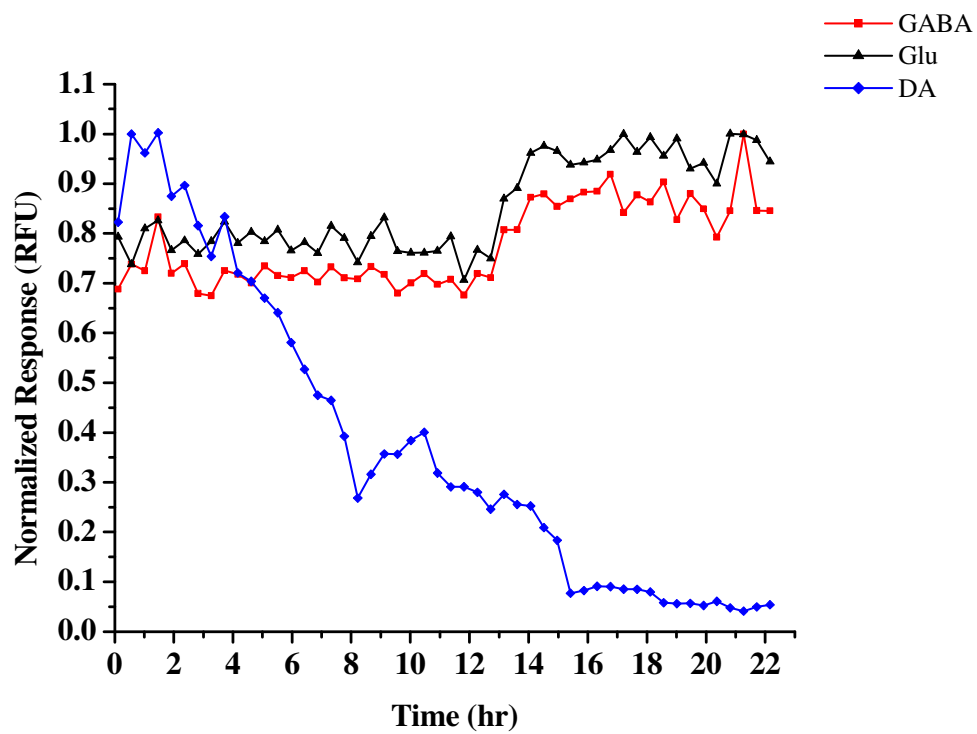
Figure 4.4. Stability plot for NDA/CN- derivatized amino acid and biogenic amine neurotransmitters.

Figure 4.5. Glu and GABA data from 2.5 minute microdialysis sampling. (A) Percent change in Glu and GABA over the time course of the experiment; (B) Percent change in DA over the time course of the experiment. 3-MPA was administered at t = 0 minutes in both. Boxes represent the time in which a steady-state concentration of 3-MPA was achieved in each region. The arrow represents the time in which the infusion was stopped.

a trend toward decreased levels immediately after the administration of the 3-MPA and continues until approximately 30 minutes after the cessation of the 3-MPA intravenous (i.v.) infusion.

The biogenic amine neurotransmitter results are illustrated in Figure 4.5(B). Again, only DA and its metabolites, DOPAC and HVA, show any deviations from basal values as was observed in Chapter 3. DA shows equivalent biphasic spiking activity comparable to the results previously obtained using a 5 minute sampling frequency. DOPAC and HVA also had similar trends with decreases from basal levels (see Figure 3.16).

A more detailed picture of the biogenic amine neurotransmission, especially for DA, was illustrated using this 2.5 minute temporal resolution. More detail was introduced within both of the phasic DA spikes. However, not much information was gained in terms of the amino acid neurotransmission. A biphasic trend in Glu was possibly emerging, but it was still difficult to confirm this using the data collected (n = 1 rat).

Using 2.5 minute temporal resolution did not prove to be very beneficial in obtaining a greater understanding of the neurochemical changes observed with the 3-MPA seizure model. In order to gain a more thorough picture of the biphasic activity of DA and the possibility of biphasic activity within Glu, the temporal resolution was increased even further to 60 seconds.

4.3.5. 60 Second Temporal Resolution

For this set of experiments, the sampling frequency was increased to 60 seconds over the time periods from 10 – 30 minutes (to encompass the first phasic activity of DA) and 40 – 75 minutes (to encompass the second phasic activity of DA). Figure 4.6(A) displays the amino acid neurotransmitter data from a collection of 3 experiments using this 60 second microdialysis sampling. A very interesting observation arises upon the investigation of the Glu data. The biphasic activity in Glu, which was thought to be observed after using 2.5 minute temporal resolution, was confirmed. Between the time frames of 5 – 25 minutes and 40 – 65 minutes, Glu activity significantly spiked ($p < 0.05$ and $p < 0.10$, respectively). There was also a sustained increase in Glu during the final 30 minutes of the experiment. The activity of GABA was consistent with what was previously observed (see Figure 3.14). GABA significantly decreased to varying degrees between 10 – 70 minutes as was expected ($p < 0.05$ and $p < 0.01$). This 60 second sampling frequency proved to be advantageous in the case of Glu when compared against the 5 minute sampling of Glu discussed in Chapter 3. Figure 4.6(B) portrays the average Glu data from this investigation superimposed onto the average Glu data from the 5 minute temporal resolution. It was shown that having the higher sampling frequency did help to detect an increased number of spiking events with the Glu data. The biphasic activity in Glu was not detected until the microdialysis collections were reduced from 5 minutes to 60 seconds.

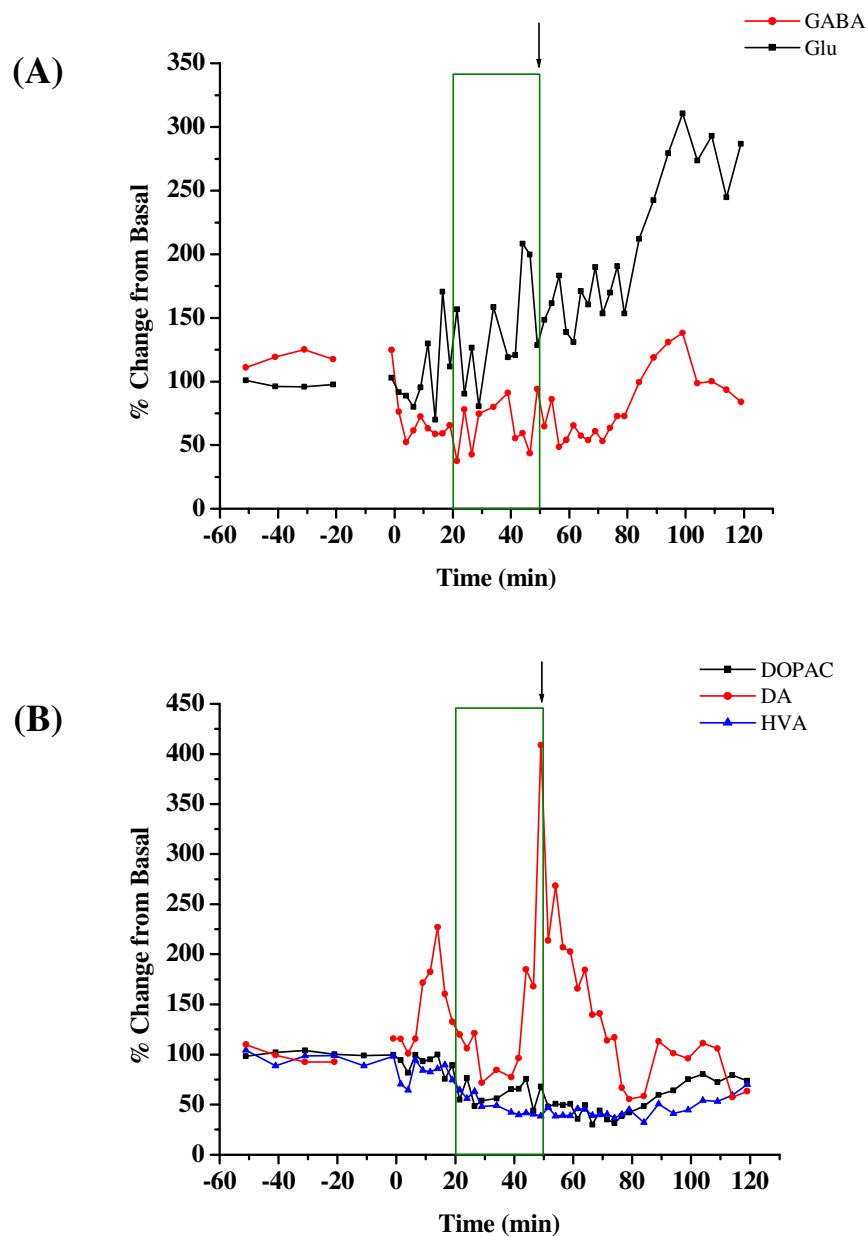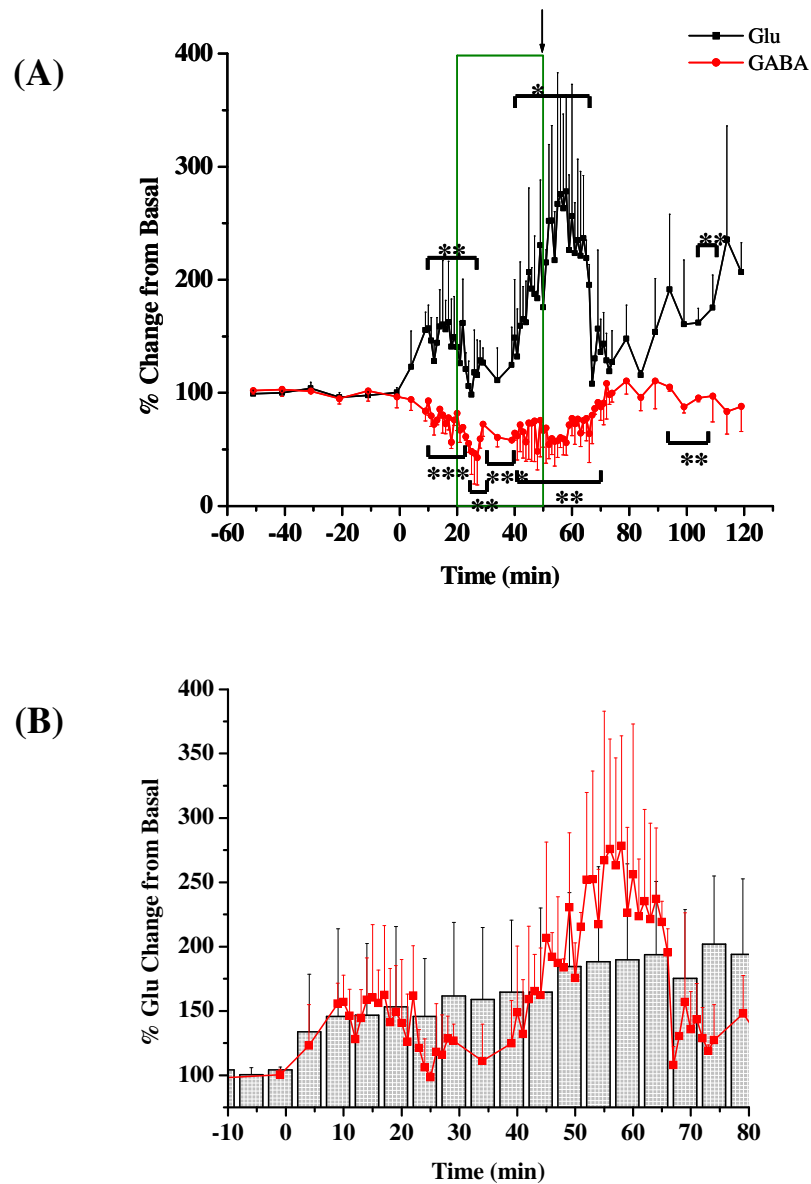Figure 4.6. Glu and GABA data from 60 second microdialysis sampling. (A) Percent change in Glu and GABA over the time course of the experiment; (B) 60 second microdialysis sampling superimposed onto 5 minute microdialysis sampling for DA. Red circles represent 60 second samples and gray histograms represent the 5 minute sampling. Plot is magnified to show areas of significance. 3-MPA was administered at $t = 0$ minutes in both. All other conditions are as noted in Figure 4.4. [* = $p < 0.10$; ** = $p < 0.05$; *** = $p < 0.01$]

The biogenic amine neurotransmitter data are shown in Figure 4.7(A) (for clarity purposes, only the DA data are plotted). Noticeable upon first inspection of the data was that, again, the biphasic activity of DA was still present. These biphasic changes were significant ($p < 0.10$ and $p < 0.05$) when compared to the basal values. The 60 second microdialysis sampling illustrated, in more detail, the working knowledge of the DA neurotransmission than the 5 minute sampling did (see Figure 3.16). Figure 4.7(B) overlays the average DA data from this study with that of the average DA data from the 5 minute temporal resolution experiments (discussed in Chapter 3). It was again observed that, while the overall biphasic DA activity was still present, the activity was much more defined. There were instances of inflections noted within each phase using the 60 second collections which were not observed using the 5 minute collections.

Using 60 second temporal resolution with microdialysis sampling proved to be beneficial in gaining more knowledge about the amino acid and biogenic amine neurotransmitters, in particular Glu and DA. The biphasic activity within both Glu and DA proved to be very interesting in this research as it allowed for a better correlation between the two neuronal systems as was illustrated by the 60 second sampling intervals. This will be discussed in Section 4.3.6.

4.3.6. Glutamatergic - Dopaminergic Correlation?

As discussed in Section 3.3.1., it has been debated heavily over the past two decades about the relationship which Glu and DA share in terms of their neuronal
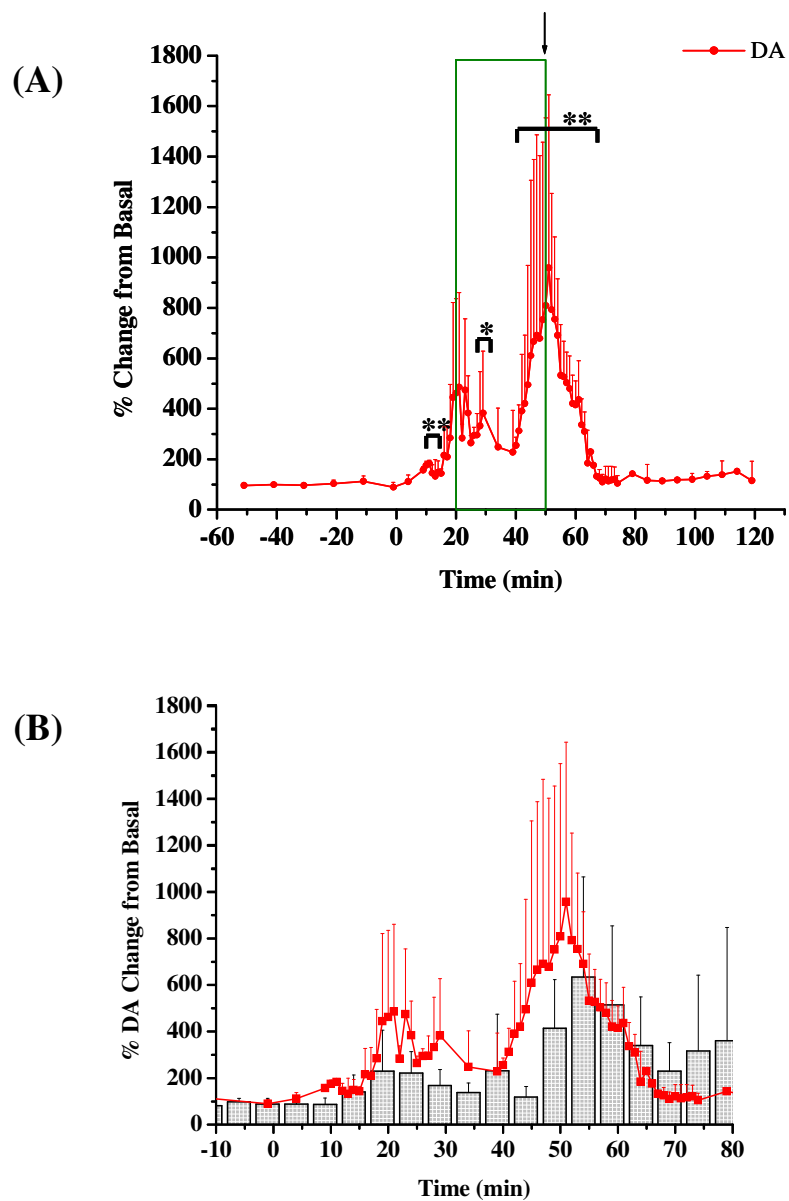
Figure 4.7. DA data from 60 second microdialysis sampling. (A) Percent change in DA over the time course of the experiment; (B) 60 second microdialysis sampling superimposed onto 5 minute microdialysis sampling for DA. Red circles represent 60 second samples and gray histograms represent the 5 minute sampling. Plot is magnified to show areas of significance. 3-MPA was administered at t = 0 minutes in both. All other conditions are as noted in Figure 4.4. [* = p < 0.10; ** = p < 0.05]

activity. Authors have argued for the glutamatergic modulation of dopaminergic neuronal activity [29-36] while others have argued for the dopaminergic modulation of the glutamatergic neuronal activity [37, 38]. Other authors additionally argue the role of Glu and DA to be a dual excitatory-inhibitory one. For example, Leviel *et al*. [39] showed that the perfusion of Glu at low concentrations (10^{-8} M) caused an increase in the release of DA while the perfusion of Glu at higher concentrations (10^{-4} M) proved to cause a decrease in the amount of DA observed. Using the 60 second microdialysis sampling and further analysis of the collected data, two different hypotheses have been developed to help explain the findings believed to link the activity of Glu and DA within the striatum.

In Chapter 3, it was discussed that the time trends relating the onset of changes in Glu and/or DA as well as the time between the phasic activities could relay some knowledge of a correlation between the two. Table 4.2(A) displays the time trends observed from the 60 second microdialysis sampling for Glu. This was possible as a direct result of the faster temporal resolution achieved with 60 second sampling. Table 4.2(B) shows the same type of time trend data DA. It was observed that the first phasic increase in Glu occured before DA ($p < 0.01$), and the second phasic increase in Glu occured at approximately the same time as the second phasic increase in DA. It was hypothesized that the first phasic increase in Glu actually causes the first phasic increase in DA. Several authors have reported that Glu acts as a non-specific ionotropic receptor agonist, activating both NMDA and AMPA receptors when released into the synaptic cleft [31, 40-42]. The activation of NMDA

Table 4.2. Time trends for excessive glutamate and dopamine using 60 second microdialysis sampling.

(A)		Median Time (t) for 1ˢᵗ Glu Spike (min)	Median Time (t) for 2ⁿᵈ Glu Spike (min)	Δt (min)
	Rat 1	15	55	40
	Rat 2	17	56	39
	Rat 3	18	60	42
	Avg ± SD	17 ± 2	57 ± 3	40 ± 2

(B)		Median Time (t) for 1ˢᵗ DA Spike (min)	Median Time (t) for 2ⁿᵈ DA Spike (min)	Δt (min)
	Rat 1	20	51	31
	Rat 2	23	53	30
	Rat 3	24	57	33
	Avg ± SD	22 ± 2	54 ± 3	31 ± 2

Table 4.3. ECoG data from 60 second microdialysis sampling.

	60 mg/kg bolus + 50 mg/kg/min infusion: 5 minute sampling[a]	60 mg/kg bolus + 50 mg/kg/min infusion: 60 second sampling[b]
Latency to Seizure Onset (s)	363.2 ± 148.8	438.0 ± 165.5
Number of Seizures Detected	592 ± 187	830 ± 62
Average of the Average Seizure Duration (s)	0.87 ± 1.78	0.6 ± 0.2
R_{max}	71.8 ± 22.2	25.4 ± 1.5

a: n = 12 rats
b: n = 3 rats

and AMPA receptors caused a subsequent activation in locomotor activity, and furthermore an increase in the release of DA. This was further validated by the observed convulsions in the animal and the latency to seizure onset (as shown in ECoG data in Table 4.3). The seizure onset times consistently preceded the observed release in the neurotransmitters. For example, the first seizure activity in the animal was observed consistently to occur on average 9.6 minutes before the first phasic activity in Glu. DA has its first phasic response exactly 5 minutes later.

The second phasic activity in both Glu and DA was hypothesized to arise from the modulatory effect DA has over Glu. This was due to the start of the second phasic release in DA which consistently occurred before the start of the second phasic release for Glu. As mentioned above, excess Glu release activates both NMDA and AMPA receptors. Konradi [38] revealed that upon activation of an NMDA receptor, the DA D_1 receptor acts to facilitate the further release of Glu. The other major DA receptor, the D_2 receptor, acts to facilitate the release of Glu when the AMPA receptor is activated.

While investigating which mechanism may be causing the observed trends in *this* study, a more in depth analysis of the research discussed in Chapter 3 involving cyclothiazide (CTZ) proved to be somewhat confounding. CTZ is known to resensitize AMPA receptors which have been desensitized due to excess Glu activity in the synaptic cleft [2, 43]. When CTZ was constantly perfused into the brain, no significant increase was observed for Glu during the 3-MPA seizure model (see Figure 3.19). However, the first phasic increase in DA disappeared and the second

phasic increase was still present. This was proof that the first phasic response was more than likely caused by Glu modulating the release of DA. The puzzling portion of the CTZ data arises from the second phasic release of both Glu and DA. No increase in Glu was observed throughout the entirety of the experiment when CTZ was present, but a phasic increase was still observed for DA. If this excess DA release were modulating either NMDA or AMPA receptors, an increased response should be noted for Glu. Since there was not a second increase noted for Glu, another mechanism appears to be playing a role.

Another question which arises is why, or how, does the DA stop being excessively released in each phase? The answer to this may lie with the $GABA_A$ and/or $GABA_B$ receptors. DA neurons are also known to have, in addition to AMPA and NMDA receptors, $GABA_A$ and $GABA_B$ receptors located on their spines [40]. Upon the activation of either GABA receptor, the membranes become hyperpolarized and the DA activity is decreased. There was a noted correlation in the times in which GABA made a return towards basal values as well as when DA falls back to basal values. For example, in Figure 4.6(A), although GABA remained decreased throughout the majority of the experiment, it did return towards basal values on two occasions. The first of these occurred at approximately the 30 minute time point. DA, shown in Figure 4.7(A), at the 30 minute time point is just falling to basal values. The second GABA return towards basal values was at approximately 65 minutes. When the corresponding DA data was observed for this time frame, it was shown to fall abruptly back to its basal level. These data would now indicate a possible role of

the GABA receptors in the overall mechanism of action implemented due to the 3-MPA seizure model.

An alternative way to investigate the Glu and DA data is a way in which the 3-MPA seizure model is considered as a model which produces hypoxic and/or ischemic events. The striatum is an area of the brain very susceptible to hypoxia and ischemia [44]. This is mainly due to the deep, centralized location of the striatum within the brain, as well as the numerous dopaminergic neurons located within the striatum. These factors also allow for the striatum to be a site for acidification, occurring when glucose becomes utilized for anaerobic glycolysis instead of oxidative metabolism [45]. It is believed that lactic acid production increases as a result of hypoxia and/or ischemic events [46]. The lactic acid accumulation in the tissue is linearly accompanied by an intracellular, as well as an extracellular lowering of the pH [47, 48]. It has been shown that upon lactic acid buildup in the striatum, DA is excessively released [49]. This excess release of DA can be cytotoxic, resulting from both enzymatic and non-enzymatic oxidation processes which generate reactive oxygen species (ROS) [50, 51]. Research involving both Glu and DA has concluded that the formation of free radicals due to ischemia can facilitate the release of Glu, and that this increased release of Glu can further facilitate the release of DA [52, 53].

Research by Remblier *et al.* describes a study involving the addition of lactic acid to the perfusion medium which aided in the formation of lactacidosis within the striatum [45, 54]. The outcome of this work led to an observed biphasic increase in

the DA activity, but only a monophasic increase for the Glu activity within the striatum. It was concluded that the first phasic release of DA was due to the excessive release of Glu (Glu excitotoxicity) as well as ROS formation. The second phasic release in DA (not accompanied by Glu release) was thought to be purely due to ROS formation. These data could help to explain the some of the trends observed with the data collected from the 60 second microdialysis samples using the 3-MPA seizure model. This theory agreed that the excessive Glu release observed modulates the first phasic release of DA observed. However, the second phasic Glu response was not validated using this theory. A further investigation into ROS production using the 3-MPA seizure model would be of great interest. Figure 4.8 provides a schematic detailing the effects encountered upon an ischemic event within the striatum. Oxygen deprivation and a depletion of energy stores have a great affect on cellular metabolism, eventually leading to depolarization of the neuron, and the release of an excessive amount of Glu. The subsequent activation of the Glu ionotropic receptors cause the uptake of extra Ca^{2+}, which is known to trigger cascading second-messenger systems, eventually leading to cell death [1, 53].

4.4. Conclusions

From this research, increasing the microdialysis sampling time within the striatum from 5 minutes to 2.5 minutes did not prove to be a dramatic improvement in the amount of knowledge received about the neurochemical events as related to the 3-MPA chemical seizure model. However, increasing the temporal resolution to the 60
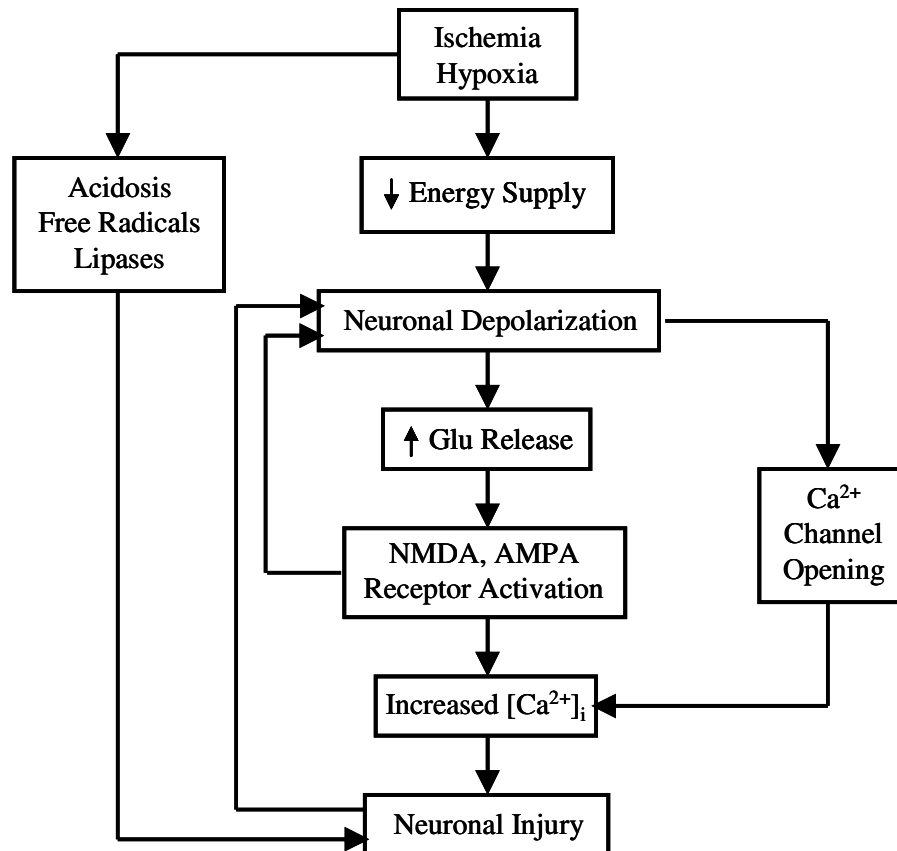
Figure 4.8. Potential pathway for neuronal damage within striatum resulting from an ischemic or hypoxic episode. Adapted from Siegel *et al.* [1].

second time scale proved to be very valuable in assessing the neurochemical changes. The 60 second temporal resolution was sufficient in this research, showing an increase in the amount of information attainable on the neurotransmitter systems versus 5 minute resolution. If other brain regions or endogenous chemical messengers are studied; however, the temporal resolution may need to be enhanced appropriately with consideration of the parameters mentioned in Section 4.1.1.

The changes which were observed in the neurotransmitters, especially Glu and DA, were hypothesized to be part of a mechanism which relates the neuronal activities of the two. It was possible that Glu was regulating the initial release of DA via the activation of DA D_2 receptors located on the AMPA receptors. It was also hypothesized that the changes observed in Glu and DA functions could be related to ischemic events within the striatum. The second phasic release of DA could be related to either hypoxic or ischemic events which occurred as a result of the 3-MPA seizure model. Further experimentation should be performed in order to evaluate whether one or both of these hypothetical situations were occurring.

4.5. References

[1]. Siegel, G.J., Agranoff, B.W., Albers, R.W., Fisher, S.K., and Uhler, M.D., eds. *Basic Neurochemistry: Molecular, Cellular, and Medical Aspects*. 6th ed. **1999**, Lippincott Williams & Wilkins: Philadelphia.

[2]. Vyklicky, L., Patneau, D.K., and Mayer, M., *Modulation of excitatory synaptic transmission by drugs that reduce desensitization at AMPA/Kainate receptors.* Neuron, **1991**, 7: 971-984.

[3]. Adams, R.N., *Probing brain chemistry with electroanalytical techniques.* Anal. Chem., **1976**, 48: 1128A-1137A.

[4]. Wightman, R.M., Strope, E., Plotsky, P., and Adams, R.N., *In vivo voltammetry: monitoring of dopamine metabolites in CSF following release by electrical stimulation.* Brain Res., **1978**, 159: 55-68.

[5]. Budygin, E.A., Kilpatrick, M.R., Gainetdinov, R.R., and Wightman, R.M., *Correlation between behavior and extracellular dopamine levels in rat striatum: comparison of microdialysis and fast-scan cyclic voltammetry.* Neurosci. Lett., **2000**, 281: 9-12.

[6]. Budygin, E.A., Phillips, P.E.M., Robinson, D.L., Kennedy, A.P., Gainetdinov, R.R., and Wightman, R.M., *Effect of acute ethanol on striatal dopamine neurotransmission in ambulatory rats.* J. Pharmacol. Exp. Ther., **2001**, 297: 27-34.

[7]. Greco, P.G., Meisel, R.L., Heidenreich, B.A., and Garris, P.A., *Voltammetric measurement of electrically evoked dopamine levels in the striatum of the anesthetized Syrian hamster.* J. Neurosci. Methods, **2006**, 152: 55-64.

[8]. Robinson, D.L., Venton, J.L., Heien, M.L.A., and Wightman, R.M., *Detecting subsecond dopamine release with fast-scan cyclic voltammetry.* Clin. Chem., **2003**, 49: 1763-1773.

[9]. Gorji, A., Stemmer, N., Rambeeck, B., Jurgens, U.H., May, T.W., Pannek, H.W., Behne, F., Ebner, A., Straub, H., and Speckmann, E.-J., *Neocortical microenvironment in patients with intractable epilepsy: potassium and chloride concentrations.* Epilepsia, **2006**, 47: 297-310.

[10]. Obrenovitch, T.P. and Zilkha, E., *High extracellular potassium, not extracellular glutamate, is required for the propagation of spreading depression.* J. Neurophysiol., **1995**, 73: 2107-2114.

[11]. Bert, L., Parrot, S., Robert, F., Desvignes, C., Denoroy, L., Suaud-Chagny, M.-F., and Renaud, B., *In vivo temporal sequence of rat striatal glutamate, aspartate and dopamine efflux during apomorphine, nomifensine, NMDA and PDC in situ administration.* Neuropharmacology, **2002**, 43: 825-835.

[12]. Parrot, S., Bert, L., Mouly-Badina, L., Sauvinet, V., Colussi-Mas, J., Lambas-Senas, L., Robert, F., Bouilloux, J.-P., Suaud-Chagny, M.-F., Denoroy, L., and Renaud, B., *Microdialysis monitoring of catecholamines and excitatory amino acids in the rat and mouse brain: recent developments based on capillary electrophoresis with laser-induced fluorescence detection - a mini-review.* Cell. Mol. Neurobiol., **2003**, 23: 793-804.

[13]. Bert, L., Robert, F., Denoroy, L., Stoppini, L., and Renaud, B., *Enhanced temporal resolution for the microdialysis monitoring of catecholamines and excitatory amino acids using capillary electrophoresis with laser-induced fluorescence detection: Analytical developments and in vitro validations.* J. Chromatogr. A, **1996**, 755: 99-111.

[14]. Lada, M.W., Vickroy, T.W., and Kennedy, R.T., *High temporal resolution monitoring of glutamate and aspartate in vivo using microdialysis on-line with capillary electrophoresis with laser-induced fluorescence detection.* Anal. Chem., **1997**, 69: 4560-4565.

[15]. Tucci, S., Rada, P., Sepulveda, M.J., and Hernandez, L., *Glutamate measured by 6-s resolution brain microdialysis: capillary electrophoretic and laser-induced fluorescence detection application.* J. Chromatogr. B, **1997**, 694: 343-349.

[16]. Tao, L. and Nicholson, C., *Diffusion of albumins in rat cortical slices and relevance to volume transmission.* Neuroscience, **1996**, 75: 839-847.

[17]. *Handbook of Capillary Electrophoresis*. 2nd ed, ed. J.P. Landers. **1997**, Boca Raton: CRC Press, Inc.

[18]. Harris, D.A., *Quantitative Chemical Analysis*. 5th ed. **1999**, New York: W. H. Freeman and Company.

[19]. Cunico, R.L., Gooding, K.M., and Wehr, T., *Basic HPLC and CE of Biomolecules*. **1998**, Richmond: Bay Bioanalytical.

[20]. Karger, B.L., *Capillary Electrophoresis: Overview and Perspective*, in *High Performance Capillary Electrophoresis*. **1998**, John Wiley & Sons, Inc.: San Diego. p. 3-24.

[21]. Siri, N., Lacroix, M., Garrigues, J.-C., Poinsot, V., and Couderc, F., *HPLC-fluorescence detection and MEKC-LIF detection for the study of amino acids and catecholamines labelled with naphthalene-2,3-dicarboxyaldehyde* Electrophoresis, **2006**, 27: 4446-4455.

[22]. Peng, Y., Liu, F., and Ye, J., *Determination of phenolic acids and flavones in Lonicera japonica Thumb. by capillary electrophoresis with electrochemical detection.* Electroanalysis, **2005**, 17: 356-362.

[23]. Peng, Y., Ye, J., and Kong, J., *Determination of Phenolic Compounds in Perilla frutescens L. by Capillary Electrophoresis with Electrochemical Detection.* J. Agric. Food Chem., **2005**, 53: 8141-8147.

[24]. Qian, J., Wu, Y., Yang, H., and Michael, A.C., *An integrated decoupler for capillary electrophoresis with electrochemical detection: application to analysis of brain microdialysate.* Anal. Chem., **1999**, 71: 4486-4492.

[25]. Dawson, L.A., Organ, A.J., Winter, P., Lacroix, L.P., Shilliam, C.S., Heidbreder, C., and Shah, A.J., *Rapid high-throughput assay for the measurement of amino acids from microdialysates and brain tissue using monolithic C18-bonded reversed-phase columns.* J. Chromatogr. B, **2004**, 807: 235-241.

[26]. Shah, A.J., de Biasi, V., Taylor, S.G., Roberts, C., Hemmati, P., Munton, R., West, A., Routledge, C., and Camilleri, P., *Development of a protocol for the automated analysis of amino acids in brain tissue samples and microdialysates.* J. Chromatogr. B, **1999**, 735: 133-140.

[27]. Hurd, Y.M. and Ungerstedt, U., *Cocaine: an in vivo microdialysis evaluation of its acute action on dopamine transmission in rat striatum.* Synapse, **1989**, 3: 48-54.

[28]. Shou, M., Ferrario, C.R., Schultz, K.N., Robinson, T.E., and Kennedy, R.T., *Monitoring Dopamine in Vivo by Microdialysis Sampling and On-Line CE-Laser-Induced Fluorescence.* Anal. Chem., **2006**, 78: 6717-6725.

[29]. Aultman, J.M. and Moghaddam, B., *Distinct contributions of glutamate and dopamine receptors to temporal aspects of rodents working memory using a clinically relevant task.* Psychopharmacology, **2001**, 153: 353-364.

[30]. Jedema, H.P. and Moghaddam, B., *Glutamatergic control of dopamine release during stress in the rat prefrontal cortex.* J. Neurochem., **1994**, 63: 785-788.

[31]. Kretschmer, B.D., *Modulation of the mesolimbic dopamine system by glutamate: Role of NMDA receptors.* J. Neurochem., **1999**, 73: 839-848.

[32]. Nieoullon, A., Kerkerian, L., and Dusticier, N., *Presynaptic controls in the neostriatum: Reciprocal interactions between the nigro-striatal dopaminergic neurons and the cortico-striatal glutamatergic pathway.* Exp. Brain Res., **1983**, Supp. 7: 54-65.

[33]. Pistis, M., Ferraro, L., Pira, L., Flore, G., Tanganelli, S., Gessa, G.L., and Devoto, P., *Δ^9-Tetradydrocannabinol decreases extracellular GABA and increases extracellular glutamate and dopamine levels in the rat prefrontal cortex: an in vivo microdialysis study.* Brain Res., **2002**, 948: 155-158.

[34]. Shimizu, N., Duan, S., Hori, T., and Oomura, Y., *Glutamate modulates dopamine release in the striatum as measured by brain microdialysis.* Brain Res. Bull., **1990**, 25: 99-102.

[35]. Takahata, R. and Moghaddam, B., *Target-specific glutamatergic regulation of dopamine neurons in the ventral tegmental area.* J. Neurochem., **2000**, 75: 1775-1778.

[36]. Youngren, K.D., Daly, D.A., and Moghaddam, B., *Distinct actions of endogenous excitatory amino acids on the outflow of dopamine in the nucleus accumbens.* J. Pharmacol. Exp. Ther., **1993**, 264: 289-293.

[37]. Bamford, N.S., Zhang, H., Schmitz, Y., Wu, N.-P., Cepeda, C., Levine, M.S., Schmauss, C., Zakharenko, S.S., Zablow, L., and Sulzer, D., *Heterosynaptic dopamine neurotransmission selects sets of corticostriatal terminals.* Neuron, **2004**, 42: 653-663.

[38]. Konradi, C., ed. *Dopamine modulation of responses mediated by excitatory amino acids in the neostriatum.* Catecholamines: Bridging Basic Science with Clinical Medicine, ed. D.S. Goldstein, G. Eisenhofer, and R. McCarty. **1998**, Academic Press: San Diego. 724-729.

[39]. Leviel, V., Gobert, A., and Guibert, B., *The glutamate-mediated release of dopamine in the rat striatum: further characterization of the dual excitatory-inhibitory function.* Neuroscience, **1990**, 39: 305-312.

[40]. Chen, B.T. and Rice, M.E., *Synaptic regulation of somatodendritic dopamine release by glutamate and GABA differs between substantia nigra and ventral tegmental area.* J. Neurochem., **2002**, 81: 158-169.

[41]. David, H.N., Ansseau, M., and Abraini, J.H., *Dopamine-glutamate reciprocal modulation of release and motor responses in the rat caudate-putamen and nucleus accumbens of "intact" animals.* Brain Res. Rev., **2005**, 50: 336-360.

[42]. Desce, J.M., Godeheu, G., Galli, T., Artaud, F., Cheramy, A., and Glowinski, J., *L-glutamate-evoked release of dopamine from synaptosomes of the rat striatum: involvement of AMPA and NMDA receptors.* Neuroscience, **1992**, 47: 333-339.

[43]. Trussell, L.O., Zhang, S., and Raman, I.M., *Desensitization of AMPA receptors upon multiquantal neurotransmitter release.* Neuron, **1993**, 10: 1185-1196.

[44]. Smith, M.L., von Hanwehr, R., and Siesjo, B.K., *Changes in extra- and intracellular pH in the brain during and following ischemia in hyperglycemic and in moderately hypoglycemic rats.* J. Cereb. Blood Flow Metab., **1986**, 6: 574-583.

[45]. Remblier, C., Pontcharraud, P., Tallineau, C., Piriou, A., and Huguet, F., *Lactic acid-induced increase of extracellular dopamine measured by microdialysis in rat striatum: evidence for glutamatergic and oxidative mechanisms.* Brain Res., **1999**, 837: 22-28.

[46]. Siesjo, B.K., *Acidosis and ischemic brain damage.* Neurochem. Pathol., **1988**, 9: 31-88.

[47]. La Manna, J.C., Giffith, J.K., Cordisco, B.R., Lin, C.W., and Lust, W.D., *Intracellular pH in rat brain in vivo and in brain slices.* Can. J. Physiol. Pharmacol., **1992**, 70: 5269-5277.

[48]. Much, W.A. and Hansen, A.J., *Extracellular pH changes during spreading depression and cerebral ischemia: mechanisms of brain pH regulation.* J. Cereb. Blood Flow Metab., **1984**, 4: 17-27.

[49]. Globus, M.Y.-T., Busto, R., Dietrich, W.D., Martinez, E., Valdes, I., and Ginsberg, M.D., *Effect of ischemia on the in vivo release of striatal dopamine, glutamate and γ-aminobutyric acid studied by intracerebral microdialysis.* J. Neurochem., **1988**, 51: 1455-1464.

[50]. Graham, D.G., *Oxidative pathways for catecholamines in the genesis of neuromelanin and cytotoxic quinones.* Mol. Pharmacol., **1978**, 14: 633-643.

[51]. Hasting, T.G., *Enzymatic oxidation of dopamine: the role of prostaglandin H synthase.* J. Neurochem., **1995**, 64: 919-924.

[52]. Pelligrini-Giampietro, D.E., Cherici, G., Alesiani, M., Carla, V., and Moroni, F., *Excitatory amino acid release from rat hippocampal slices as a consequence of free-radical formation.* J. Neurochem., **1988**, 51: 1960-1963.

[53]. Pelligrini-Giampietro, D.E., Lombardi, G., Cherici, G., Carla, V., and Moroni, F., *Excitatory amino acid release during in vitro and in vivo models of ischemia: are free radicals involved?*, in *Excitatory Amino Acids and Brain Ischemia: Pharmacological and Clinical Aspects*, G. Biggio, et al., Editors. **1989**, Pergamon Press: Oxford. p. 45-56.

[54]. Remblier, C., Jolimay, N., Wahl, A., Pariat, C., Piriou, A., and Huguet, F., *Extracellular dopamine and catabolites in rat striatum during lactic acid perfusion as determined by in vivo microdialysis.* Brain Res., **1998**, 804: 224-230.

Chapter 5.

Dual-Electrode Detection for Capillary Electrophoresis:
Feasibility of a New Dual-Detector Design

5.1. Introduction

5.1.1. Background and Significance

While CE-LIF and CE-UV proved promising for the increased temporal resolution analysis of microdialysis samples, the analysis of the samples was inconvenient. Since the NDA/CN$^-$ derivatized dopamine (DA) samples had a high rate of degradation, the available autosampler for the CE-LIF could not be employed. Also, during the analysis glutamate (Glu) and g-aminobutyric acic (GABA), the sensitivity of the LIF detector was not sufficient to monitor DA. In this situation, the samples had to be analyzed twice on different dynamic range settings in order to monitor all of the neurotransmitters of interest.

Since the NDA/CN$^-$ derivatives are also electroactive, electrochemical detection coupled to CE (CE-EC) is an attractive alternative to using CE-LIF. EC detection is much cheaper to implement, relatively simple to setup, and has competitive limits of detection (LODs) versus LIF detection. Subnanomolar detection limits for dopamine (DA), norepinephrine (NE) and serotonin (5-HT) have been reported recently by Weng *et al*. using CE-EC [1]. As discussed in Chapter 1, CE lends itself easily to miniaturization. Microchip CE has emerged as a growing trend over the past few years [2, 3]. EC detection for microchip CE is a very popular

detection scheme due to its inexpensive design and ease of integration [4]. A microchip CE-EC method has recently been reported to provide LODs for glutamate (Glu) and aspartate (Asp) of ~200 nM [5]; Kong *et al*. have achieved LODs for DA of 650 nM [3]. Along with the above mentioned advantages of EC detection, the properties of wide linear dynamic ranges and excellent selectivity in biological matrices make the detection scheme a unique alternative [2, 4].

5.1.2. Amperometric Detection for Capillary Electrophoresis

The basis for EC detection results from the generation of an electrical signal which arises from the interaction of three electrodes. The working electrode (WE), the reference electrode (RE), and the auxiliary electrode (AE) are placed into a solution containing the analytes of interest [6]. EC detection can be broken into two main classifications, potentiometric and faradaic techniques [7]. Potentiometry is the measure of the difference in the potential of two electrodes being held at a constant current [7]. This potential difference is related to the concentration of the analyte in solution. Faradaic techniques are based on applying a controlled potential to a solution of analytes and monitoring the current output which arises from the oxidation or reduction of the analytes [7]. This measurable current is used to relay information regarding the concentration of the analytes.

Two common forms of faradaic techniques are voltammetry and amperometry [8]. This discussion will focus primarily on amperometry. Amperometry allows for the oxidation or reduction (redox) of analytes to occur at the surface of the electrode,

thereby allowing a measurable current to pass through the electrochemical cell (Equation 5.1). In the three-electrode setup, redox reactions occur at the WE, the RE

$$O + ne^- \rightleftharpoons R \qquad (5.1)$$

is comprised of a reversible redox couple (*e.g.* Ag/AgCl) and maintains a constant reference potential, and the AE to complete the circuit [7]. The controlled potential which is applied to the WE is received from a potentiostat. When a potential is applied to the WE, an excess of charge is developed on the surface of the electrode. The solvent molecules and the electrolyte species orient towards the electrode surface to counter this charge build up. This interaction is known as the electrical double-layer and extends from the surface of the electrode approximately 1 – 10 nm [9]. Only molecules within this double-layer are affected during an EC experiment.

The measurable current resulting from the applied potential comes directly

$$Q = nFN \qquad (5.2)$$

from Faraday's law as shown in Equation 5.2 [6-8]. Q is the charge (coulombs), n is the number of the electrons transferred (equivalents per mole), F is Faraday's constant (96,485 coulombs per equivalent), and N is the number of moles undergoing the reaction. Faraday's Law displays the linear relationship between the charge passing through the EC cell and the quantity of the chemical reaction which has taken

place. For the purposes described in these studies, the measurement of the current

generated from the WE is important. The first derivative of Faraday's law, shown in

$$i(t) = (dQ/dt) = nF(dN/dt) \qquad (5.3)$$

Equation 5.3, displays a rate equation relating the electrical response (current) to the

rate of a chemical reaction.

EC detection is a powerful electroanalytical detection scheme commonly

coupled with CE for the routine analysis of biological samples [10]. However, the

coupling of the separation and detection techniques presents potential problems.

Special precautions must be taken when arranging the EC cell containing the

separation capillary and the electrode. This is primarily due of the differences in

currents generated from the separation voltage within the capillary and the applied

potential at the microelectrode. It is of critical importance that the current due the

separation voltage be isolated from the current due to the applied potential at the

surface of the WE. There are two common strategies for isolating these currents

when coupling CE to EC detection, on-column detection and end-column detection

[10].

5.1.2.1. On-Column Detection

On-column detection implies the WE is on, or inside (also known as in-

capillary) the separation capillary [10]. Figure 5.1 displays a typical single carbon
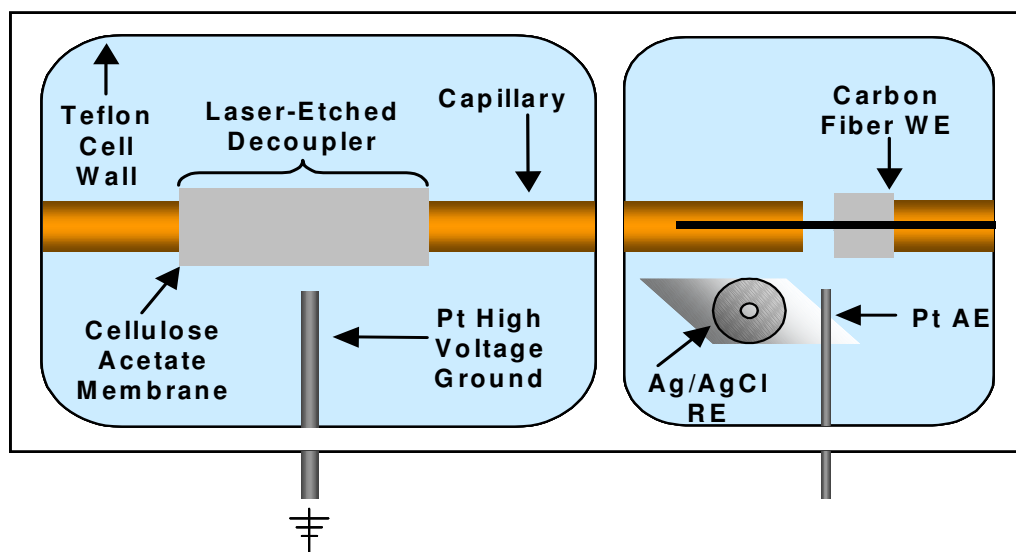
Figure 5.1. Single-electrode CE-EC schematic using on-column detection. Adapted from Osbourn [11].

fiber (CF) electrode inserted into the outlet end of the separation capillary, a design commonly employed in our laboratory. Other electrode materials can be employed in a similar fashion, including Au/Hg amalgam [12], copper [13, 14], and diamond [15].

In on-column detection, the separation current needs to be isolated from the current of the WE, or the analyte signal will be masked [10]. The isolation of the separation current from the EC detector can be accomplished using an electrical decoupler. The electroosmotic flow (EOF) will help to carry the analytes of interest across the decoupler, towards the microelectrode. The first electrical decoupler made from porous glass was introduced by Wallingford and Ewing [16]. This decoupler consisted of fracturing the capillary and adding a porous glass sleeve over the fracture. Since its initiation, the decoupler has undergone many transformations, including a bare fracture [17], a bare fracture with a Nafion polymer coating [18, 19], hydrofluoric acid (HF) acid etching of the capillary [20, 21], and a laser-etched opening in the capillary coated with a cellulose acetate polymer [22] in order to create the optimal design.

The main advantage of this detection design is no loss of the analyte due to the diffusion away from the WE, and ease and reproducibility of electrode placement. The main limitation lies in the difficulty to manufacture and maintain the decoupler due to its fragile nature.

5.1.2.2. End-Column Detection

End-column detection implies that the WE is positioned outside of the outlet end of the separation capillary as shown in Figure 5.2(A). In this design, the need for an electrical decoupler is negated since the WE is not actually inside the separation capillary [10]. The current due to the separation voltage is minimal to non-existent at the surface of the WE. This is due primarily to the voltage drop across the length of the capillary being sufficient to shield the majority of the separation current [23, 24]. The separation currents can be kept minimal by the employment of small i.d. (25 μm) separation capillaries, low concentration (ionic strength) buffers, or low separation buffers. Improvements have been made to the end-column detection design through the implementation of HF acid etching. HF etching dissolves the inner walls of the separation capillary, thereby increasing the i.d. of the separation capillary nearest to outlet in a conical pattern [24-26]. In this manner, the electrode can be inserted into the separation capillary very close to the end of the HF etched portion (the original i.d. of the capillary) as shown in Figure 5.2(B).

The main advantage of this design is that it does not require an electrical decoupler. However, even the improved design of HF etching is not without issues. In these designs, it has been shown that the current from the separation voltage was not effectively shielded at the EC detector, resulting in a shift in the half-wave potentials for the analytes of interest [27, 28]. Other limitations of end-column detection include the difficult and reproducible alignment of the WE with the outlet
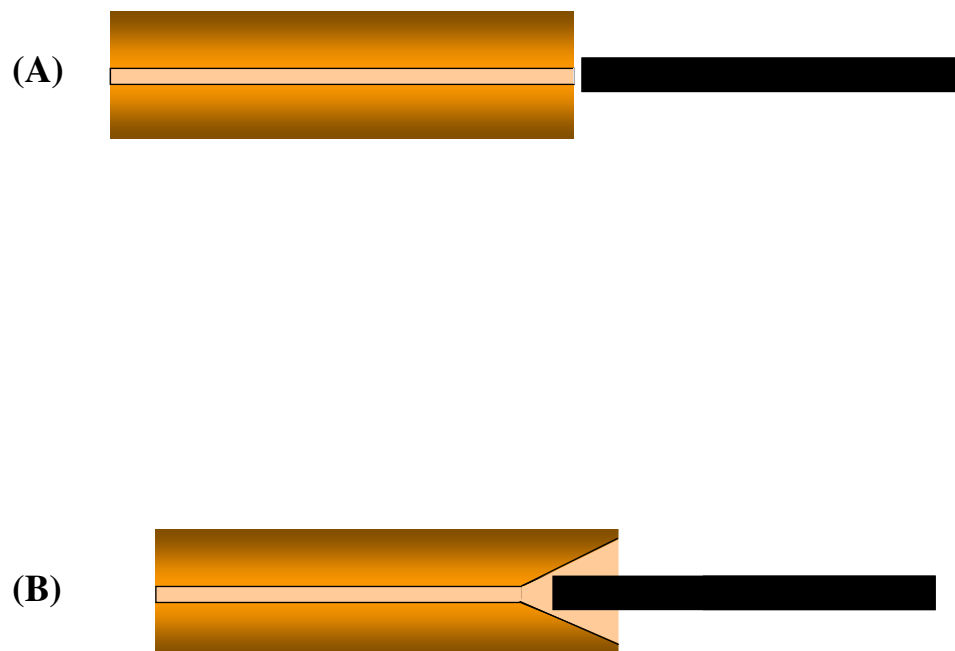
(A)

(B)

Figure 5.2. Schematic of end-column detection for CE. (A) Conventional end-column detection with CF electrode outside of separation capillary; (B) Improved end-column detection using HF etching with CF electrode placed into the separation capillary.

of the separation capillary, and the loss of sensitivity which occurs as the analyte diffuses in solution away from the separation capillary to the WE.

5.1.3. Dual-Electrode Detection for Capillary Electrophoresis

The problems of limited dynamic range from the use of a single detector and decreased sensitivity can be overcome quite easily by employing the use of dual-electrode detection. For example, dual-electrode detection was developed for liquid chromatography (LC) for the purpose of increasing the sensitivity and selectivity of the analysis [29-32]. Figure 5.3 illustrates the different possibilities for the configuration of the dual-electrode detector. Using the dual-electrode in the "series" mode, the chemical reversibility of compounds of interest can be exploited at the different electrodes by selectively oxidizing the analytes at the first electrode and then reducing the analytes at the second electrode as shown in Figure 5.3(A). Using the dual-electrode in the "parallel-adjacent" mode, the peak identification can be enhanced by measuring the current ratios of the peaks while holding both electrodes in either the oxidation or reduction mode as shown in Figure 5.3(B). Also, when using the dual-electrode in the "parallel-opposed" mode, the redox chemistry of an analyte can be exploited to enhance its sensitivity via redox cycling as shown in Figure 5.3(C).

The first dual-amperometric detection for CE was developed in 1994 for the detection of cysteine and cystine [33]. A Au/Hg amalgam electrode wire was placed upstream to reduce cystine and a Au/Hg amalgam disk electrode was placed
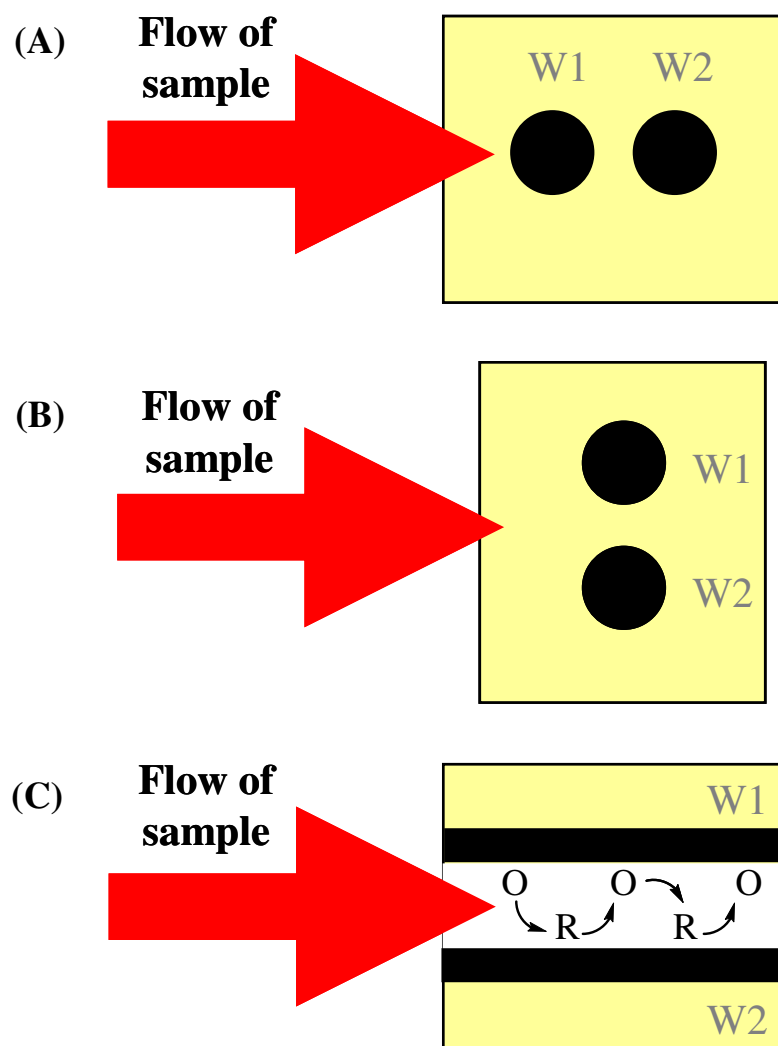
Figure 5.3. Different possible configurations for dual-electrode detection in LC. (A) "series" mode; (B) "parallel-adjacent" mode; (C) "parallel-opposed" mode.

downstream for the detection of cysteine oxidation. This work was soon followed by Zhong *et al*. with a ring-disk and a parallel carbon electrode [34]. Both designs were used in the end-column format for the detection of biogenic amine neurotransmitters with LODs of 5 μm. A design by Voegel and Baldwin was the first "integrated" dual-electrode approach [35]. In this work, dual separation capillaries were used with sputter-coated electrodes on the outlet end. In another approach by Zhong and Lunte, a series dual-Au/Hg electrode was developed using a tubular upstream electrode and a disk electrode downstream for the detection of thiol- and disulfide-containing peptides from a tryptic digest of ribonuclease A [12]. A second "integrated" dual electrode design was implemented by Holland *et al*. using platinum wires for the detection of a mixture of phenolic acids [36]. The upstream electrode was inserted into the end of the capillary and bent over the edge of the capillary and glued into place. A second downstream electrode was placed over the outlet of the capillary perpendicular to the first and glued to the sides of the separation capillary. LODs for the phenolic acids tested ranged from 1.2 – 4.7 μM. Alternatively, a parallel-opposed dual-electrode scheme was employed by Chen *et al*. in order to employ redox cycling to enhance the sensitivity over conventional CE-EC [37, 38]. LODs for DA were reported as 12 nM.

5.1.4. Specific Aims of Research

The goal of this research was to develop an analytical detection scheme employing conventional CE with dual-parallel electrode detection in order to

circumvent some of the main issues surrounding single detection schemes, including the need for enhanced selectivity within a complex biological sample and enhanced sensitivity of the detector. This new dual-parallel electrode design provided for operation in a variety of detection modes, including the "series" and "parallel-opposed" modes for redox cycling and the "parallel-adjacent" mode for monitoring the peak ratios within an electrophoretic analysis. These modes of operation were demonstrated using a variety of analytes.

The analytes of interest chosen for this feasibility study were the well known redox couple, hydroquinone (H_2Q) and benzoquinone (BQ), and a mixture of phenolic acids including 3,4-dihydroxybenzoic acid (3,4-DHBA), 4-hydroxybenzoic acid (4-HBA), syringic acid (SA), and ferulic acid (FA) as shown in Figure 5.4. H_2Q and BQ were chosen primarily for an investigation into the differences in the amount of redox cycling observed within the dual-parallel electrode design as a result of any changes that occur in flow velocity. The phenolic acids were chosen for the development of a separation and also determining the amount of redox cycling within a mixture and obtaining selective peak identification by monitoring current ratios.

5.2. Materials and Methods

5.2.1. Chemicals / Reagents

Methanol, hydrofluoric acid, hydrochloric acid, sodium hydroxide, hydroquinone (H_2Q), and benzoquinone (BQ) were obtained from Fisher Scientific (Pittsburgh, PA). H_2Q was used as received; however, BQ was purified via a
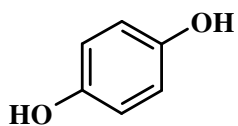
Hydroquinone (H₂Q)

$pKa \sim 10.33$ **(most acidic)**
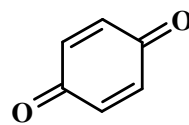
1,4-Benzoquinone (BQ)
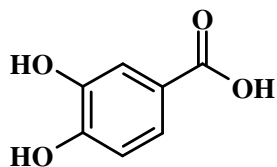
3,4-Dihydroxybenzoic acid (3,4-DHBA)

$pKa \sim 4.45$ **(most acidic)**
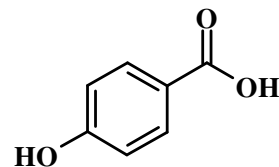
4-Hydroxybenzoic acid (4-HBA)

$pKa \sim 4.57$ **(most acidic)**
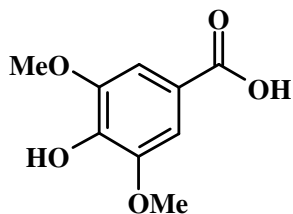
Syringic acid (SA)

$pKa \sim 4.33$ **(most acidic)**
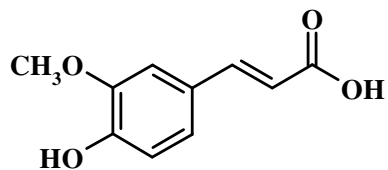
Ferulic acid (FA)

$pKa \sim 4.04$ **(most acidic)**

Figure 5.4. Analytes of interest in this research. The pKa values were obtained using SciFinder® Scholar 2006.

sublimation reaction prior to use. 2-(N-Morpholino)ethanesulfonic acid (MES), sodium bicarbonate, sodium tetraborate decahydrate, tetradecyltrimethylammonium bromide (TTAB), 3,4-dihydroxybenzoic acid (3,4-DHBA), 4-hydroxybenzoic acid (4-HBA), syringic acid (SA), and ferulic acid (FA) were obtained from Sigma-Aldrich (St. Louis, MO). Cellulose acetate was obtained from Aldrich (Milwaukee, WI). All solutions were prepared in 18.2 MΩ distilled, deionized water (Labconco, Kansas City, MO) and filtered through 0.22 µm pore size membrane filters prior to use unless otherwise noted.

5.2.2. Instrumentation

5.2.2.1. Dual-Parallel Electrode Fabrication

The goal of the new design of the dual-parallel electrode was to have the electrodes function in all 3 configurations of dual-electrode detection (see Figure 5.3), including the "series" and "parallel-opposed" configurations simultaneously and the "parallel-adjacent" configuration in order to enhance the selectivity and sensitivity of biological measurements. The design for this dual-parallel electrode was based upon the previously designed single carbon fiber (CF) electrode (refer to Figure 5.1). The modification to the single CF electrode design involved the addition of a second 33 µm CF to the outside of the original electrode. Figure 5.5 schematically displays the new dual-parallel electrode design. Briefly, two single 33 µm CF (AVCO Specialty Materials, Lowell, MA) electrodes were fabricated by threading the CF through fused silica capillary (105 µm o.d., 40 µm i.d.) leaving approximately 1.5 mm of exposed
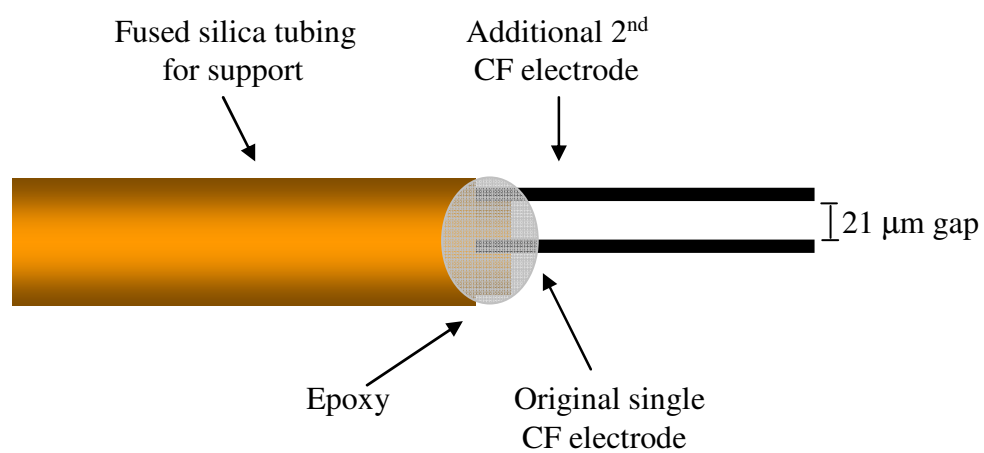
Figure 5.5. Schematic of new design for dual-electrode.

CF at the tip of one and 2.5 mm exposed at the tip of the other. These ends represent the two WE. The opposite ends of the CF were inserted into a 23 gauge needle which had an opening bored into the side. Each single CF electrode was inserted through the needle until it reached the opening in the side, and a drop of silver paste (Ted Pella, Redding, CA) is added to make the electrical connection for the WE. These two single electrodes were UV glued together, and the longer length of CF was UV glued to the parallel piece of capillary. The distance between the electrodes in this design was 21 µm. The combined electrodes were fed through a section of fused silica capillary (360 µm o.d., 250 µm i.d.) for rigidity and support. Both electrodes were then trimmed using a razor blade to a length of approximately 1 - 1.5 mm.

5.2.2.2. Laser-Etched Decoupler for Capillary Electrophoresis

The electrical decoupler was prepared as described previously in a design by Osbourn and Lunte [22]. Briefly, a 35-W CO2 laser (M25 Class, Universal Laser, Denver, CO) was used to etch the fused silica capillaries to create the electrical decouplers. The laser was set to an engraving speed of 3.1% and power of 8%. A 50 µm i.d. separation capillary was taped down to a glass plate leaving the region to be etched by the laser exposed. The laser was focused on the glass plate, and the etch pattern was printed by the laser using a CorelDraw software program (Corel Corporation, Ontario, Canada). The electrical decoupler was located 1.5 cm from the detection end of the capillary and consisted of 35 lines and each line was etched 8 times in order to efficiently create an opening into the lumen of the capillary.

After the laser-etched holes had been made, a 40.6 μm o.d. tungsten wire was threaded through the detection end of the capillary just past the decoupler. The decoupler was then coated with a 6% (w/w) cellulose acetate solution (prepared in acetone) by dragging a drop of the solution across the laser-etched holes. This was repeated 10 - 12 times until the holes were filled with a uniform layer of cellulose acetate polymer. The decoupler was then placed under a 100-W light bulb for 5 minutes to evaporate any residual acetone, thereby increasing the viscosity of the cellulose acetate coating, not allowing any of it to enter and potentially block the inside of the capillary. The capillary was then heated in an oven for 1 hour at 90 ºC to cure the cellulose acetate. After removal of the tungsten wire, the capillary was placed into a Teflon cell as depicted in Figure 5.1. The reservoir surrounding the decoupler was filled with 0.1 N NaOH to soak the decoupler for a period of 1 hour. The capillary was flushed with 0.1 N NaOH at 10 psi during this time period. This resulted in open pores within the cellulose acetate decoupler which allowed for the passage of ions. The capillary was then soaked in BGE continually after this.

5.2.2.3. CE-EC Setup

Electrophoresis was performed using a high voltage (0 – 30 kV) power supply (Spellman High Voltage, Hauppauge, NY). The anodic end of the capillary was isolated in a Plexiglas box containing an interlock for the user's safety. Uncoated fused silica capillaries (Polymicro Technologies, Phoenix, AZ) with dimensions of either 25 μm i.d. and 80 cm length, or 50 μm i.d. and 75 cm length were used as the

separation capillaries. The capillary was placed into the EC cell which contained the BGE and served as the cathodic reservoir (when operating in normal polarity).

In order for the dual-parallel electrode to be inserted into either a 25 or 50 μm i.d. separation capillary, a modification had to be made to the capillary outlet. This involved submerging the outlet of the capillary into 49% HF acid for a period of time. The resulting diameter of the opening at the outlet of the capillary was sufficient for the insertion of the dual-electrode. This will be discussed further in Section 5.3.1.

Electrodes were prepared as described in Section 5.2.2.1. The electrodes were placed into BGE and pre-treated by applying a ±1.5 V square waveform at 100 Hz for 20 seconds. A platinum auxiliary electrode and a Ag/AgCl reference electrode (Bioanalytical Systems, West Lafayette, IN) were used. The CF working electrodes were controlled by two LC-4C potentiostats (Bioanalytical Systems, West Lafayette, IN). All applied potentials reported were against a Ag/AgCl reference electrode. Data acquisition was performed by Chrom&Spec software (Ampersand International, Inc., Beachwood, OH) at a frequency of 10 Hz per channel.

5.2.3. CE Methodology

5.2.3.1. Hydroquinone/Benzoquinone

All injections were performed by hydrodynamically injecting (10 psi for 2 seconds) each standard onto the capillary (50 μm i.d., 75 cm length, laser-etched cellulose acetate decoupler). The BGE for this research was 25 mM MES, pH 5.5. The separation voltage was -15 kV.   The dual-electrodes were inserted a depth of

700 μm. The oxidation potential used to detect H_2Q was +400 mV versus Ag/AgCl, and the reduction potential for BQ was -200 mV versus Ag/AgCl.

5.2.3.2. Phenolic Acids

All samples were injected electrokinetically (-12 kV for 1 second) onto the capillary (25 μm i.d., 80 cm length, no decoupler). The BGE for this research was 75 mM sodium tetraborate, 0.5 mM TTAB, pH 8.4 with 0.1 M HCl. The separation voltage was -12 kV. The dual-electrodes were inserted a depth of 400 μm. The oxidation and reduction potentials used to detect the phenolic acids were +700 mV and -400 mV versus Ag/AgCl, respectively.

5.3. Results and Discussion

5.3.1. HF Etching of Capillaries

For the coupling of either 25 or 50 μm separation capillaries with the newly designed dual-electrode detector, the i.d. of the outlet end of the capillary had to be increased. A method of HF acid etching the outlet end of the capillary introduced by Sloss and Ewing was incorporated for this purpose [24]. Briefly, the capillary was placed through a rubber septum and then fitted into the lid of a plastic vial which contained 2 mL of 49% HF acid. Parameters, including the inclusion of the polyimide coating and the length of time spent in the HF acid, were varied in order to optimize the proper etching protocol. Immediately after removal from the 49% HF

Table 5.1. HF etching optimization.

Initial Capillary i.d. (μm)	Condition Tested	HF Etch Time (min)	New Capillary i.d. at Tip (μm)[a]	Maximum Insertion Depth of Dual-Electrode (μm)[a]
50	3 mm polyimide removed	20	~120	~280
50	3 mm polyimide removed	40	~175	~350
50	polyimide intact	40	~200	~575
50	polyimide intact	60	~300	~825
25	polyimide intact	90	~300	~1100

a: average of n = 3 capillaries

acid, the capillary was placed into a 1 M sodium bicarbonate solution in order to neutralize any remaining HF acid from further etching the capillary inner wall. The results from the HF etching are summarized in Table 5.1. It was determined that for the 50 μm i.d. capillary, the optimum HF etching conditions in order to keep the polyimide coating intact was to etch for 60 minutes. This provided a significant magnification to the capillary i.d. at the outlet allowing for the maximal insertion of the dual-electrode as pictured in Figure 5.6. It should be noted that the HF acid etching of the 50 μm i.d. capillary should occur before the laser-etched decoupler is
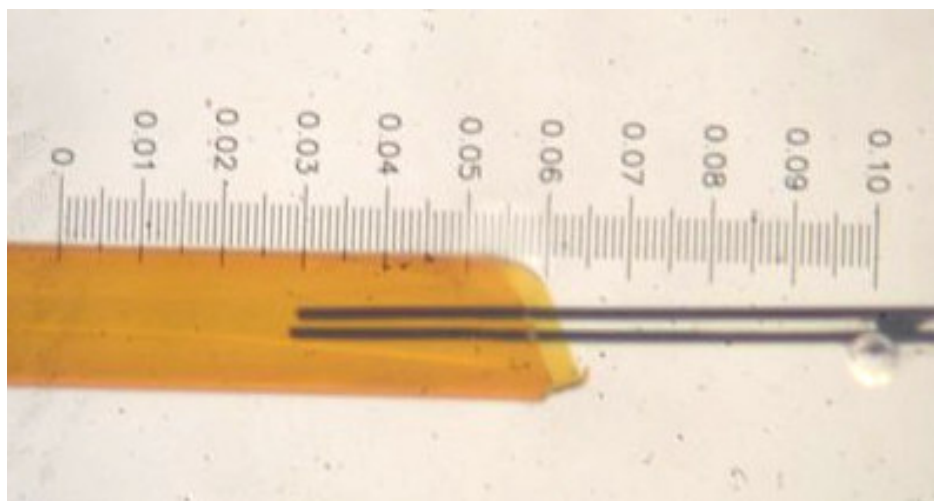
Figure 5.6. Dual-electrode detector inserted into an HF etched capillary.

coated with cellulose acetate as the HF acid fumes will dissolve the polymer coating. For the 25 μm i.d. capillary, an etch time of 90 minutes, with the polyimide coating intact, was acceptable in producing an increased capillary i.d. at the outlet and enabled the insertion of the dual-parallel electrode detector.

5.3.2. Hydroquinone / Benzoquinone

The H_2Q/BQ couple is commonly used to study redox chemistry. Figure 5.7 displays this redox couple. The redox couple was chosen for this research because of its reversible nature and its ease of detection at the CF electrode. A 100 μM concentration of each H_2Q and BQ was used to create respective hydrodynamic voltammagrams (HDVs) which are shown in Figure 5.8.

To first test the H_2Q/BQ redox couple, flow-injection analysis (FIA) was performed by hydrodynamically injecting each standard individually (10 psi for 2 seconds) and then applying 10 psi to push the H_2Q or BQ towards the detector. One WE was set to +400 mV ($W_{(+400)}$) and the second WE was set to -200 mV ($W_{(-200)}$) versus Ag/AgCl. Figures 5.9(A) and (B) display typical results from an FIA experiment for H_2Q and BQ, respectively. The black trace in each electropherogram displays the results from a single electrode CE-EC experiment. When the second electrode is activated, the electropherogram takes on the form of the red trace. The same injection was also performed with only having $W_{(-200)}$ active for an injection of H_2Q, and $W_{(+400)}$ active for BQ. No peak was observed when these conditions were
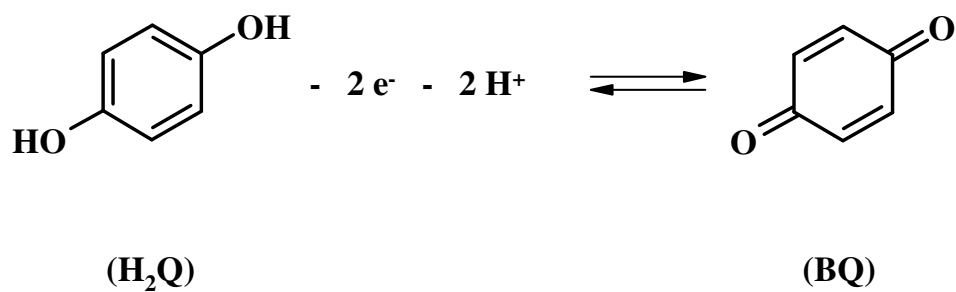
Figure 5.7. H$_2$Q/BQ redox couple.
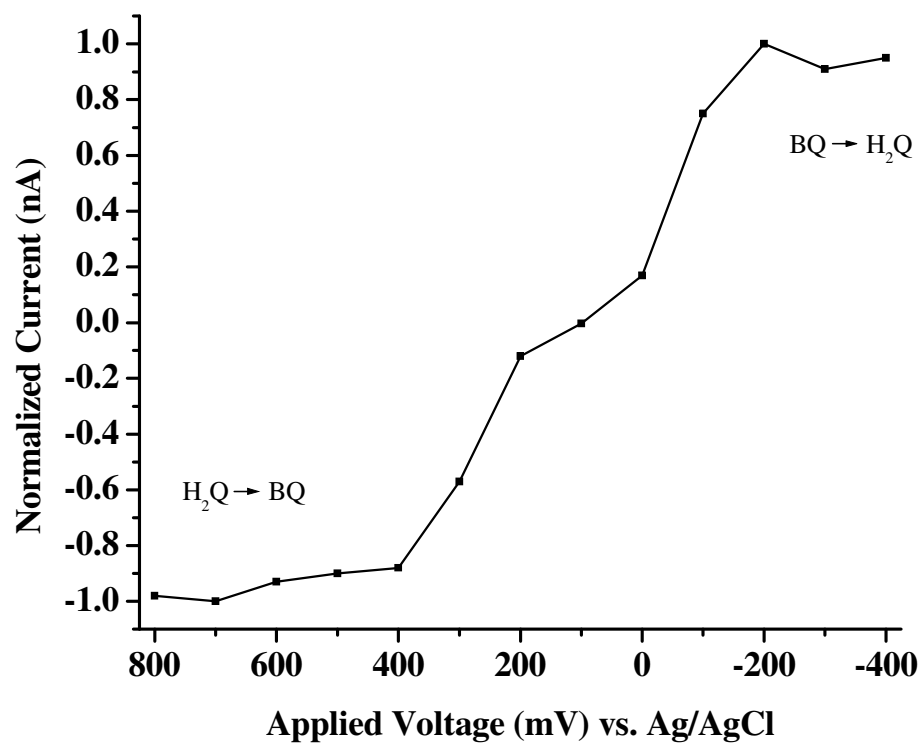
Figure 5.8. HDVs for H_2Q and BQ. CE-EC parameters as noted in Section 5.3.2.
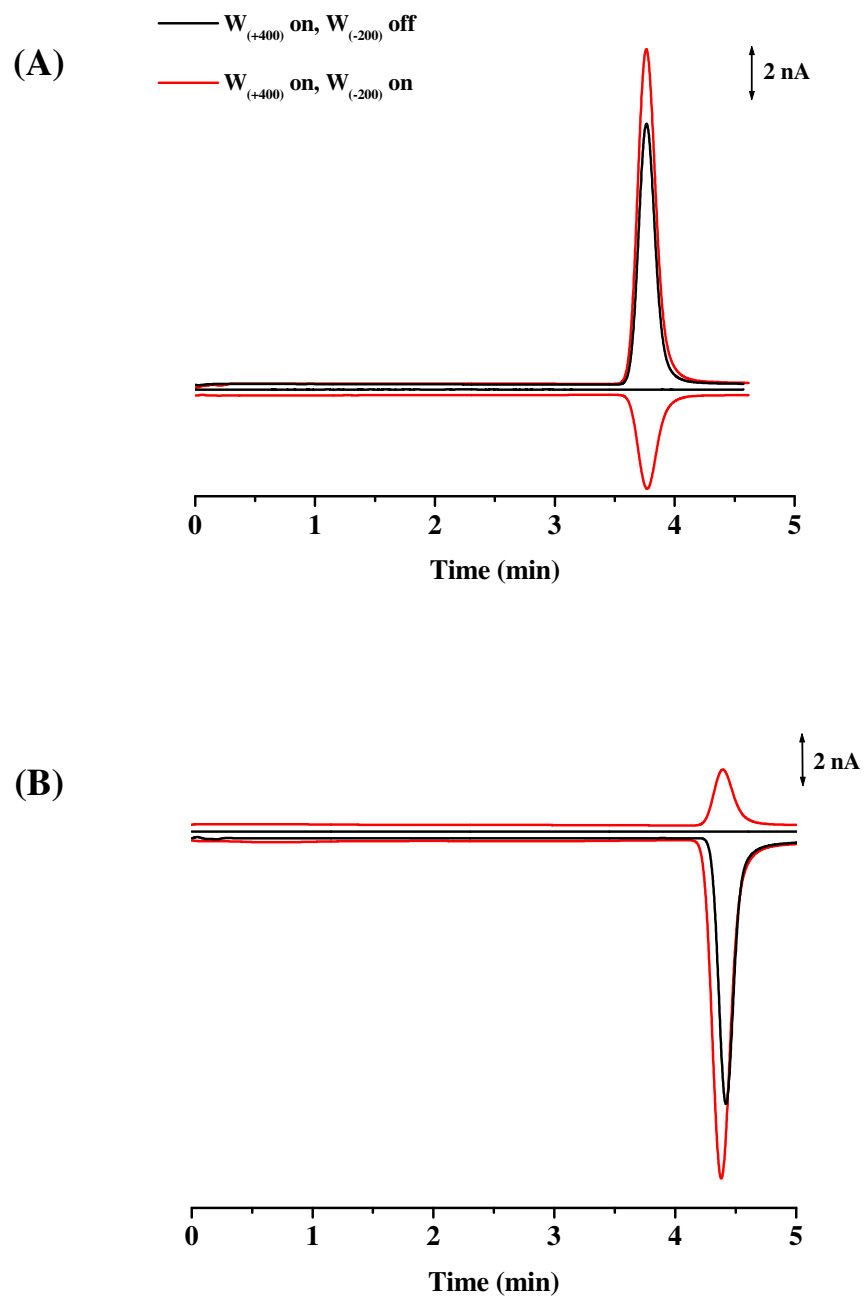
Figure 5.9. FIA traces for H$_2$Q and BQ. CE-EC parameters as noted in Section 5.3.2. (A) Injection of H$_2$Q; (B) Injection of BQ.

employed proving the peaks previously observed were true representations of what is occurring at each WE. Table 5.2 summarizes the numerical data from the FIA experiments. The collection efficiencies were calculated by taking the ratio of the area of each analyte peak at the downstream electrode to its area at the upstream electrode.

Table 5.2. FIA analysis of H_2Q and BQ.

Compound	Collection Efficiency	Estimated Single LOD[a] (nM)	Signal Enhancement	Estimated Dual LOD[b] (nM)
H_2Q	28%	1.3	22%	1.0
BQ	16%	2.1	22%	1.6

a: only $W_{(+400)}$ active
b: both $W_{(+400)}$ and $W_{(-200)}$ active

This experiment was repeated using capillary electrophoresis (CE) instead of FIA. CE was performed at +15 kV in order to considerably slow the velocity of the analytes. Figures 5.10(A) and (B) display typical electropherograms received from an injection of H_2Q and BQ, respectively. The numerical data from these experiments are tabulated in Table 5.3. The analyte peaks shown in Figure 5.10 are very broad when compared to typical CE peaks. This is one drawback of using an
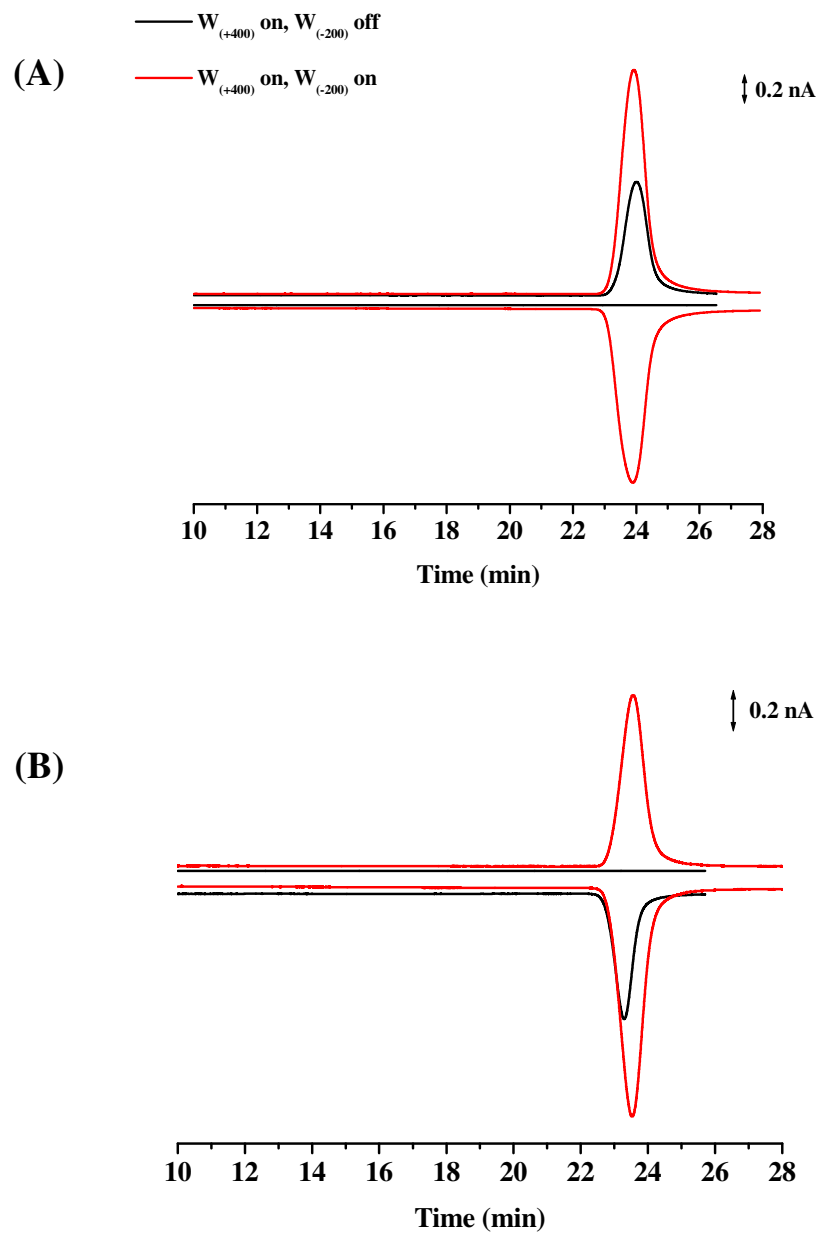
Figure 5.10. Electropherograms for H₂Q and BQ. CE-EC parameters as noted in Section 5.3.2. (A) Injection of H₂Q; (B) Injection of BQ.

Table 5.3. Electrophoretic analysis of H_2Q and BQ

Compound	Collection Efficiency	Estimated Single LOD[a] (nM)	Signal Enhancement	Estimated Dual LOD[b] (nM)
H_2Q	85%	46.4	50%	23.4
BQ	75%	47.5	45%	26.2

a: only $W_{(+400)}$ active
b: both $W_{(+400)}$ and $W_{(-200)}$ active

electrical decoupler. After the decoupler, the separation capillary turns into a "detection" capillary where phenomena such as laminar flow and band-broadening can occur [19]. Also, the HF acid etched portion of the capillary, which surrounds the electrodes, helps to contribute to the diffusion and band-broadening characteristics.

In both of these experiments, the dual-electrode system is acting in the "series" configuration since subsequent reduction occurs after an injection of H_2Q (and *vice versa* for BQ), and in the "parallel-opposed" configuration since signal enhancement is observed due to redox cycling. The estimated LODs of H_2Q and BQ decreased upon activation of the downstream electrode. This was possible due to the redox cycling between the two CF electrodes. Tables 5.2 and 5.3 also show the signal enhancement, or current increase, obtained at the upstream electrode upon activation of the downstream electrode. It should be noted that both the collection efficiencies

and the signal enhancements are greater for H_2Q and BQ with CE rather than with FIA. To explain this, the apparent mobility (μ_{app}) for the two analytes was considered. Equation 5.4 shows a variation on Equation 1.12 (Chapter 1) used for the

$$\mu_{app} = L_d L_t / Vt \qquad (5.4)$$

analysis of the μ_{app}. This equation was used to calculate the μ_{app} for the analytes using both FIA and CE, where L_d is the effective capillary length in centimeters, L_t is the total capillary length in centimeters, V is the applied voltage in Volts, and t is the migration time in seconds. For the FIA calculations, V was excluded. Table 5.4 summarizes these data.

Table 5.4. Apparent mobilities of H_2Q and BQ using FIA and CE.

Compound	Analysis Mode	μ_{app} (cm^{2}V^{-1}sec^{-1})
H_2Q	FIA	25
BQ	FIA	21.8
H_2Q	CE	0.000256
BQ	CE	0.000261

The decreased mobilities of both H$_2$Q and BQ in CE contribute to the corresponding increases observed in their collection efficiencies. These decreased mobilities also contribute to the increases observed in the amount of redox cycling in CE compared to FIA as shown in Table 5.5. Equation 5.5 displays an empirical formula used to

$$RC = 1 + CE^2 + CE^4 + CE^6 + \ldots = 1 / (1\text{-}CE^2) \qquad (5.5)$$

calculate the amount of redox cycling between electrodes based upon the collection efficiencies [39]. As shown, the amount of redox cycling (*RC*) was calculated based upon the increase in current, or collection efficiency (*CE*), from the regeneration of the analyte at W$_{(+400)}$ after a series of subsequent reduction and oxidation cycles. The first complete oxidation-reduction-oxidation cycle is equivalent to *CE*^{2}. For a large number of terms, Equation 5.5 can equate to $1 / (1 - CE^2)$ for simplicity. The calculated values for redox cycling were obtained using Equation 5.5. The experimental values for redox cycling take into account the actual observed signal enhancement, a caveat of Equation 5.5. The values correlate quite reasonably. This geometric series does provide a good estimate of the amount of redox cycling that would be expected only by knowing the value of the collection efficiency. However, it does not take into account the conversion efficiencies at each electrode throughout each cycle. A value of 100% was assumed for the conversion efficiency when Equation 5.5 was employed.

Table 5.5. Redox cycling of H_2Q and BQ using FIA and CE.

Compound	Analysis Mode	Calculated Redox Cycling	Experimental Redox Cycling
H_2Q	FIA	1.1	~ 1.0
BQ	FIA	1.0	~ 1.0
H_2Q	CE	3.6	~ 1.7
BQ	CE	2.3	~ 1.8

Further experimentation is needed using this dual-electrode design. Parameters such as the determination of a linear working range and reproducibility upon multiple injections as well as between different dual-electrode fabrications require additional examination.

5.3.3. Phenolic Acids

A mixture of 4 phenolic acids (3,4-DHBA, 4-HBA, SA, and FA) were investigated for the further investigation of the new dual-electrode design in a separation mode.   A 100 µM concentration of this mixture was used to create respective HDVs which are shown in Figure 5.11.
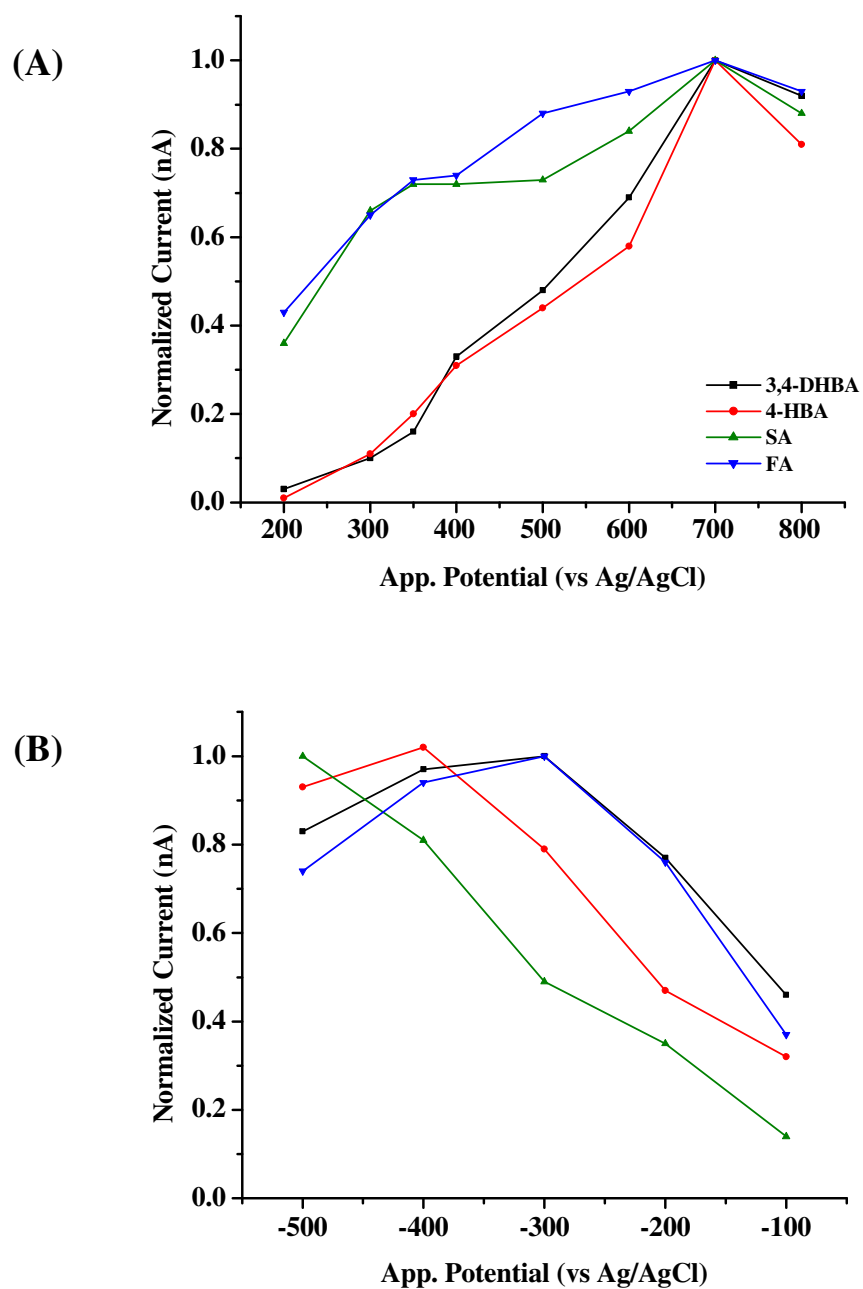
Figure 5.11. HDVs for mixture of phenolic acids. CE-EC parameters as noted in Section 5.3.3. (A) Oxidation HDV; (B) Reduction HDV.

The dual-electrode design was first tested in the "parallel-opposed" configuration. The first WE was set to + 700 mV ($W_{(+700)}$)and the second WE was set to -400 mV ($W_{(-400)}$) versus Ag/AgCl. Figure 5.12 displays a typical electropherogram from a mixture of phenolic acids. The black trace was indicative of only $W_{(+700)}$ being active. Upon activation of $W_{(-400)}$, the electropherogram takes on the form of the red trace. Table 5.6 summarizes the data obtained from these dual-electrode experiments. Again, it was noticed that the dual-electrode was acting both in "series" and "parallel-opposed" configurations. The observed collection efficiencies are very similar to those reported in literature for these acids in both

Table 5.6. Electrophoretic analysis of phenolic acids in "parallel-opposed" configuration.

Compound	Collection Efficiency	Estimated Single LOD[a] (nM)	Signal Enhancement	Estimated Dual LOD[b] (nM)
3,4-DHBA	27%	48.8	21%	38.6
4-HBA	6%	3.3	16%	2.7
SA	13%	39.7	16%	33.4
FA	21%	42.9	24%	32.7

a: only $W_{(+700)}$ active
b: both $W_{(+700)}$ and $W_{(-400)}$ active

Figure 5.12. Electropherograms for mixture of phenolic acids using dual-electrode in "parallel-opposed" configuration. CE-EC parameters as noted in Section 5.3.3. [1 = 3,4-DHBA; 2 = 4-HBA; 3 = SA; 4 = FA].

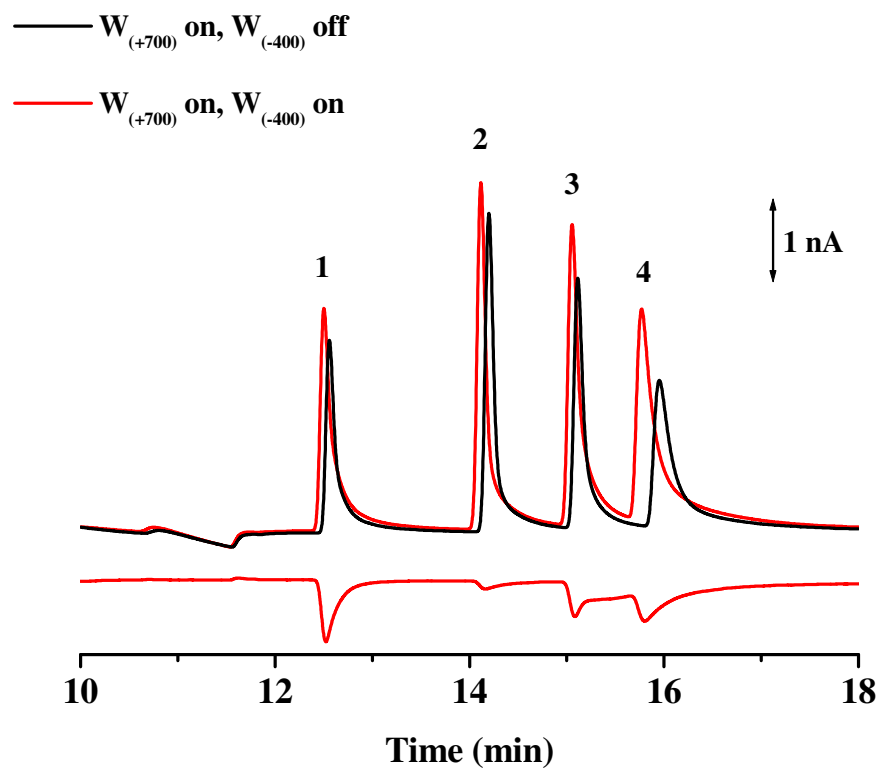LC-EC and CE-EC. Holland *et al.* [36] reported collection efficiencies for 35% for 3,4-DHBA and 18% for FA using CE-EC, while Lunte *et al.* [40] reported collection efficiencies of 13% for SA and 18% for FA using LC-EC. Again, the estimated LODs were reduced due to the redox cycling which occurred.

The dual-electrode design was next operated in the "parallel-adjacent" configuration. The first WE was set to +350 mV ($W_{(+350)}$) and the second WE was set to +700 mV ($W_{(+700)}$) versus Ag/AgCl. $W_{(+350)}$ was chosen as the operating potential from the oxidation HDV (Figure 5.11(A)). Typically, the chosen potential would produce approximately 50% of the signal at the second electrode. This research showed +350 mV to be an optimum potential as SA and FA possessed approximately 70% of the signal output and 3,4-DHBA and 4-HBA had approximately 20% of the signal output. Figure 5.13 displays typical electropherograms collected in the "parallel-adjacent" configuration. The expected and obtained current ratios between the two traces are shown in Table 5.7. From these data, the dual-electrode appeared to perform as expected with the actual measured current ratios corresponding to the expected ratios from the HDV.

Again, further experimentation is needed using this dual-electrode design. The parameters which need further examination are the determination of a linear working range and reproducibility upon multiple injections as well as between different dual-electrode fabrications.
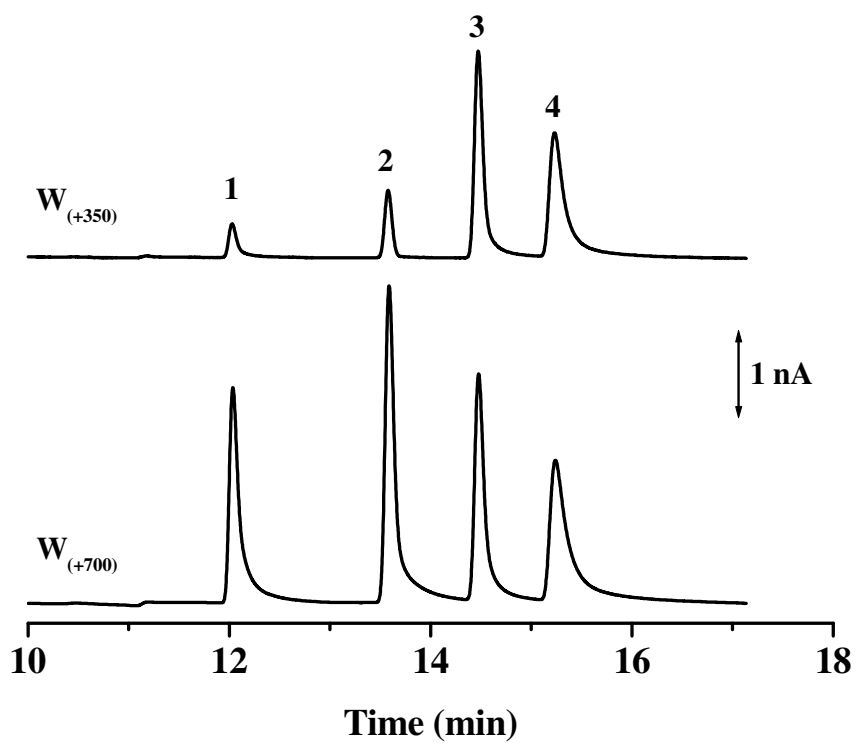
Figure 5.13. Electropherograms for mixture of phenolic acids using dual-electrode in "parallel-adjacent" configuration. CE-EC parameters as noted in Section 5.3.3. [1 = 3,4-DHBA; 2 = 4-HBA; 3 = SA; 4 = FA].

Table 5.7. Electrophoretic analysis of phenolic acids in "parallel-adjacent" configuration. ($W_{(+350)}$ / $W_{(+700)}$).

Compound	Current Ratio from HDV	Current Ratio from Electropherogram
3,4-DHBA	0.15	0.16
4-HBA	0.19	0.20
SA	0.70	0.72
FA	0.73	0.73

5.4. Conclusions

A new design for an on-capillary dual-electrode detector for CE-EC has been described. The new dual-electrode detector was shown to perform successfully using either a 50 μm i.d. capillary with a laser-etched cellulose acetate decoupler as well as a 25 μm i.d. capillary without a decoupler. HF acid etching was used to create a larger opening at the outlet end of the capillary to facilitate the insertion of the dual-electrode detector.

The H$_2$Q/BQ redox couple, as well as a mixture of phenolic acids, was tested with the dual-electrode detector acting simultaneously in the "series" and "parallel-opposed" configuration. These data showed that decreased flow velocities provided an increase in the collection efficiencies and subsequently, the amount of redox cycling. With the dual-electrode detector operating in the "parallel-adjacent" configuration, comparative current ratios were obtained with those predicted from the HDVs.

5.5. References

[1].   Weng, Q., Xu, G., Yuan, K., and Tang, P., *Determination of monoamines in urine by capillary electrophoresis with field-amplified sample stacking and amperometric detection.* J. Chromatogr. B, **2006**, 835: 55-61.

[2].   Du, Y. and Wang, E., *Capillary electrophoresis and microchip capillary electrophoresis with electrochemical and electrochemiluminescence detection.* J. Sep. Sci., **2007**, 30: 875-890.

[3].   Kong, Y., Chen, H., Wang, Y., and Soper, S.A., *Fabrication of a gold microelectrode for amperometric detection on a polycarbonate electrophoresis chip by photodirected electroless plating.* Electrophoresis, **2006**, 27: 2940-2950.

[4].   Xu, J.-J., Wang, A.-J., and Chen, H.-Y., *Electrochemical detection modes for microchip capillary electrophoresis.* Trends Analyt. Chem., **2007**, 26: 125-132.

[5].   Sandlin, Z.D., Shou, M., Shackman, J.G., and Kennedy, R.T., *Microfluidic electrophoresis chip coupled to microdialysis for in vivo monitoring of amino acid neurotransmitters.* Anal. Chem., **2005**, 77: 7702-7708.

[6].   O'Shea, T.J., *Electrochemical Detection for Capillary Electrophoresis*, in *Pharmaceutical and Biomedical Applications of Capillary Electrophoresis*, S.M. Lunte and D.M. Radzik, Editors. **1996**, Elsevier: Oxford.

[7].   Bard, A.J. and Faulkner, L.R., *Electrochemical Methods: Fundamentals and Applications*. 2nd ed. **2001**, New York: John Wiley and Sons, Inc.

[8].   Brett, C.M.A. and Brett, A.M.O., *Electrochemistry: Principles, Methods, and Applications*. **1993**, Oxford: Oxford University Press.

[9].   Fisher, A.C., *Electrode Dynamics*, ed. R.G. Compton. **1996**, Oxford: Oxford University Press.

[10].   Lunte, S.M., Martin, R.S., and Lunte, C.E., *Capillary Electrophoresis /Electrochemistry*, in *Electroanalytical Methods for Biological Materials*, A. Brajter-Toth and J.Q. Chambers, Editors. **2002**, Marcel Dekker, Inc.: New York.

[11].   Osbourn, D.M., *Instrumentation and Methods for Capillary Electrophoresis*. **2003**, University of Kansas: Dissertation.

[12]. Zhong, M. and Lunte, S.M., *Tubular-wire dual electrode for detection of thiols and disulfides by capillary electrophoresis/electrochemistry.* Anal. Chem., **1999**, 71: 251-255.

[13]. Huang, X. and Kok, W.T., *Determination of sugars by capillary electrophoresis with electrochemical detection using cuprous oxide modified electrodes.* J. Chromatogr. A, **1995**, 707: 335-342.

[14]. Zhou, J. and Lunte, S.M., *Direct determination of amino acids by capillary electrophoresis/electrochemistry using a copper microelectrode and zwitterionic buffers.* Electrophoresis, **1995**, 16: 498-503.

[15]. Shin, D., Sarada, B.V., Tryk, D.A., Fujishima, A., and Wang, J., *Application of diamond microelectrodes for end-column electrochemical detection in capillary electrophoresis.* Anal. Chem., **2003**, 75: 530-534.

[16]. Wallingford, R.A. and Ewing, A.G., *Capillary zone electrophoresis with electrochemical detection.* Anal. Chem., **1987**, 59: 1762-1766.

[17]. Linhares, M.C. and Kissinger, P.T., *Use of an on-column fracture in capillary zone electrophoresis for sample introduction.* Anal. Chem., **1991**, 63: 2076-2078.

[18]. O'Shea, T.J., Greenhagen, R.D., Lunte, S.M., Lunte, C.E., Smyth, M.R., Radzik, D.M., and Watanabe, N., *Capillary electrophoresis with electrochemical detection employing an on-column Nafion joint.* J. Chromatogr. A, **1992**, 593: 305-312.

[19]. Park, S., Lunte, S.M., and Lunte, C.E., *A perfluorosulfonated ionomer joint for capillary electrophoresis with on-column electrochemical detection.* Anal. Chem., **1995**, 67: 911-918.

[20]. Qian, J., Wu, Y., Yang, H., and Michael, A.C., *An integrated decoupler for capillary electrophoresis with electrochemical detection: application to analysis of brain microdialysate.* Anal. Chem., **1999**, 71: 4486-4492.

[21]. Hu, S., Wang, Z.-L., Li, P.-B., and Cheng, J.-K., *Amperometric detection in capillary electrophoresis with an etched joint.* Anal. Chem., **1997**, 69: 264-267.

[22]. Osbourn, D.M. and Lunte, C.E., *Cellulose acetate decoupler for on-column electrochemical detection in capillary electrophoresis.* Anal. Chem., **2001**, 73: 5961-5964.

[23]. Huang, X., Zare, R.N., Sloss, S., and Ewing, A.G., *End-column detection for capillary electrophoresis.* Anal. Chem., **1991**, 63: 189-192.

[24]. Sloss, S. and Ewing, A.G., *Improved method for end-column amperometric detection for capillary electrophoresis.* Anal. Chem., **1993**, 65: 577-581.

[25]. Powell, P.R., Woods, L.A., and Ewing, A.G., *Characterization of etched electrochemcial detection for electrophoresis in micron inner diameter capillaries.* J. Sep. Sci., **2005**, 28: 2540-2545.

[26]. Woods, L.A. and Ewing, A.G., *Etched electrochemical detection for electrophoresis in nanometer inner diameter capillaries.* Chemphyschem, **2003**, 4: 207-211.

[27]. Matysik, F.-M., *Improved end-column amperometric detection for capillary electrophoresis.* J. Chromatogr. A, **1996**, 742: 229-234.

[28]. Wallenborg, S.R., Nyholm, L., and Lunte, C.E., *End-column amperometric detection in capillary electrophoresis: influence of separation-related parameters on the observed half-wave potential for dopamine and catechol.* Anal. Chem., **1999**, 71: 544-549.

[29]. Fenn, R.J., Siggia, S., and Curran, D.J., *Liquid chromatography detection based on single and twin electrode thin-layer electrochemistry: application to the determination of catecholamines in blood plasma.* Anal. Chem., **1978**, 50: 1067-1073.

[30]. Roston, D.A. and Kissinger, P.T., *Identification of phenolic constituents in commerical beverages by liquid chromatography with electrochemical detection.* Anal. Chem., **1981**, 53: 1695-1699.

[31]. Roston, D.A. and Kissinger, P.T., *Series dual-electrode detector for liquid chromatography/electrochemistry.* Anal. Chem., **1982**, 54: 429-434.

[32]. Schieffer, G.W., *Dual coulometric-amperometric cells for increasing the selectivity of electrochemical detection in high-performance liquid chromatography.* Anal. Chem., **1980**, 52: 1994-1998.

[33]. Lin, B.L., Colon, L.A., and Zare, R.N., *Dual electrochemical detection of cysteine and cystine in capillary zone electrophoresis.* J. Chromatogr. A, **1994**, 680: 263-270.

[34]. Zhong, M., Zhou, J., Lunte, S.M., Zhao, G., Giolando, D.M., and Kirchhoff, J.R., *Dual-electrode detection for capillary electrophoresis/electrochemistry.* Anal. Chem., **1996**, 68: 203-207.

[35]. Voegel, P.D. and Baldwin, R.P., *Electrochemical detection in capillary electrophoresis with dual-parallel on-capillary electrodes.* Electrophoresis, **1998**, 19: 2226-2232.

[36]. Holland, L.A., Harmony, N.M., and Lunte, S.M., *Characterization of an integrated on-capillary dual electrode for capillary electrophoresis-electrochemistry.* Electroanalysis, **1999**, 11: 327-330.

[37]. Chen, D.-C., Chang, S.-S., and Chen, C.-H., *Parallel-opposed dual-electrode detector with recycling amperometric enhancement for capillary electrophoresis.* Anal. Chem., **1999**, 71: 3200-3205.

[38]. Chen, D.-C., Zhan, D.-Z., Cheng, C.-W., Liu, A.-C., and Chen, C.-H., *Determination of urine catecholamines by capillary electrophoresis with dual-electrode amperometric detection.* J. Chromatogr. B, **2001**, 750: 33-39.

[39]. Bjorefors, F., Strandman, C., and Nyholm, L., *Electrochemical detection based on redox cycling using interdigitated microarray electrodes at μL/min flow rates.* Electroanalysis, **2000**, 12: 255-261.

[40]. Lunte, C.E., Kissinger, P.T., and Shoup, R.E., *Differential mode detection with thin-layer dual-electrode liquid chromatography/electrochemistry.* Anal. Chem., **1985**, 57: 1541-1546.

Chapter 6.

Conclusions and Future Work

6.1. Summary of Dissertation

6.1.1. Design of a Chemically-Induced Seizure Model

A chemically-induced seizure model was developed using the known convulsant, 3-mercaptopropionic acid (3-MPA). An LC-EC method was developed in order to quantitatively monitor the pharmacokinetics (PK) of 3-MPA in different brain regions. This was the first report in which 3-MPA was monitored *in vivo* while simultaneously recording the electrical activity within the cerebral cortex. A 3-MPA dosing method was developed in which a loading dose was administered intravenously (i.v.), immediately followed by a constant infusion of the convulsant. The purpose of this dosing scheme was to maintain a steady-state of the convulsant within the brain. This allowed for the concentration of the 3-MPA to act as an independent variable while manipulations such as anticonvulsant dosing were performed on the animal model. The creation of a controllable seizure model using 3-MPA allowed for the pharmacodynamics (PD) analysis of the neurochemical changes associated with the different stages within the model.

Future work regarding further development of this 3-MPA seizure model would involve variations in both the dose and time of the convulsant. In the developed 3-MPA seizure model, the animal was held in a steady-state of seizure

activity for a maximum time of 30 minutes. This timeframe appeared to be a physiological limitation for the rat model. Maintaining a controllable steady-state of convulsant concentration within the brain while reducing the 3-MPA concentration, thereby reducing the intensity of the obtained seizures, would make for interesting correlations to be made with the accompanying neurochemical changes. Also, varying the 3-MPA dosing scheme by using on-off cycles of dosing (during the constant infusion period) would allow for better experimental control over the physiological barriers which were present during the 30 minute period of steady seizure activity. The use of awake animals would be of interest in the further development of this 3-MPA seizure model. An awake animal would present a model more closely related to human epilepsy. The use of anesthetics, such as ketamine [1, 2] and isoflurane [3], has been shown to suppress seizure activity, thereby not giving a true representation of the dynamics of the epileptic activity.

6.1.2. Analysis of Neurochemical Activity **In Vivo**

Using LC, the amino acid and biogenic amine neurotransmitters were monitored during the application of the 3-MPA chemical seizure model. Within the striatum, significant changes were observed for both glutamate (Glu) and γ-aminobutyric acid (GABA) which were sustained over a period of time. It was hypothesized that this was a result of the desensitization of the Glu receptors. Upon the intracranial perfusion of cyclothiazide (CTZ), the Glu levels significantly decreased compared to the previous experiments. An increase in the level of GABA

was also observed, hypothesizing an increase in the inhibition of the $GABA_A$ receptor by CTZ. A large and reproducible biphasic increase in dopamine (DA) release was observed within the striatum with a resulting decrease in 3,4-dihydroxyphenylaceic acid (DOPAC) and homovanillic acid (HVA), both metabolites of DA. The changes in DA, unfortunately, could not be explained using the experimental parameters instituted. Therefore, in order to gain a more in depth explanation of the neurochemical changes which pertain to the elicited seizures, the analytical methodology was enhanced.

Using CE methodology, the temporal resolution of the microdialysis sampling was increased within the striatum from 5 minutes to 60 seconds. This enhancement in the temporal resolution provided a dramatic improvement in the amount of knowledge obtained about the neurochemical events, especially Glu and DA transmission, as related to the 3-MPA chemical seizure model.

The changes which were observed in the Glu and DA neurotransmitters were thought to be part of a mechanism relating the neuronal activities of the two. Glu was thought to possibly be regulating the initial release of DA via the activation of DA D_2 receptors located on the NMDA receptors. It was also hypothesized that the changes observed in Glu and DA functions were related to hypoxic and/or ischemic events within the striatum.

Future work regarding the analysis of the neurochemical activity resulting from the 3-MPA seizure model would include looking into a correlation between neurotransmitters, such as Glu and DA, and the ionic concentrations of both

potassium (K^+) and calcium (Ca^{2+}). Information regarding K^+ and Ca^{2+} changes within the striatum would reveal further knowledge on the relationship of AMPA and NMDA receptors to the obtained results. Also, monitoring the extracellular pH, lactic acid content, and free radical formation would be helpful in explaining the excessive release activity of both Glu and DA and their relationship to ischemic events.

6.1.3. Development of a Dual-Electrode Amperometric Detector for Capillary Electrophoresis

A new design for an on-capillary dual-electrode detector for CE-EC was described. The new dual-electrode detector was shown to perform successfully using either a 50 μm i.d. capillary with a laser-etched cellulose acetate decoupler and also a 25 μm i.d. capillary without a decoupler. HF acid etching was used to create a larger opening at the outlet end of the capillary to facilitate the insertion of the dual-electrode detector.

The hydroquinone (H_2Q) / benzoquinone (BQ) redox couple and a mixture of phenolic acids were tested with the dual-electrode detector acting simultaneously in the "series" and "parallel-opposed" configuration. These data showed that decreased flow velocities provided an increase in the collection efficiencies and subsequently, the amount of redox cycling. With the dual-electrode detector operating in the "parallel-adjacent" configuration, comparative current ratios were obtained with those predicted from the hydrodynamic voltammagrams (HDVs).

Future work regarding the newly designed dual-electrode amperometric detector should focus on its versatility and applicability. To further demonstrate the

238

function aspect of the dual-parallel electrode, analytes which are not chemically reversible need to be analyzed (*e.g.* 5-hydroxyindole-3-acetic acid (5-HIAA) or ascorbic acid). The analysis of cations, specifically amino acid and biogenic amine neurotransmitters, should be conducted within biological samples to further demonstrate the applicability of the dual-parallel electrode design. As for the overall dual-electrode design, a smaller gap between the electrodes could be investigated. This parameter may help to enhance the amount of redox cycling beyond that already obtained.

The newly designed dual-parallel electrode detector could be implemented for the analysis of faster temporal resolution microdialysis sampling. When using EC detection, the biogenic amines do not need to be derivatized because they are natively electroactive. The addition of perchloric acid allows the microdialysis sample to remain stable for several days. The increased sample stability and improved sensitivity from redox cycling could be advantageous in coupling the dual-parallel electrode detector to an automated commercial CE instrument. This coupling would allow for the advantages of an autosampler and refrigerated sample storage conditions on the commercial CE to be combined with those of the dual-parallel electrode design for high-throughput analysis of microdialysis samples.

6.2. Future Directions

The research discussed throughout this dissertation could be used to benefit alternative treatments used for epilepsy. The 3-MPA seizure model would allow for

the study of the neurochemical changes associated with automated seizure prediction and blockage therapies. The arena of predicting impending seizures in advance of their onset has been an area of much growth over the past 5 years [4]. Being able to block seizures, just before or at their onset, would offer a tremendous advancement in the surgical and medical management of epilepsy [4]. A library of knowledge has been created regarding the use of frequency-dependent electrical stimulation for blocking, or stopping, seizure activity. It has been determined that low (1 Hz) and high (>100 Hz) stimulation frequencies can suppress seizure activity [5, 6], while mid-range (40 – 60 Hz) stimulation frequencies actually enhance the observed seizure activity [7]. Clinical observations have shown remarkable reductions in the number of seizures in which patients endure on a daily basis. Kerrigan *et al*. [8] have noted a mean reduction in seizure frequency of $\geq 54\%$ (maximum reduction of 75%), while Osorio *et al*. [9] have reported seizure reductions of $\geq 58.8\%$ (maximum reduction of 100%).

While clinically observed to function remarkably well, the aforementioned electrical stimulation therapies are purely anecdotal, lacking a general understanding of the neurochemistry behind their effectiveness. Microdialysis could be employed during the various portions of the automated seizure prediction and blockage therapies to assist in circumventing these issues. The 3-MPA seizure model could be employed for use as the basis of generalized epileptic seizures. Electrodes placed strategically within different brain regions could act both to record the electrical activity leading up to and during a seizure event, and to stimulate the selected brain

region to impede the event. High temporal microdialysis sampling would be beneficial during the entirety of such a study. Vital neurochemical information from these experiments could be used for the advancement of the ability to predict the onset of epileptic seizures as well as stopping the seizure events before or at their onset.

6.3. References

[1].   Borris, D.J., Bertram, E.H., and Kapur, J., *Ketamine controls prolonged status epilepticus.* Epilepsy Res., **2000**, 42: 117-122.

[2].   Corssen, G., Little, S.C., and Tavakoli, M., *Ketamine and Epilepsy.* Anesth. Analg., **1973**, 53: 319-335.

[3].   Larsen, M., Hegstad, E., Berg-Johnsen, J., and Langmoen, I.A., *Isoflurane increases the uptake of glutamate in synaptosomes from rat cerebral cortex.* Br. J. Anaesth., **1997**, 78: 55-59.

[4].   Iasemidis, L.D., Shiau, D.-S., Pardalos, P.M., Chaovalitwongse, W., Narayanan, K., Prasad, A., Tsakalis, K., Carney, P.R., and Sackellares, J.C., *Long-term prospective on-line real-time seizure prediction.* Clin. Neurophysiol., **2005**, 116: 532-544.

[5].   Lian, J., Bikson, M., Sciortino, C., Stacey, W.C., and Durand, D.M., *Local suppression of epileptiform activity by electrical stimulation in rat hippocampus in vitro.* J. Physiol., **2003**, 547: 427-434.

[6].   Osorio, I., Frei, M.G., Manly, B.F.J., Sunderam, S., Bhavaraju, N.C., and Wilkinson, S.B., *An introduction to contingent (closed-loop) brain electrical stimulation for seizure blockage, to ultra-short-term clinical trials, and to multidimensional statistical analysis of therapeutic efficacy.* J. Clin. Neurophysiol., **2001**, 18: 533-544.

[7].   You, Z.-B., Tzschentke, T.M., Brodin, E., and Wise, R.A., *Electrical stimulation of the prefrontal cortex increases cholecystokinin, glutamate, and dopamine release in the nucleus accumbens: an in vivo microdialysis study in freely moving rats.* J. Neurosci., **1998**, 18: 6492-6500.

[8].   Kerrigan, J.F., Litt, B., Fisher, R.S., Cranstoun, S., French, J.A., Blum, D.E., Dichter, M., Shetter, A., Baltuch, G., Jaggi, J., Krone, S.B., M., Rise, M., and Graves, N., *Electrical stimulation of the anterior nucleus of the thalamus for the treatment of intractable epilepsy.* Epilepsia, **2004**, 45: 346-354.

[9].   Osorio, I., Frei, M.G., Sunderam, S., Giftakis, J., Bhavaraju, N.C., Schaffner, S.F., and Wilkinson, S.B., *Automated seizure abatement in humans using electrical stimulation.* Ann. Neurol., **2005**, 57: 258-268.